STATEMENT BY THE CANDIDATE

As required by the University Ordinance 770, I wish to state that the work embodied in this thesis titled “RADIO/X-RAY/GAMMA-RAY MONITORING OF MICRO-QUASARS” forms my own contribution to he research work carried out under the guidance of Dr. V.H. Kulkarni at the Department of Physics, University of Mumbai,Kalina Campus, Mumbai - 400 098 this work has not been submitted for any other degree of this or any other University. Whenever reference have been made to previous works of others, it has been clearly indicated as such and included in the Bibliography.

Signature of candidate

Mamta D. Pandey

Certified by

Signature of Guide

Dr. V. H. Kulkarni

DEDICATED

TO MY

BELOVED FAMILY

STATEMENT REQUIRED UNDER 0.771

0.771. Each candidate for the Degree shall send three written or printed copies of his thesis embodying the results of his research and starting whether the work is based on the discovery of new facts by the candidates or of new relations of facts observed by other and how the work tends to the general advancement of knowledge. The candidate shall further forward statement indicating the sources from which his information has been derived and the extent to which his information has been derived and the extent to which he has based his work on the work of others, and shall indicate which portion or portions of his thesis he claims as original. Where a candidate presents a joint work, he shall clearly state the portion in which his own contribution as distinguished from the portion contributed by his collaborator. This statement shall be certified as correct by the University teacher, as well as the candidate. The candidate may also forward with his application three copies of any original contribution or contributions to the advancement of knowledge on the subject selected by him for his thesis or any cognate subject published by him independently or jointly with others upon which he relies in support of his candidature. The thesis shall be written or printed in English, so that when the subjects-matter of the thesis relates to a modern European or Modern Indian Language, it may, with the previous permission of the Board of University Teaching for subjects in the Faculties of Arts and Science, be written or printed in that language.

1]. This thesis presents a detailed first ever study of the micro-quasars at low radio frequencies. The data from other wavelengths are also used to understand the multi-wavelength nature of these sources. It is based on the following objectives:

(i) Relativistic outflows, or ‘Jets’, represent one of the most obvious, important and yet poorly-explained phenomena associated with accreting relativistic objects, including X-ray binaries. Detailed investigations have revealed a rich phenomenology and clear patter of behavior which have provided unique insight into the coupling of accretion

and outflow close to relativistic objects. In this thesis we study the radio properties of micro-quasars monitored at 1280, 610 and 235 MHz with the Giant Metrewave Radio Telescope (GMRT) over a period of 3 years. And we study X-ray properties of micro-quasars using RXTE/ASM satellite data. We also performed the first ever low frequency radio study of newly discovered Gamma-ray emitting sources detected by the INTEGRAL satellite. The first ever low radio frequency studies done on these sources was with the motivation gained from the high frequency results. The investigation is applied to the known population of sixteen micro-quasars as well as newly discovered ones. The result is used to study various astrophysical phenomenon and confirm/check various theoretical assumptions.

(ii) Nine among the sixteen sources have been positively detected with the GMRT which includes six High Mass X-ray binaries and three Low Mass X-ray Binaries. Among the nine sources emitting at low frequencies five are persistent and four are transient. Four sources are absorbed at low frequencies.

(iii) In the case of three persistent systems the contemporaneous data suggest a flat spectrum at high frequencies with inverted spectra at low frequencies i.e. below 2 GHz (where $S_\nu \propto \nu^\alpha$). A spectral turnover below 2 GHz is seen for most of the sources. We provide different models for radio emissions at low frequencies and discuss the synchrotron self absorption model and the low frequency resrviour model in detail.

(iv) Refractive interstellar scintillation becomes dominant at low frequencies hence the GMRT data was checked for refractive interstellar scintillation effects. From our observations we confirm that only Cyg X-1 and SS433 are affected by refractive interstellar scintillation and Sco X-1, LS5039, XTE J1118+480, and LSI+61303 are most likely to be affected by scintillation.

(v) The famouse micro-quasar, GRS 1915+105 was observed during three different radio outburst. A comparision with the simultaneous data at higher frequencies suggest that there is a formation of temporary lobes at the end of the radio jet as seen in quasars.

These regions are formed due to adiabatic expansion of radio emitting plasma in an ambient medium. The density of the medium is too poor, to slow down the expansion. The magnetic field is temporarily trapped in these lobes providing adequate energy for the emission of low frequency nonthermal radiation. This is an important addition in the morphology of micro-quasars from our observations.

(vi) Thus, these studies have provided several new results, which are useful for understanding a complex system like micro-quasars. It will also hopefully stimulate further research in terms of theoretical understanding of the properties of the black hole X-ray binaries, and in understanding the generation and maintenance of magnetic field in the complex jet medium.

(v) Motivated with above important results, we have also carried out follow up observations of newly discovered X-ray binaries by the INTEGRAL satellite in order to find new micro-quasar candidates. Four newly discovered hard X-ray sources turn out to be possible micro-quasar candidates based upon the follow up radio and other multi-wavelength observations.

2]. Proper references have been made where the work of others is described in the thesis. The rest of the thesis can be claimed as original.

3]. The work presented here is done under the guidance of Dr. V. H. Kulkarni, department of Physics, University of Mumbai. Part of the work presented in this thesis is done in collaboration with the other senior scientist, Prof. A. P. Rao and Dr. Ishwara Chandra at the National Centre for Radio Astrophysics, Tata Institute of Fundamental Research, Pune, Prof. R. K. Manchanda at the Tata Institute of Fundamental Research, Mumbai, and, Prof. P. Durouchoux at the Astronomy department of Center of Atomic Energy, Saclay, France.

Part of the work presented in this thesis has been published. A list of publications has been attached along with the copies of the published papers.

Certified that the above statements are true.

Signature of Candidate

Mamta D. Pandey

Signature of Guide

Dr. V. H. Kulkarni

RADIO/X-RAY/GAMMA-RAY MONITORING OF MICRO-QUASARS

A Thesis submitted
to the
University of Mumbai
for the
Ph.D. (Science) Degree
in Physics

Submitted By
MAMTA D. PANDEY

Under the Guidance of
Dr. V.H. Kulkarni

Department of Physics,
Kalina Campus, University of Mumbai,
Mumbai - 400 098
INDIA

April 2006

Contents

List of Figures

List of Tables

ACKNOWLEDGEMENTS

I thank Prof. Pramesh Rao and Dr.Ishwara-Chandra for introducing me to my thesis problem. They have provided me all the help, guidance and encouragement needed during these years. They have solved various queries related to my thesis problem and regarding AIPS. They have always been available for scientific and personal discussions. They have always encouraged me tackle problems independently. I express my deep gratitude to them for being humble and patient towards me. I also thank them for patiently revising my thesis. I specially thank Dr.Ishwara-Chandra and Prof. Pramesh Rao for spending his valuable time on my thesis reading and correction.

I am obliged to Prof. R. Manchanda, who supported and encouraged me to do research in Radio astronomy. He also got the financial assistance from the Department of Space for this research work. This research was supported under RESPOND programme of ISRO. He has helped in various aspects related to this thesis work and have provided guidance and assistance in carrying out this work. In particular, I am greatful to all of them for paying adequate attention to my work in spite of their heavy occupancy. It has been a great pleasure to interact with them and learn various things over the years.

I am thankful to my collaborator Prof. Ph. Durouchoux for being a source of enthusiasm and encouragement in this field of research. He is full of new ideas and is one among a few enthusiastic scientists, I have met. I am thankful to him for reading and commenting my papers and thesis. I am also thankful to him for inviting me to CEA to work with him and providing me the financial support. I also thank Mrs. Durouchoux for inviting me for dinner at their place and having interesting discussions about various cultures.

I am thankful to Prof. V. H.Kulkarni, my official supervisor, for taking considerable interest in my work since the beginning and also for the guidance in various matters pertaining to the thesis work. Without his support this thesis was not possible. I know him since my M. Sc. days, he has always been very understanding and kind towards students. We use to often go to him for advise related to our career in research. He has always been a source of encouragement for the Physics department students. I am thankful to him for reading my thesis. I would also like to thank Dr. S. Gupta, Dr. A. M. Narsale, Dr. Yadav, Dr. Kothari, Dr. Dubey, Dr. M. Press, Dr. S. B. Patel and other university professors for encouraging and supporting me all these years.

My special thanks to Prof. R. Nityananda and Prof. V. K. Kulkarni who have been kind and understanding towards me and have provided me the library, computational and hostel facility in NCRA. With their support, encouragement and guidance, my stay in NCRA was possible. In particular, I would like to place my sincere thanks to Prof. R. Nityananda for arranging adequate support from the RRI Trust during my crucial days and for providing me a loan from the RRI Trust to help me during my first visit to CEA. He has been very considerate and approchive towards me. He is one of the best teachers, I have ever met. My sincere thanks to Prof. V. K. Kulkarni for introducing me to NCRA and radio astronomy. Without his initial support it was not possible for me to carry out my research in radio astronomy. He has helped me many times in AIPS and scientific matters. He was always available to hear my problems and has advised me over various matters.

I am thankful to the Director of NCRA for his support during my long stay in NCRA, Pune and for allowing me to use the GMRT facility. He has also allotted me the ToO observing facility, while my source flared. I am also thankful to the GMRT staff for carrying out my observations smoothly. In particular, I would like to thank the GCC for various helps. I would also like to thank the operators for carrying out my observations and for being helpful and friendly during the observation runs. I also thank the librarian for allowing me to use the NCRA library.

I would like to thank Prof. G. Swarup, Prof. V. K. Kulkarni, and Prof. S. Ananthkrishnan for showing interest and excitement throughout this work and in my progress. We have always had great discussions. I would love to mention my heartfelt thanks to Mrs. Vani Kulkarni, Mrs. Parvati Rao, and Mrs. Sudha Ananthkrishnan for inviting me for delicious meals at their home and having lively discussions. They have been affectionate and kind towards me.

Several people have taken interest in this work and helped me in various ways before I converged into this thesis. Prof. A. R. Rao, Prof. A. Kembhavi, Prof. P. Agarwal, Prof. M. N. Vahia, Prof. Shreekumar, Prof. Bhatt, Prof. Acharya, Prof. D. Bhattacharya, Prof. Gopal-Krishna, and Prof. D. J. Saikia have shown interest in knowing the details of my work and results. And have always encouraged me. I am also thankful to Dr. J. Rodriguez, Dr. D. Green, Dr. G. Pooley, Dr. P. Wita, Dr. J. Paredes, and Dr. S. Corbel, who have gone through my papers and provided valuable comments. And I sincerely thank Dr. J. Malzac, Dr. A. Marcowith, Dr. P. O. Petrucci, Dr. J. Rodriguez and Dr. S. Chaty who have shown interest in knowing the details of my work and results.

I would also like thank the rest of the faculty at NCRA for their various kindness during the past several years. My sincere thanks to Dr. S. Roy for clearing my queries about AIPS and Mr. Sandeep Sirothia for helping me in various aspects. He was always available to solve my queries and has spent considerable time, whenever approached. I thank C. Konar, and A. Hota for various valuable help during my initial days in NCRA. I would like to thank Dr. Sarala, Mrs. U. Konar, Mrs. M. pal, Dr. S. pal, Mrs. A. Hota, Ms. B. Bhattacharya, Mr. J. Roy, Mr. Nirupum, and, Ms. Ekta and all my friends at NCRA for interesting discussions, support and various kinds of help over the years.

Finally I would like to thank my family and loved ones, who has always been a firm support for me. Their help, faith and education has always helped me in my life.

Mamta D. Pandey

PUBLICATIONS

(a) Published Papers:

(1) “GMRT observations of the field of INTEGRAL X-ray sources- I”. M. Pandey, R. K. Manchanda, A. P. Rao, P. Durouchoux, Ishwara-Chandra, 2006, Astronomy & Astrophysics, 446, pp.471-483

(2) “Low frequency radio monitoring of Cygnus X-1
and Cygnus X-3”. M. Pandey, A. P. Rao, G. G. Pooley, P. Durouchoux, R. K. Manchanda, C. H. Ishwara-Chandra, 2006, Astronomy & Astrophysics, 447, pp.525-532

(3) “GMRT observations of the field of INTEGRAL X-ray sources- II”. M. Pandey, A. P. Rao, R. Manchanda, P. Durouchoux, C. H. Ishwara-Chandra, 2006, Astronomy & Astrophysics, inpress

(4) “Low Frequency Radio Observations of GRS 1915+105 with GMRT”. C. H. Ishwara-Chandra, A. P. Rao, M. Pandey, R. Manchanda, P. Durouchoux, 2005, Chinese Journal of Astronomy & Astrophysics, Vol. 5 Supplement, pp. 87-92

(b) Papers submitted for Publication:

(1) “Low frequency radio monitoring of microquasars”. M. Pandey, A. P. Rao, P. Durouchoux, R. K. Manchanda, C. H. Ishwara-Chandra, 2006, Astronomy & Astrophysics, Submitted

(2) “Low frequency monitoring of GRS 1915+105”. M. Pandey, A. P. Rao, G. G. Pooley, C. H. Ishwara-Chandra, R. K. Manchanda, P. Durouchoux, 2006, Astronomy & Astrophysics, Submitted

(c) Papers in Conference Proceedings:

(1) “GMRT Observations of X-Ray Binaries Including New INTEGRAL Sources”.

Proceedings of the International conference on *5th INTEGRAL workshop on The INTEGRAL Universe*, 2004, M. Pandey, P. Durouchoux, R. K. Manchanda, A. P. Rao, C. H. Ishwara-Chandra, G. G. Pooley, SP-552, p-699

(2) “Low frequency Radio observations of Cyg X-1 and Cyg X-3”.
M. Pandey, A. P. Rao, R. K. Manchanda, P. Durouchoux, Ishwara-Chandra, 2006
Proceedings of the COSPAR Colloquium on *Spectra and Timing of Compact X-ray Binaries*, TIFR,

January 17-21, Accepted, in press

(3) “GMRT Observations of the field of INTEGRAL X-ray sources”.
M. Pandey, R. K. Manchanda, P. Durouchoux, A. P. Rao, Ishwara-Chandra, 2006,
Journal of Astronomy & Astrophysics, Submitted.

ABBREVIATION

AGNs: Active Galactic Nucleis
AIPS: Astronomical Image Processing System
ASM: All Sky Monitor
ATCA: Australia Telescope Compact Array
BH: Black Hole
BHC: Black Hole Candidate
COMPTON-GRO :Compton Gamma Ray Observatory
CS : Companion star
DISS: Diffractive Inter Stellar Scintillation
EGRET:Energetic Gamma Ray Experiment Telescope
EVN: European VLBI Network
GLAST: Gamma-ray Large Area space Telecsope
GBI: Green Bank Interferometer
GMRT: Giant Metrewave Radio Telescope
HESS: High Energy Spectroscopic System
HMXBs: High mass X-ray binaries
INTEGRAL: INTErnational Gamma-Ray Astrophysics Laboratory
ISS: Inter Stellar Scintillation
LMXBs: Low mass X-ray binaries
MERLIN: Multi-Element Radio Linked Interferometer Network
QPO: Quasi periodic oscillation
RXTE: Rossi X-ary Timing Explorer
NCRA: National Center for Radio Astrophysics
NRAO: National Radio Astronomy Observatory
NS: Neutron star
NVSS:NRAO VLA Sky Survey
P: Persistent
RFI: Radio Frequency Interference
RISS: Refractive Inter Stellar Scintillation
SSA: Synchrotron self absorption
T: Transient
TIFR: Tata Institute of Fundamental Research
VLA: Very Large Array
VLBA: Very Long Baseline Array
VLBI: Very Long Baseline Interferometry
XRBs: X-ray binaries

Chapter 1

Introduction

In modern astronomy, the mysteries of accretion-ejection phenomenon remains far from solved. A good understanding of accretion-ejection physics will give insight in the behavior of compact objects and to understand intrinsic coupling between accretion process and ejection of jets. This phenomenon can be analyzed by radio/X-ray/gamma-ray studies of X-ray binaries present in our galaxy: a replica of distant quasars. The solar mass black hole systems present in our galaxy accret matter from the nearby companion stars. The accretion process gives rise to 6.4 keV Iron fluorescence K-line broadening in relativistic accretion disc. This allows to study the gravitational effects in most extreme conditions and thus to test the General Relativity theory.

It is crucial to understand the emission mechanism at various wavelengths, at work in these sources (thermal, synchrotron, inverse Compton) and derive the connection between the accretion onto compact objects and the formation of collimated jets. This will lead to the understanding of the nature of relativistic jets that are seen elsewhere in the universe. These systems acts as a local laboratory to study the accretion-ejection effects seen in quasars at a much shorter time scale of the order of a few hours to days. Since they are closer than the Active Galactic Nuclei (AGNs), the very high energy cosmic rays could be detected and prodiced in these systems. Thus to understand the physics of extra-galactic quasars and X-ray binaries it is important to look at both the class of sources and to use the knowledge of one class to understand the other.

1.1 Microquasars

Microquasars are the subset of X-ray binary (XRBs) stellar systems which consists of a normal star and a compact object, which may be a neutron star (NS) or a black hole (BH). The normal star is a main sequence star of O or B type super-giant and generally referred as ‘companion star’ (CS). The compact object has strong magnetic fields, rapid rotation, strong gravity and accrets matter from the companion star, occasionally at super-Eddington rates, and causes the formation of accretion disk and radio emitting jets. They are known as micro-quasars since their morphology is similar to that of distant quasars, which has supermassive black holes at the centers of active galactic nuclei and powerful radio emitting jets.

There are a few differences between Galactic micro-quasars and extra-galactic quasar:

(i) The masses of the compact objects in micro-quasars are a factor of 10^{6-9} smaller than those of quasars. Therefore, the variability time scales of micro-quasars are also shorter by similar amount as compared to quasars.

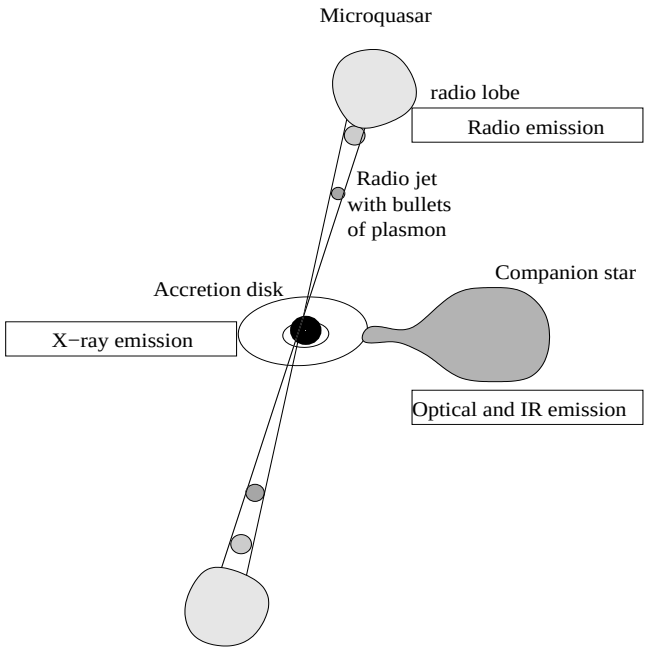

Figure 1.1: Schematic illustration of a micro-quasar showing various components emitting at different wavelengths

(ii) Jets in quasars are seen mostly on one side, whereas in micro-quasars jets are often seen on either side.

(iii) Microquasars provide the circumstance to study the accretion and jet ejection at much shorter time scale as compared to quasars.

The three basic ingredients of micro-quasars are the central compact object, the accretion disk, and relativistic jets (refer fi gure 1.1). The accretion disk predominantly emits in X-rays. In BH X-ray spectrum, the soft thermal component is believed to originate from an optically thick, geometrically thin accretion disc (Shakura & Sunyaev 1973), and the power law component is produced by comptonization of ′seed′ photons in a hot, rarefi ed′corona′ of (quasi-)thermal electrons (Shapiro, Lightman & Eardly 1976; Sunyaev & Titarchk 1980; Haardt & Maraschi 1991; Poutanen & Svensson 1996). The accreted matter from the accretion disk gets heated giving rise to optical emission. The disk also undergoes expansion coincident in phase with the X-ray activity. This cools the disk material giving rise to infrared emission from the system. The existence of corona at the base of the jet has been well established from the evidence of a turnover in the infrared-optical band. The disk matter is occasionally thrown out from the system in the form of radio jets. Microquasars belong to the class of radio emitting X-ray binaries (REXBs) (refer fi g. 1.2).

Radio jets have been commonly observed in some of these systems apparently showing superluminal motions during fl aring stages at high radio frequencies. The jets emits via synchrotron process. The radio light curve shows ′quiescent′ and ′fl aring ′ phases of the source and can be further classifi ed into 3 subclasses, viz Superluminal fl aring stage, plateau stage and mini fl aring stage e.g. GRS 1915+105 (Mirabel et al. 1994). They show rapid day-to-day variable radio fl ux density during fl aring phase. However, in quiescent phase these sources are expected to have nearly constant fl ux. Few micro-quasars, viz. LS 5039, LSI+61303 are known to have gamma-ray counter parts. Based on the observational evidences, models have been proposed for gamma-ray emissions from the radio jets. It

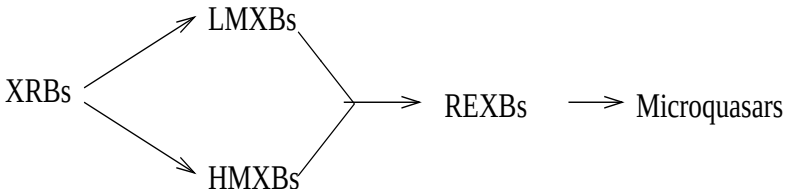

Figure 1.2: X-ray binaries: classification; XRBs: X-ray binaries, LMXB: Low mass X-ray Binaries; HMXB: High mass X-ray binaries; REXBs: Radio emitting X-ray binaries

is proposed that the non-thermal electrons encounter shocks with the ISM and get accelerated giving rise to gamma-ray emissions. More detailed observations are required with highly sensitive gamma-ray instruments to explore this poorly observed and understood part of the micro-quasar spectrum.

1.1.1 List of micro-quasars and their parameters

There are 16 known micro-quasars till date. Table 1.1 lists various information about these sources. The top part of the table lists micro-quasars associated with high mass companion star and the bottom with low mass companion star. Column 1 and 2 gives a list of all the known micro-quasars and the type of the compact object respectively. Column 3 and 4 lists the masses of the compact object and the companion star respectively. Column 5 lists their distance and Column 6 lists their X-ray luminosity. High resolution radio interferometric techniques like VLBI have given direct evidence of the presence of collimated jets and unresolved radio sources. The transient and persistent behavior of the radio jets known from the literature is listed in Column 7. Radio jets have been mapped for most of these sources and references are listed in the Column 8 of the table.

It can be seen from the Table 1.1 that REXBs with high mass companion stars are persistent emitters at radio wavelength and the one with low mass companion star are transient in behavior.

The observed radio emission from micro-quasars is mostly due to synchrotron radiation in the jet. The radio emission from the source's inner regions is obscured by the ionized wind from the companion star (Hjellming and Han 1995).

The refractive index, n, of the medium for radio waves of frequency $\omega = 2\pi\nu$ is

$$n = \sqrt{1 - (\frac{\omega_p}{\omega})^2} = \sqrt{1 - (\frac{\nu_p}{\nu})^2} \tag{1.1}$$

where

$$\omega_p \propto \sqrt{\frac{4\pi N_e e^2}{m_e}} \tag{1.2}$$

ω_p is the plasma frequency, N_e, m_e and e are the density, mass and charge of the electron respectively. Close to the source, N_e is high, therefore n will be imaginary and the radio transmission will be attenuated. Thus any detectable radio transmission will come only from regions far away enough from the source where $\nu_p < \nu$. The minimum distance for which this condition is met lies between 10^{12} and 10^{15} cm (Hjellming 1988). Microquasars with massive companion star eject larger amount of matter covering the distance beyond 10^{12} cm. Thus persistent radio emissions have been detected in micro-quasars with high mass companion star e.g. micro-quasar SS433 (Hjellming and Han 1995).

In the next section a brief description of XRBs and their classification based upon the mass of the companion star is given.

Table 1.1: List of known micro-quasars and their parameters

Source	Type	$M_{compact}$ (M_{sun})	M_{CS} (M_{sun})	Dist (Kpc)	L_{edd} (ergs/sec)	Radio-type $\geq$2GHz
HMXB						
LSI+61303[1]	BHC	2±	-	2	2.5×10^{38}	p
V4641 sgr[2]	BHC	9.6	3.1	10	12×10^{38}	t
LS 5039[3]	BHC	5	-	2.55	4×10^{38}	p
SS433[4,5]	BHC	11±5	19	4.8	13.7×10^{38}	p
Cyg X-1[6]	BHC	10.1	31	2.5	12.6×10^{38}	p
Cyg X-3[7,8]	BHC	17	-	9	21.25×10^{38}	p
LMXB						
XTE J1118+480[9]	BHC	6.9±0.9	0.3	1.9	8.6×10^{38}	t
Cir X-1[10,11]	NSC	1.1±1.4	-	5.5	1.4×10^{38}	p
XTE J1550-564[12]	BHC	9.4	0.9	5.3	11.7×10^{38}	t
Sco X-1[13]	NSC	1.4	-	2.8	1.8×10^{38}	p
GRO J1655-40[14,15]	BHC	7.02	2.4	3.2	8.8×10^{38}	t
GX339-04[16]	BHC	5.8±0.5	-	4	7.3×10^{38}	t
1E1740.7-2942[17,18]	BHC	-	-	8.5	-	p
XTE J1748-288[19]	BHC	$\geq$4.5	-	$\geq$8	5.6×10^{38}	t
GRS 1758-258[20]	BHC	-	-	8.5	-	p
GRS 1915+105[21,22]	BHC	14±4	1.5	12.5	17.5×10^{38}	t

BHC= black hole candidate, p= persistent, t= transient, Massi et al. (2001)[1], Hjellming et al. (2001)[2], Paredes et al. (2000)[3], Margon (1984)[4], Spencer (1984)[5], Stirling et al. (2001)[6], Schalinski et al. (1993)[7], Marti et al. (1998)[8], Mirabel (2000)[9], Stewart et al. (1993)[10], Fender et al. (1998)[11], Hannikainen et al. (2001)[12], Fomalont et al. (2001)[13], Hjellming&Rupen (1995)[14], Tingay et al. (1995)[15], Gallo et al. (2004)[16], Mirabel et al. (1992)[17], Rodriguez&Mirabel (1999)[18], Hjellming et al. (1998)[19], Rodriguez et al. (1993)[20], Mirabel&Rodriguez (1994)[21], Fender et al. (1999)[22]

1.1.2 X-ray binaries: the superset of micro-quasars

In this section XRBs are discussed in brief and differences in the properties based upon the mass of the companion star are mentioned.

XRBs are the superset of Galactic micro-quasars and the brightest X-ray sources in our galaxy. They are stellar systems formed by two stars of non-similar physical properties which rotate around each other. They are conventionally divided into two classes: the low-mass XRBs (LMXB) and the high-mass XRBs (HMXB) (Bradt and McClintock 1983), based on the ratio of X-ray to optical luminosity, L_{opt}

$$\beta = \left(\frac{L_X(2-10keV)}{L_{opt}(3000-7000A^o)}\right) \leq 10 \tag{1.3}$$

For a HMXB, β is less than 10. while for a LMXB, this ratio is greater than 10. This division based on optical and X-ray luminosities coincides with a division based on the mass of the companion star. This is because if the companion star is an early type massive star it will dominate the optical luminosity.

Since the HMXB have more massive companion star they tend to be younger than LMXB. The

HMXB are population I objects and are concentrated in the Galactic plane. LMXB, in contrast, tend to be population II objects and their spatial distribution shows no preference for the Galactic plane, although they tend to be concentrated towards the Galactic center. The HMXB also tend to have stronger magnetic fields than the LMXB, due to better confinement of magnetic field lines in HMXBs. A consequence of the lower average magnetic fields of LMXB is that the accretion disk extends closer to the accreting star where the radiation flow is high. This can photo-ionize and heat the inner accretion disk which can modify the X-ray spectrum.

The mass of the companion star influences significantly the accretion processes in the micro-quasars and the formation of disc. In the next section we discuss a few mechanisms of accretion.

1.2 Accretion of matter and formation of disc in micro-quasars

X-radiations of high luminosity may result due to mass exchange occurring between companion star and compact object. The gravitational potential energy of the in falling matter is converted to kinetic energy resulting in the formation of accretion disc around the compact object. The mass exchange can occur in three different ways:

1.2.1 Types of accretion processes

1- Roche-lobe overflow of the companion star:-
For a micro-quasar with a low mass companion star, the mass transfer can lead to large fluxes of X-rays only through Roche-lobe overflow. The location between the two stars in a binary system, where the gravitational pull from the compact star is equal and opposite to that of the companion star, is called as Roche-lobe. Ideally in a close binary system, (i.e. small orbital radius), this point lies near the surface of the normal star. In these systems, this point acts as a "funnel point" for significant mass to flow out towards the compact star for accretion. In the case of Roche-lobe overflow, the angular momentum of the accreting material forms a differentially rotating disk. The material in this accretion disk is slowly spiraled around the compact object due to its intense gravitational pull. It heats up to temperatures over 1,000,000 degrees and, therefore, shines brightly in X-rays.

2- Enhanced stellar wind from the companion star:-
Microquasars with massive companion star emit stellar wind driven by its own radiation pressure. This wind orbits around the NS or BH by forming an accretion disk. The compact object captures a fraction of the wind and converts the potential energy of the accreted plasma into X-rays.

3- Capture of circumstellar material from a Be companion star:-
A Be star is a B star (hot star) which is rotating at a high speed that leads to an instability, the material streams out from the equatorial plane and an expanding atmosphere is formed. This introduces strong emission lines of hydrogen and neutral helium into the stellar spectrum. The capture and accretion of this material by the compact star is known to be the source of many of the observed transient micro-quasars. These micro-quasars are known to throw off large amounts of matter from their equatorial regions at apparently random intervals. The X-ray characteristics in this system is characterized by the accretion rate of the binary system. Intense X-ray emission is released from the inner region of the accretion disk where it falls onto the compact star. This process is explained briefly in section 1.2.2.

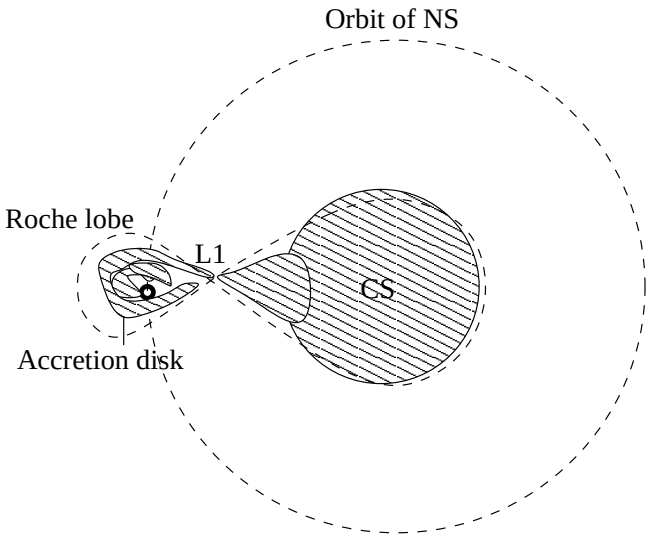

Figure 1.3: Accretion of matter by the compact object from the companion star is shown via Roche-lobe overflow. The compact object is marked with bolder circle

1.2.2 Accretion disk properties

A micro-quasar is in orbital motion around the common center of gravity, and the matter leaving the companion star has an angular momentum (J), which leads to a spiraling of the matter around the compact object. The stream of matter orbits around the compact object with a radius determined by J and the mass of the compact object (M_X). Different layers of matter spiraling in the accretion disk will have different velocities and temperature gradients depending upon their distance from the compact object. Viscosity effects within the accretion disk may redistribute the angular momentum, i.e. some of the material will pick up the angular momentum and spiral out-wards, whereas other material will spiral in-wards. This leads to formation of an accretion disk (Longair 1994). The matter will drift in-wards until it reaches the last stable orbit, called 'inner radius' of the accretion disk (R_{in}), which for a non rotating black hole is approximately three times the Schwarzschild radius. The Schwarzschild radius is the radius at which the escape velocity of the matter equals the speed of light (r_s):

$$r_s = \frac{2GM_X}{C^2} \tag{1.4}$$

$$R_{in} = 3r_s = 9\frac{M_X}{M_{sun}} \qquad (km) \tag{1.5}$$

Viscosity results in to transport of angular momentum and dissipation of heat due to frictional force within the accretion disk. The amount of friction depends upon the orbital speed of the gas around the compact object. At the inner disk, the temperature (T_{in}) reaches maximum upto (Longair 1994),

$$T_{in} = 2 \times 10^7 (\frac{M_X}{M_{sun}})^{-1/4} \qquad ({}^0K) \tag{1.6}$$

Thus for a binary of 1 solar mass, the matter around the last stable orbit is heated upto tens of million degrees, therefore emitting predominantly in the X-ray band.

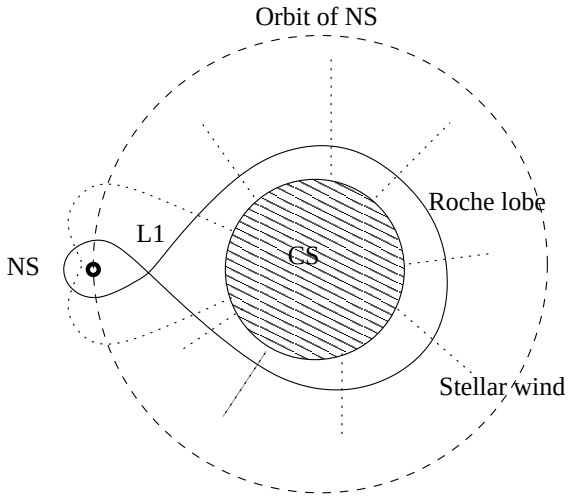

Figure 1.4: The matter from the wind of the companion star is accreted by the compact object

The accretion luminosity can be written as:

$$L = \eta \dot{m} c^2, \tag{1.7}$$

where η, the efficiency of energy conversion, expresses here how compact an object (with radius R) is: $\eta = 1/2(r_s/R)$ (Longair 1994). η for white dwarf is 0.0001 and for neutron star is 0.1. As a comparison, the release of nuclear fusion energy occur in the conversion of four protons into helium gives $\eta = (4m_p - m_{He})/4m_p = 7 \times 10^{-3}$. Thus, accretion in neutron stars already is an order of magnitude more efficient as an energy source as compared with nuclear energy generation (Longair 1994).

However, there is a limit in energy release by accretion. If the force generated by radiation pressure exceeds then gravitational force of the compact object, then accretion of gas ceases. The expression for that luminosity limit referred as, the Eddington luminosity, is (Longair 1994),

$$L_E = 1.3 \times 10^{38} (\frac{M_X}{M_{sun}}) \qquad ergs^{-1} \tag{1.8}$$

It can be seen from Table 1.1 that all the micro-quasars are very luminous X-ray sources.

1.3 Ejection of matter and formation of Jets

The perturbation in the accretion disk of micro-quasars results into removal of matter from the system in the form of radio jets. Radio observations with high spatial resolution during the past decade have shown that a small number of micro-quasar jets display blobs which move with an apparent velocity larger than the velocity of light (superluminal motion) away from the core of the X-ray source. The lifetimes of these blobs as radio emitters is short (a few days to weeks) as compared to their repeated time scale of ejection. The generally accepted notion is that two-sided jets are emitted by these X-ray sources.

1.3.1 Physical properties of Jets

Radio emission from the jets of micro-quasars are due to non-thermal processes and have high brightness temperature and polarization. This non-thermal continuum radiation arises in the jet from the optically thin medium due to synchrotron emission from the relativistic electrons spiraling in a magnetic field. Because of synchrotron losses, the most energetic electrons lose energy fastest leading to faster decay of higher frequency radio emission, which leads to modification of the radio spectral index, particularly at the high frequency region. Determining the detailed shape of the relativistic electron distribution within the jet medium is important because it allows one to acquire critical information concerning the physical conditions of the source emitting regions. In particular, if simple assumptions are satisfied, it is potentially possible to use the synchrotron spectrum to estimate the brightness temperature, age, size and magnetic field in the emitting region within the jet medium. The next section describes the theory on which the synchrotron mechanism is based.

1.3.2 Synchrotron radiation from a single energy particle

Consider an electron having a velocity V and moving in a magnetic field of induction B. The electron will experience a force from the magnetic field $(F = eV \times B/c)$ experiencing an acceleration $\dot{V}$;

$$\dot{V} = \frac{e}{mc}\sqrt{1-\frac{V^2}{c^2}}V \times B \tag{1.9}$$

The electron describes a circular radius of r,

$$\frac{V^2}{r} = \frac{eV \times B}{mc}\sqrt{1-\frac{V^2}{c^2}} = \frac{ec}{E}V \times B \tag{1.10}$$

$$rBsin\theta = \frac{mcV}{e\sqrt{1-\frac{V^2}{c^2}}} \tag{1.11}$$

where, E = total energy of the particle, r is the radius and m is its rest mass. Since $\dot{V}$ is normal to V, the magnitude of velocity does not change. From this equation and the right hand rule for particles in a magnetic field we see that the particles are confined to helical paths along the field lines. The radius of this helical path around the field line is inversely proportional to the strength of the field B. The stronger the field the smaller the radius (Moffet et. al. 1962). Also notice that the radius of the helical path is proportional to the mass. If the electron were non-relativistic ($V << c$), it would radiate like a dipole rotating at the electron cyclotron frequency;

$$\nu_m = \frac{V}{2\pi r} \tag{1.12}$$

$$\nu_m = \frac{eBsin\theta}{2\pi mc} = \frac{eB_\perp}{2\pi mc} \tag{1.13}$$

where $B_\perp = Bsin\theta$ is the component of the magnetic field perpendicular to the electron's path. The angle θ is the angle between V and B. The gyration frequency for a relativistic electron will be reduced because of the increased effective mass of the particle:

$$\nu_g = \frac{eB_\perp\sqrt{1-\frac{V^2}{c^2}}}{2\pi mc} = \nu_m\sqrt{1-\frac{V^2}{c^2}} \tag{1.14}$$

If the electron is highly relativistic, the transformation from its rest system to the system of the observer will compress the forward lobe of the dipole radiation pattern into a small cone with its axis along V and with a half-angle ζ of the order;

$$\zeta = \sqrt{1 - \frac{V^2}{c^2}} = \frac{m_0 c^2}{E} = mc^2 \tag{1.15}$$

For a very distant observer the motion of the electron in a direction parallel to B will not effect the angle between B and the line of sight toward the electron. The observer remains on the cone swept out by V, and he detects a succession of synchrotron pulses repeating at the Doppler-shifted gyration frequency;

$$\nu_g' = \frac{\nu_g}{1 - \frac{Vcos^2\theta}{c}} = \frac{\nu_g}{sin^2\theta} \tag{1.16}$$

Here $Vcos\theta$ is the electron's velocity of translation parallel to B and $Vcos^2\theta$ is the component of that velocity in the direction of the observer. Since the electron is highly relativistic, $V/c = 1$ and $1 - \frac{Vcos^2\theta}{c} = sin^2\theta$.

The width of each synchrotron pulse seen by the observer is approximately equal to the time required for the electron to move through an angle 2ζ about B, as seen by the observer at the moment when the electron is moving towards him. To the observer the electron's angular velocity about B does not appear to be constant. On the average it has the value $\dot{V}/V = 2\pi\nu_g$, but as the electron approaches the observer this rate is "blue shifted" by a factor $1/(1-V/c) = (1+V/c)/(1-V^2/c^2) = 2/(1-V^2/c^2)$. Thus the pulse width appears to be;

$$\delta t = \frac{2\zeta}{\dot{V}/V}\frac{1}{2}(1 - \frac{V^2}{c^2}) = \frac{\zeta(1 - \frac{V^2}{c^2})}{2\pi\nu_g} = \frac{(1 - \frac{V^2}{c^2})^{3/2}}{2\pi\nu_g} \tag{1.17}$$

Because the pulses recur with frequency ν_g', the frequency spectrum of the radiation is a series of spikes at all harmonics of ν_g'. Most of the energy will be radiated in those harmonics which yield frequencies of the order of $(2\pi\delta t)^{-1}$, i.e., at frequencies;

$$\frac{1}{2\pi\delta t} = \frac{\nu_g}{(1 - \frac{V^2}{c^2})^{3/2}} = \nu_g' sin^2\theta(\frac{E}{mc^2}^3) = \frac{\nu_m}{1 - \frac{V^2}{c^2}} = \nu_m(\frac{E}{mc^2})^2 \tag{1.18}$$

The order of these harmonics is proportional to E^3, but $\nu_g' \propto E^{-1}$, the actual value of the frequency of maximum emission is proportional to E^2 (Moffet et. al. 1962). For $E >> mc^2$ the harmonics are so closely spaced that the spectrum is essentially a continuum. The frequency near which the emission is a maximum is called the *critical frequency* for synchrotron emission and is conventionally defined as 3/2 of the above expressions, or

$$\nu_c = \frac{3e}{4\pi mc} B_\perp (\frac{E}{mc^2})^2 = C_1 B_\perp E^2 \tag{1.19}$$

The constant $C_1 = 6.266 \times 10^{18}$ in cgs units or 16.08 from practical units in which ν_c is expressed in MHz, $B_\perp$ in micro gauss, and E in GeV. Thus a 3 GeV electron in a field of 10 micro gauss would radiate most of its energy at frequencies near 1500 MHz.

The power spectrum of the emission from a single electron is calculated by taking the Fourier transform of the electric field in the synchrotron radiation spikes. The field is computed from the Lienard-Wiechert potentials produced by the moving electron. The total power emitted, $p(E,\nu)d\nu$,

by an electron of energy E, in all the directions and polarizations, between frequencies ν and $\nu + d\nu$ is

$$p(E,\nu)d\nu = \frac{3^{1/2}e^3}{mc^2} B_\perp(\nu\ /\nu_c) \int_{\nu\ /\nu_c}^{\infty} K_{5/3}(\eta)d\eta d\nu = 4\pi C_2 B_\perp F(\nu\ /\nu_c)d\nu \tag{1.20}$$

where

$$F(x) = x\int_x^{\infty} K_{5/3}(\eta)d\eta \tag{1.21}$$

The frequency dependence of the spectrum is contained in the function $F(\nu\ /\nu_c)$, which is an integral of the modified Bessel function $K_{5/3}(\eta)$. The constant $C_2 = 1.865 \times 10^{23}$ in cgs units.

The rate at which the electron losses energy is the integral of equation (1.20) over all frequencies;

$$-\frac{dE}{dt} = \int_0^{\infty} p(E,\nu)d\nu = 4\pi C_2 B_\perp \int_0^{\infty} F(\nu\ /\nu_c)d\nu = 4\pi C_2 B_\perp \nu_c \int_0^{\infty} F(x)dx \tag{1.22}$$

The definite integral at the right in equation (1.22) is equal to $8\pi/(9\sqrt{3})$, so

$$-\frac{dE}{dt} = 4\pi C_2 B_\perp \nu_c \frac{8\pi}{9\sqrt{3}} = \frac{32\pi^2}{9\sqrt{3}} C_1 C_2 B_\perp^2 E^2 = C_3 B_\perp^2 E^2 \tag{1.23}$$

where the constant $C_3 = 2.368 \times 10^{-3}$ in cgs units. The solution of the differential equation (1.23) for the electron energy as a function of time is;

$$E(t) = [C_3 B_\perp^2 (t + t_{1/2})]^{-1} = E_0(1 + t/t_{1/2})^{-1} \tag{1.24}$$

where $t_{1/2}$, the time required for the electron to lose half of its initial energy E_0, is;

$$t_{1/2} = \frac{1}{C_3 B_\perp^2 E_0} \tag{1.25}$$

The decay is not exponential, so $t_{1/2}$ is not a 'half-life' in the usual sense. Thus an electron with an initial energy of 3 GeV, trapped in an effective field of 10 micro gauss, will radiate half its energy in a bit less than 3×10^7 yrs. The radiation from a single electron is elliptically polarized.

1.3.3 Emission from an ensemble of particles

The synchrotron radiation which an observer detects from a particular element of volume in a radio source comes from all electrons having the same pitch angle. Thus the spectrum of the emission from that volume element is the integral of the equation (1.20) over the energy distribution of electrons with the appropriate pitch angle. If the *volume emissivity* at frequency ν, in the direction θ (per unit of volume, frequency, and solid angle) is $\varepsilon_\nu(\theta)$ and if $n(E,\theta)$ is the number density of electrons with energy E and pitch angle θ, (per unit of energy and solid angle), then

$$\varepsilon_\nu(\theta) = \int_0^{\infty} n(E,\theta)p(E,\nu)dE \tag{1.26}$$

It is assumed that the angular speed ζ of the emission from a single electron is negligible small (Moffet et. al. 1962). The total number density of electrons with energy E is the integral of $n(E,\theta)$ over all solid angles, $n(E) = \int_0^{\infty} n(E,\theta)d\omega$. If the electrons have an isotropic distribution of pitch angles, then

$n(E,\theta) = n(E)/4\pi$. A further assumption is that the source is stationary, i.e. it is not expanding with relativistic velocities. Let the electron energy distribution in the ensemble be given by power law. Let the number of electrons per unit volume of the source and having energies between E and $E+dE$ be

$$n(E)dE = n_0 E^{-\gamma} dE \tag{1.27}$$

This distribution prevails over a limited energy range $E_1 < E < E_2$, thus the total number density of electrons,

$$n_e = \int_{E_1}^{E_2} n(E)dE \tag{1.28}$$

and the total electron energy density is,

$$u_e = \int_{E_1}^{E_2} n(E)E\,dE \tag{1.29}$$

Combining equations (1.20), (1.28) and (1.29) and assuming an isotropic pitch-angle distribution, the emission at frequency ν and in direction θ per unit volume, frequency, and solid angle is

$$\varepsilon_\nu(\theta) = \int_{E_1}^{E_2} p(E,\nu)n(E,\theta) = \int_{E_1}^{E_2} p(E,\nu)\frac{n(E)}{4\pi}dE = \frac{3^{1/2}e^3}{4\pi mc^2}B_\perp F(\nu/\nu_c)n_0 \int_{E_1}^{E_2} E^{-\gamma}dE \tag{1.30}$$

In this equation ν_c and E must be related through equation (1.19). If a change of variables is made from E to ν/ν_c, above equation becomes,

$$\varepsilon_\nu(\theta) = (\frac{1}{2})\frac{3^{1/2}e^3}{4\pi mc^2}(\frac{3e}{4\pi m^3c^5})^{-(\gamma-1)/2} n_0 B_\perp^{(\gamma+1)/2}\nu^{-(\gamma-1)/2}\int_{\nu/\nu_2}^{\nu/\nu_1} x^{(\gamma-3)/2}F(x)dx \tag{1.31}$$

or

$$\varepsilon_\nu(\theta) = \frac{1}{2}C_2 n_0 B_\perp^{(\gamma+1)/2}(C_1/\nu)^{(\gamma-1)/2}G(\nu/\nu_1,\nu/\nu_2,\gamma) \tag{1.32}$$

where $G(\nu/\nu_1,\nu/\nu_2,\gamma)$ is the definite integral on the right in equation (1.31) and is a function of the electron spectral index and of the distance of the observed frequency ν from the cutoff frequencies ν_1 and ν_2 (the critical frequencies corresponding to energies E_1 and E_1). Thus a power-law electron distribution with exponent $-\gamma$ has given rise to a power-law emission spectrum with exponent $-(\gamma-1)/2$,

$$\varepsilon_\nu(\theta) \propto B_\perp^{(\gamma+1)/2}\nu^{-(\gamma-1)/2} \tag{1.33}$$

where $\alpha = -(\gamma-1)/2$ is the emission spectral index.

The function $G(x_1,x_2,\gamma)$ is a measure of the contributions of the electrons with various critical frequencies to the emission at the particular frequency ν. Thus G reflects the behavior of $F(\nu/\nu_c)$.

The typical non-thermal source will have a spectral index $\alpha = -0.7$, but a blackbody will radiate with $\alpha = 2$.

1.3.4 Modification of the power-law spectrum

A radio source of a randomly oriented magnetic field which contains a power-law distribution of relativistic electrons, $n(E) = n_0 E^{-1/2}$, has a spectrum which is proportional to the emissivity $\varepsilon_\nu(\theta)$, where

$$\varepsilon_\nu(\theta) = \frac{1}{2}C_2 n_0 B_\perp^{(\gamma+1)/2}(C_1/\nu)^{(\gamma-1)/2}G'(\nu/\nu_1,\nu/\nu_2,\gamma) \tag{1.34}$$

provided the source region is optically thin at all frequencies of interest (Moffet et. al. 1962). Furthermore, if the cutoff frequencies are sufficiently far removed from the frequencies of observations, the cutoff function G' will be independent of frequency, and the spectrum will follow a strict power law,

$$\varepsilon_\nu(\theta) \propto \nu^\alpha \tag{1.35}$$

The power law emission spectrum will be modified if the electron energy distribution as well as conditions which affect the radio spectrum directly, are modified.

If there is a sharp low-energy cutoff in the electron spectrum at an energy corresponding to a critical frequency ν_1, then if the observed frequency is below ν_1 the intensity of the radio emission is proportional to $\nu^{1/3}$, independent of γ (Moffet et al. 1962). At the other end of the electron energy spectrum, if there were an abrupt high-energy cutoff, the radio emission would drop exponentially for frequency above the critical frequency corresponding to the cutoff energy reflecting the behavior of $F(\nu/\nu_c)$, which defines the single particle emission spectrum.

The frequency dependence of $\nu^{1/3}(i.e., \alpha = 1/3)$, is the sharpest low frequency cutoff that can be obtained in a pure synchrotron spectrum, unmodified by absorption or other process.

Since a number of radio sources show low frequency spectra which rise more steeply i.e., $\alpha = +2$, some combination of absorption processes must alter the observed intensity distribution. The important absorption processes are; (i) Thermal absorption (TA) and (ii) Synchrotron self absorption (SSA).

These absorption processes can be understood with the aid of some concept of radiation transfer. If I_ν is the specific intensity of radiation $(ergs^{-1}cm^2Hz^{-1}str^{-1})$, the equation of transfer specifies the change in I_ν as the radiation traverses a distance ds within the source.

$$dI_\nu = (\varepsilon_\nu - k_\nu I_\nu)ds \tag{1.36}$$

where, ε_ν = emissivity per unit volume, frequency and solid angle and k_ν = absorption coefficient.

The solution of transfer equation

$$I_\nu(s) = I_\nu(0)e^{-\tau(s,0)} + \int_0^s \varepsilon_\nu e^{-\tau(s,s')}ds' \tag{1.37}$$

where, τ = optical depth and $\tau(s,s') = \int_{s'}^{s} k_\nu ds''$ Consider a homogeneous slab with thickness l, in which ε_ν and k_ν are constant and isotropic refer figure 1.3. The optical depth is then $\tau(s,s') = \int_{s'}^{s} k_\nu ds''$ and for propagation directly through the slab the solution to the transfer equation is,

$$I_\nu(l) = I_\nu(0)e^{-k_\nu l} + \frac{\varepsilon_\nu}{k_\nu}[1 - e^{-k_\nu l}] \tag{1.38}$$

Suppose $I_\nu(0) = 0$ i.e., no radiation enters and
the source is optically thin $(\tau = k_\nu l << 1)$,

$$I_\nu(l) = \varepsilon_\nu l \tag{1.39}$$

If the radiation passes through a purely absorbing layer and emission is negligible small, its intensity is reduced by a factor $e^{-\tau} = e^{-k_\nu l}$.

And if the source is optically thick $(\tau = k_\nu l >> 1)$, then

$$I_\nu(l) = \frac{\varepsilon_\nu}{k_\nu} \tag{1.40}$$

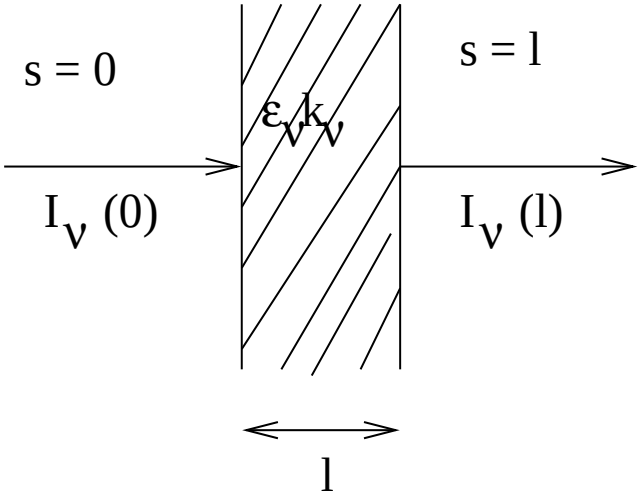

Figure 1.5: Transfer of radiation through a homogeneous slab of material with thickness l and with emissivity ε_ν and absorption coeffi cient k_ν

Thermal absorption: is due to scattering of thermal electrons by the ions in a plasma. In such a scattering, a photon may be emitted or absorbed as the electron is accelerated by the coulomb fi eld of the ion. This mechanism produces the thermal radio emission from HII regions. Thermal absorption signifi cantly modifi es the radiation received from the synchrotron source within or behind the main body of the associated source or from the sources whose radiation must pass through ionized region in our galaxy. The thermal absorption coeffi cient at radio frequencies is given as,

$$k_\nu \propto n^2 T^{-3/2} \nu^{-2.1} \tag{1.41}$$

If ν_T = cutoff frequency at which the optical depth $(\tau = k_\nu l = 1)$and below this the intensity of the source would fall as $e^{-\tau} = e^{-(\nu/\nu_t)^{-2.1}}$ (Moffet et al. 1962)

Thus thermal absorption can produce sharp low frequency cutoff in the spectrum of the radio source. If a large number of thermal electrons are mixed with the relativistic plasma in a synchrotron source, the low-frequency behavior is given by,

$$I_\nu = \frac{\varepsilon_\nu}{k_\nu} = \frac{\nu^{-(\gamma-1)/2}}{\nu^{-2.1}} \tag{1.42}$$

If $\alpha_0 = \frac{-(\gamma-1)}{2}$ = spectral index above ν_t (source is optically thin) then low frequency spectral index, $\alpha = 2.1 + \alpha_0$

Synchrotron self absorption (SSA): is due to re-absorption of the radiation through synchrotron mechanism in a source with a suffi ciently high intensity (of synchrotron radiation). If this takes place, the SSA will drastically modify the spectrum of the source at low frequency.

The absorption at frequency ν is the difference between the upward transitions from states with energies $E - h\nu$ to states with energy E and the stimulated downward transitions between the same states. At given energy E the upward rate of transitions per unit of volume, frequency, and solid angle is $I_\nu(\theta) B_{12} n(E - h\nu, \theta)$ and the downward rate is $I_\nu(\theta) B_{21} n(E, \theta)$. The Einstein coeffi cients B_{12} and

B_{21} depend on the direction of motion of the electrons. Let θ be the pitch angle between the direction of propagation of electrons with respect to the magnetic field.

Each transition adds or subtracts one photon of energy $h\nu$ from the pencil of radiation $I_\nu(\theta)$. The absorption coefficient k_ν is the integral of the transition rates over all energies, divided by the intensity, or

$$k_\nu(\theta) = -\frac{1}{I_\nu(\theta)}\frac{dI_\nu(\theta)}{ds} = h\nu\int_0^\infty [B_{12}n(E-h\nu,\theta) - B_{21}n(E,\theta)]dE \tag{1.43}$$

The Einstein coefficients are related as:

$$w(E)B_{21} = w(E-h\nu)B_{12}, \qquad A_{21}/B_{21} = 2h\nu^3/c^2, \tag{1.44}$$

where the $w(E)$ are the statistical weights and A_{21} is the coefficient for spontaneous emission. The latter may be related to the radiation rate $p(E,\nu)$ for a single electron from equation (1.20) by noting that the volume emissivity is just

$$\varepsilon_\nu(\theta) = h\nu\int_0^\infty A_{21}[n(E,\theta)]dE, \tag{1.45}$$

and identifying this with the previously defined emissivity from equation (1.26),

$$\varepsilon_\nu(\theta) = \int_0^\infty [p(E,\nu)n(E,\theta)]dE, \tag{1.46}$$

Thus $A_{21} = p(E,\nu)/h\nu$. Since $p(E,\nu)$ depends on the pitch angle θ through the factor $B_\perp$, the Einstein coefficients will also depend on pitch angle.

The statistical weight of an electron with energy between E and $E+dE$ is equal to the volume in momentum space which it can occupy. For an electron with momentum P this volume equals $4\pi P^2 dP$; for a relativistic electron $P = E/c$, so the statistical weight is given by

$$w(E)dE = 4\pi E^2 dE/c^3. \tag{1.47}$$

From equation (1.19) we can see that emission takes place only when $h\nu << E$, so approximately $w(E-h\nu) = w(E)(1-2h\nu/E)$. The difference in the electron densities may be approximated in the same way, $n(E-h\nu,\theta) = n(E,\theta) - h\nu(dn/dE) = n(E,\theta)[1-(h\nu/n)(dn/dE)]$. Then, for the first order in $h\nu/E$, the expression for the absorption coefficient becomes,

$$k_\nu(\theta) = \frac{c^2}{2h\nu^3}\int_0^\infty n(E,\theta)[\frac{2h\nu}{E} - \frac{h\nu}{n(E,\theta)}\frac{dn(E,\theta)}{dE}]p(E,\nu)dE \tag{1.48}$$

$$k_\nu(\theta) = -\frac{c^2}{2\nu^2}\int_0^\infty E^2\frac{d}{dE}[\frac{n(E,\theta)}{E^2}]p(E,\nu)dE \tag{1.49}$$

We assuming that the electrons have an isotropic velocity distribution and a power-law spectrum has a limited range of energies $E_1 < E < E_2$. Here we replace $n(E,\theta) = n(E)/4\pi$. This reduces the limits of the integrals to E_1 and E_2. Thus $n(E) = n_0E^{-\gamma}, d[n(E)/E^2]/dE = -(\gamma+2)n_0E^{-(\gamma+3)}$, and the absorption coefficient then becomes

$$k_\nu(\theta) = \frac{c^2}{8\pi\nu^2}(\gamma+2)n_0\int_{E_1}^{E_2} E^{-(\gamma+1)}p(E,\nu)dE \tag{1.50}$$

The equation (1.50) is similar to that for synchrotron emission from a similar ensemble of electrons, equation (1.30), except that the exponent of E in the integrand is reduced by one, and factor $(\gamma+$

$2)c^2/2\nu^2$ is added. Thus making similar changes in variables, we obtain the absorption coefficient in terms of the cutoff frequencies ν_1 and ν_2 as (refer Moffet et al. 1962)

$$k_\nu(\theta) = \frac{c^2}{2}\frac{3^{1/2}e^3}{4\pi mc^2}(\frac{3e}{4\pi m^3c^5})^{\gamma/2}(\gamma+2)n_0B_\perp^{(\gamma+2)/2}\nu^{-(\gamma+4)/2}(\gamma+2)\int_{\nu/\nu_1}^{\nu/\nu_2}x^{(\gamma-2)/2}F(x)dx \qquad (1.51)$$

Above equation is similar to (1.31) evaluated with $(\gamma+1)$ in place of γ. Thus it is equal to the function $G(\nu/\nu_1,\nu/\nu_2,\gamma+1)$. Using this function, we get

$$k_\nu(\theta) = \frac{c^2}{2}C_2C_1^{\gamma/2}n_0B_\perp^{(\gamma+2)/2}\nu^{-(\gamma+4)/2}G(\nu/\nu_1,\nu/\nu_2,\gamma+1) \qquad (1.52)$$

Equation (1.52) refers to radiation traveling in direction θ with respect to a homogeneous magnetic field B. If the magnetic field is tangled in a random way, the mean absorption is obtained by multiplying by a geometrical factor. Using function $G'(\nu/\nu_1,\nu/\nu_2,\gamma+1)$ in the expression for mean absorption coefficient,

$$k_\nu = \frac{c^2}{2}C_2C_1^{\gamma/2}n_0B_\perp^{(\gamma+2)/2}\nu^{-(\gamma+4)/2}G'(\nu/\nu_1,\nu/\nu_2,\gamma+1) \qquad (1.53)$$

The absorption coefficient has frequency dependence of $\nu^{-(\gamma+4)/2}$ while that of the emissivity is $\nu^{-(\gamma-1)/2}$. A source of diameter l will become optically thick at a frequency such that $k_\nu l \geq 1$, and at frequencies below the cutoff the emission of the source will have $\varepsilon_\nu/k_\nu \propto \nu^{5/2}$. Below the cutoff for SSA the spectral index is $\alpha = +2.5$, independent of γ. This differs from the blackbody spectral index of +2 because a power-law distribution was specified instead of a Maxwell-Boltzmann distribution for the electron energies.

SSA conditions occurring may be stated directly in terms of observable properties of a radio source, like, its angular dimensions and flux density at the Earth (Slish et al. 1963 and Williams et al. 1963). From eq. (1.39) we see that at frequencies well above cutoff, the specific intensity I_ν of a source in the form of a homogeneous slab with thickness l is $\varepsilon_\nu l$. The flux density S_ν of the radiation received at the Earth is the product of I_ν times the solid angle subtended by the source,

$$S_\nu = I_\nu\Delta\Omega = \varepsilon_\nu l\Delta\Omega \qquad (1.54)$$

For frequencies well above cutoff, the flux obeys the power-law $S_\nu = S_0(\nu/\nu_0)^\alpha$ where $\alpha = -(\gamma-1)/2$, and ν_0 is some frequency in the region above cutoff.

Defining the cutoff frequency for SSA, ν_s as the frequency for which $k_\nu l = 1$. In the absence of absorption, flux at this frequency would be $S_s^* = S_0(\nu_s/\nu_0)^\alpha$. Than at cutoff frequency, above equation becomes,

$$\varepsilon_\nu/k_\nu = S_s^*/\Delta\Omega \qquad (if \quad \nu = \nu_s) \qquad (1.55)$$

The emissivity and opacity are given in equation (1.34) and (1.53) respectively. Taking ratio we have,

$$\frac{1}{c^2}C_1^{-1/2}B^{-1/2}\nu_s^{5/2}[\frac{G'(\nu_s/\nu_1,\nu_s/\nu_2,\gamma)}{(\gamma+2)G'(\nu_s/\nu_1,\nu_s/\nu_2,\gamma+1)}] = \frac{S_s^*}{\Delta\Omega} \qquad (1.56)$$

or

$$\nu^{5/2} = c^2C_1^{1/2}B^{1/2}S_s^*F'/\Delta\Omega \qquad (1.57)$$

where $1/F'$ is the function in brackets in above equation.

Intensities of many small diameter radio sources decrease at frequencies below a few hundred MHz. This can be attributed to SSA and useful to predict angular diameters of these sources. If

$\Delta\Omega = \theta^2$, where θ is measured in arc seconds, ν_s in MHz, B in gauss and S in flux units of 10^{-26} $Wm^{-2}Hz^{-1}$, we get,

$$\theta^2 = 900 S_s^* F' B^{1/2} \nu_s^{-2.5} \tag{1.58}$$

The observable quantities ν_s and S_s^* determine the value of $\theta/B^{1/4}$ where dependence of θ on the value of B is assumed to be weak.

Thus the cutoff frequency for SSA is that at which the surface brightness temperature of the source becomes comparable to the kinetic temperature of the electrons which emit the radiation. For non-Maxwellian electron energy distributions we define this kinetic temperature as $kT \sim E$. From the Rayleigh-Jeans law, the brightness temperature T_b is,

$$2kT_b\nu^2/c^2 = S_0(\nu/\nu_0)^\alpha/\Delta\Omega \tag{1.59}$$

or

$$kT_b = c^2 S_0(\nu/\nu_0)^\alpha/(2\nu^2\Delta\Omega) \tag{1.60}$$

The relevant electrons are those with critical frequencies equal to cutoff frequency, thus from equation (1.19) E and ν_s can be related as,

$$kT \sim E \sim (\nu_s/C_1B)^{1/2} i \tag{1.61}$$

setting $kT = kT_b$,

$$(\frac{\nu_s}{C_1B})^{1/2} \sim \frac{c^2 S_0(\nu_s/\nu_0)^\alpha}{2\nu_s^2\Delta\Omega} = \frac{c^2 S_s^*}{2\nu_s^2\Delta\Omega} \tag{1.62}$$

which agrees with equation (1.57)

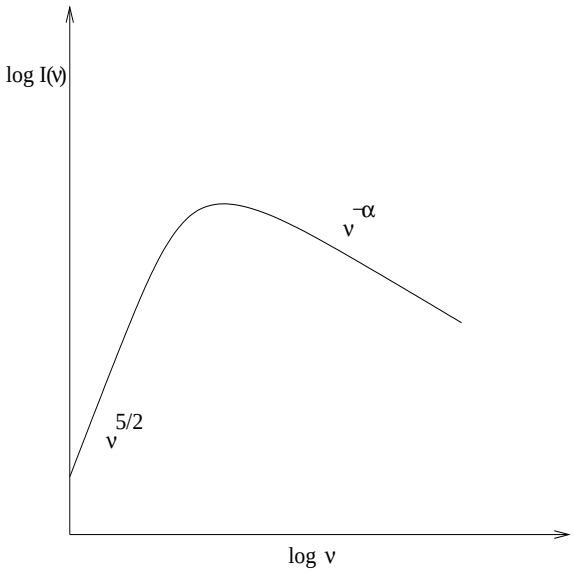

Figure 1.6: The spectrum of a source of synchrotron radiation which exhibits the phenomenon of SSA

The SSA in the source of high brightness and small size θ produces a sharp fall in the flux densities at lower frequencies. For the sources at lower brightness the fall-off occurs at much lower frequencies (refer figure 1.7). This is due to absorption by ionized hydrogen.

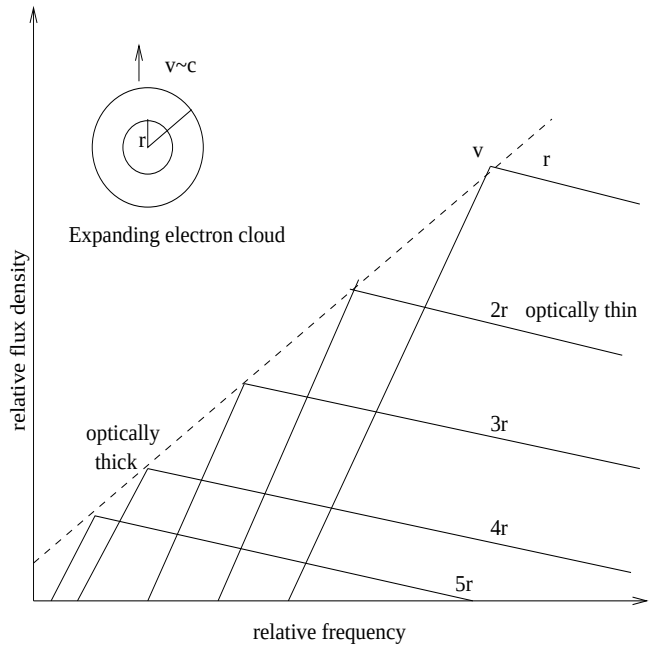

Figure 1.7: The spectrum of a uniformly expanding cloud. With the increase in the radius, the spectrum shifts at lower frequencies and lower flux densities. The cloud which was optically thick initially becomes optically thin at lower frequencies with time

The study of expanding blobs of plasmon suggests that magnetic fi led strength, B, and the energy, E, of the relativistic electrons trapped inside the blobs, will decrease inversely proportional to the square of the radius, r (Shklovsky et al. 1965). This leads to decrease in the observed flux density as

$$S_\nu \propto r^{-2(2\alpha+1)} \tag{1.63}$$

Where, for constant expansion r is substituted by t. The frequency of maximum flux density also depends on r, as

$$\nu_{max} \propto r^{-(4\alpha+5)/(\alpha+2.5)} \tag{1.64}$$

Assuming an expanding electron cloud with initial radius, r_0, it can be seen from above equations that the flux density at a fi xed frequency, ν_0 will increase until the cloud has become optically thin, and then decreases as shown in the fi gure.

1.3.5 Widely accepted model from radio observations

It is important to follow the long term spectral evolution of individual sources in the radio window inorder to construct an unifi ed spectral model that can be used to represent the spectra of all the micro-quasars. The necessary elements of such models have been deduced from a simple appraisal of the observational data from radio interferometers. It is accepted that radio emission from micro-quasars is synchrotron in origin (as discussed in earlier sections) (Hjellming & Han 1995; Mirabel & Rodriguez 1999; Fender 2000). A persistent synchrotron-emitting source should exhibit a two-component spectrum with a spectral index of $+2.5$ below the frequency at which self-absorption becomes signifi cant. The spectral index is α above this frequency. Hjellming & Johnston (1998) present a theoretical model to explain the persistent radio emission from micro-quasars by assuming adiabatic expansion

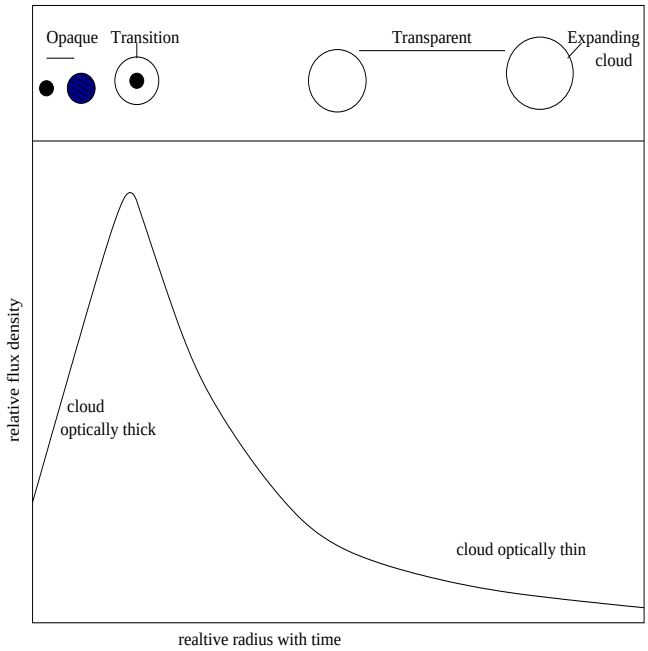

Figure 1.8: The spectrum of a source of synchrotron radiation which exhibits the phenomenon of SSA. It shows the variation in the flux density at a fixed frequency. The bubble is initially optically thick and as it expands it becomes transparent

dominated by lateral expansions. For flaring events they consider spherical bubbles of relativistic plasma expanding under its own higher lateral pressure. The higher frequency emission comes from the inner regions of the compact radiating plasma cloud and the lower frequency emission comes from the outer layers due to the increased optical depth for the inner layers (van der Lann, 1966; Hjellming and Johnston, 1988).

Synchrotron bubble model

Consider a spherical cloud of relativistic electrons with the energy distribution $n(E)dE = n_0 E^{-\gamma} dE$ confined to the range $E_1(t) \leq \mathrm{E} \leq E_2(t)$, and emitting synchrotron radiation. Let r be the radius of the cloud expanding at the rate $\dot{r}$. They radiate as they are accelerated in a magnetic field of strength B. Initially, the cloud is sufficiently thick at all radio frequencies. The condition that the brightness temperature of the radio source cannot exceed the equivalent temperature of the electrons is chiefly responsible for the synchrotron radiation at any given frequency yields, refer equation (1.58), (van der Lann 1966),

$$\theta \propto C S_m^{1/2} \nu_m^{-5/4} B_\perp^{1/4} \tag{1.65}$$

or

$$\nu_m = C B^{1/5} \theta^{-4/5} S_m^{2/5} = C B^{1/5} \theta^{-4/5} \left(S_0 (\nu_s/\nu_0)^{(\gamma-1)/2}\right)^{2/5} \tag{1.66}$$

where ν_m is the frequency at which the spectral curve reaches a maximum, and C is a constant. For synchrotron radiation volume emissivity $\varepsilon_\nu \propto \nu^{-(\gamma-1)/2}$ while the absorption coefficient $k_\nu \propto \nu^{-(\gamma+4)/4}$, and for this reason it follows that the frequency dependence of the spectral curve takes the

form

$$S_\nu \propto \frac{\varepsilon_\nu}{k_\nu}[1-e^{-\tau(\nu)}] \propto \nu^{5/2}[1-e^{-\tau(\nu)}] \tag{1.67}$$

where the optical depth $\tau(\nu) = \int k_\nu dl \propto \nu^{-(\gamma+4)/2}$. For frequencies $\nu << \nu_m$ the flux density is given by

$$S_\nu = k_1 B_\perp^{-1/2} \theta^2 \nu^{5/2} \tag{1.68}$$

while at $\nu >> \nu_m$

$$S_\nu = k_2 n B_\perp^{(\gamma+1)/2} \theta^3 \nu^{-(\gamma-1)/2} \tag{1.69}$$

where k_1 and k_2 are constants. The magnetic flux is conserved

$$B = B_0 (r/r_0)^{-2} \tag{1.70}$$

and the relativistic gas cools adiabatically, so that for an individual particle

$$E = E_0 (r/r_0)^{-1} \tag{1.71}$$

while the angular diameter, of course, varies as

$$\theta = \theta_0 (r/r_0) \tag{1.72}$$

In this model, particles neither enter nor escape the reservoir after the initiating event, so that

$$\frac{d}{dt} r^3(t) n_0 \int_{E_1 t}^{E_2 t} E^{-\gamma} dE = 0 \tag{1.73}$$

Thus it follows that, for $\nu << \nu_m$

$$S(\nu, r/r_0) = S_0(\nu)(r/r_0)^3 \tag{1.74}$$

and for $\nu >> \nu_m$

$$S(\nu, r/r_0) = S_0(\nu)(r/r_0)^{-2\gamma} \tag{1.75}$$

where r/r_0 is the relative radius of the source. Thus,

$$\nu_m(r/r_0) = \nu_{m0}(r/r_0)^{-(4\gamma+6)/(\gamma+4)} \tag{1.76}$$

From equations above, the variation of the maximum flux density follows:

$$S_m(r/r_0) = S_{m0}(r/r_0)^{-(7\gamma+3)/(\gamma+4)} \tag{1.77}$$

The evolution of the spectrum thus seems to be very simple. The spectral curve, $logS(\nu)$-$log\nu$ plane, does not change, but moves down and towards the left i.e. to lower frequencies and lower flux densities. Thus observing such a source at one frequency will show the maximum flux density to increase rapidly at first, reach a maximum and then decrease more gently. Simultaneous observations at a lower frequency will show the same fractional rate of increase, but the maximum will be reached later and have smaller value. Thus,

$$\dot{\nu}_m/\nu_m = -(\frac{(4\gamma+6)}{(\gamma+4)})\dot{r}/r; \qquad \dot{S}_m/S_m = -(\frac{(7\gamma+3)}{(\gamma+4)})\dot{r}/r \tag{1.78}$$

and for $\nu << \nu_m$, $\dot{S}_m/S_m = 3\dot{r}/r = 3/t$; and for $\nu >> \nu_m$, $\dot{S}_m/S_m = -2\gamma\dot{r}/r = -2\gamma/t$.
Thus to calculate $(S(\nu, r/r_0))$, the flux density at a given frequency one can use expression (1.78),

(1.87), and (1.88). Or,
under the optically thick conditions,

$$\frac{S_p}{S_s} = (\frac{r_p}{r_s})^3 = t^3 \tag{1.79}$$

and under the optically thin conditions,

$$\frac{S_c}{S_p} = (\frac{r_c}{r_p})^{-2p} = t^{-2p} \tag{1.80}$$

Here S_s, S_p and S_c are the observed flux densities at the start, peak and end of the flare and r_s, r_p and r_c are the corresponding radii of the bubble.

1.3.6 Modifications of the electron spectrum

The spectrum of a radio source will also be modified due to the change in the electron distribution from a power-law dependence on energy. A change of $\Delta\gamma$ in the electron spectral index will be reflected as a change $\Delta\alpha = -\Delta\gamma/2$ in the radio spectral index.

Let the electron distribution in a radio source follow a strict power law initially. After some time t it departs from power-law, since electrons with different energies lose energy at different rates. The principal loss mechanisms are(i) losses by synchrotron emission and by inverse Compton effect, both proportional to E^2, (ii) losses by radiation during collisions with heavy particles in the plasma (bremsstrahlung losses) and losses due to expansion of the source, both of which are proportional to E, and (iii) losses by ionizing atoms or molecules of the plasma, which are independent of energy.

The rate of change of $n(E,t)$, the density of electrons having energy E at time t, is obtained by counting up the gains and the losses in an energy interval dE during a time interval dt. The result is,

$$\frac{\delta n(E,t)}{\delta t} = -\frac{\delta}{\delta E}[\frac{dE}{dt}n(E,t)] + q(E,t), \tag{1.81}$$

where $q(E,t)$ is the rate at which electrons of energy E are supplied to the volume element under consideration.

Thus the rate of energy loss per electron is,

$$-\frac{dE}{dt} = a + bE + cE^2 \tag{1.82}$$

If electrons are continuously being ejected with a power-law spectrum $q(E) = KE^{-\gamma_0}$, an equilibrium energy distribution is eventually reached with,

$$n(E,t) = \frac{K}{\gamma_0 - 1}\frac{E^{-(\gamma_0-1)}}{a + bE + cE^2} \tag{1.83}$$

Over restricted ranges of energy this function may approximate a simple power-law with an index of $-(\gamma_0-1)$, $-\gamma_0$, $-(\gamma_0+1)$, depending on which type of energy loss mechanism predominates.

If the particle injection is not continuous, but it is initially supplied with electrons having a power-law energy distribution of index $-\gamma_0$ and an isotropic velocity distribution. And if synchrotron losses predominate, than the emission spectrum will develop a discontinuity, changing from $\alpha = \alpha_0 = -(\gamma_0-1)/2$ at low frequencies to $\alpha = (4\alpha_0/3-1) = -(2\gamma_0+1)$ at high frequencies. The frequency at which discontinuity appears will decrease with time t as

$$\nu = 3.4 \times 10^8 B^{-3} t^{-2} \tag{1.84}$$

Table 1.2: Slope of a radio spectrum and the loss mechanism

Slope	Distribution of electrons	Spectral index	Loss mechanism
αE	$n(E,t) \propto E^{-(\gamma_0-1)}$	$\alpha_1 = -(\gamma_0-2)/2$	Low frequency (bremsstrahlung + adiabatic expansion)
αE^2	$n(E,t) \propto E^{-\gamma_0}$	$\alpha_1 = -(\gamma_0-1)/2$	Intermediate (synchrotron emission + inverse Compton effect)
α	$n(E,t) \propto E^{-(\gamma_0+1)}$	$\alpha_1 = -\gamma_0/2$	High frequency (loss by ionizing atom or molecule, independent of E)

ref:(1)- Moffet et al. 1962

where B is the magnetic fi eld in the source region (refer Moffet et al. 1962).

A source formed by the injection of mono-energetic electrons into a magnetic fi eld will develop a power-law electron spectrum with index -2 and with a lower energy cutoff which decreases with time according to equation (1.25). The two important loss mechanisms prominent at low frequencies is discussed in detail below.

Compton Loss: In a synchrotron source of extremely high luminosity and small size it is possible for a signifi cant number of collisions to occur between relativistic electrons and radio frequency photons. The interaction is inverse to Compton effect (energetic photons and electrons at rest). Thus the process in radio source is often called as inverse Compton effect. It contributes signifi cantly to energy losses of the electrons and scattered photons may be detected in another part of the spectrum. The expression for rate at which the electron energy decreases due to scattering of photons is

$$-\frac{dE}{dt} \propto u_{ph} E^2 \tag{1.85}$$

where u_{ph} is the photon energy density (refer Moffet et al. 1962). The above equation is analogous to equation (1.23) for the rate of energy loss due to synchrotron radiation.

Expansion Loss: Let a cloud of well-tangled magnetic fi eld, of strength B and containing relativistic electrons, expand isotropically and adiabatically from radius r to $r' = fr$. Then the product Br^2 will be conserved since total magnetic flux is conserved. If the expansion is slow compared to gyration time of the relativistic particles, the magnetic flux enclosed by each particle orbit will be conserved, requiring a change in electron energy $E \propto B^{1/2}$. If the energy spectrum of the electrons is

$$n(E)dEdV = n_0 E^{-\gamma} dE dV, \tag{1.86}$$

then the effect of the expansion on E, dE, and dV will cause n_0 to vary as $r^{-(\gamma+2)}$. Thus,

$$r \sim r' = fr, \qquad B \sim B' = f^{-2}B, \tag{1.87}$$

$$E \sim E' = f^{-1}E, \qquad n_0 \sim n_0' = f^{-(\gamma+2)} n_0 \tag{1.88}$$

If the source is optically thin, the luminosity at constant frequency will change as

$$L_\nu = (4/3)\pi r^3 \varepsilon_\nu \propto r^3 n_0 B^{(\gamma+1)/2} \propto f^3 f^{-(\gamma+2)} f^{-(\gamma+1)}, \tag{1.89}$$

$$L_\nu \sim L_\nu' = f^{-2\gamma} L_\nu \tag{1.90}$$

The decrease of luminosity with size is large; since $\alpha = 0.75$ typically, we have $L_\nu \propto f^{-5}$. For optically thick source of very small size which are observed to vary in intensity and represent an evolutionary sequence in size and intensity with time expands due to adiabatic expansion. In the region where such a source is optically thick it has,

$$L_\nu = 4\pi r^2 B_\nu = 4\pi r^2 \varepsilon_\nu / k_\nu \propto r^2 B^{-1/2} \propto f^3 \tag{1.91}$$

Thus at frequencies above the cutoff due to SSA the luminosity increases at a given frequency as f^3, while at frequencies where the source is optically thin we have $L_\nu \propto f^{-2\gamma}$. The change in cutoff frequency may be calculated by substituting the relation (1.69) and (1.70) and requiring $k_\nu r \sim 1$ at $\nu = \nu_s$.

$$\nu_s \propto f^{-(4\gamma+6)/(\gamma+4)} \tag{1.92}$$

The flux density near the cutoff frequency,

$$S_s^* \propto f^{-(7\gamma+3)/(\gamma+4)} \tag{1.93}$$

the shape of the spectrum remains unchanged; and gets translated to lower intensity and lower frequency.

In this section we have discussed in detail the general emission mechanism at radio wavelength related to all the REXBs of which micro-quasars form a subset. However, each micro-quasar has shown specific properties of its own and there exists a strong correlation in the X-ray state and radio emission of micro-quasars. Next section deals with the interesting observational results seen in these sources.

1.4 Observational properties of Microquasars

In the previous sections we have discussed briefly the theory of micro-quasars. In confirmation of theory of micro-quasars, the properties based on the observations are discussed in this section. Multi wavelength observations of micro-quasars are studied in detail to understand the emission mechanism of these sources at various wavelengths. We discuss further the X-ray states and their correlation with the radio emission. The properties of these sources at multi-wavelengths is also discussed.

1.4.1 X-ray states and the correlation with the radio emission

A radio emitting X-ray binary is called transient, if at least one outburst occurs with a flux variation of more than 2-3 orders of magnitude greater than the normal flux (McClintock & Reimmllard 2003). This outburst may last for several days to months. This is directly related to a variation of the accretion disk. Some micro-quasars are always observed in one state, while some may switch from one to another state. Microquasars exist in 3 basic X-ray states; as defined below

1- High/Soft state: Most of the power emerges at around $\sim$1 keV and a power-law index $\geq$2, in the X-ray spectrum.
(a)- The soft state spectra of these sources is produced by comptonization of soft photons from the cool accretion disk by non-thermal electrons in the corona (Poutanen & Coppi 1998, Gierlinski et al. 1999).
(b)- The X-ray spectrum is a composite of multi color disk black body plus power law tail. In this case an optically thick disk is assumed. The energy generated by viscosity is locally dissipated in

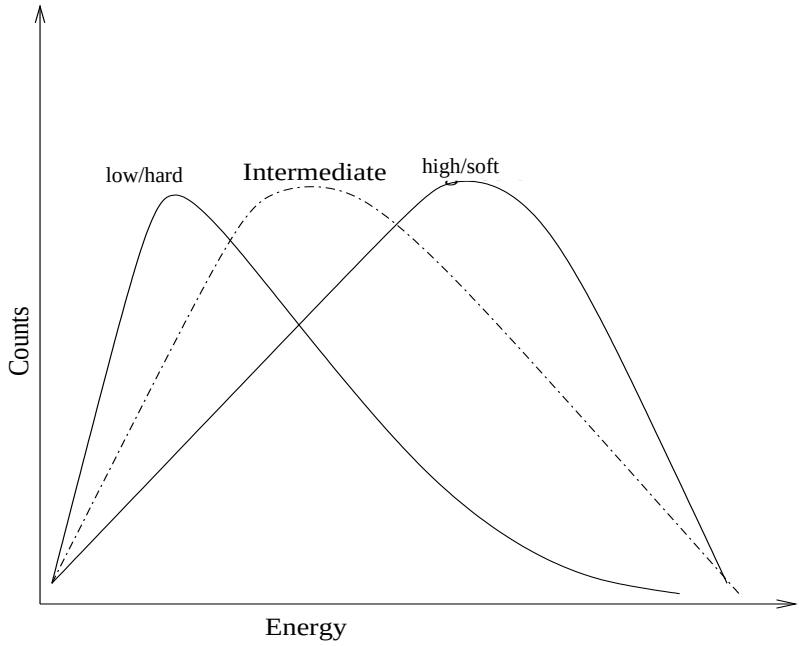

Figure 1.9: X-ray spectrum of a binary star in low/hard, intermediate, and high/soft states. The low/hard state is characterized by hard power-law tail

blackbody radiation. The disk spectrum is a superposition of spectra with temperatures varying from a low value T_{out} at the outer edge to a maximum T_{in} at the inner edge (i.e. at the inner radius R_{in}) of the disk.
The power-law component in the X-ray spectrum is the result of inverse Compton scattering of low-energy disk photons by electrons. These electrons have a power-law or at least a hybrid distribution (consisting of thermal and non-thermal electrons) that can be located in the coronal regions (Zdziarski et al. 2001).
(c)- The radio flux density drops signifi cantly during this state e.g. GX 339−04 (Fender et al. 1999). The outfbw may be physically suppressed during this state via inverse Compton losses. The electrons in the luminous disk scatters the radio photons so rapidly that, the electrons no longer produce synchrotron emission.

2- Intermediate state: Most of the power emerges between $\sim$ 1-100 keV
(a)- The thermal(disk) and non-thermal(power-law) spectral components may be present. Intermediate state is a much rarer state.
(b)- There is no proper radius coverage during this state. However, observations reveal fairly bright and variable radio emission during this state giving rise to transient jets (Kuulkers et al. 1999, Fender & Pooley 1998). It is similar to very high/soft state, but at lower luminosity levels; however, good radio coverage is needed to understand the system in this state.

3- Low/Hard state: Most of the power emerges at around $\sim$100 keV and with power-law photon index $\sim$1.6
(a)- The thermal comptonization is responsible for the hard state spectra of these sources
(b)- The long tail at $\sim$ 1 MeV is produced by non-thermal particles in a tail of otherwise almost

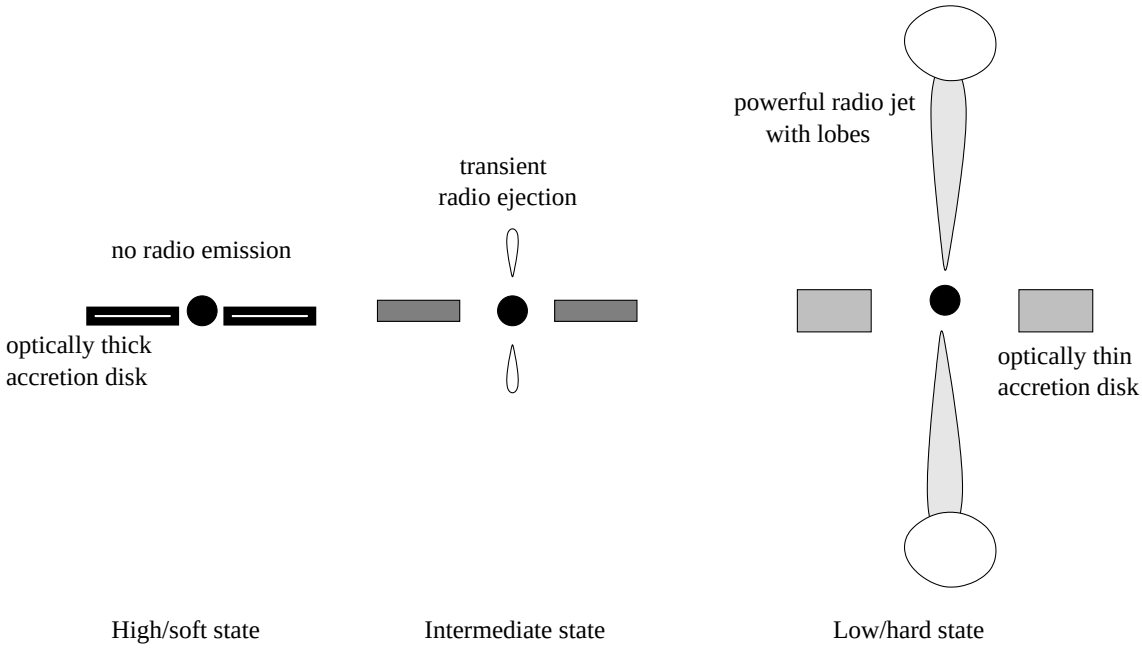

Figure 1.10: Disk-jet connection in a micro-quasar depends upon the X-ray state of the source. In high/soft state no radio jet formation takes place. In intermediate state marginal radio emission is detected. And in low/hard state radio jets moving with apparently superluminal speeds are detected

Maxwellian distribution
(c)- The Compton component arises due to reflection of coronal emission by the accretion disk. It is a signature of the transformation of the thin accretion disk in the vicinity of the black hole into a hot geometrically thick flow emitting hard X-rays e.g. Cyg X-1
(d)- Quasi-periodic oscillations with time-scale of several minutes in X-ray and in IR or radio band are a signature of episodic disk-removal/variation and plasma bubble ejection.

1.4.2 Observed properties of radio jets

Several types of radio jets have been imaged for micro-quasars using radio interferometers (VLA, VLBA, EVN, MERLIN, ATCA etc). Jets can be broadly grouped into:

1- Compact jets: The jet emission which is not at superluminal speed and unresolved at milliarcsecond scale resolution is suggested to be compact in nature. This type of jet displays a flat or inverted radio spectral index ($\alpha \geq 0$, where $S_\nu \propto \nu^{-\alpha}$), as one would expect from optically thick synchrotron emission in a continuous jet flow (Fender 2001). The flat spectrum has been shown to extend upto mm, IR and probably optical wavelengths. The X-ray emission could be interpreted as optically thin synchrotron emission produced at the base of the jet (Gallo, Fender, & Pooley 2003). The presence of compact jets is inferred in micro-quasars where high resolution imaging is not possible due to their variable flux density and position in the sky, e.g. GX339−04. VLBA has resolved compact jet in GRS 1915+105 during so called 'plateau state' (Dhawan, Mirabel, & Rodriguez 2000, Fuchs et al. 2003). In Cyg X−1 the compact jet is present in low/hard X-ray state (Stirling et al. 2001).

2- Discrete ejection: These ejection take place during 'state transitions' in black hole candidates e.g. GRS 1915+105 (Mirabel & Rodriguez 1994, Fender et al. 1999) and GRO J1655−40 (Hjellming & Rupen 1995; Tingay et al. 1995). Here the radio emission rapidly evolves to an optically thin spectrum (negative spectral index α). This can be due to adiabatic expansion of the relativistic electron cloud e.g. Sco X−1 (Fomalont et al. 2001), Cyg X-3 (Mioduszewski et al. 2001, Marti et al. 2000, Marti et al. 2001).

3- Large-scale jets: Parsec-scale radio jets have been imaged for hard X-ray sources, 1E1740.7−2942 and GRS 1758−258 (Mirabel et al. 1992, Marti et al. 2002). Since these sources have been found most of the times in the low/hard state, the large-scale jets are thought to result from the long-term action of steady jets in ISM, e.g. XTE J1550-564 (Corbel et al. 2002).

An interesting case that does not fit in any of the classes mentioned above is that of LS 5039, where a compact radio jet with discrete components has been detected at AU-scales (Paredes et al. 2000). Also the radio spectral index is $\alpha \sim -0.5$, indicative of optically thin emission, in contrast with the flat spectral index detected in the low/hard state of BHC. This suggests that the compact jet is build up in the superposition of subsequent discrete ejection, although this is just a preliminary idea.

1.4.3 Gamma-ray emissions from the radio jets

On the far end of the spectrum, micro-quasars appear as a possible explanation for some of the unidentified sources of high energy gamma−rays detected by the experiment EGRET on board the satellite COMPTON−GRO (Paredes et al. 2005). Microquasars are recent additions in this field of high energy astrophysics. Gamma−ray emissions from these sources are being discussed based upon the presence of gamma−ray emitting counterparts detected within the field of micro-quasars. However, the high energy part of the spectrum is most poorly known, due to the lack of sensitive and high resolution instruments. The synchrotron jet emission traveling at high velocity may encounter relativistic shocks in the Inter Stellar Medium (ISM) giving rise to gamma−ray emissions. It is important to note here that the emission at the end of the jet is mainly dominant at low radio frequencies. The micro-quasars, LS 5039 and LSI+61303 are the best representative of the proposed gamma−rays emissions from this class of sources (Paredes et al. 2005).

No detailed micro-quasar survey at gamma−ray wavelength has been performed in recent past, as these sources are faint emitters at this wavelength. Highly sensitive gamma−ray instruments with low background noise are desired to carry out this survey. The very recent high resolution Cerenkov telescope facility, called High Energy Stereoscopic System (HESS) has detected a compact TeV gamma-rays emitting counterpart for the micro-quasar LS 5039. This result has opened a new window to explore the nature of micro-quasars. We performed a follow up radio observations of the newly discovered gamma-ray emitting sources discovered by the INTEGRAL satellite with the aim to find new micro-quasar candidates and increasing their population. The INTEGRAL gamma-ray satellite was launched in Oct 2002, during the starting of this research and about 60 new class of sources are discovered up todate. Most of these are XRBs. The lifetime of INTEGRAL satellite is upto 2006. However, future satellite missions like the Gamma-ray Large-Area Space Telescope (GLAST) operating in high-energy gamma-ray regime (10 MeV to about 500 GeV) will be launched soon and will solve the puzzle of gamma-ray emissions from the radio jets of micro-quasars. This will be discussed briefly in chapter 5.

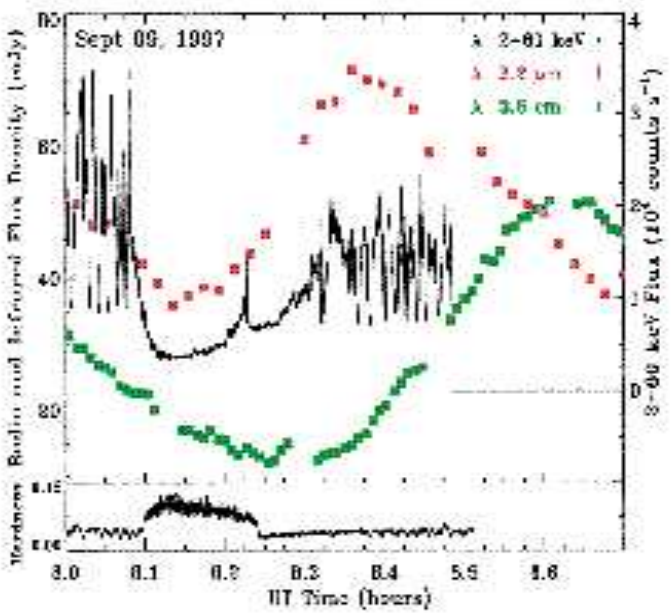

Figure 1.11: GRS 1915+105; within 1/2 h, and X-ray dip, followed by IR and radio peaks is observed revealing the disk jet connection in a micro-quasar. In the bottom panel the X-ray hardness ratio is plotted. (Mirabel et al. 1998, Fig. 3)

1.4.4 Results from multi wavelength observations

We discuss below the spectacular results obtained by multi wavelength observations on two interesting micro-quasars.

GRS 1915+105: is one of the most famous micro-quasar. It has shown various interesting variability trends in the X-ray and the radio light curve (Belloni et al. 2000, Fender et al. 1997, et al. 1998, Eikenberry et al. 1998). Apparent super luminal motions were detected in GRS 1915+105 with relativistic jet velocity of 0.92c (Mirabel et al. 1994). During recent multi wavelength campaign the source was observed 3 times in the plateau state, before and after a major radio and X-ray flare. It showed a strong and steady, optically thick radio emission corresponding to powerful compact jets resolved in the radio images. It also showed a bright near-infrared emission and a strong QPO at 2.5 Hz in the X-rays with a power law dominated spectrum with cutoff in the 3-300 keV range (Fuchs et al. 2004, Fuchs et al. 2003).

SS433: is the brightest micro-quasar at the radio wavelengths ($\sim$ 300 mJy at 13 cm). It is known to have a companion with an orbital period of 13.1 d, a large disc and two highly collimated relativistic jets moving at $\nu \sim 0.26c$. The disc makes an angle of $\sim 78^0$ with the line of sight, while the jet precesses with the axis at an angle of $\sim 19^0$ (Margon 1984) with a periodicity of about 162.15 d. VLBA observations of SS433 at 18 cm in Nov 1998 shows a core and semi-stationary hot spots on either sides. The length of the jet on west side is shorter than the jet on the east side (Mioduszewski et al. 2005). The multi-wavelength observations showed that this source suggest that it exhibits chaotic optical variability on time-scales of as small as 10s (Revnivstev et al. 2004). An evidence

of synchrotron emission in IR was found in the western lobe of SS433 (Fuchs et al. 2001). Many spectral components were detected for SS433, suggesting more observations in the optical and UV spectrometry (Gies et al. 2002). A sharp variation in intensity on time-scales of a few minutes in the X-ray, IR and radio wavelengths were reported by (Chakrabarti et al. 2005). Differential photometry in the IR observations clearly indicates signifi cant intrinsic variations on short time-scales of minutes. A signature of delay of about two days between the IR and radio signals is also reported for these observation. The X-ray spectrum yielded double Fe line profi les which corresponded to red and blue components of the relativistic jet (Chakrabarti et al. 2005).

Thus deeper look in the system shows more complex behavior. The detailed investigations on micro-quasars at multi-wavelength have revealed a rich phenomenology and clear patterns of behavior which has provided insights into the coupling of accretion and outfbw close to relativistic objects.

1.5 Motivation of present work

As can be seen from the above discussions that systematic observations for micro-quasars were carried out at centimeter wavelengths in past and RXTE is carrying out daily monitoring of these sources at X-ray wavelengths since 1996 upto date. However, systematic study of these sources were never carried out at meter wavelengths and the behavior of these sources at low frequencies was unknown. Most of the observations at centimeter wavelengths were performed after triggering alerts of changes in the X-ray states. Various interesting results has come out on micro-quasars at high frequencies (GHz and above). However, these sources were most poorly studied at low radio frequencies (below 1 MHz). Multi-wavelength campaign have been carried out in past to understand the disk-jet connection and various models are proposed in this connection. As discussed above, many theoretical predictions like estimation of turnover frequency at which SSA occurs, the relation between radio emitting region at high and low radio frequencies etc, are yet to be confi rmed observationally. The radio spectra at meter-wavelengths could not be explored due to non availability of sensitive instruments operating at these frequencies.

The motivation of this thesis work is to carry out a systematic study of the observational properties of micro-quasars in low frequency radio domain -an unexplored region so far. Observational signatures available from X-ray and gamma-ray wave-bands are used to arrive at a phenomenological model for the origin of relativistic jets. The main emphasis of this work is to study the radio spectra of micro-quasars at low radio frequencies. This leads to the modeling of the sources geometry and physics of jets in the X-ray sources. From the spectral turnover at radio frequencies we aim to derive important parameters such as size of the emitting region and its magnetic fi eld strength. Also as these sources are counterparts of distant quasars, various large scale phenomenon in quasars will be studied at shorter time scale. Our statistical study of micro-quasars may also reveal different aspects of the diverse phenomenology that each new object of this class has shown and may help in discovering new micro-quasar candidates (based on their variability trends in the radio light curve). Various theoretical and observational features may be understood with our devoted monitoring campaign on the statistical study of micro-quasars. With the motivation of developing a clear understanding of the characteristics of micro-quasars at low frequencies and to unravel the complete morphology and emission processes of these sources, we carried out this statistical monitoring campaign.

The second aim of this thesis work is to carry out radio surveys of newly discovered XRBs from the INTEGRAL gamma-ray satellite. The motivation is to discover new micro-quasar candidates among this new class of XRBs emitting at gamma-ray wavelengths and to increase their population. The information at other wavelengths can be used to confi rm the nature of the new possible micro-

quasar. With the information of the radio counterparts of the gamma-ray sources, the exact position of the source could be determined. And follow up IR and optical observations can be performed based on the radio position. With the systematic monitoring at radio and X-ray wavelengths the variability nature and the disk-jet connection can be confirmed. The information about the radio morphology and precise position of the other sources which do not belong to the micro-quasar category forms one of the by product of this survey. The second interest was the detection of the variable field sources lying outside the position error circle of the INTEGRAL sources.

For this purpose we have selected a list of 16 well known micro-quasars and a list of forty newly discovered X-ray binaries from the gamma-ray satellite called *INTEGRAL*. We have performed an in-depth analysis of various radio observations and used the available data from X-ray and gamma-ray to compliment our results.

The REXBs are highly variable sources at various wavelengths. They show a rich class of diversity in radio and X-ray windows and have added an important understanding in the study of Galactic variable sources. It is important to combine data from various wavelengths since it helps in understanding the conditions in the accretion disk which are required for the production of radio emissions and large scale radio jets. The main observational work was carried out at low frequency radio wavelengths using the state-of-art facility of Giant Metrewave Radio Telescope (GMRT) and the archival monitoring data from the X-ray and gamma-ray satellites was used to interpret the results.

Chapter 2

Observation and data analysis

This chapter describes the observation, reduction and analysis methods used in the studies presented in this thesis. It starts with the explanation of the sample selection of sources based on the results from literature survey. A brief introduction is given to the various radio, X-ray and gamma-ray instruments whose data has been used extensively to meet the objectives of this thesis. Most of the data in this thesis is acquired at very low radio frequencies with the GMRT. In the radio domain, interferometry techniques are used for imaging purpose. It is a synthesized way of imaging where the data is in the Fourier domain of visibilities and the image is a Fourier transform of the visibilities. This research was carried out at very low radio frequencies were 3D imaging techniques become relevant. The imaging procedure and the quality of the acquired data is discussed precisely in this chapter. The radio data at low frequencies is also known to be affected by Inter Stellar Scintillation (ISS). At GMRT frequencies Refractive Inter Stellar Scintillation (RISS) become dominant, hence ISS phenomenon is described briefly at the end of this chapter.

2.1 Sample selection and observing strategy of sources

For this, the sample selection was made with a two-fold aim of exploring the low frequency nature of micro-quasar and increasing the population of micro-quasar by carrying out radio survey of newly discovered XRBs. Accordingly, a list consisting of the known micro-quasar is prepared. These sources have been systematically studied for the first time over a duration of 3 years to explore their behavior at low frequencies. This forms the main aim of this research. The second list consists of sources newly discovered by the gamma-ray satellite INTEGRAL. Follow up observations with GMRT were performed on them to identify new micro-quasar candidates.

2.1.1 Selection of Micro-quasar

The sample selection was made with the plan of studying the long term variability behavior (of the order of a few weeks) and the short term flaring episodes (of the order of a few hours) of micro-quasar. This sample was chosen after detailed literature survey on micro-quasar. The sources which have shown resolved radio jets in VLBI observations are selected. Initially observations were performed with GMRT at 1.28 GHz on a few micro-quasar which had confirmed detection at 1.420 GHz from the NRAO VLA Sky Survey (NVSS). Some more confirmed micro-quasars were added later, (refer Table 1.1 for the sample list). This list consists of sample of all the micro-quasars known during our

observations. All the sources were monitored systematically between 2003 and 2005 at 0.610 and 0.235 GHz.

There are couple of REXBs which may be micro-quasar candidates. While we prepared our sample list, we did not included the sources which do not show confirmed micro-quasar properties as mentioned in chapter 1. It may be possible that a few among these left out sources may be now confirmed micro-quasar. Our sample list contains all the well studied micro-quasar that has shown frequent activities in X-ray and radio windows.

2.1.2 Selection of INTEGRAL sources

A new group of hard X-ray emitting binaries were discovered by the INTEGRAL satellite during last three years. First ever follow up radio observations were performed on these sources with the GMRT at 0.235, 0.61 and 1.28 GHz, in order to provide information of their nature, to look for the possible counter parts and to identify new micro-quasar candidates. A couple of sources could not be observed by GMRT due to position constraints.

2.1.3 Observing strategy

Micro-quasar are highly variable Galactic sources. As seen in chapter 1, they show interesting variability trends at various times scales of the order of a few hours to days. Each micro-quasar was monitored for roughly one hour at several epochs between 2003 – 2005. The observing strategy was planned such that the variability trends at larger time span and the short term flaring episodes could be studied at low radio frequencies. With this scientific plan, the sources in the flaring stage were immediately observed with GMRT at 1.28 GHz and at its unique dual frequency (0.61/0.235 GHz) setting. The flaring sources were observed under Target of Opportunity programme (ToO) for five to six hours continuously during at least one week, in order to get the complete evolution of the radio outburst in time. With simultaneous dual frequency observations, a more complete spectral picture of the source was obtained. The observations were performed only when micro-quasar were in low/hard X-ray state, which initiates radio outbursts (refer chapter 1 for details).

Based on our initial results of a few positive detection at 1.28 GHz, we had planned our monitoring (snapshot) observations at lower frequencies. Four micro-quasar were re-observed for more than 4 hours due to interesting radio light curve properties seen in the initial observing sessions. GRS 1915+105 is the most extensively studied micro-quasar. It was observed for the largest time span of observations under ToO to explore for the first time the low frequency radio behavior of this source during flaring episodes.

Chapter 1 highlights the importance of multi wavelength observations on these sources. Therefore RXTE/ASM archival data was used to interpret the X-ray states of these sources and to derive the radio – X-ray correlation. The near simultaneous radio data with Ryle telescope at 15 GHz was also used to get the information about the high frequency part of the radio spectra of micro-quasar.

In the case of INTEGRAL sources follow up observations were performed with GMRT at 0.61 and 1.280 GHz, immediately after the discovery of new source. In all a total of 40 sources were observed for a duration of 30 min each. Based on the information about radio counter parts, four sources were selected as possible micro-quasar and repeated observations were performed on them to look for their radio variability trends.

2.2 Instruments

This section describes briefly the instruments used to acquire data for this research work. The performance parameters for each instruments are mentioned in the subsections below. GMRT observations at low radio frequencies (MHz) were complemented with the near-simultaneous high frequency (GHz) data with Ryle Telescope. The archival data from Green Bank Interferometer (GBI) was used to study the long term radio light curve of persistent micro-quasar. The information about the X-ray state of the source was obtained from the RXTE/ASM monitoring data. And the information about the newly discovered hard XBs came from the INTEGRAL catalog and Astronomer's Telegrams (ATELS). The RXTE/ASM and INTEGRAL monitoring data are publicly available.

2.2.1 Giant Metrewave Radio Telescope (GMRT)

GMRT is an unique facility for radio astronomical research using the Metrewave lengths range of the radio spectrum. It is built by National Center for Radio Astrophysics (NCRA- TIFR). It is located at a site about 80 km north of Pune, India. GMRT consists of 30 fully steerable gigantic parabolic dishes of 45m diameter each spread over distances of upto 25 km. It is a highly sensitive instrument with

Figure 2.1: Giant Metre-wave Radio Telescope array in India

high angular resolution and has ability to image diffuse radio emission. The dishes are arranged in a 'Y'-shaped confi guration with fourteen dishes located more or less randomly in a compact central array in the region of about 1 sq km. And the remaining sixteen dishes are spread out along the 3 arms with the longest interferometric baseline of about 25 km. The whole array acts like a single gigantic dish of 25 kilometer in diameter. And the multiplication or correlation of radio signals from all the 435 possible pairs of antennas (or interferometers) over several hours enable the formation of radio images of celestial objects. There are six frequency bands of operation centered around 0.050, 1.53, 0.233, 0.325, 0.610 and 1.420 GHz. All these feeds provide dual polarization outputs. In

Table 2.1: Design parameters of GMRT

	Freq. (MHz)				
	151	235	325	610	1420
Primary Beam (Degrees)	3.8	2.5	1.8	0.9	0.4
System Temperature(K)	450	180	100	90	70
Antenna Temperature(K/Jy/Antenna)	0.35	0.3	0.35	0.3	0.25
Synthesized Beam (arcsec)					
whole array	20	13	9	5	2
Central square	420	270	200	100	40
Largest Detectable source (arcmin)	68	44	32	17	7
Sensitivity (rms image noise mJy/ 1 MHz/ 1 min)					
whole array	5.2	3.9	1.2	1.2	1.2
Central square	10.4	7.8	2.4	2.4	2.4
Usable frequency range (MHz)					
Reliable	???	235–240	315–335	590–630	1000–1450
Best rms sensitivity					
while imaging (mJy)	???	1	0.5	0.2	0.05

some configurations, dual-frequency observations (0.61 and 0.235 GHz simultaneous observations) are also possible. The highest angular resolution achievable ranges from about 60 arcsec at the lowest frequencies to about 2 arcsec at 1.4 GHz.

The design is completely indigenous and relatively cheap with light-weight, low-cost dishes. The 'SMART' concept, i.e. Stretch Mesh Attached to Rope Trusses has been used in designing the dishes. Table 2.1 gives the design parameters and performance of the GMRT. It can be seen from the table that GMRT is the best observing facility at International level operating at Metrewave lengths.

The data for research related to this thesis work has been acquired with GMRT at 0.233, 0.61 and 1.28 GHz.

2.2.2 Other facilities

Ryle Telescope: is an 8-element interferometer operating at 15 GHz (2cm wavelength). The elements are equatorially mounted 13 m Cassegrain antennas, on an (almost) E-W baseline. Four aerials are mounted on a 1.2 km rail track, and the others are fixed at 1.2 km intervals. A variety of configuration is available between 18 m and 4.8 km baselines. This facility is best suited for high-resolution imaging, as the mobile aerials are arranged along the track, to give uniform baseline coverage upto 4.8 km. For low-brightness astronomy the mobile aerials are arranged in a 'compact array', with a maximum baseline of about 100 m. All aerial pairs are correlated, so some long baseline data are always available, even in the 'compact array' configuration. The primary beam is 6 arcmin (FWHM) and the synthesized beam is 30 arcsec at 15 GHz. The rms noise is typically 10-12 mJy. For details of data acquisition and telescope performance refer Pooley & Fender (1997).

As the RT is an E-W instrument, most imaging observations involve 12-hour observations in order to fill the synthesized aperture (calibration observations are routinely interleaved). Another

Figure 2.2: Ryle Telescope array at Cambridge

consequence of the geometry is that it is not practical to image sources near the equator, or in the south. The flux monitoring of galactic variable sources is one of the main scientific programs of RT.

The near-simultaneous monitoring data on persistent micro-quasar have been used in this thesis work to interpret the radio spectra of the sources. The longitudes of the GMRT and Ryle Telescope differ by 74 deg (5 hr), so the observations are usually not exactly simultaneous; in the worst cases the nearest 15-GHz observation is separated by 2 days from the GMRT observation. Interesting results about the spectral turn over and inverted spectrum at low frequencies could be derived only with the help of RT data. The near-simultaneous observations have added interesting ingredients into the existing morphology of micro-quasar.

Green Bank Interferometer (GBI): the archival data from the Green Bank radio Interferometer has been used in this thesis to get the information available at centimeter wavelengths. The observation and data reduction was carried out by the GBI team and public data on the radio monitoring (radio light-curves) of micro-quasar is used in this thesis.

The *Green Bank Interferometer* is a 3-element interferometer located in Green Bank, West Virginia, US and is operated by the National radio Astronomy Observatory (NRAO), US. It consists of three radio telescopes of 26m diameter with a baseline of 2400 m. It operates simultaneously at 2 frequencies 2.25 and 8.3 GHz with 35 MHz bandwidth. The resolution is 3 arc seconds fringe at 8.3 GHz and 11 arc seconds at 2.2 GHz. The sensitivity is 6 mJy (2.2 GHz) and 10 mJy (8.3 GHz). *GBI* has monitored almost all the interesting micro-quasar from 1996 onwards. Details of data analysis and monitoring with GBI is presented in Ray et al. (1997). The monitoring was stopped due to lack of funding in Oct, 2000. The flux density between 15 mJy to 20 mJy from this telescope is dominated by noise.

RXTE/ASM: the *Rossi X-ray Timing Explorer (RXTE)* is a satellite for observations of X-radiations

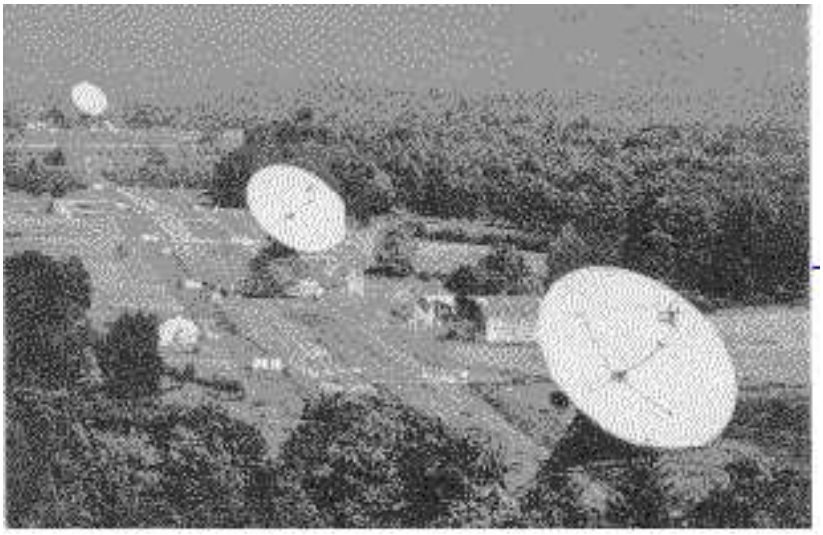

Figure 2.3: Green Bank Interferometer array in United states

Table 2.2: Design parameters and performance of ASM

Energy band	2-10 keV
Energy resolution	$\sim$ 20% in 2-10 keV
Scan time	90 m, 80% of the sky per orbit
Angular resolution	0.2^0
Spatial resolution	$3' \times 15'$
Detectors	3 Scanning shadow cameras
Collecting area	180 cm^2 without masks
Net area	90 cm^2 (3 detectors)
Sensitivity	20 mCrab in 90 m

in 2 – 250 keV range. The most important feature of RXTE is the time resolution in combination with wide-band X-ray spectral capability. It has moderate spectral resolution, to explore the variability of X-ray sources. In this thesis data from the ASM has been used extensively. The table 2.2 lists the design parameters of this instrument. The three instruments on *RXTE* are the Proportional Counter Array (PCA), co-pointed with detectors on the High Energy X-Ray Timing Experiment (HEXTE), and the All-Sky Monitor (ASM). The first two are for pointed observations while the last monitors the X-ray sky, scanning 70% of the sky in each satellite orbit. The details of design and description are given in Levine et al. 1996.

The daily monitoring data was analyzed to obtained the X-ray light curve of micro-quasar before GMRT observations. The X-ray light curve gives information about the X-ray activity of the source. It has been seen from GMRT monitoring data that there exists an anti-correlation in the radio–X-ray light curve. As discussed in chapter 1, when the source is in low/hard X-ray state, radio emissions were detected at low frequencies. Radio emissions were quenched when the source was in high/soft state.

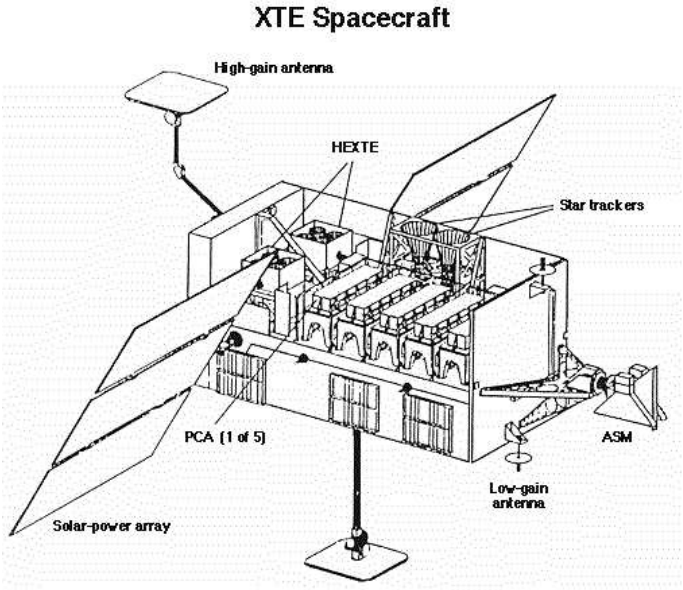

Figure 2.4: RXTE/ASM spacecraft

INTEGRAL: (INTErnational Gamma-Ray Astrophysics Laboratory) is an astronomical satellite for observing the gamma-ray sky. After satellites such as CGRO (Compton Gamma-Ray Observatory) and GRANAT, INTEGRAL represents the next step in gamma-ray sky observation. The INTEGRAL satellite was launched on October 17, 2002 by a Russian PROTON launcher. It is a highly eccentric orbit (blue ellipse) with a revolution period around the Earth (blue disc) of 3 sidereal days. The use of INTEGRAL is planned for 2 years at least, with possible two-year extensions decided every second year. Fig. 2.5 shows the INTEGRAL spacecraft. It consists of four scientific instruments: the spectrometer SPI (foreground cylinder), the imager IBIS (big square in the back), the two X-ray monitors JEM-X (1 & 2) (the two circles between IBIS and SPI), and the optical monitoring camera OMC (small conical tube at the left of JEM-X). INTEGRAL to observes the astronomical source simultaneously in the optical, X-rays and gamma-rays. This facility is first in its kind. Gamma-rays unlike visible light, cannot be deflected with a glass lens or a mirror hence, special method was used to construct this gamma-ray instrument. This method uses a pattern of transparent and opaque elements, the so-called coded mask. The detectors register the shadow of the pattern which is then used to reconstitute the location of the incoming rays. INTEGRAL's instruments for the high-energy range (spectrometer, imager and X-ray monitor) resort to the use of the coded mask technique. The spectrometer SPI (Spectrometer on INTEGRAL) provides spectral analysis of gamma-ray point sources as well as extended sources over an energy range between 20 keV and 8 MeV (electron-volt). The imager IBIS (Imager on Board the INTEGRAL Satellite) has been optimized for fine imaging and precise detection of radiation sources. IBIS achieves an angular resolution of 12 arcmin over an energy range between 15 keV and 10 MeV (electron-volt). This instrument mainly observes compact objects, such as neutron stars and black holes.

It has given a successful performance since its launch. About, 60 new gamma-ray emitting sources were discovered by this satellite since last 3 years. This has added up into the better understanding of the gamma-ray sky.

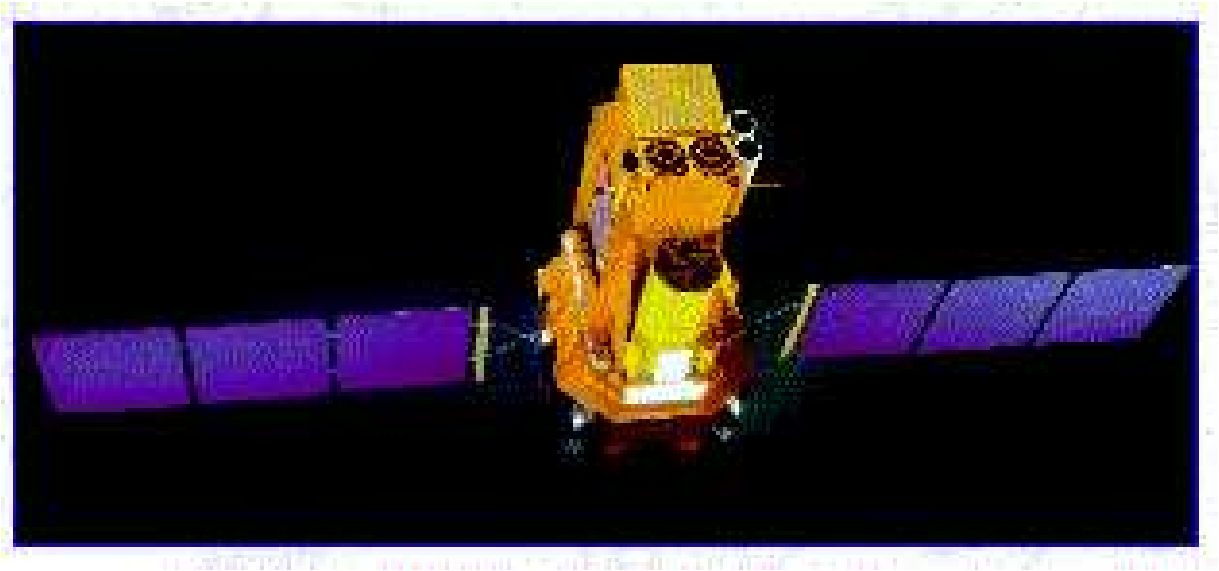

Figure 2.5: INTEGRAL Gamma-ray satellite

Table 2.3: Design parameters and performance of INTEGRAL

Energy band	15 keV - 10 MeV
Field of View	IBIS- 9 X 9, SPI- 16
Area	IBIS- 2600 cm^2 (CdTe array) + 3100 cm^2 (CsI array), SPI- 500 cm^2 (Ge array)
Energy resolution	IBIS- 2 keV (FWHM) at 1 MeV
Angular resolution	IBIS- 12 arcmin in 15 keV - 10 MeV, SPI- 2

2.3 Data acquisition and reduction

The data acquired with GMRT was mainly used in this research. Whereas the archival data and information from other instruments were extensively used to study the multi wavelength nature of micro-quasar. The data from GBI, RXTE/ASM, and GBI are publicly available in standard format on archive. We have downloaded these data and plotted the light curves using standard plotting tools.

In this section we discuss only about data acquisition with radio interferometer like, GMRT. The analysis and imaging techniques are discussed in detail here. At low frequencies various issues that has to be taken into account while imaging are also discussed. The archived data and information obtained by other instruments are discussed at the end of this chapter.

2.3.1 Data acquisition with radio interferometers

Imaging at radio wavelengths require high sensitivity and resolution as the radio signals are weak. Higher sensitivity demands larger collecting area of the antennae. And good resolution is necessary for resolving the nearby sources. The resolution of an antennae is proportional to λ/D, where λ is the wavelength of observation, and D is the diameter of the antennae dish. At lower wavelengths like X-ray and optical, λ is small and the desired resolution can be achieved by relatively small mirrors.

However, at radio wavelengths one needs a big antennae of several tens of kilometers diameter in order to obtain the desired resolution which is clearly infeasible. Thus interferometric techniques are commonly used at these wavelengths. The principle is to use several smaller dishes spread over an area of the hypothetical giant dish in a feasible confi guration. The signals from all the antennas are combined in a constructive interference. Each "small" antenna receives electric signal from the source. The complex multiplication of the two electric signals is called complex visibility from two antennae. the radio intensity of a source is the Fourier transform of the complex visibility from two antennae. A combination of two antennae is called a baseline. Hence for "n" antennae, there will be n(n-) baselines. Complex visibility is a function of U and V, where U is the east-west projection of the baseline in wavelength units and V is the north-south projection of the baselines. One measures the visibilities from the source and the corresponding Fourier transform gives the synthesis map of the fi eld of view.

Visibility of a radio source:

Consider a radio source at a distance R emitting radio waves which reaches us in time t. The time variable electric fi eld vector received by the antenna is $E(R,t)$. An electromagnetic wave will propagate away and eventually arrive at the observer at r (Cornwell & Perley, 1999). Let the electric fi eld at point $P_1'(x_1',y_1',z_1')$ at the source be given by $\varepsilon(P_1')$. The fi eld $E(P_1)$ at the observation point is $P_1(x_1,y_1,z_1)$

$$E(P_1) = \int (\varepsilon(P_1')\frac{e^{-ikD(P_1',P_1)}}{D(P_1',P_1)})d\Omega_1) \tag{2.1}$$

where $D(P_1',P_1)$ = distance between P_1' and P_1. Similarly $E(P_2)$ is the fi led at some other observing point $P_2(x_2,y_2,z_2)$. Then the cross-correlation between these two fi elds,

$$< E(P_1)E^*(P_2) >= \int (\varepsilon(P_1')\varepsilon^*(P_2'))\frac{e^{-ik[D(P_1',P_1)-D(P_2',P_2)]}}{D(P_1',P_1)D(P_2',P_2)}d\Omega_1 d\Omega_2 \tag{2.2}$$

If the emission from the source is spatially incoherent, i.e. $\varepsilon(P_1')\varepsilon^*(P_2') = 0$, when $P_1' = P_2'$ then,

$$< E(P_1)E^*(P_2) >= \int (I(P_1')\frac{e^{-ik[D(P_1',P_1)-D(P_1',P_2)]}}{D(P_1',P_1)D(P_1',P_2)}d\Omega_1 \tag{2.3}$$

where $I(P_1')$= intensity at point (P_1'). The sources is assumed to be lying on a celestial sphere of radius r, thus we have $x_1' = rcos(\theta_x) = R_l$, $y_1' = rcos(\theta_y) = R_m$ and $z_1' = rcos(\theta_z) = R_n$. (l, m, n) are direction cosines in uvw co-ordinate plane and $l^2+m^2+n^2 = 1$. Also $d\Omega = dldmdn/(1-l^2-m^2-n^2)^2$. With the assumption of the sky (2-D) and with $r_1 - r_2 = \lambda(u,v,0)$ we can represent baseline coordinates-uvw in terms of λ as, $u = (x_2-x_1)/\lambda$, $v = (y_2-y_1)/\lambda$, and $w = (z_2-z_1)/\lambda$. A synthesis radio telescope utilizes the earth rotation to improve the UV-coverage. Due to Earth's rotation, a few hours of observations can give good UV-coverage. The spatial coherence function $< E(P_1)E^*(P_2) >$ can thus be written as

$$< E(P_1)E^*(P_2) >= \frac{1}{R^2}\int (I(l,m)e^{-ik[l(x_2-x_1)+m(y_2-y_1)+n(z_2-z_1)]})\frac{dldm}{\sqrt{1-l^2-m^2}} \tag{2.4}$$

Or,

$$< E(P_1)E^*(P_2) >= \frac{1}{R^2}\int (I(l,m)e^{-ik\lambda[lu+mv+nw]})\frac{dldm}{\sqrt{1-l^2-m^2}} \tag{2.5}$$

Thus

$$< E(P_1)E^*(P_2) >= \int (I(l,m)e^{-i2\pi[lu+mv+nw]})\frac{dldm}{\sqrt{1-l^2-m^2}} = V(u,v,w) \tag{2.6}$$

This is the fundamental relationship between the visibility and source brightness distribution in radio interferometry. In general

$$V\nu(u,v,w) = \int (I\nu(l,m)A\nu(l,m)e^{-i2\pi[lu+mv+w(\sqrt{1-l^2-m^2})]}\frac{dldm}{\sqrt{1-l^2-m^2}} \quad (2.7)$$

$V\nu(u,v,w) =< E(P_1)E^*(P_2) >= V\nu(r_1,r_2)$ is the time averaged expectation value of the complex conjugate of the signals $E(P_1)$ and $E(P_2)$. In the case of GMRT it is averaged for 16 seconds. $A\nu(l,m)$ is the far fi led normalized antenna reception pattern (the primary beam). (u, v, w) are the projected co-ordinates of the antennae and I(l, m) is the source brightness distribution (the image). Equation 2.7 is the relation between the spatial coherence function and modifi ed Intensity distribution $I(l,m)/\sqrt{(}1-l^2-m^2)$. Inverse Fourier transform of this visibility leads to the estimation of the intensity of this source.

In the next section the data analysis, imaging and the quality of the data at low radio frequencies are discussed.

2.3.2 Observation and data reduction

At radio wavelengths, the target source is observed interleaved with observations of the calibrators. The flux density scale is set by observing the flux calibrators. This is a standard compact source of known flux density. It is observed during the start and end of the observation run. The slow time variations of complex antenna based gain are corrected using periodic observation of a source of known structure, refereed to as the "secondary calibrator". The secondary calibrator is chosen to lie within 10-15 of the target source so that the phase variation corrections due to antenna based complex gains reflect the phase variations of the target source. These phase variations occurs due to instrumental phase and gain drifts, atmospheric gain and phase variations. It is observed alternately with the target source.

The perform observations with GMRT, one has to submit scientifi c proposals to the GMRT time allotting committee (GTAC) twice in a year. The observation proposals are refereed by the GTAC and the observation time is allotted accordingly for a given observation cycle (A0n). Observation proposals for fi ve continuous cycles, i.e. A03–A07 were submitted to GMRT for observing micro-quasar and INTEGRAL sources. Seventeen observations were performed on all these sources. Also eighteen ToO observations were performed at dual frequencies i.e. 0.61/0.235 GHz simultaneously, during the radio activity of GRS 1915+105 in 2003 and 2004. In all 34 data sets at each frequency, i.e. 0.61 and 0.235 GHz have been analyzed for this research work. Table 2.3 lists the details of our observations.

As seen in the table radio snapshot observations (of duration 40 min) were carried out with the GMRT at 0.235 GHz, 0.61 GHz and 1.280 GHz with a bandwidth of 6/16/32 MHz using the GMRT. The data was acquired at 128 channels with a sampling time of 16 s. For the ToO observations the same strategy was used with repeated scans of 40 m duration over the alloted time scale of the order of a few hours. The visibility data from GMRT was recorded in the lta (long term accumulation) format and analyzed using the Astronomical Image Processing System (AIPS). AIPS is standard interactive software developed by National Radio Astronomy Observatory. The lta data was converted into FITS format (AIPS readable) using GMRT softwares listscan and gvfi ts. The dual frequency data was divided into independent frequencies while using listscan. The non-working antennas during the observation run can be deleted or flagged outside AIPS using ltaflag. The multi-source visibility data is then imported in AIPS using the task 'FITLD' and stored in UVDATA format. The FITS and UVDATA format of the data contains the information about the observation in tables like source table

Table 2.4: Details of observations with GMRT

Cycle	period	hours of observation	frequency (MHz)	no. of observations
A03	Mar 2003	40	610/235 & 1280	3
A04	Jul 2003	40	610/235	3
A05	Apr 2004	39	610/235	3
A06	Aug 2004	40	610/235	4
A07	Jan 2005	34	610/235	3
ToO	Jun 2003 & Jun 2004	50	610/235	18

SU, frequency table FQ, antenna table AN and history table HI. The uv data is indexed by the task 'INDXR' and NX and CL (version 1) tables are created. The CL table is simply used as a template by the AIPS to calibration programme to determine the time resolution for the subsequent CL and antenna gain tables, SN. To reduce the radio data one calibrates the phase calibrator and apply the gains of the phase calibrator to the target source. Next paragraph discusses the reduction procedure in detail.

The flux density of the calibrator is proportional to the amplitude of the visibility function V. AIPS uses the task 'GETJY' to scale the visibilities of the phase calibrator into flux density. The flux density of the standard flux calibrators like 3C48, 3C286, 3C147, etc used for scaling are stored in AIPS and obtained by using task 'SETJY'. This task enters source information into the source (SU) table. While calibrating the calibrators one chooses a reference antenna (among the 30 GMRT antennas) and a reference channel (among the 128 channels). All the antenna baseline visibility data with respect to this channel is plotted to identify and flag the bad or RFI affected scans of the data. Only clean data can give the expected flux and phase corrections needed to calibrate the calibrators. The task 'VPLOT' is run to check the dead antenna and time stamps. The task 'UVFLG' is used to flag these bad data which can cause errors in gain calibration. To plot the visibility amplitudes as a function of $\sqrt{(u^2+v^2)}$ the task 'UVPLT' is used. The data diverging from the expected values are identified and flagged using task 'TVFLG' and 'UVFLG'. These are powerful tasks to identify data with very high or very low visibilities as a function of baselines.

The antenna based complex gains vary slowly over a time scale of a few tens of minutes. The obtain a stable performance of array over several hours of observations, these relative phase variations between the antennas have to be corrected. Linear interpolation corrects well these phase variations over a time scale of 35 m. It is recommended to observe the phase calibrator after every 35-40 min of observation on the target source. The Very Large Array (VLA) Calibrator Manual was used to select the best phase calibrators near the target source. The task 'CALIB' is used to calibrate the antenna based complex gains for the calibrators. This stores the complex gain solutions in SN table. The task 'CLCAL' then applies the complex gain solutions to the calibrators and stores the solutions in the CL table (version 2). One can plot the solutions of SN and CL tables by using task 'SNPLT'. If the data is calibrated well then these solutions look smooth without sudden jumps. Data editing and calibration is an iterative process which is repeated until the data looks sufficiently healthy.

Once the calibrators are calibrated for single channel, the next step is to calculate the channel dependent antenna based complex gains for all the 128 channels of the band of 16 MHz for the GMRT. These antenna based band shape and residual fixed delay errors give rise to antenna based complex gains variations across the passband. These variations in the complex gains have to be corrected in

order to ensure the stability of the system in the observation band. The calibrators with significant flux density having good signal to noise ratio are used for the corrections of channel dependent antenna based complex gains. The average gain per channel is computed. This procedure is known as band-pass calibrations and its is performed by using the task 'BPASS' in AIPS. The linearly interpolated values of the gain per channel obtained using 'BPASS' is applied to the multi-source data by using the task 'SPLAT'. The channels with gain below 0.9 are not considered in this procedure, so that channels with lower gains are rejected. This ensures that the channel dependent complex gains i.e. calibrations are applied to the whole data. This task also collapses all the channels in the band into one channel and thus increases the signal to noise ratio. The data is compressed and easy to handle. In the case of very low frequency observations for example 0.235 GHz, the w-term in equation 2.7 is not negligible and causes band width smearing (explained in detail later). Thus to take into account this effect, the data is collapsed into six channels with each channel corresponding to 8 collapsed channels. The channel collapsed data is then recalibrated as mentioned above to re-ensure that all the gain corrections are RFI free and accurate to calibrate the source. The data is again flagged as some bad data may appear after channel collapsing. The target source is then calibrated with respect to the secondary calibrator to correct for its phase and amplitude. The task 'UVPLT' is used to see the visibility distribution of the source. If the target is a compact source, the visibility plot is constant with respect to baseline. And if the target source is extended then the visibility plot is a delta function with respect to baseline. In case the target source has both the features then the visibility plot is a combination of constant and delta function with respect to baseline. The calibrated target source data is then extracted from the multi source data file using the task 'SPLIT'.

2.3.3 Synthesis Imaging

The visibility pattern of the source is used to construct image. The task 'IMAGR' in AIPS is used to make the image of the source from the 'SPLIT' file. The task works on the principle mentioned in subsection 2.3.1. IMAGR performs the task of Fourier inversion and CLEANing of the visibilities to obtain the brightness distribution. Equation 2.7 shows the 2-D Fourier transform relation between surface brightness and visibility. Since GMRT has finite number of antennas in an aperture synthesis array, the uv-coverage is not continuous. Let for all the measured (u,v) points S(u, v) = 1 and 0 otherwise. Thus the visibilities can be represented as,

$$V(u,v)S(u,v) = \int\int I(l,m)e^{2i\pi(ul+vm)}dldm \tag{2.8}$$

Inverting above equation and using convolution theorem, we get

$$I^D = I * DB \tag{2.9}$$

where DB is the Fourier transform of S. DB is the transfer function of the telescope for imaging and is referred to as the Dirty Beam. I^D is the raw image produced by an earth rotation aperture synthesis telescope like GMRT and is referred to as the Dirty Map. This map is created when the IMAGER is run on the 'SPLIT' file of the target source. After Fourier inversion, the IMAGER task uses the 2D CLEANing algorithm based on Fast Fourier Transform. All the dominant sources in the field are selected for this task. It uses point-source component model and finds and subtracts one component at a time. This method works well for small diameter objects like micro-quasar. A self calibration on the data was performed to correct for phase related errors which can scatter power to the low flux density regions and produce artifact in the image. The self-calibration algorithm averages

the gains of the model provided to the visibility data. It divides the average of visibility data to the average of model. If the ratio is constant or zero for e.g. like a point source then the self-calibration is accurate. The procedure is repeated until reasonable accuracy is achieved. Like CLEAN this task interprets the visibility data in the missing baselines by inserting best fitting assumptions from the source structure supplied as a reference model. The task 'CALIB' is used to compute the new visibility data of the target source by applying the antenna gain corrections to the visibility with respect to the source structure model. These gain corrections can be constrained by controlling the number of input clean components (non-negative), signal to noise ratio and restricting the failed solutions. This phase corrected data is then used to make the new image of the target source. The IMAGR and CALIB procedures are carried it iteratively to obtain the final CLEAN image with the expected rms noise.

For observations at 0.235 GHz a 3-D imaging technique in AIPS is used to correct for wide field imaging errors. A detailed description about the standard imaging technique is given above. In the case of 3-D imaging the w-term corrections are applied. The In the 2-D imaging the source brightness distribution was approximated only to the tangential plane at the phase center in the sky rather than on the surface of the celestial sphere. At very low frequencies like 0.235 GHz, where the antenna primary beams are larger of the order of a few degrees and the radio emission from sources is also on large scale, the 2-D assumption breaks. The term $w\sqrt{(1-l^2-m^2)}$ is often referred to as w-term and arises due to the fact that fringe rotation effectively phases the array for a point source in the sky at the phase center direction. A wave front from the point away from the phase tracking center but on the surface of the sphere will carry an extra phase, not due to geometry of the array but because of its separation from the phase center. Thus the phase of the wavefront measured from a properly phased array carries information about the source structure and the w-term is the extra phase due to the spherical geometry of the problem. Thus in the case of 2-D imaging the sky is approximated by a 2-D plane close to the phase tracking center and the w-term is ignored. This works well for small field of view. Sufficiently far away from the phase center, the w-term must be taken into account. This can be done by approximating the sky as d 2-D plane and shifting the visibility by the w-term. This is equivalent to shifting the phase center and corresponds to a shift of the equivalent point in the image plane. Since the w-term is a function of image co-ordinates this term is different to different parts of the sky. Thus the image is divided into multiple facets where 2-D approximation works well. This corrects for the non-co planarity of baselines. The number of facets required at a given frequency depends upon the relation, $N_{planes} = \lambda B/D^2$ (Cornwell & Perley, 1999), where λ is the wavelength of observation, B is the longest baseline separation (25 Km for GMRT) and D is the antenna diameter (45 m for GMRT). A small part of the sky (corresponding to the size of each facet) centered around each facet is then imaged by shifting the phase center of the visibility to the center of the facet and then performing the normal 2-D inversion and CLEANing. After self calibration the facets are mosaiced to construct the sky using the task 'FLATN'. The CLEAN image was finally used to generate the radio light curve by using the task 'DFTPL'.

The signal measured with GMRT is the ratio of antenna temperature and system temperature. The system temperature increases significantly in the field near Galactic plane at low radio frequencies, i.e 0.610 and 0.235 GHz, hence gain depression corrections or system temperature corrections were applied to the flux densities of the radio sources lying at the galactic plane. The gain depression corrections were measured by putting off the Automatic level Control (ALC) of all the antenna and stabilizing the self power to a lower level, so that the system does not gets saturated at lower frequencies. The self power of each antenna was measured on the flux calibrator- a region far from the Galactic center and on the target source.- a region close the Galactic plane. The ratio of the self powers of the target source and the flux calibrator was calculated and applied to the measured flux

density of the source at 0.235 GHz, to account for the decrease in the gain.

2.3.4 Discussion on the data quality

Micro-quasar are mJy (relatively weaker) strength source at meter-wavelengths. They are mostly crowded in the Galactic plane and mainly towards the Galactic center. It is important to carefully flag (removal of RFI) the data at low frequencies and acquire the desired rms (noise) inorder to detect the faint sources. The observations show that the noise in the Galactic center is relatively higher. Hence, the noise in some of the images of micro-quasar were higher than the expected values listed in the table 2.1. Also the noise was higher at lower frequencies due to increased local Radio Frequency Interference (RFI) and increase in system temperature. The data at 1.280 GHz was the cleanest and many data sets at 0.235 GHz were discarded due to RFI problems. During some observations a few antennas were not in working condition due to technical problems, this has also contributed into the increase in the noise of the image. It can be noted that the noise was smaller during longer observation runs as the signal to noise (S/N) was higher.

During our observations many of the transient sources were not detected, hence for transient sources the upper limit ($3 \times rms$) is considered as the reference radio flux density. The details of our observation on individual sources is listed in chapter 3. It is important to note that, a few transient sources (GRS 1915+105, V4641 Sgr, and GX339-04) were detected by GMRT during radio outbursts before 2003 and detailed results have been published elsewhere (Ishwara-Chandra et al. 2004, Ishwara-Chandra et al. 2005a, Ishwara-Chandra et al. 2005b).

The low frequency radio data is also affected by bandwidth smearing. As seen earlier the visibility data is integrated over the bandwidth $\Delta\nu$ (16 MHz) for better signal to noise ratio. However, the assumption is $\Delta\nu$ is a single frequency ν_0 which is the central frequency of the band. In this case, the u and v co-ordinates and the visibilities are corrected only for ν_0. Bandwidth smearing is directly proportional to $\Delta\nu/\nu_0$. This effect can be reduced if the band is split into many frequency channels with smaller channel widths and later the sub bands are stacked together to increase the sensitivity. The bandwidth smearing is taken care in GMRT by dividing the data in 2 bands, the lower and upper sides band. The data is collected from both the side bands and later added to increase the signal to noise ratio. In this way all the data acquired by GMRT was corrected for bandwidth smearing.

The low frequency radio data acquired at GMRT are also affected by Ionospheric Scintillation and the interpretation of the data is affected by Inter Stellar Scintillation (ISS). Scintillation can cause variations in signal amplitude, phase, angle-of-arrival, and Faraday rotation. The ionospheric scintillation are caused by spatial irregularities in the refractive indices of the ionosphere. The effect decreases with increase in the wave frequency. It is dependent upon the angle between the ray path and the earth's magnetic field which may be more important than elevation-angle dependence. Thus it is most severe in the equatorial region within 20^0 of the magnetic equator, north and south, and in high latitudes, where two regions of peak scintillation activity have been reported i.e. auroral oval and polar cap above 80^0 latitude. Equatorial scintillation are strongest after sunset (near 20 hours Local Time) near equinoxes, i.e., March-April and October-November. The amplitude and phase scintillation results in a reduction in the signal-to-noise ratio and rapid phase changes of the radio signal. This effect is dominant at lower frequencies.

In addition to the ionospheric scintillation, the interpretation of the radio data at low frequencies are also affected by ISS. Due to this an increase in the percentage variability of the radio flux density of the source was seen. The errors due to scintillation in the data interpretation cannot be corrected. Various models to solve the ISS problem are existing. One of the most widely accepted model used to check for the variability in the source flux density due to ISS was developed by Cordes et al. 2004.

I have used this model to calculate the expected variability time scale in the source flux density of micro-quasar. In most of the cases these time scales are long enough so not to affect the source. The ISS phenomenon is discussed in detail in Appendix B.

2.3.5 Data at other wavelengths

We have used radio data on micro-quasars at centimeter wavelengths from GBI and Ryle Telescope at 2.3/8.2 GHz and 15 GHz respectively, to study the nature of these sources at centimeter wavelengths. The observation and data reduction is carried out by GBI and Ryle groups, and we have only used publicly available radio monitoring data (light-curves) on these sources. We do not describe the analysis technique used by these groups. The data relevant to this research was downloaded from 'http://www.gb.nrao.edu/fgdocs/gbi/plgbi/plgbi.html' and radio light curves were plotted using the standard plotting tools. The GBI data at 2.3 and 8.2 GHz is acquired simultaneously, hence information about the radio spectra of these sources could be derived (as discussed in chapter 3). The archival data is available only upto October 2000 as mentioned earlier. Since, there is no overlap in GMRT and GBI data, the GBI data is only used for studying the nature of radio emission from these sources at centimeter wavelengths.

The Ryle telescope is monitoring micro-quasars Cyg X-1, CYg X-3, GRS 1915+105 regularly. This data at 15 GHz is near simultaneous in time with respect to GMRT data. Hence the 15 GHz data is used to study the radio spectra of these source from centimeter to meter wavelengths. The 15 GHz data is also used to look for radio flares at higher frequencies. And the information is used to organize the ToO observations on the flaring sources at lower frequencies with the GMRT.

The ASM monitoring data is analyzed by the MIT instrumentation team into a standard product of light curves in three different energy ranges plus the combined (sum) range is available at 'http://xte.mit.edu'. The energy range are soft (1 – 3 keV), medium (3 – 5 keV) and hard (5 – 12 keV) X-rays regime. This data is also in the public archive. The data relevant to this research was downloaded and X-ray light curves were plotted using the combined range, using standard plotting tools. The hardness ratio used is equivalent to the ratio of counts/sec in hard to counts/sec in medium X-ray regime.

Most of the monitoring data from the INTEGRAL Gamma-ray satellite is regularly published. Although data from this satellite has not been used in this thesis, some preliminary near simultaneous observations have established the prospects of future study of micro-quasar systems (viz., Cyg X-1) with this satellite and GMRT. There was one overlapping observation of GMRT and INTEGRAL on the micro-quasar Cyg X-1. In the next chapter we have discussed about this overlapping observation and we have also discussed the behavior of this source based on the near simultaneous radio/X-ray/Gamma-ray data. The were no other overlapping observations on the remaining micro-quasars with GMRT and INTEGRAL satellite.

Since, its launch, the INTEGRAL Gamma-ray satellite has discovered many new gamma-ray emitting sources. We carried out the first ever low frequency radio survey of these newly discovered gamma-ray sources by the INTEGRAL satellite. X-ray binaries discovered by this satellite were extensively studied and the data from the RXTE/ASM, and other sources (DSS, NVSS, 2MASS) if available, was used to derive the nature of these sources at multi-wavelengths.

We have also used the information about the position, variability and spectra, available from the monitoring data on these new discovered sources by the INTEGRAL satellite, to derive the nature of these sources.

In the next chapters, I will discuss about the results obtained from our study on X-ray sources. In chapter 3, we will discuss about the results of low frequency study performed on sixteen micro-

quasars and in chapter 4, we will discuss about the results of low frequency survey performed on forty gamma-ray sources discovered by the INTEGRAL satellite.

Chapter 3

Low Frequency Radio Monitoring of Micro-quasars

X-ray binaries are known to be strong radio emitters (Hjellming and Han 1995; Fender and Hendry 2000) with variable radio light curves. The non-thermal part of their radio spectra and polarization features suggests that the radio emission is due to synchrotron radiation mechanism. Radio jets have been resolved in many sources using higher resolution radio observations at cm wavelengths. The emission model involves jets of relativistic matter emitting synchrotron radiation in the form of jets. Although these sources have been extensively studied at centimeter wavelengths, their nature at low radio frequencies is the part of present thesis.

We have started a programme to monitor all the known micro-quasars at low radio frequencies using GMRT. Sixteen X-ray binaries and known micro-quasar candidates have been extensively monitored for the first time at low radio frequencies at 0.235, 0.61 and 1.28 GHz, using GMRT between June 2003 to Jan 2005. Nine out of sixteen sources have been detected positively by GMRT which includes all the six HMXBs and three low LMXBs. Radio emission models for prominent sources are discussed in this chapter. The radio luminosity and the equipartition magnetic field from centimeter-(GHz) to meter-wavelength (MHz) is calculated for all the detected sources. The strength of the magnetic field is calculated assuming a equipartition of energy between the magnetic fields and that of relativistic particles. Some XRBs show high variability at low radio frequencies due to Refractive Interstellar Scintillation (RISS). RISS dominates at meter wavelengths which may lead to flux density fluctuations, hence scintillation time scale for each micro-quasar was calculated.

We have plotted the RXTE/ASM X-ray light curve for all the sixteen known micro-quasars. Based on the light-curves, the sources can be classified in to: (a) persistent, (b) quasi-persistent and (c) transient sources. From the analysis of these types and the information about their companion star the persistent or transient nature of the radio jet can be inferred. Characteristic evidence for a relationship between radio and X-ray emission from prominent sources are also discussed in this chapter. This chapter summarizes the main observational results obtained by us and different models for the production of low frequency radio emissions.

3.1 Introduction

The XRB, Sco X-1, containing an accreting NS was the first X-ray source identified as a radio source (Hjellming and Han 1995). With the extensive study of GRS 1915+105, the understanding of radio

emission from XRBs was significantly brought forward. Radio jets have been commonly observed in this system apparently showing superluminal motions during flaring stages at high resolution radio observations. The radio light-curve in the case of GRS 1915+105 shows 'quiescent' and 'flaring' phases of the source and can be further classified into 3 subclasses, viz., superluminal flaring stage, plateau stage and mini flaring stage e.g. GRS 1915+105 (Mirabel et al. 1994). They show variability in timescales ranging from minutes to several days during flaring phase; however, in quiescent phase these sources show nearly constant flux. There exists a good correlation in the X-ray and radio emission from these sources. The flaring state, the quiescent and plateau states show different radio spectral properties. It is important to investigate the basic behavior of X-ray light curve and the radio spectra from centimeter to meter-wavelengths in these sources. Various interesting characteristics of micro-quasars have been studied at high radio frequencies ($\geq$ 2 GHz) (Fender et al. 2000); however, the low frequency characteristics is not yet explored.

We have carried out a systematic low frequency radio monitoring of micro-quasars using the GMRT (Pandey et al. 2004) to explore for the first time the low frequency behavior of these jet sources. The radio observations were carried out at 0.235 GHz, 0.61 GHz and 1.28 GHz with a bandwidth of 6/16/32 MHz using the GMRT. The flux density scale was set by observing the primary calibrator 3C286 and 3C48. Phase calibrators were interleaved with 25 min scans on each micro-quasar. The visibility data recorded from GMRT was converted into FITS file and analyzed using the Astronomical Image Processing System (AIPS) using standard procedures. The data acquisition and analysis procedure is discussed in detail in chapter 2.

As seen in Fig. 3.1 all the micro-quasars are unresolved with GMRT. System temperature correction was applied to the flux densities, as explained in chapter 2. A self calibration on the data was performed to correct for phase related errors and to improve the image quality. Wide-field 3-D imaging technique was used to generate maps at 0.235 GHz.

The following sections present the results of our monitoring on micro-quasars. The goal of these observations were to search for radio flares and continuous emissions from micro-quasars during active X-ray state (low/hard state). In the next section We will describe the nature of radio emission based on the light curve obtained from archival data from GBI. We will also discuss the crude classification scheme for the RXTE/ASM X-ray light curve. Based on the information of the X-ray light curve and the mass of companion star, the nature of the radio emission can be derived. Finally, we will discuss the results of our low frequency observations and we will compare various parameters at centimeter and meter-wavelengths.

3.2 Classification based on light curves of micro-quasars

With a view to summaries the known behavior in the scope of our study and to establish the correlation at X-ray and radio wavelengths on all the sources available in our sample, we have used the archival data from the GBI and the RXTE/ASM X-ray monitoring campaign. In this section we plot the centimeter wavelength radio and X-ray light curve of micro-quasars and derive some interesting characteristics.

3.2.1 Radio properties

To study the nature of micro-quasars at centimeter wavelengths we have compiled and analyzed the available radio data on these sources from various telescopes at high radio frequencies. The Green Bank Interferometer (GBI), West Virginia, operated by NRAO, provides data for a number of X-ray

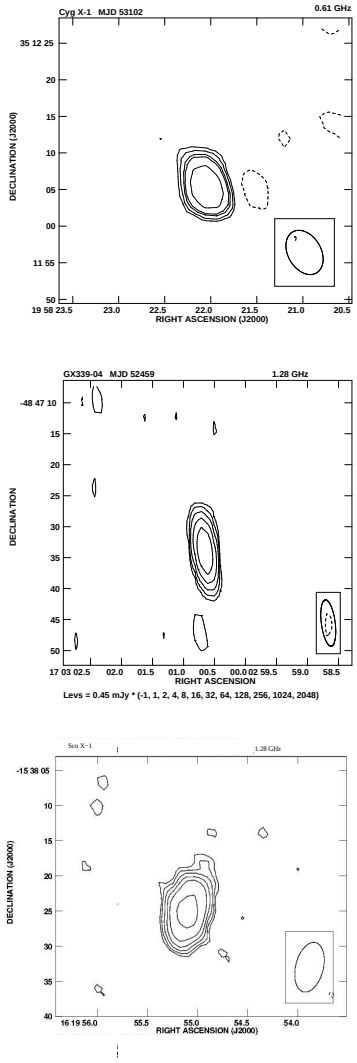

Figure 3.1: Radio image of micro-quasars Cyg X-1, GX339-04 and Sco X-1 observed with GMRT at 0.61 and 1.28 GHz.

sources that were monitored during its several years of operation between 1996 – 2000. The radio light curve at simultaneous dual frequency, viz., 2.2 GHz and 8 GHz were obtained with 10 min averaging time on each source. The typical rms is below 20 mJy and 15 mJy at 2.2 GHz and 8 GHz respectively and the flux density between 20 mJy and 15 mJy is dominated by noise. We have plotted the radio light curve for persistent micro-quasars in Fig. 3.2 and 3.3.

It can be seen from the figures that these persistent sources are highly variable and show frequent flaring activity. Based on such monitoring campaigns these sources are classified as persistent and transient in nature at centimeter wavelengths. This information is listed in table 3.1. The radio data on transient sources are not plotted here as they are not detected on most occasions.

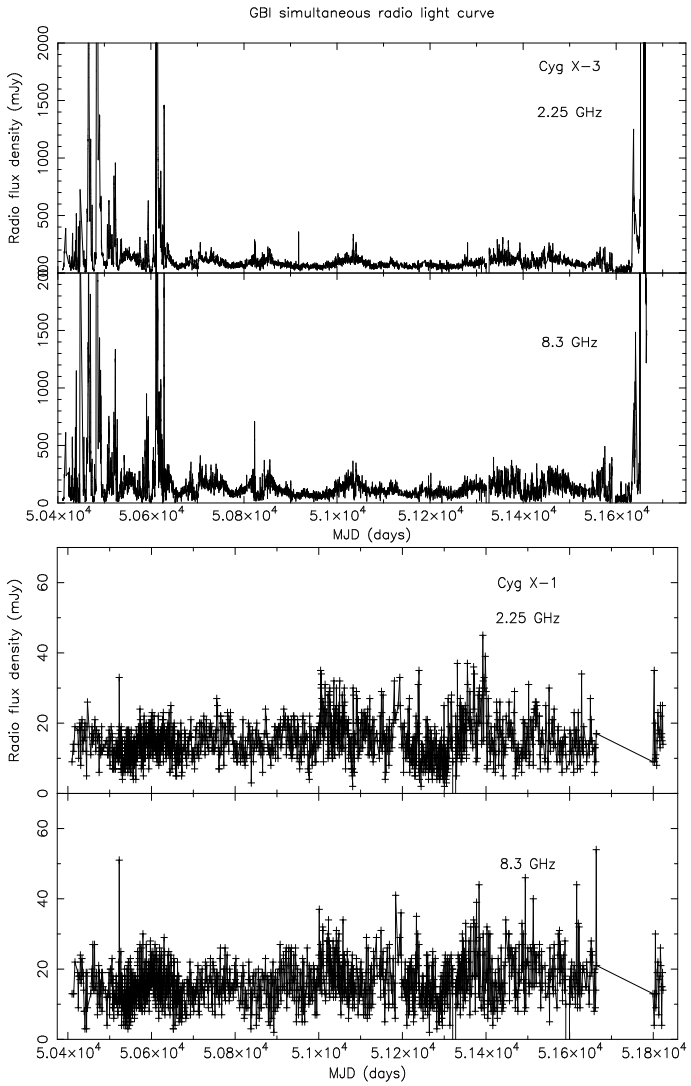

Figure 3.2: GBI radio light-curve at 2.2 and 8.2 GHz for persistent micro-quasars Cyg X-3 and Cyg X-1

3.2.2 X-ray properties

The RXTE All Sky Monitor provides the X-ray light curve for all the micro-quasars in three sub-energy bands (or ″colors″), viz soft, medium and hard. The X-ray light curve for each micro-quasar was generated using the sum band intensity to look for common pattern in these sources. Based on the common trends seen in the data, the X-ray light curve for the micro-quasars can be roughly grouped into 3 types:

- X-ray light curve with no flaring events (A)- persistent
- X-ray light curve with rare flaring events (B)- quasi-persistent
- X-ray light curve with frequent flaring events (C)- transient, as shown in Fig. 3.4 and listed in table 3.1.

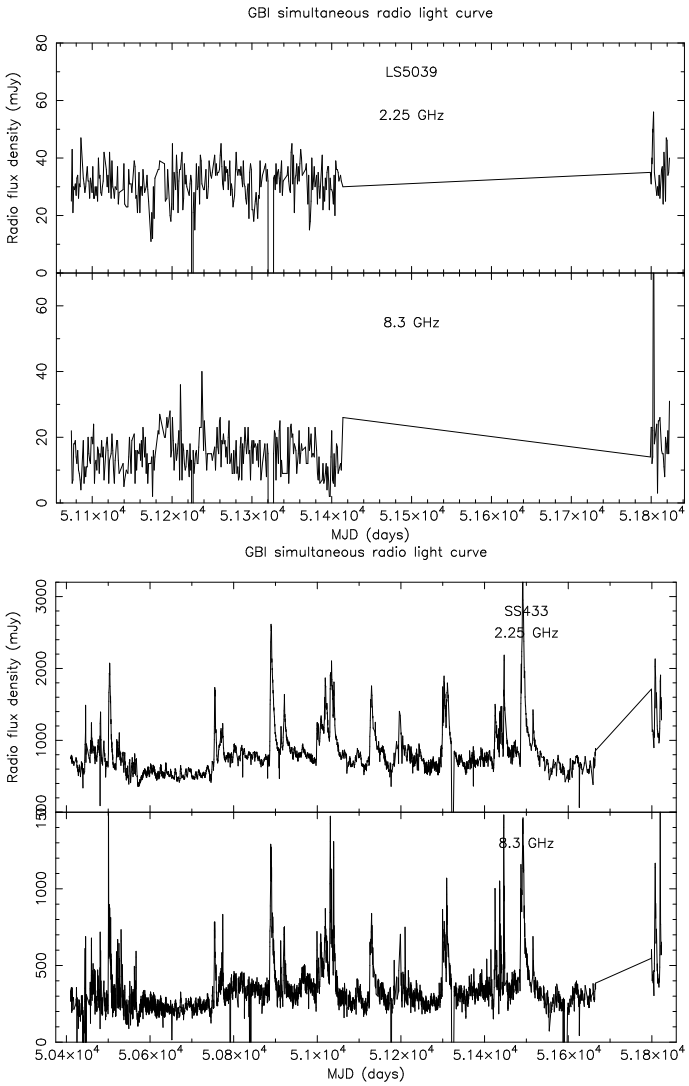

Figure 3.3: GBI radio light-curve at 2.2 and 8.2 GHz for persistent micro-quasars LS 5039 and SS433

This classifi cation of X-ray light curves provide the signatures that suggests whether X-ray binaries are persistent or transient in nature in radio. It can be seen from table 3.1 that the X-ray light curve in the case of HMXBs is mainly type (A) or (C) except for V4641 Sgr which is of type (B). The X-ray light curve in the case of LMXBs is mainly type (B) or (C) except for Cir X-1 and Sco X-1 which are type (A).

Thus, it can be seen from the table 3.1 that, there are in all 6 HMXBs which are persistent in radio. Depending upon their radio emission these sources are further classifi ed as:

- Persistent high mass REXBs that are always detected in radio. Five HMXBs, viz., LSI+61303, LS 5039, SS433, Cyg X-1, and Cyg X-3 are persistent at high frequencies i.e., above 2 GHz and 4 are also persistent at low frequencies i.e. below 2 GHz except Cyg X-1 (Pandey et al. 2005b).

- The high mass X-ray binary V4641 Sgr shows transient behavior at radio wavelengths.

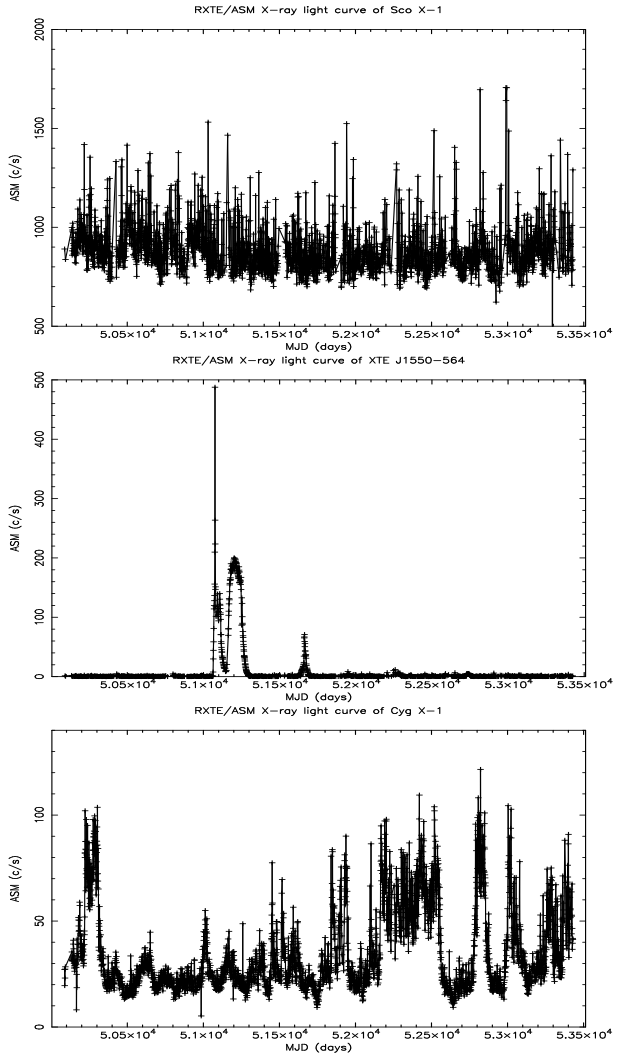

Figure 3.4: Three types of RXTE/ASM X-ray light-curve of Micro-quasars are shown here. *Top* Persistent light-curve (A), *Middle* Quasi persistent light-curve (B) and *Bottom* Transient light-curve (C)

There are in all 10 LMXBs belonging to the category of REXBs. They are further grouped into:

- Persistent low mass REXBs, viz Cir X-1, Sco X-1, GRS J1758−258 and 1E1740.7-2942 at high radio frequencies. At low radio frequencies only Sco X-1 is persistent. GRS J1758−258 and 1E1740.7−2942 were never detected.

- The LMXBs, viz, XTE J1118+480, XTE J1550−564, GRO J1655−40, GX339−04, XTEJ1748−288 and GRS 1915+105 show transient behavior at high radio frequencies. However, at low frequencies only GX339−04 and GRS 1915+105 were detected during radio flares. XTE J1550−564 was not observed with GMRT due to declination constraints. GRO J1655−40, XTE J1118+480, and, XTE J1748−288, which are not frequently detected at high frequencies, were also never detected at low frequencies, as listed in Table 3.1.

	Source	Dist. kpc	Accr. disc type	X-ray type	Radio type $\geq$2GHz	Jet size (AU)
	HMXB					
01.	LSI+61303	2$\pm$	A	-	p	10-700
02.	V4641 Sgr	9.6	B	-	t	-
03.	LS 5039	5	A	-	p	10-10^3
04.	SS433	11$\pm$5	A	t	p	10^4-10
05.	Cyg X-1	10.1	C	-	p	40
06.	Cyg X-3	17	C	t	p	10^4
	LMXB					
07.	XTE J1118+480	6.9$\pm$0.9	B	-	t	$\leq$0.03
08.	Cir X-1	1.1$\pm$1.4	A	p	p	$\geq 10^4$
09.	XTEJ1550	9.4	B	-	t	10^8
10.	Sco X-1	1.4	A	-	p	40
11.	GRO J1655$-$40	7.02	B	t	t	8000
12.	GX339-04	5.8$\pm$0.5	B	-	t	$\leq$4000
13.	1E1740.7$-$2942	8.4	B	p	p	10^5
14.	XTE J1748$-$288	$\geq$4.5	B	t	t	10^4
15.	GRS 1758$-$258	8.4	B	p	p	10^5
16.	GRS 1915+105	14$\pm$4	C	t	t	10-10^4

Table 3.1: Nature of micro-quasars based on light curve

[1]ref:(1)- J. M Paredes et al. 2005, arXiv.astro-ph/0409226, Chinese journal of A&A, (2)- J. Greiner et al. 2000, arXiv.astro-ph/9912326, (3)- http://www.johnstonsarchive.net/relativity/bhctable.html, ND= Not detected, NO= Not observed, p= persistent, t= transient

Source	MJD	Freq (MHz)	Detection	S_ν (mJy)	RMS (mJy b$^-$1)
XTE J1118+480	52459	1280	No	<0.33	0.11
	52694	610/235	No	<2.55/<5	0.85/1.6
	52699	610/235	No	<2.25/<4.77	0.75/1.59
	52702	610/235	No	<1.95/<6.60	0.65/2.20
	52855	1280	No	<0.54	0.18
	52898	610/235	No	<3.54/<6.99	1.18/2.33
	53220	610/235	No	<3.78/<6.06	1.26/2.02
	53377	610/235	No	<3.51/<9.12	1.17/3.04
	53391	610/235	No	<3.99/<8.34	1.33/2.78
GRO J1655-40	52459	1280	No	<0.36	0.12
	52694	610/235	No	<2.04/6.03	0.68/2.01
	52699	610/235	No	<1.68/<5.67	0.56/1.89
	52702	610/235	No	<2.25/<6.60	0.75/2.20
	52849	1280	No	<0.27	0.09
	52855	1280	No	<0.30	0.10
	53377	610/235	No	<2.22/<6.9	0.74/2.3

Table 3.2: Details of observations on transient micro-quasars XTE J1118+480 and GRO J1655-40 with GMRT

Thus, we infer that if the source is a HMXB with the X-ray light curve of type (A) or (C), it shows persistent radio emission. And if the source is a LMXB with the X-ray light curve of type (B) or (C) then it is transient in nature at radio wavelengths. This gives an important clue for radio observations on newly detected XRBs. We have applied this correlation to a newly detected INTEGRAL source IGR J17303-0601 and IGR J18406−0539 which showed transient and persistent behavior respectively in radio. The detailed discussion about this source is presented in Chapter 4.

In table 3.1, columns 1, 2, 3, and 5 lists the general properties of micro-quasars. Column 4 and 6 shows the radio behavior of these sources at centimeter and meter-wavelengths respectively.

In the next section we will discuss in detail the results of our monitoring on fourteen micro-quasars with GMRT at 0.235, 0.61 and 1.28 GHz.

3.3 Results of low frequency monitoring on micro-quasars

The monitoring campaign was carried with GMRT for three years to study the nature of radio spectra of micro-quasars at low frequencies (Pandey et. al. 2006e). Based on the results obtained from the observations, the sources are classified and discussed below.

3.3.1 Micro-quasars with no radio detection at low frequencies

Five micro-quasars, viz., XTE J1118+480, GRS 1758−258, XTE J1748−288 , GRO J1655−40 and 1E1740.7−2942 were extensively monitored with GMRT at various frequencies but never detected. Table 3.2 and 3.3 shows the observation details. The flux density quoted in the table is 3σ upper limit. All the sources belonging to this category are LMXBs. Among these three sources, viz., XTE J1118+480, GRO J1655−40, and XTE J1748−288 are reported to be transient and two sources viz.,

Source	MJD	Freq (MHz)	Detection	S_ν (mJy)	RMS (mJy b$^-$1)
XTE J1748−288	52849	1280	No	<0.237	0.079
	53127	610/235	No	<3.18/<6.39	1.06/2.13
	53107	610/235	No	<3.03/<3.78	1.01/1.26
	53379	610/235	No	<2.94/<6.09	0.98/2.03
	53391	610/235	No	<3.06/<6.27	1.02/2.09
GRS 1758-258	52459	1280	No	<0.66	0.22
	52694	610/235	No	<3.21/<4.38	1.07/1.46
	52699	610/235	No	<2.34/<5.85	0.78/1.95
	52702	610/235	No	<2.40/<3.69	0.80/1.23
	52707	610/235	No	<3.09/<6.12	1.03/2.04
	52849	1280	No	<0.60	0.2
	52855	1280	No	<0.27	0.09
	53127	610/235	No	<3.48/<4.35	1.16/1.45
	53379	610/235	No	<2.91/<3.93	0.97/1.31
	53391	610/235	No	<3.42/<6.27	1.14/2.09
	53392	610/235	No	<3.33/<5.49	1.11/1.83
1E1740.7-2942	52459	1280	No	<0.27	0.09
	52694	610/235	No	<3.27/<4.62	1.09/1.54
	52699	610/235	No	<3.42/<4.56	1.14/1.52
	52702	610/235	No	<3.66/<6.18	1.22/2.06
	52707	610/235	No	<3.57/<6.09	1.19/2.03
	52849	1280	No	<0.39	0.13
	52855	1280	No	<0.6	0.20
	52897	610/235	No	<3.63/<6.12	1.21/2.04
	53107	610/235	No	<2.73/<6.18	0.91/2.06
	53379	610/235	No	<3.12/<4.17	1.04/1.39
	53392	610/235	No	<3.48/<6.09	1.16/2.03

Table 3.3: Details of observations on transient micro-quasars XTE J1748−288, GRS 1758-258, and 1E1740.7-2942 with GMRT

GRS 1758−258 and 1E1740.7−2942 are persistent in nature at centimeter wavelengths (table 3.1). The RXTE/ASM X-ray light curve of these sources are quasi-persistent in nature and have show occasional flaring (one or two) episodes at the time scale of nine years as seen in Fig. 3.5 (top) suggesting that these sources have stable accretion disk. It is important to note that 1E1740.7−2942 and GRS 1758−258 are very faint sources of the order of $\sim$0.35$\pm$0.11 mJy at 20 cm (Mirabel et. al. 1993) and $\sim$0.21$\pm$0.04 mJy at 6 cm (Rodriguez et. al. 1992) at centimeter wavelengths respectively. (http://www.aim.univ-paris7.fr/CHATY/Microquasars/micro-quasars.html). Thus the non detection of these sources at meter-wavelengths may be due to higher detection limit of GMRT. It should be also noted that our observations were not timed during X-ray active states for these sources and, hence we may have missed the chance of detection at low radio frequencies.

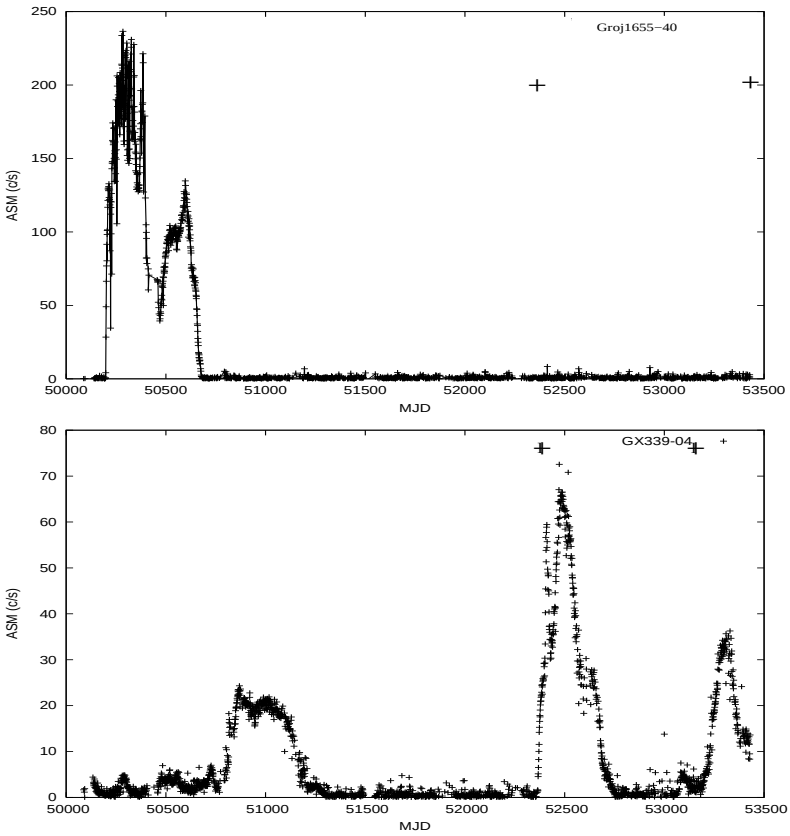

Figure 3.5: X-ray light of transient micro-quasar GRO J1655-40 with no X-ray activity and micro-quasar GX339-04 with occasional X-ray activity during GMRT observations since MJD 52459. The + shows the period, during which the GMRT observations were performed.

3.3.2 Microquasars with occasional radio detection at low frequencies

Two micro-quasars, viz., V4641 Sgr and GX339-04 fall under this category. The accretion disk is quasi-persistent (B) in both the cases. They have shown rare X-ray activity since past several years. During our observations in 2002, both the sources were in X-ray active states. The source has moved into low/hard X-ray state at the end of the X-ray flare. This resulted in positive detection at radio wavelengths. V4641 Sgr was detected at 1.28 GHz with a flux density of 49.41 mJy and GX339-04 was detected at a flux density of 15.20 mJy at 1.28 GHz. After 2002, both the sources have shown no X-ray activity, see figure 3.5 (bottom). They were not detected during most of the observations. On 3rd Aug, 2004, GX339-04 again showed a X-ray flare and went into low/hard X-ray state. Simultaneous (0.61 and 0.235 GHz) observations performed with GMRT at this epoch. The source was detected at a flux density of 4.20 mJy at 0.61 GHz and the upper limit at 0.235 GHz was $\leq$6 mJy. The spectral index was -0.37 ($S_\nu \propto \nu^\alpha$). The non detection of the source at 0.235 GHz agrees with the synchrotron bubble model. The just-born synchrotron emitting plasma is initially optically thick and emits only at higher frequencies. The radio emissions are detected at low frequencies with a delay, when the ejected plasma expands and emits at lower energies.

Source	MJD	Freq (MHz)	Detection	S_ν (mJy)	RMS (mJy b$^-$1)
V4641 Sgr	52849	1280	No	$<$0.6	0.20
	52855	1280	Yes	49.41$\pm$1.13	0.40
	52897	610/235	No	$<$2.50/$<$3.87	0.83/1.29
	53107	610/235	No	$<$3.36/$<$5.34	1.12/1.78
	53126	610/235	No	$<$2.88/$<$4.11	0.96/1.37
	53377	610/235	No	$<$2.64/$<$4.35	0.88/1.45
	53379	610/235	No	$<$3.27/$<$6.27	1.09/2.09
	53391	610/235	No	$<$3.12/$<$6.12	1.04/2.04
	53392	610/235	No	$<$2.82/$<$3.87	0.94/1.29

Table 3.4: Details of observations on transient micro-quasar V4641 Sgr with GMRT

3.3.3 Microquasars with persistent radio emission at low frequencies

Six persistent micro-quasars fall under this category viz., Cyg X-1, Cyg X-3, Sco X-1, LSI+61303, LS 5039, and SS433. Among these sources Cyg X-1, Cyg X-3, Sco X-1 and LSI+61303 show spectral turnover at low radio frequencies due to Synchrotron self-absorption (SSA). This is consistent with the standard model which considers a compact jet geometry. The higher frequency emission comes from the inner regions of the compact radiating plasma cloud and the lower frequency comes from the outer layers due to the increased optical depth at low frequencies (van der Lann, 1966; Hjellming and Johnston, 1988). If the jet is optically thick, SSA will result into the spectral turn over at low radio frequencies; however, if the jet is optically thin, then the plasma will continue to expand adiabatically, with no signature of turn over even at lower frequencies. The model is discussed in detail in chapter 1. Such clear turnover at low frequencies give important information about the source and its ambiance. We will discuss in detail these four sources with the new results obtained at low frequencies below.

There were fourteen observations performed on the micro-quasar, SS433 and only 2 snap short observations performed on LS 5039. Both these sources show no signature of turn over at low frequencies; however, the spectral index obtained from simultaneous 610 and 235 MHz show values ranging from -0.7 to -1, suggesting marginal changes in the optical depth during flare. We will briefly discuss the radio spectrum of these source in the later part of this chapter.

Cyg X-1: is a HMXB source, bright in X-rays with mass in excess of $7M_\odot$ (Gies & Bolton 1986) and at a distance of $\sim$2.5 kpc. The companion star in the case of Cyg X-1 is an O9.7 Iab super-giant (V1357 Cyg, HDE 226868). The companion star shows a strong stellar wind (Persi et al. 1980) almost filling the Roche lobe of the binary (Bolton 1972). A radial velocity of $v \sin i$ = 76 km s^{-1} is measured for the system (Gies & Bolton 1982).

The X-ray and radio emission vary over a wide range of time-scales, including modulation at the 5.6 days orbital period (Brocksopp et al (1999) and Gleissner et al (2004). The source is mostly in low/hard X-ray state and rarely goes to high/soft state. The radio emission at centimeter wavelengths is suppressed during the high-soft states (Hjellming, Gibson & Owen 1975) (see Fig. 3.6). In the low/hard X-ray state the radio emission is highly variable, but persistent in nature. The source shows rare radio outburst. The radio spectral index α, defined as $S \propto \nu^\alpha$, is close to zero in the range 2 – 220 GHz (Fender et al 2000). Jet emission in Cyg X-1 has also been observed at milliarcsec resolution during the low-hard state at 8.4 GHz (Stirling et al. 2001). Cyg X-1 jet is less dramatic (in terms of

Source	MJD	Freq (MHz)	Detection	S_ν (mJy)	RMS (mJy b$^-$1)
GX339-04	52459	1280	Yes	15.20±0.30	0.15
	52694	610/235	No	<3.15/<6.09	1.05/2.03
	52699	610/235	No	<3.12/<4.56	1.04/1.52
	52702	610/235	No	<3.63/<5.4	1.21/1.8
	52707	610/235	No	<2.4/<6.48	0.80/2.16
	52796	1280	No	<0.24	0.08
	52799	1280	No	<0.18	0.09
	52829	610/235	No	<3.03/<3.69	1.01/1.23
	52849	1280	No	<0.33	0.11
	52855	1280	No	<0.24	0.08
	52897	610/235	No	<3.27/<3.69	1.09/1.23
	53102	610/235	No	<2.70/<3.27	0.90/1.09
	53104	610/235	No	<2.61/<4.02	0.87/1.34
	53106	610/235	No	<3.12/<5.37	1.04/1.79
	53107	610/235	No	<2.34/<3.48	0.78/1.16
	53126	610/235	No	<4.20/<6.27	1.40/2.09
	53181	610/235	No	<2.94/<6.03	0.98/2.01
	53220	610/235	Yes	4.20±0.12/<6.09	0.96/2.03
	53377	610/235	No	<2.82/<5.10	0.94/1.70
	53379	610/235	No	<3.09/<4.08	1.03/1.36
	53391	610/235	No	<3.12/<6.27	1.04/2.09
	53392	610/235	No	<2.49/<6.06	0.83/2.02

Table 3.5: Details of observations on transient micro-quasar GX339-04 with GMRT

rapid variability and relativistic outflows) as compared to jets observed in other micro-quasars, e.g. Cyg X-3 (Mioduszewski et al 2001), GRS 1915+105 (Dhawan et al. 2000), IE 1740.7−2942 (Mirabel et al. 1992), and GRS 1758-258 (Rodríguez et al. 1992). Gallo et al. (2005); however, suggest that the jet may be inflating a large (5 pc) shell-like structure around the X-ray source, implying that its contribution to the outflow of energy in this system is dominant.

GMRT monitoring of Cyg X-1: Table 3.6 presents the GMRT data at 0.235, 0.61 and 1.28 GHz. At 0.235 GHz observing frequency of GMRT, the observing bandwidth is reduced due to less available RFI free band. Thus the noise is higher. Also since these sources lie in the Galactic plane where the background noise is high, the system temperature increases. This leads to a decrease in the antenna gain and, hence System temperature correction, Tsys is applied to all the measure flux densities. It can be seen from our observations, that the mean flux of Cyg X-1 at 0.61 and 0.235 GHz are ∼8.5 mJy and ∼9.9 mJy respectively and the source is highly variable at radio wavelengths.

Figure 3.6 shows the low-frequency flux density from GMRT plotted against the closest

available 15-GHz flux density. Different markers are used for the three GMRT frequencies. There is a clear correlation between the high- and low-frequency data, which is somewhat complicated by the upper limits on some of the GMRT flux densities, but is nevertheless convincing.

The X-ray/radio correlation: the radio light curve at 15-GHz, the X-ray light curve from the

Source	MJD	Freq (MHz)	Detection	S_ν (mJy)	α	$S_{\nu(15GHz)}$ (mJy)	RMS (mJy b$^-$1)	X-ray state
Cyg X-1	52796	1280	No	$<$0.93		13	0.31	H-S
	52799	1280	Yes	10.1$\pm$0.96		22	0.3	H-S
	52827	610/235	No	$<$1.5 /$<$4.08		8	0.5/1.36	H-S
	52829	610/235	No	$<$1.2 /$<$4.02		13	0.4/1.34	H-S
	52845	1280	No	$<$0.6		6	0.2	H-S
	52848	1280	No	$<$0.9		6	0.3	H-S
	52855	1280	Yes	5.40$\pm$0.21		22	0.2	Int
	52891	610/235	Yes	5.80$\pm$1.63 /7.36$\pm$2.02	-0.25	15	0.7/1.52	L-H
	53037	1280	Yes	9.20$\pm$0.04		15	0.2	Int
	53102	610/235	Yes	9.07$\pm$0.43 /10.01$\pm$2.43	-0.10	22	0.4/1.70	L-H
	53104	610/235	No	$<$2.7 /$<$5.49		27	0.9/1.83	L-H
	53107	610/235	Yes	10.03$\pm$0.12/7.81$\pm$1.83	0.26	26	0.7/1.34	L-H
	53127	610/235	No	$<$2.73 /$<$4.53		16	0.9/1.51	L-H
	53377	610/235	No	$<$2.10 /$<$4.29		6	0.7/1.43	H-S
	53379	610/235	No	$<$3.30 /$<$5.49		6	1.1/1.83	H-S
	53381	610/235	yes	7.30$\pm$0.12 /9.73$\pm$2.80	-0.30	16	0.7/1.62	Int
	53391	610/235	yes	8.40$\pm$0.12 /11.97$\pm$1.66	-0.37	20	0.9/1.41	Int
	53392	610/235	yes	8.40$\pm$0.12 /12.26$\pm$2.07	-0.39	16	0.8/1.55	Int

Table 3.6: Details of observations on Cyg X-1 with GMRT

RXTE/ASM X-ray count-rate and hardness ratio HR2 for Cyg X-1 from Mar, 2003 to Jan, 2005 are shown in Fig. 3.7. It can be seen from the figure that the X-ray state of the system showed gradual changes over this period. The source went into high/soft state for three distinct periods each lasting 1 – 2 months. It can be clearly seen from the figure that the radio flux density at 15 GHz is suppressed during this state. On one occasion an exceptional

flare was recorded in the 15 GHz data, on Feb. 20.27, 2004 with a radio flux density of 140 mJy. Unfortunately, there was no GMRT observation performed on this date.

During June 7-11, 2003, there were near simultaneous observations of the source with GMRT, Ryle Telescope, RXTE/ASM, and INTEGRAL satellite. The source was switching from low/hard to high/soft state. The gamma-ray observations by INTEGRAL satellite was performed by Malzac et. al. 2006. Based on the 15 GHz radio, RXTE/AMS X-ray data and the INTEGRAL data Malzac et. al. 2006 claim that, both spectral and variability properties of the source indicate that Cygnus X-1 was in an Intermediate State. The multi-wavelength data suggests that, the jet power appears to be anti-correlated with the disc luminosity and unrelated to the coronal power. This suggests a different mode of coupling between the jet, the cold disc, and the corona in Intermediate States. This is in sharp contrast with previous results obtained for the Low Hard State. It was inferred that, the bolometric luminosity jumps by a factor of about 2 during the transition hard to soft, suggesting a radiatively inefficient accretion flow in the Low Hard State.

During GMRT observations, the source was not detected on June 6, 2003, when the source was in low/hard state and later it was detected on June 9, 2003, when it was in intermediate state. It should be noted from table 3.6, that the data at 15 GHz mimics a similar pattern. It can be clearly inferred from the multi-wavelength data, that a shift in the peak of the spectrum at various wavelengths is seen. When the spectrum enters in the intermediate state on 7th June, 2003 from the low/hard state

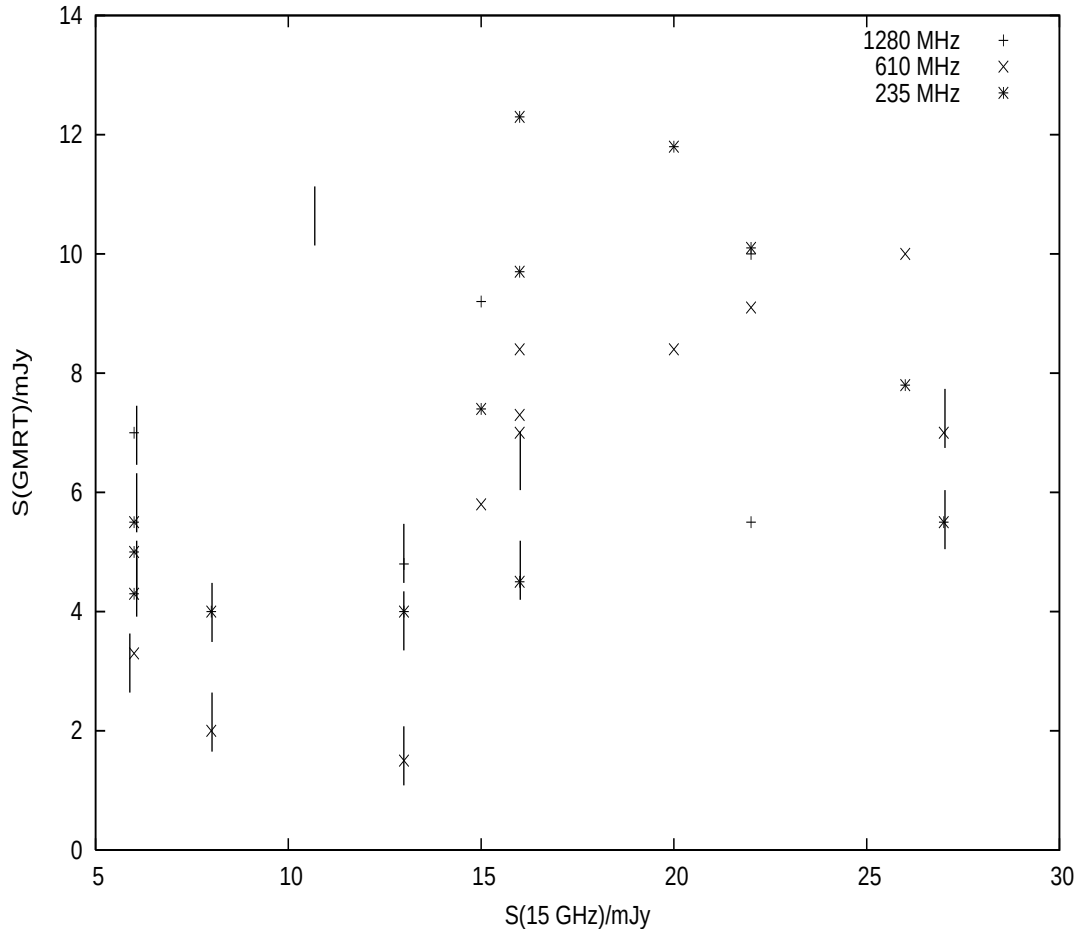

Figure 3.6: Flux–flux plot for Cyg X-1 showing the low-frequency GMRT flux densities (0.235 GHz, 0.61 GHz, 1.28 GHz) and the closest 15-GHz measurement. The upper limits are marked with bars in the figure

on 6th June, 2003, the peak of the emission spectrum moves at lower energies. Thus, the source was detected with a stronger flux at radio wavelengths during the end of the intermediate state i.e., on 9th April, 2003. This delay in the gamma-ray/X-ray to radio was approximately of the order of 2 days, as seen from our data.

With this near simultaneous monitoring observation we have derived the behavior of the source in the intermediate state at radio/X-ray/gamma-ray wavelengths.

Spectral and temporal nature of Cyg X-1: is rather quite interesting. Cyg X-1 is a persistent and variable flat-spectrum source over the range 2 to 220 GHz (Fender et al. 2000). It is clear from Table 3.6 and Fig. 3.6 that Cyg X-1 was detected at low frequency only once in high/soft state. The source was always detected in low/hard and intermediate states. Thus it is confirmed from our observations at meter wavelength and the data at centimeter wavelength that, the high/soft state suppresses the radio emission. The wide band radio spectrum of the source suggests that, the radio spectrum rises

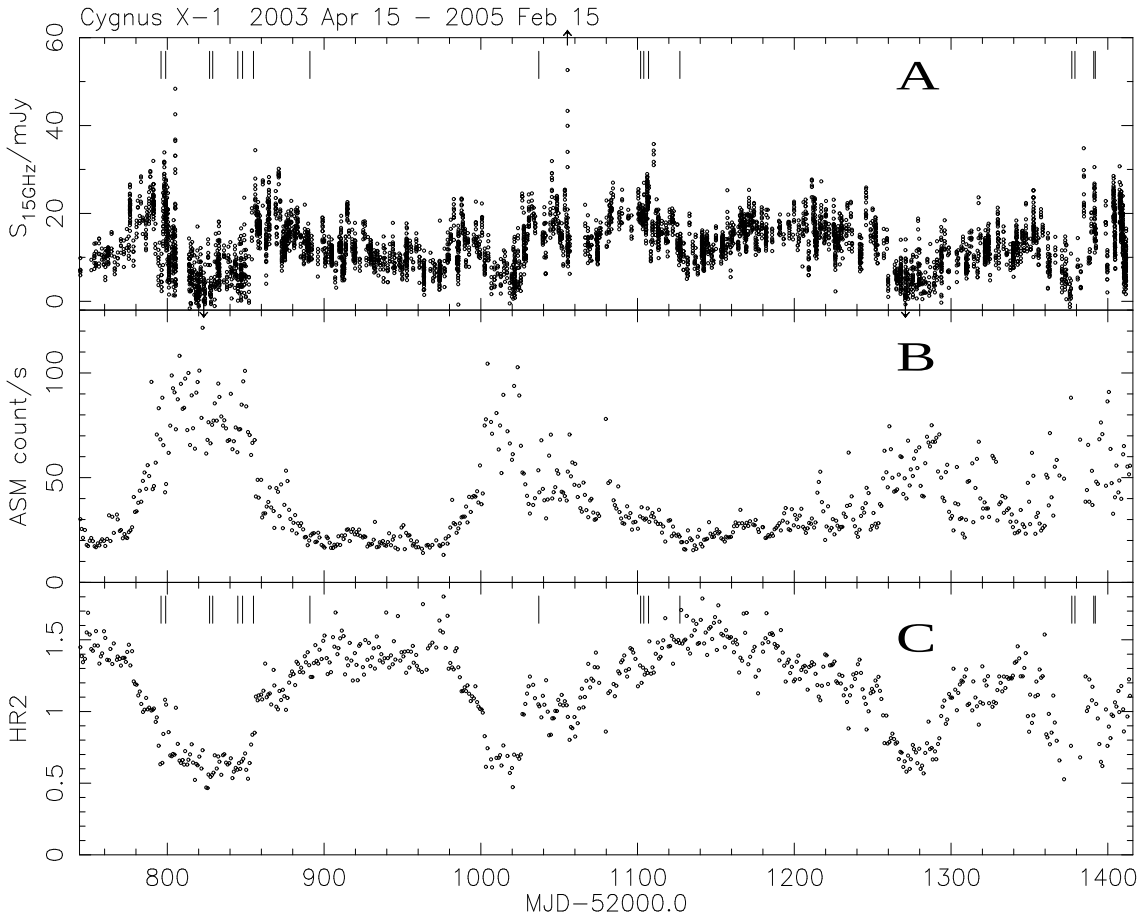

Figure 3.7: Cygnus X-1: Radio (15 GHz) (top) and RXTE/ASM (middle) light-curves; ASM hardness ratio HR2=(5–12)keV/(3–5)keV (bottom) during the interval MJD 52796 = 2003 Jun 06 to MJD 53392 = 2005 Jan 22. The dates of GMRT observations are marked with vertical lines.

from the GMRT observing frequencies to 15 GHz. The data at 0.235 and 0.61 GHz is simultaneous and the data at 15 GHz is near simultaneous. The spectrum is inverted between 0.61 and 15 GHz and flatter at lower frequencies, as shown in figure 3.8. It should be noted that the flux density at centimeter wavelengths is noise dominated. The flux density of the source shows high variability at lower frequencies. Part of the variation of radio emission from Cyg X-1 is associated with the X-ray state of the system, and is therefore intrinsic. A further part may be associated with propagation through the interstellar medium; in particular, refractive interstellar scintillation (RISS) may introduce amplitude variations (Rickett, 1990). We used the NE2001 code made available by Cordes & Lazio (1993) to estimate the propagation parameters for Cyg X-1.

The NE2001 code estimates that the transition frequency (above which the scattering is weak, and therefore the intensity fluctuations is small) is around 6 GHz. The angular broadening is estimated as 2.47 mas at 0.235 GHz, 0.3 mas at 0.61 GHz and 0.06 mas at 1.28 GHz. The scattering disc is therefore about 7.5×10^{11}m at 0.235 GHz, 1×10^{11}m at 0.61 GHz and 2×10^{10}m at 1.28 GHz. If we assume that typical transverse velocities involved (the source or the medium) are near 100 km s^{-1},

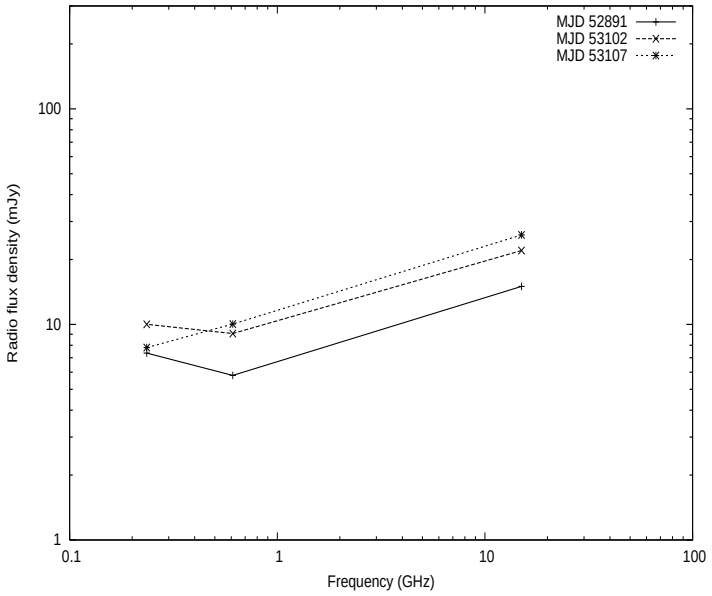

Figure 3.8: Radio spectra for Cyg X-1 at various epochs are ploted in this figure. The spectra is inverted at low frequencies

we derive timescales of 45, 5 and 1 days at the three frequencies. These are clearly in the same area as those of the observed fluctuations in the GMRT data, so it is quite possible that RISS is a contributing factor. We note; however, two important points. The angular size of the (transient) radio jet mapped at 8.4 GHz by Stirling et al. (2001) is 10 mas: the low-frequency emission may originate in a region of this size (or larger), and the scintillation bandwidths estimated by the NE2001 code are 27.65, 30, and 100 MHz at 0.235, 0.61, 1.28 GHz.

Proposed geometry of Cyg X-1 radio jet: from the above results, we conclude that the radio spectrum of Cyg X-1 is flat at centimeter (2 – 220 GHz) and meter (0.235 – 1.28 GHz) wavelengths with a decreases in the flux density below 2 GHz. It is important to note that the radio flux density at centimeter wavelengths is noise dominated (refer chapter 2). Considering this fact, the radio spectrum of the source is proposed to consists of two components; the persistent high frequency emitting component and the variable low frequency component. Both of these components imply the presence of a continuous jet with discrete plasmoids or clouds of electrons emitting synchrotron radiation. The behavior of the source can be explained by adiabatically expanding plasmoids in conical jets (Hjellming et al. 1988). Fig. 3.9 shows the sketch of this model. In this model, compact plasmoids are ejected continuously at the base of the jet and expand adiabatically within the jet medium. The low frequency emission from the newly ejected plasmoids will be absorbed due to SSA in an optically thick medium because of its highly compact nature and high magnetic field. The plasmoid will still be visible at high radio frequencies (Miller-Jones et al. 2004). As the plasma expands under its internal pressure, it will become optically thin and emit over the whole radio- frequency band, although at a lower intensity.

The observed flat radio spectrum can thus be explained by superposition of individual SSA plas-

mons with differing age and decay time profile. If a combination of size and the magnetic field are such that opacity effects are only important for the younger population, an inverted (or overall flat) spectrum is seen.

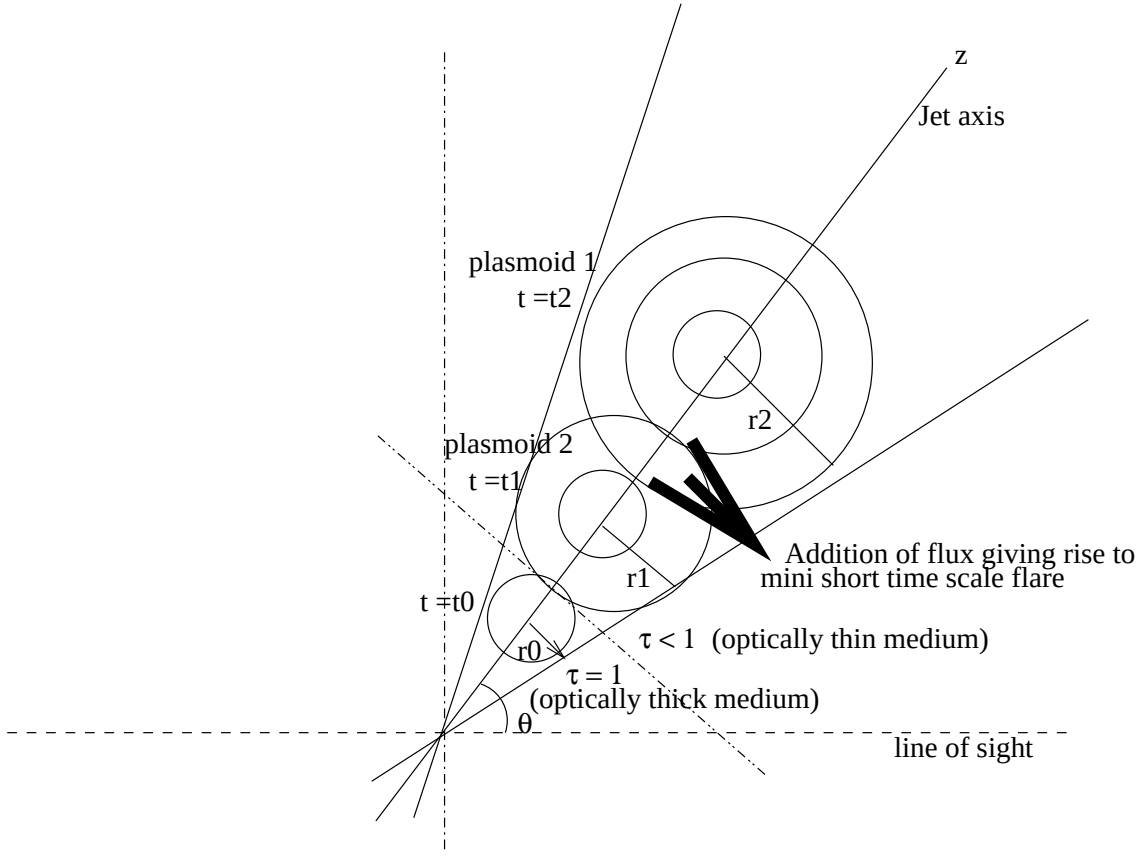

Figure 3.9: Model for the Cyg X-1 jet. The bold arrow marks the region where two plasmons of different age profile and speed may merge giving rise to increase in radio flux density

Thus, we conclude that, the radio emission in Cyg X-1 is mainly due to a continuous outflow of either compact plasmoids or electron clouds within the jet medium with different age profile and slow decay rate.

Discussion: in this section, the low frequency nature of Cyg X-1, is discussed for the first time, along with its temporal behavior, after monitoring observations of these sources over three years at various frequencies. It was noted that, Cyg X-1 is transient in nature with a mean radio flux of $\sim$8.5 mJy, and the source is detected at low radio frequencies only when the high frequency radio flux crosses the mean threshold of 15 mJy. The near simultaneous multi-wavelength monitoring (radio/X-ray/Gamma-ray) data on the source shows a shift in the peak of the spectrum from shorter to longer wavelengths. The delay in the peak is of the order of $\sim$2 days. The spectral characteristics of the source also show spectral turn over at lower frequencies. If continuous blobs of plasmoids are emitted within the jet medium with larger lifetime for the individual blobs, a flatness in the radio spectra can

be understood in the case of Cyg X-1. The positive detection of Cyg X-1 at 0.235, 0.61 to 1.2 GHz on several occasions, along with the spectral turnover at low frequencies, conclusively supports the synchrotron origin of the radio photons contrary to its ambiguous thermal or non-thermal nature as concluded from earlier measurements (Fender et al. 2000).

Rigorous calculations were performed to look for the effect of refractive interstellar scintillation at low frequency on the data of this source. The present data clearly indicate that the source visibility above a threshold luminosity seen in Cyg X-1 is due to this effect. However, the variability at high frequencies is intrinsic to the source and least affected by interstellar scintillation. Finally, we discussed a jet emission model for the source in which synchrotron radiation-emitting plasmoids originate at the base of the conical jet and the observed spectral features due to the superposition of many such plasmoids with different age profile. Thus detailed spectral measurements in the m-cm regime (low frequency radio) combined with simultaneous X-ray data can provide a clear understanding of the emission mechanisms in these sources.

Cyg X-3: is an X-ray binary system that does not seem to fit easily into the established classes of these systems. It has a 4.8-hr orbital period, and is located in the Galactic plane at a distance of $\sim$10 kpc (Predehl et al. 2002; Dickey 1983; Mason et al. 1979). The optical counterpart of the X-ray source is a WR star (van Kerkwijk et al. 1996), that is not visible in the optical band because of heavy interstellar extinction, but is clearly seen above $\sim 0.8\mu$m. The infrared data also shows a 4.8-hr modulation corresponding to the orbital period as seen in X-rays (Hanson et al. 1999). The source exhibits two spectral states of low-hard and high-soft similar to Cyg X-1 and has been observed up to 500 keV during the flare mode. The quasi-periodic oscillations with periods between 50 – 1500 s are the key characteristics of the source (van der Klis & Janson 1985). Detailed analysis of the X-ray spectrum suggests that the total number of X-ray photons seems to be conserved at all times irrespective of the state, and the observed spectrum is consistent with a thermal source embedded in a hot plasma and enveloped in a cold hydrogen shell (Manchanda 2002). The X-ray light curve of the source in the 2-12 keV band from the RXTE/ASM data shows frequent spectral changes between the high-soft to low-hard states, thereby suggesting large changes in the accretion rate on to the compact object.

At radio wavelengths, Cyg X-3 is the most luminous X-ray binary in both its quiescent and flaring states (Waltman et al. 1995). Huge radio outbursts have been reported in Cyg X-3, during which the flux density can increase up to levels of $\sim$20 Jy; radio emission is suppressed ("quenched") to levels below 1 mJy for some days before large radio flares (Waltman et al. 1994). Jet-like structures with repeated relativistic ejection have been observed at various radio frequencies (e.g. Schalinski et al. 1998). On an arc-second scale, two-sided jets have been seen from the source in the N-S orientation, whereas a highly-relativistic ($\beta \geq 0.81$), one-sided jet with the same orientation has been reported on milli-arcsec scales with the VLBA (Martí et al. 2001; Mioduszewski et al. 2001).

GMRT monitoring of Cyg X-3: Table 3.7 shows the details of GMRT observations on Cyg X-3 at various frequencies (Pandey et. al. 2004, Pandey et. al. 2006c, Pandey et. al. 2006d, Pandey et. al. 2006e). It can be seen from the table that the noise at 0.235 GHz is the highest. All the flux quoted in the table are corrected for Tsys. There were in all fifteen observations performed on this source and it was detected in all the observations. The source is highly variable at radio wavelengths.

Temporal characteristics in the radio band and their association with the X-ray emission: in

Source	MJD	Freq (MHz)	Detection	S_ν (mJy)	α	$S_{\nu(15GHz)}$ (mJy)	RMS (mJy b$^-$1)	X-ray state
Cyg X-3	52797	1280	Yes	57.90±0.88		70	0.4	L-H
	52800	1280	Yes	90.40±1.03		110	0.3	L-H
	52830	610/235	Yes	41.18±4.38/13.26±1.38	1.19	115	0.8/1.24	L-H
	52849	1280	Yes	62.40±1.43		190	0.4	L-H
	52856	1280	Yes	53.50±1.38		132	0.3	L-H
	52892	610/235	Yes	9.24 ±0.81/4.90±1.06		73	0.7/1.30	L-H
	53037	1280	Yes	21.14±0.14		51	0.3	L-H
	53105	610/235	Yes	19.14±0.12/16.25±2.23	0.17	45	1.1/1.78	L-H
	53107	610/235	Yes	17.16±0.08/15.69±3.31	0.09	70	0.8/1.21	L-H
	53127	610/235	Yes	53.85±1.26/23.51±3.96	0.87	50	1.1/1.76	L-H
	53128	610/235	Yes	38.94±2.88/20.18±3.22	0.69	73	0.8/1.13	L-H
	53378	610/235	Yes	41.45±1.93/14.65±7.61	1.09	130	0.9/1.36	H-S
	53379	610/235	Yes	39.34±0.72/13.32±5.06	1.13	130	0.7/1.27	H-S
	53392	610/235	Yes	36.04±1.83/11.18±3.83	1.23	170	0.9/1.26	H-S
	53393	610/235	Yes	53.84±3.04/49.24±9.63	0.09	170	0.8/1.33	H-S

Table 3.7: Details of observations on Cyg X-3 with GMRT

Table 3.7 we summarize the radio flux densities of the source as measured simultaneously during various observations with GMRT and from the near simultaneous Ryle Telescope data. Figure 3.10 shows a flux–flux plot for Cyg X-3 for the GMRT and 15-GHz data. The last 4 GMRT observations, all at 0.235 and 0.61 GHz, were made during the high-soft state. The mean flux density at that frequency was 20.25 and 33.2 mJy, compared with 18 and 22.7 mJy respectively for the 6 previous data points; the 15-GHz mean value was also higher; 150 mJy compared with 71 mJy for the corresponding 6 data points. The radio spectra for CygX-3 is inverted at low radio radio frequencies, as shown in Fig. 3.11.

Figure 3.12 shows the 15-GHz and RXTE ASM data for the whole period. The timing of the GMRT observations is again marked with vertical lines in Fig. 3.12. We reestablish that the radio/X-ray correlation is the opposite of that for Cyg X-1. McCollough et al (1999) report both anti-correlations (in the quiescent state) and correlations (in the flaring state) between the hard X-ray flux (20–100 keV, as measured by BATSE) and the cm-wave radio flux density of Cyg X-3. It can be seen from the figure 3.12, that no large flares were observed during this interval. The radio emission is in the 'quiescent' state, typically 50 to 200 mJy at 15 GHz. For the time-range 53380−53392, the X-ray spectrum softens: the RXTE ASM ratio HR2 falls consistently below 2, and the radio emission starts to become more erratic. This behavior faded away after another month or so, and the source returned to the quiescent state.

We investigated the possibility that RISS might be important in the case of Cyg X-3. The propagation conditions are severe, than for the case of Cyg X-1: the path length is much longer, and it has been known for some time (e.g. Wilkinson et al, 1994) that the scatter-broadening for this source is extreme. The NE2001 model is consistent, it suggests angular broadening of the order of a few arcsec at 0.235, 0.61, 1.28 GHz. The corresponding timescales would be many years, and the narrow scintillation bandwidth (2 Hz) would suppress any observed scintillation. We conclude that RISS is not relevant to this study of Cyg X-3.

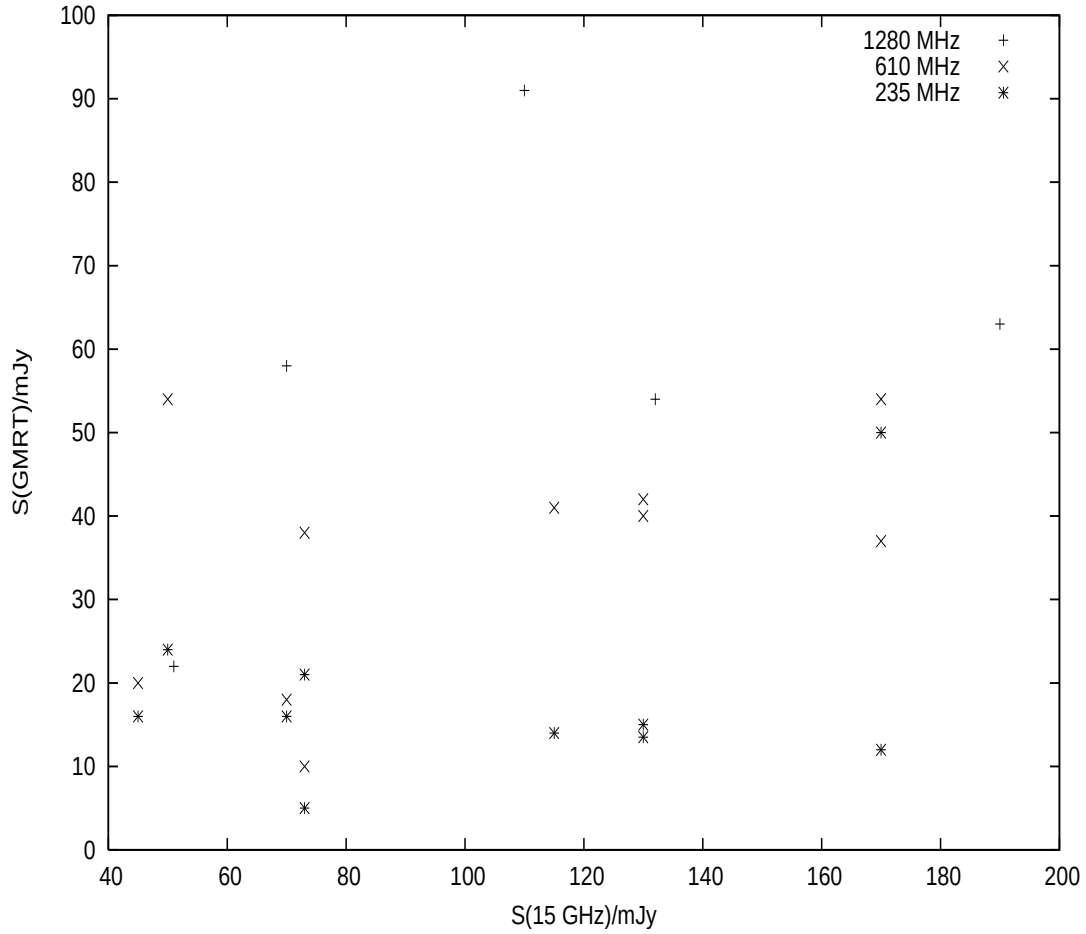

Figure 3.10: Flux–flux plot for Cyg X-3 showing the low-frequency GMRT flux densities (0.235 GHz, 0.61 GHz, 1.28 GHz) and the closest 15-GHz measurement

Spectral behavior and the emission geometry: as seen from the data in Table 3.7 and Fig. 3.12, Cyg X-3 is a persistent radio source at all wavelengths. Cyg X-3 is more luminous at higher frequencies. The data in Table 3.7 and Fig. 3.11, clearly indicates a low frequency turnover in the source spectrum below 1 GHz. As discussed earlier, such behavior can arise due to synchrotron self absorption of the compact radio emitting plasma in an optically thick medium. The observed variability of the flux density is consistent with the assumption of a discrete ejection/plasmoid in adiabatic expansion. The ejection rate and/or lifetimes of plasmoids in Cyg X-3 are probably lower/shorter than in Cyg X-1 with little or no overlap of the spectra associated to the single discrete ejection. The spectrum and the fact that the radio emission is persistently at high level may therefore imply an uninterrupted low-rate ejection.

Discussion: the first ever low frequency nature of Cyg X-3, is presented in this section based on the three years of monitoring with the GMRT at various frequencies. It was noted that, Cyg X-3 is

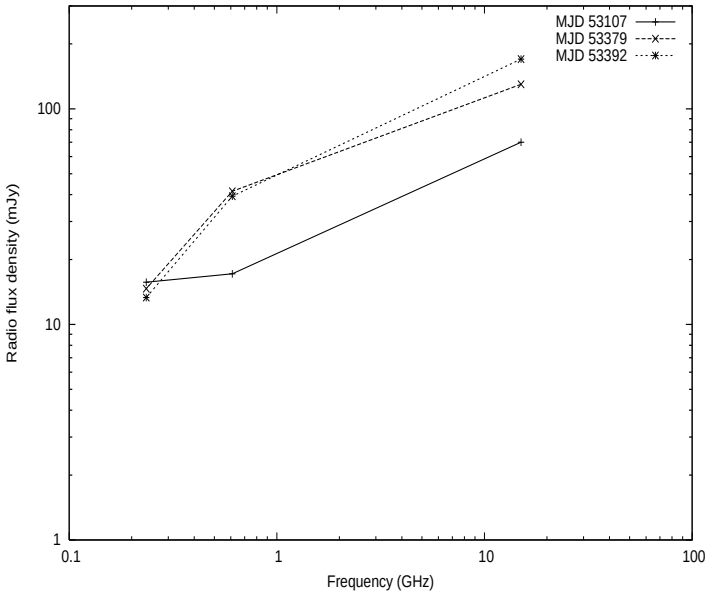

Figure 3.11: Radio spectra for Cyg X-3 at various epochs are ploted in this figure. The spectra is inverted at low frequencies

persistent source at low frequencies. The spectral characteristics of the source also show spectral turn over at lower frequencies. The spectrum of Cyg X-3 suggests that continuous blobs of plasmoids are emitted within the jet medium with shorter life time.

Rigorous calculations were performed to look for the effect of refractive interstellar scintillation at low frequency on the data of this source. The scintillation in this sources is anisotropic in nature suggesting that the variability noted in the source is intrinsic in origin. Detailed spectral measurements in the m-cm regime (low frequency radio) combined with simultaneous X-ray data can provide a clear understanding of the emission mechanisms in this source.

Scorpius X-1 (Sco X-1): was the first and brightest persistent galactic X-ray source discovered. It is a prototype low mass X-ray binary composed of a compact object and a donor star that have masses of 1.4 $M_{\circ}$ and 0.42 $M_{\circ}$, respectively. The orbital period is of 18.9 hr and the compact object is accreting matter from the Roche lobe-filling companion star (Fomalont et al. 1998, Bradshaw et al. 1997). Scorpius X-1 is a micro quasar, in which the radio emissions are highly variable with compact radio morphology. The VLBA and VLBI observations on the source suggests that the source consists of two variable radio lobes, which form near the core within the timescales of a day and move diametrically outward in the NE and SW direction. The life time of these components are typically 2 days. The behavior subsequently repeats. Both the lobes are less then 3 mas in angular size. Sco X-1 also show rapid variations on time scales ranging from 20 sec to several minutes minutes along with the 3 hrs periodicity in the radio light curve (Fomalont et al. 2001).

During MOST and OSRT observations the source was not detected at 0.843 GHz ($\leq$ 2 mJy) and 0.325 GHz ($\leq$ 10 mJy; Veluswamy et al. 1989). We have extensively monitored the source at low frequencies using GMRT. The source was always detected at 1.28 and 0.61 GHz and it was not detected at 0.235 GHz (Table 3.8 and 3.9). Thus from earlier observation performed at 0.325 GHz and from our observations at 0.235 GHz, it is confirmed that Sco X-1 is absorbed below 0.61

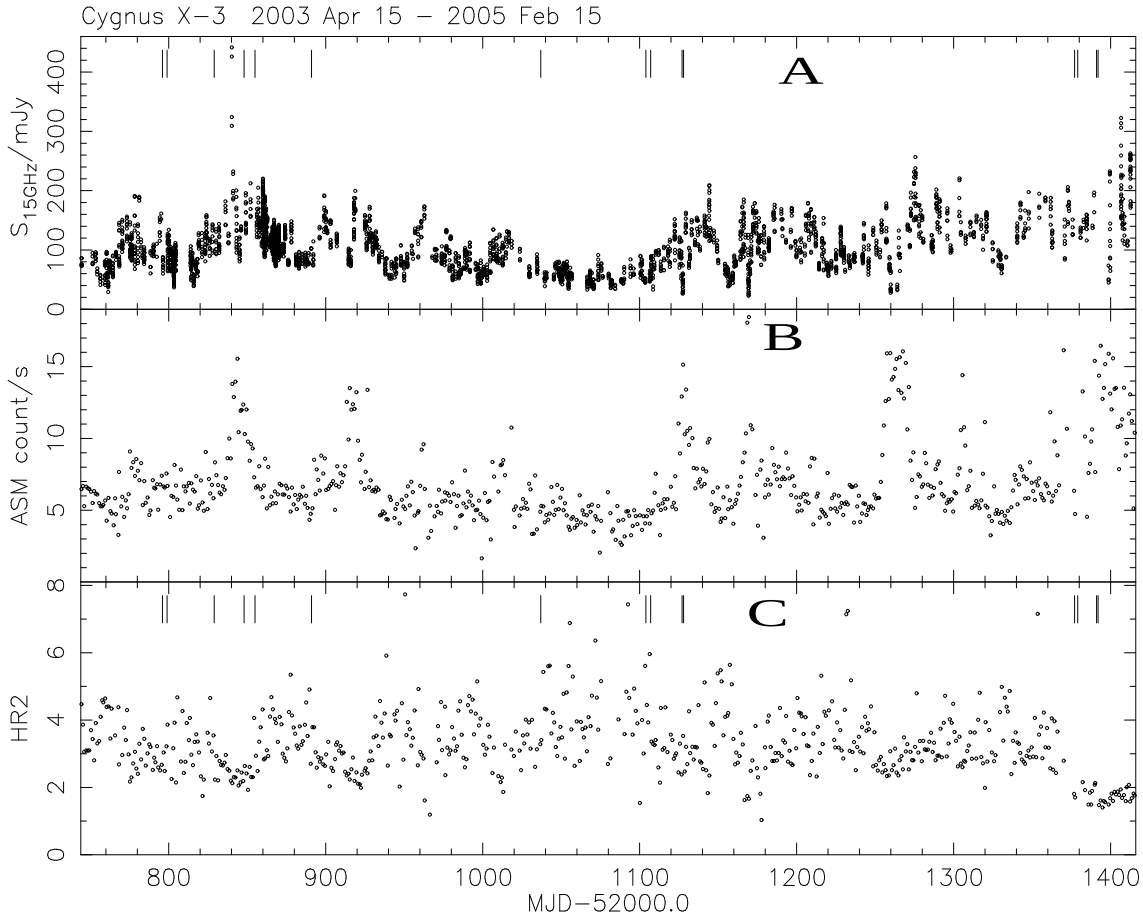

Figure 3.12: Cygnus X-3: Radio (15 GHz) (top) and RXTE/ASM (middle) light-curves; ASM hardness ratio (bottom), HR2=(5–12)keV/(3–5)keV during the interval MJD 52796 = 2003 Jun 06 to MJD 53392 = 2005 Jan 22. The dates of GMRT observations are marked with vertical lines.

GHz. The radio flux density of Sco X-1 at 0.61 GHz and 1.28 GHz is highly variable as shown in Table 3.8. The detailed study of the light-curve at low frequencies indicate a slow variation in the radio flux density. The radio image of the field also reveals an aligned triple source with the central component coincident with the star. It was believed initially that these sources were associated with Sco X-1. These are background sources which are aligned at an angle of 56^0 w.r.t Sco X-1 in NE and SW directions separated by $\sim 70''$. Their non association with the Sco X-1 was established later (Fomalont et. al. 2001). The south-west (SW) back ground source is slightly resolved by the GMRT, and the north-east (NE) back ground source is unresolved at 1.28 and 0.61 GHz. Figure 3.13, shows the radio image of Sco X-1 at 1.28 GHz with the background sources. At 0.235 GHz, Sco X-1 and the NE sources are absorbed and only SW source is detected. The details of the observation are listed in tables 3.8 and 3.9. In the case of low frequency observations at 0.327 GHz with OSRT in 1989, only SW source was detected at a flux density of 67 ± 10 mJy (Veluswamy et al. 1989). The upper limit for the NE source was ~ 10 mJy. The flux density of SW source during GMRT observations at 0.235, 0.61 and 1.28 GHz was 85 ± 12 mJy, 43 ± 7 mJy and 27 ± 12.5 mJy respectively. Thus a spectral

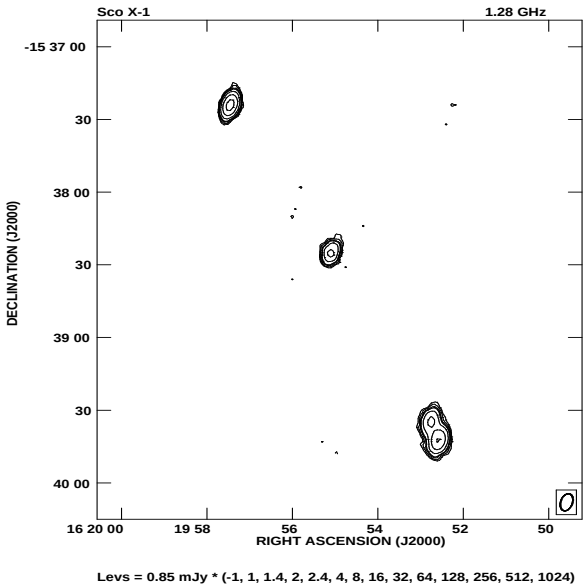

Figure 3.13: Radio image of Sco X-1 at 1.28 GHz, showing the field sources

index of -0.68 is obtained suggesting that

GMRT monitoring of Sco X-1: The details of our observations are listed in the table 3.8 (Pandey et. al. 2006e). It can be seen from the table that Sco X-1 shows persistent radio emission at 12.8 and 0.61 GHz.

Periodicity in the radio light-curve: in this section, we plot the radio light curve at 0.61 GHz for Sco X-1 for the observations greater than about 30 min scan so that slowly variable pattern at timescales of tens of minutes can be studied. To counter check, we have also plotted the light curve for a background source in the field of Sco X-1. It can be seen from the light curves that Sco X-1 shows significant slow change in the radio flux density as seen in Fig. 3.14, 3.15 and 3.16. This characteristics is also noted at centimeter wavelenths by Bradshaw et. al. 1997

The radio light-curve shows short and long term variability. It can be seen from the light-curves that the source shows significant variations within $\sim$30 m scan and shows 3 different stages of evolution of the radio emission from the source:

- The slow rising stage
- The plateau stage
- The slow decaying stage

This suggests that the bulk of the low frequency radio emission is a slowly expanding blob of matter under its own lateral pressure while moving from the optically thick to the optically thin medium.

Discussion: We have carried out an extensive study of Sco X-1 at low radio frequencies to study the variability of the source. The source shows high variability in the radio flux density. The radio

Source	MJD	Freq (MHz)	RMS (mJy b^{-}1)	S_ν (mJy) SW		S_ν (mJy) C		S_ν (mJy) NE	
Sco X-1	52796	1280	0.21	28.06		38.48		17.25	
	52798	1280	0.09	27.48		45.52		15.02	
	52799	1280	0.16	31.43		58.51		16.48	
	52849	1280	0.34	26.82		44.94		16.32	
	52855	1280	0.08	24.53		8.04		16.38	
	52897	610/235	0.85/1.88	36.03	73.02	6.48	$\leq$5.64	25.71	$\leq$5.64
	53377	610/235	1.06/1.42	50.56	97.16	24.75	$\leq$4.26	28.37	$\leq$4.26
	53391	610/235	1.08/2.09	43.26	85.13	41.25	$\leq$6.27	29.62	$\leq$6.27
	53392	610/235	1.21/1.23	42.79	84.81	51.61	$\leq$3.69	29.67	$\leq$3.69

Table 3.8: Flux density of Sco X-1 between Jun 2003-Jan 2005

Table 3.9: Flux density of radio sources in the fi eld of Sco X-1

Source	$S_{0.235}$ (mJy)	$S_{0.325}$ (mJy)	$S_{0.61}$ (mJy)	$S_{0.843}$(mJy)	$S_{1.28}$(mJy)
SW BS	85$\pm$16	67$\pm$10	43$\pm$7	35$\pm$4	27$\pm$3.5
Sco X-1	$\leq$4.97	$\leq$10	6.5 - 51.6	$\leq$2	8 - 59
NE BS	$\leq$4.97	$\leq$10	27$\pm$2.5	19$\pm$2	16$\pm$1.5

light-curve shows short and long term variability with different stages of plasma evolution. The life time of the radio emitting blob is roughly of the order of a few hours.

The variability in the radio flux density considerably increases at lower frequencies. The flux density variations may be partly explained by RISS. The scintillation time scale was calculated for Sco X-1 using NE2001 model. The expected time scales are of the order of 26.63 years and 5.25 years at 0.61 GHz and 1.28 GHz respectively; however, flux density variations at the time scale of a few days to month is seen in the case of Sco X-1. This clearly indicates that the variability in this source is intrinsic in nature.

We have also confi rmed from our observations at 0.61 GHz that all the 3 components i.e Sco X-1 and the 2 back ground sources are always detected. From table 3.9 we infer that Sco X-1 and the NE component is absorbed below 0.61 GHz due to SSA. The SW component follows a power law decay above 0.235 GHz. Based on its morphology and spectral behavior we claim that it is an extra-galactic radio source. Thus from our observations we confi rm that both these back ground sources are non variable and not associated with Sco X-1.

LSI+61303: is a HMXB with the main sequence companion star B0-B0.5 (L$\sim$10^{3}8 erg sec^{-1}). It lies at the distance of 2.0$\pm$0.2 kpc (Hutchings and Crampton 1918, Frail and Hjellming 1991). It is the only X-ray binary showing variations compatible with the orbital period at X-rays (Paredes et al. 1997; Leahy 2001), at Gamma-rays (Massi 2004; Massi et al; 2004a), at optical wavelengths in both continuum and lines (Maraschi and Treves 1981; Paredes and Figueras 1986; Mendelson and Mazeh 1989; Zamanov and Marti 2000; Liu et al. 2000; Apparao 2000). A 26.49 days orbital period is reported for the sources from various observations. At centimeter radio wavelengths the source is known to have a fl at spectrum during the initial phases of outbursts (Taylor 1996), which evolves into an optically thin spectrum. A model of adiabatically expanding cloud of synchrotron-

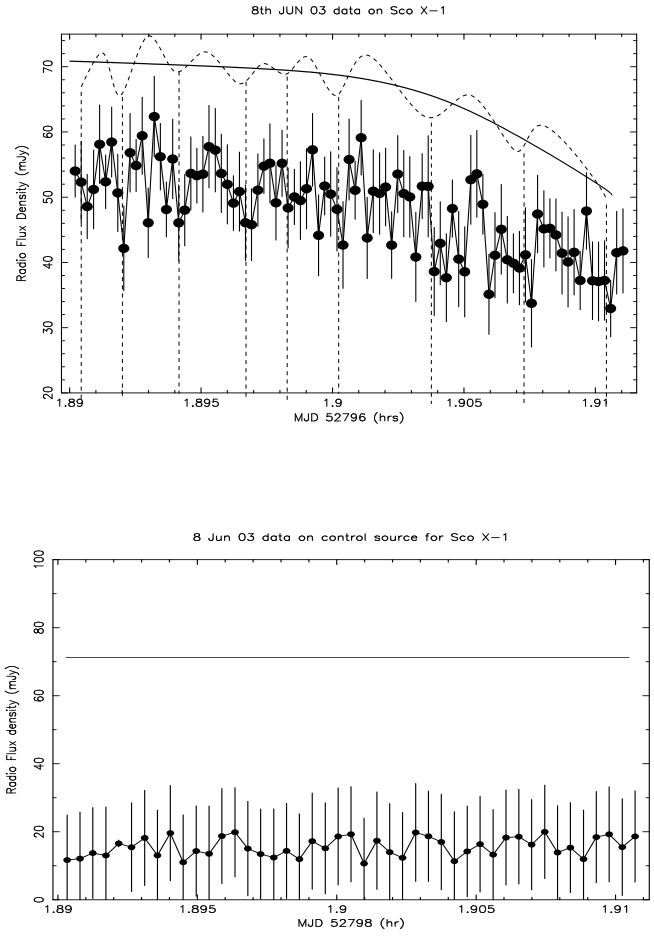

Figure 3.14: Radio light curve of Sco X-1 at 0.61 GHz showing slow decay phase

emitting relativistic electrons with continuous ejection of particles (lasting two days) explains the radio behavior (Paredes et al. 1991).

We have performed only two observations with GMRT to explore the nature of this source at low radio frequencies (Pandey et. al. 2006e). It can be see from our observations that the source is persistent and shows inverted spectrum at low radio frequencies. This indicates that the source is SSA at low radio frequencies. There is now near simultaneous Ryle Telescope data available for this source.

LS 5039: is a HMXB system at a distance of 2.55 kpc (Paredes et al. 2000). VLBA+VLA observations in 1999 revealed the micro-quasar nature of LS 5039, showing a two-sided jet at milliarcsecond scales (Paredes et al. 2002). The observations by EVN and Merlin at 5 GHz in 2000, confirm the existence of a two-sided jet structure in LS 5039 and indicate their persistent nature (Paredes et al. 2002). Recently the HESS group has reported the discovery of very high energy (VHE) gamma rays from LS 5039. The X-ray observations near the source shows an extended emission (Aharonian et al. 2005). We have performed the GMRT observations on this source with the view to explore the low frequency nature. Table 3.11 shows the details of our observation.

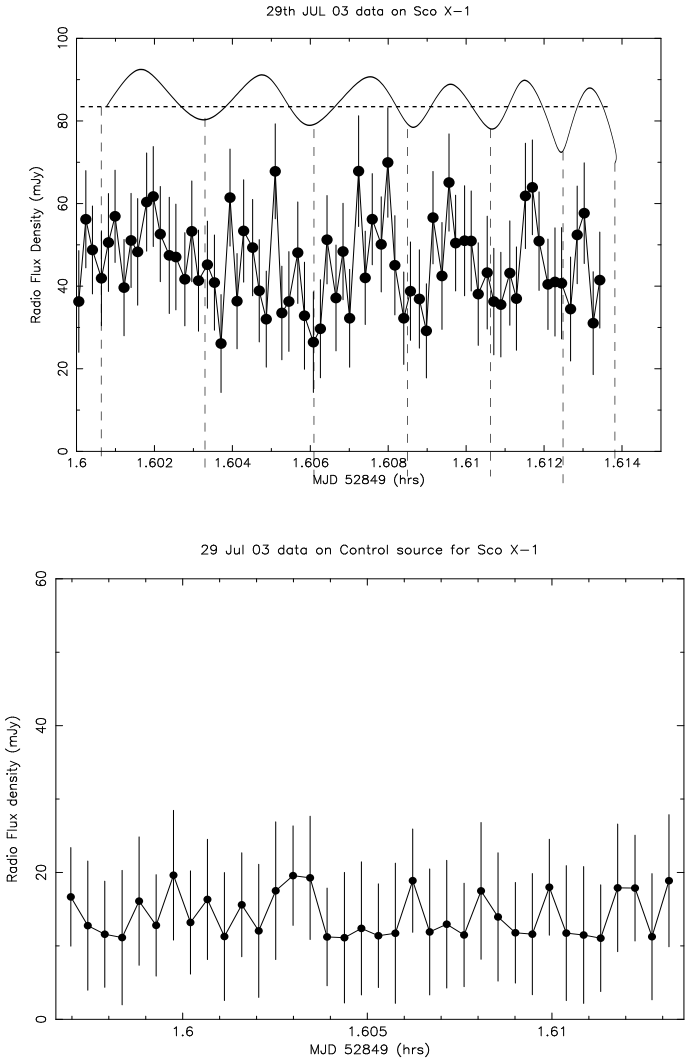

Figure 3.15: Radio light curve of Sco X-1 at 0.61 GHz showing plateau phase

Only two snap shot observations were performed on this sources. It can be seen from our observations that the source has a normal steep spectral index of -0.82. This suggests that the radio emitting synchrotron plasma is adiabatically expanding resulting into the steep spectrum radio emission. Our result also supports the nature of the source at other wavelengths. The non thermal radio emission can get Compton inverse scattered within the dense ISM and give rise to gamma-radiations. LS 5039 is an interesting source for multi wavelength studies.

SS433: is an extensively studied micro-quasar. It lies inside the Galactic supernova remnant W50. W50 is an elongated radio nebula produced by SS433 jets dues to jet interaction with the ISM (Fabrika et. al 2006). SS433 is a HMXB system showing extremely large Doppler shifts in both optical and X-ray spectral lines. These lines originate in material in the jets moving at velocities of about 26% of the speed of light. There exists a misalignment of the planes of the binary orbit and the accretion disk causing the latter to precess over a 162.5-day period. The radio jets are assumed to be tied to the

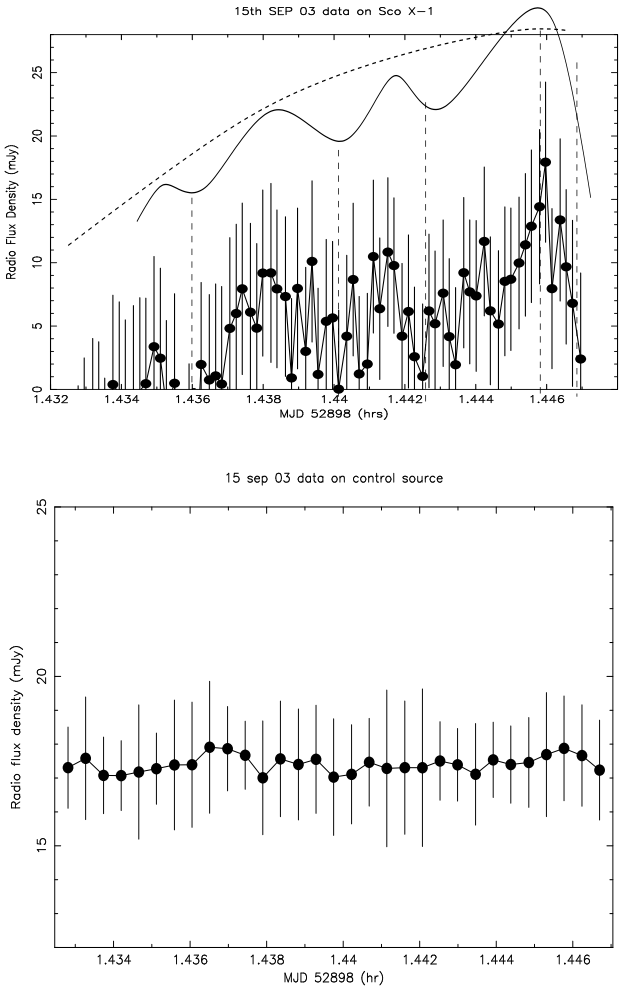

Figure 3.16: Radio light curve of Sco X-1 at 0.61 GHz showing slow rising phase

accretion disk, so they precess as well. A change in the Doppler shifts of the jet material is caused due to resulting wobble. This also causes the spectroscopic lines to move up and down the spectrum by enormous amounts. SS433 is the only relativistic jet known which produces spectral lines, which has lead to several arguments whether, the jet must be made up of baryons rather than just electrons & positron. The radio observations have shown two unique characteristics of SS433 jet: they evolve rapidly, and they precess over a large angle. The rapid evolution makes them easy to study on human time-scales – weeks to months, rather than the decades required to see interesting changes in extra-galactic sources (active galactic nuclei). The large precession angle helps to follow the evolution of the ejecta unambiguously over a substantial period, since previous and following ejection occur along different angles. The observations performed by Merlin group shows the characteristic "S-shaped" morphology of SS433's precessing jets. Several ballistic knots of radio emission within the jet medium were identified with exponential decay of time constant 16 days (Spencer et. al. 1995).

The multi-wavelength observation performed on this source during flaring stage by Chakrabarti et al. (2002) suggest a short time scale variation of 2-8 m at all the wavelengths. A delay in the radio emission of the order of $\sim$2 days is seen as compared to IR emission. The broad band spectrum

Source	MJD	Freq (MHz)	Detection	S_ν (mJy)	α	RMS (mJy b$^-$1)
LSI+61303	52891	610/235	Yes	21.70±2.21/6.27±2.43	1.30	0.83/1.23
	53377	610/235	Yes	87.32±1.04/25.63±5.44	1.28	0.93/1.54

Table 3.10: Details of observations on LSI+61303 with GMRT

Source	MJD	Freq (MHz)	Detection	S_ν (mJy)	α	RMS (mJy b$^-$1)
LS 5039	53220	610/235	Yes	28.55±3.56/65.04±7.71	-0.86	0.92/2.06
	53377	610/235	Yes	34.29±2.34/74.56±5.63	-0.81	0.74/2.03

Table 3.11: Details of observations on LS 5039 with GMRT

shows evidence of very high extinction in the optical region, possibly due to large scale obscuration of central object by matter coming from the companion wind (Paragi et al. 1999). It was reported that during Chakrabarti et al. (2002) observations the source showed negative spectral index from 0.61 to 1.28 GHz (GMRT observations), suggesting that the synchrotron radiation has emerged in optically thin regime and the self absorption frequency lies below 0.61 GHz.

GMRT monitoring of SS433: We have performed simultaneous dual frequency (610/235 MHz) radio observation of SS433 at many epochs with GMRT to explore the nature of this source further at lower frequencies (Pandey et. al. 2006e). The observations were also carried at 1.28 GHz. The details of our observations are listed in table 3.12. It can be seen from the table that the source is significantly variable and the flux at lower frequencies is higher as compared to 1.28 GHz as seen in figure 3.17.

We have also calculated the spectral index of the source from simultaneous dual frequency observations. The spectral index between 0.235 and 0.61 GHz range from 0.69 to 1.05. This range of spectral index is likely to be due to marginally different optical depth conditions at different stages of flaring.

3.3.4 GRS 1915+105: A unique micro-quasar

The first detailed low frequency radio measurements of the galactic micro-quasar GRS 1915+105 is presented in this section. The source was monitored at many epochs at 1.28 GHz, 0.610 and 0.244 GHz with the GMRT with the latter two frequencies being simultaneous observations. We have extensively used the RXTE/ASM X-ray data and 15 GHz radio data to plan the low frequency observations with GMRT. There exits a good correlation within the X-ray and radio light curve. The observations were carried out mostly during low/hard X-ray state when the source was likely to be in radio outburst phase. The source was not detected in radio during high/soft X-ray state in agreement with the known correlation between radio emission and X-ray state of GRS 1915+105.

During radio flaring states the source was detected at low frequencies with a delay as compared to 15 GHz (Pandey et. al. 2004, Pandey et. al. 2006f). Simultaneous observations at 0.610 and 0.244GHz with GMRT on many occasions do not show any signature of spectral turn over upto low radio frequency of 0.244 GHz. We propose that while the radio emission at high radio frequencies could predominantly come from compact jets, the emission at lower frequency originates in the lobes at the end of the jet which acts like a reservoir of low energy electrons. We will present the results of

Source	MJD	Freq (MHz)	Detection	S_ν (mJy)		α	RMS (mJy b$^-$1)
SS433	52459	1280	Yes	695.60±3.40			0.45
	52479	610/235	Yes	1473.64±2.04	/2972.50±1.20	-1.05	0.85/1.78
	52694	610/235	Yes	1769.68±1.70	/3830.60±3.43	-0.81	1.26/1.73
	52699	610/235	Yes	985.53±6.90	/2282.50±7.41	-0.88	1.05/1.89
	52702	610/235	Yes	1137.15±6.47	/2740.19±9.10	-0.92	1.13/2.20
	52707	610/235	Yes	1284.78±3.40	/2715.50±9.02	-0.78	0.86/2.18
	52849	1280	Yes	632.02±1.27			0.20
	52855	1280	Yes	660.00±0.14			0.24
	52897	610/235	Yes	891.68± 4.08	/2152.50±5.43	-0.92	0.71/1.66
	53102	610/235	Yes	1467.10±11.47	/2982.55±11.01	-0.74	0.91/1.75
	53104	610/235	Yes	1587.35±12.27	/3080.30±15.5	-0.69	1.02/1.66
	53107	610/235	Yes	731.50±0.14	/1725.71±6.43	-0.89	0.98/2.08
	53377	610/235	Yes	1167.75±1.36	/2380.30±10.1	-0.75	1.04/2.03
	53392	610/235	Yes	1234.97±2.78	/2957.50±07.3	-0.92	1.03/1.34

Table 3.12: Details of observations on SS433 with GMRT

low frequency monitoring on GRS 1915+105 below.

Introduction: GRS 1915+105 is a LMXB and transient source discovered in 1992 by the GRANAT satellite (Castro-Tirado et al. 1992). In this system the compact object is 14±4 solar mass with the companion K-M III star of mass $1.2\pm0.2M_\odot$ (Greiner et al. 2001). The source has shown many interesting activities at X-ray and radio wavelengths. Relativistic outflows during radio outbursts were often detected in the source (Mirabel & Rodríguez 1994). A good correlation is seen in the radio and X-ray band and the overall radio emission is correlated with its X-ray properties (eg: Harmon et al. 1997). The radio emission from the source can be broadly classified into three categories; (i) the relativistic superluminal radio jets of flux density $\sim$ 1 Jy and above at cm wavelengths, with decay time-scales of several days (Fender et al. 1999), (ii) the baby jets of $20-40$ min durations with flux density of $20-200$ mJy both in infrared (IR) and radio (Pooley & Fender 1997; Eikenberry et al. 1998) and (iii) the plateau state with persistent radio emission of $20-100$ mJy for extended durations (Muno et al. 2001). The plateau and baby jet stages show flat spectra and occur close to the accretion disk (within a few tens of AU; Muno et al. 2001). And in the case of superluminal jets, the radio emission has steep spectra and are observed at large distances ($400-5000$ AU) from the accretion disk (Fender et al. 1999; Dhawan et. al 2000). The radio emission at this distance is believed to be decoupled from the accretion disk. Even though superluminal jets and baby jets are differentiated by their spectra, decay time scales, and the distance from the accretion disk at which the emission takes place; there is an evidence for the ejection of significant amount of relativistic material even during the baby jets (Fender et. al 1999). The radio emission is believed to be due to synchrotron emission from relativistic electrons and the dominant decay mechanism is the adiabatic expansion losses (Mirabel et. al 1998). The frequency corresponding to the peak radio flux in the source spectrum depends on the energy and spectral distribution of the electrons in the emitting volume. The peak flux exhibits temporal evolution by shifting to lower frequencies, in the absence of in-situ acceleration. This results in decrease of the energy of the electrons by radiative and expansion

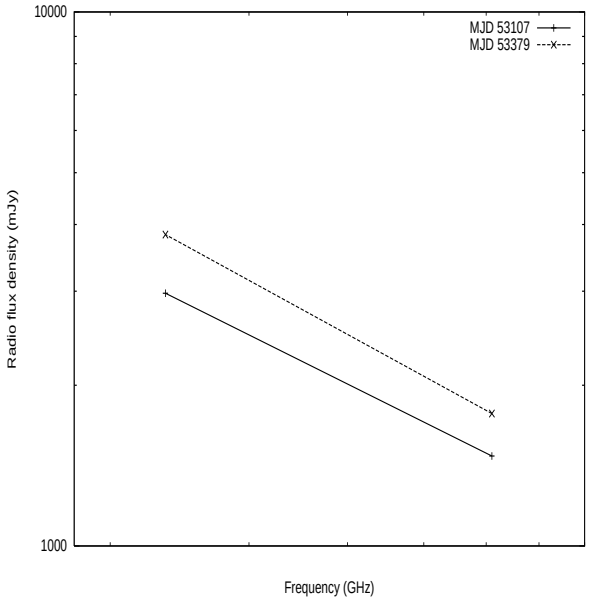

Figure 3.17: Radio spectra for SS433 at various epochs are ploted in this figure. The spectra is steep at low frequencies

losses.

In this section, we present the low frequency radio data taken with GMRT over several years and discuss the results in terms of the geometric model of the source. The details of our observations are listed in table 3.13 and 3.14.

GMRT monitoring of GRS 1915+105: the GMRT observations were performed at 0.235, 0.61 and 1.28 GHz at various epochs. The source was detected mostly in the low/hard X-ray state and the radio emissions were quenched in high/soft state. We have also listed the near simultaneous 15 GHz data available from Ryle telescope in the table.

It can be seen from the data, that during radio flares, the source was detected first at 15 GHz followed by its detection at 0.61 and 0.235 GHz. The radio images of GRS 1915+105 at 0.244 and 0.610 GHz are presented in Figure 3.18. The source has a compact morphology at both the frequencies. It is important to note that, during the detection, no evidence of spectral turn over is seen up to 0.244 GHz in most of the cases. However, clear spectral turn over is seen when the source was observed during the early stages of the flare, suggesting that the radio emitting plasma evolves from the optically thick to optically thin state during the course of the flare. Since most of the observations were performed well past the initial phase, the plasma has expanded to optically thin state by then.

In Figure 3.19, we present spectra between 0.235 and 0.61 GHz from simultaneous observations performed with gmrt along with near simultaneous observations at 15 GHz by Ryle Telescope during one of the flaring episode. The spectral index for the rest of the observations are presented in the table 3.13 and 3.14. The flux densities at these frequencies have been corrected for the increased system temperature in the direction of GRS 1915+105.

It can be seen from the table that the spectral index ranges from -0.43 and -1.74 and on one

Source	MJD	Freq (MHz)	Detection	S_ν (mJy)	$S_{\nu(15GHz)}$ (mJy)	α	RMS (mJy b$^-$1)
GRS 1915	52459	1280	Yes	33.60±0.80	15		0.25
+105	52480	610/235	Yes	45.09±2.50 /202.95±1.42	23.50	-1.58	0.84/1.38
	52694	610/235	No	<3.06 /<4.50	<20		1.02/1.50
	52699	610/235	Yes	45.9 /30.02	<15	+0.45	0.73/2.09
	52702	610/235	yes	113.5 /272.3	<15	-0.92	0.77/2.10
	52707	610/235	Yes	17.75 /78.72	<15	-1.56	0.83/1.70
	52796	1280	Yes	185±1.09	33.33		0.35
	52799	1280	No	<0.60			0.20
	52811	610/235	Yes	186.64±2.15 /756.00±58.70	<15	-1.47	0.82/1.45
	52812	610/235	Yes	161.81±2.64 /672.00±6.90	<15	-1.49	0.54/1.85
	52813	610/235	Yes	105.28±2.41 /450.58±3.78	<15	-1.53	0.48/1.26
	52814	610	Yes	94.72±1.27	25.50		0.76
	52820	610/235	Yes	81.45±1.66 /148.93±5.64	50	-0.63	0.82/2.03
	52825	610/235	Yes	89.59±1.85 /160.57±7.01	30	-0.60	0.62/1.66
	52829	610/235	Yes	48.05±1.89 /98.04±8.63	28	-0.75	1.03/1.39
	52845	1280	Yes	83.78±1.78	33.50		0.08
	52849	1280	Yes	197.54±1.84	25		0.07
	52855	1280	Yes	4.15±0.41	<15		0.08
	52891	610/235	yes	9.67±0.51 /34.46±1.31	<15	-1.33	1.03/1.46
	52897	610/235	Yes	5.09±0.17 /21.45±1.17	<15	-1.51	1.07/1.94
	52898	610/235	Yes	<2.46 /11.83±1.26	<15	-1.65	0.82/1.29
	52961	1280	No	<0.90	<15		0.30
		610/235	No	<4.02	<2.49		0.83/1.34
	52962	1280	No	<0.87	<15		0.29
		610/235	No	<5.61	<3.12		1.04/1.87
	52963	1280	No	<0.45	<15		0.15
	52974	1280	Yes	4.51±0.42	<15		0.24
	52975	1280	Yes	2.26±0.81	15		0.19
	53019	610	No	<4.20	<15		1.4
	53034	1280	No	<0.24	<15		0.08
	53037	1280	No	<0.39	<15		0.13
	53060	610/235	Yes	48.51±1.03 /157.73±7.15	92	-1.24	1.03/1.86
	53061	610/235	Yes	37.53±1.03 /133.86±5.13	85	-1.33	0.82/1.90
	53062	610/235	Yes	26.38±0.73 /108.82±7.84	80	-1.48	0.73/2.33
	53069	610/235	Yes	4.74±0.22 /24.94±4.02	170	-1.74	0.58/1.94
	53071	610/235	Yes	25.70±0.12 /38.93±8.23	150	-0.44	0.94/1.79
	53073	610/235	Yes	31.15±1.26 /85.62±6.2	120	-1.06	1.49/1.76
	53076	610/235	Yes	44.17±1.03 /129.66±11.17	110	-1.12	0.49/2.08
	53126	610/235	Yes	102.51±2.47 /174.41±9.43	75	-0.56	0.98/1.74
	53127	610/235	Yes	76.42±2.30 /124.29±3.12	75	-0.51	1.43/1.47
	53129	610/235	Yes	48.60±3.03 /76.78±7.12	50	-0.48	0.84/1.48

Table 3.13: Details of observations on GRS 1915+105 with GMRT

Source	MJD	Freq (MHz)	Detection	S_ν (mJy)	$S_{\nu(15GHz)}$ (mJy)	α	RMS (mJy b^-1)
GRS 1915 +105	53130	610/235	Yes	49.98±23.12 /118.99±6.76	40	-0.91	0.84/1.65
	53138	1280	Yes	51.51±0.89	110		0.21
	53139	610/235	Yes	202.50±3.85 /349.39±4.6	60	-0.57	0.89/1.42
	53140	610	Yes	5	<20		0.83
	53141	610/235	Yes	263.06±1.42 /419.87±2.93	50	-0.48	1.24/1.58
	53142	610/235	Yes	287.28±17.02 /434.73±1.68	55	-0.43	0.90/1.89
	53143	1280	Yes	33.6	60		0.08
	53280	1280	Yes	18.35±0.81	<15		0.51
	53299	610	Yes	8±0.61	<15		1.29
	53376	610/235	No	<3.09 /<6.03	<15		1.03/2.01
	53379	610/235	No	<3.06 /<5.46	<15		1.02/1.82
	53391	610/235	No	<2.61 /<5.97	<15		0.87/1.99
	53392	610/235	No	<2.16 /<5.46	<6.36		0.72/1.82

Table 3.14: Details of observations on GRS 1915+105 with GMRT

occasion it is +0.45 ($S_\nu \propto \nu^\alpha$; refer table 3.13 and 3.14, figure 3.19). This suggest that during the radio flaring activity , the radio emitting plasma shows evolution in the radio behavior. The source shows steep spectral behavior at the decay of the flare and flat spectral behavior during the rise of the flare. This data mimics the synchrotron bubble model, where the ejected synchrotron emitting plasma is first detected only at high frequencies due to its compact nature and later at low frequencies the plasma is optically thin. As the synchrotron emitting plasma evolves, a shift is peak of the spectrum towards lower energies is seen. Our simultaneous dual frequency data between MJD 52694 – 52707 shows the rise and the decay phase of the radio flare. The spectral index is positive during the rise of the flare, when the low frequency emissions are weak, at the initial stage. A shift in the peak of the flare at lower frequencies is seen as the synchrotron emitting plasma evolves. On MJD 52829, a new flare is added up at 15 GHz as seen from the fig. 3.19.

During most of the other observations the source was observed at the end of the flare. The continuous data during this stage suggests a steepening in the radio spectrum, than the previous day and is consistent with the expectation that the 0.244 GHz emission decays slower than 0.610 GHz. The observed spectral indices on both days suggests that the radio emission at low frequencies arises in a optically thin medium. The radiative lifetimes of the electrons are longer at these frequencies, thus the source is visible for longer duration during radio flares, as compared to higher radio frequencies. The low frequency radio emission are useful to understand several parameters such as compactness of the radio emitting plasma, the ambient medium.

Radio/X-ray correlation: We have plotted the RXTE/ASM X-ray light curve, and the 15 GHz radio light curve in Figure 3.20. The GMRT observations are marked on the 15 GHz light curve.

It can be seen from the figure that, the source is highly variable in the X-ray and radio regime and has shown frequent flaring activity in last three years. Also, with the exception of one or two flaring episodes, the flux density at 0.235 GHz is always higher as compared to 0.61 and 15 GHz. Such spectral behavior is typical of lobes of radio galaxies and quasars.

In the case of GRS 1915+105, the radio spectrum suggest that, the source is not self-absorbed and the flux density seems to increase at lower frequencies. This may be due to presence of large

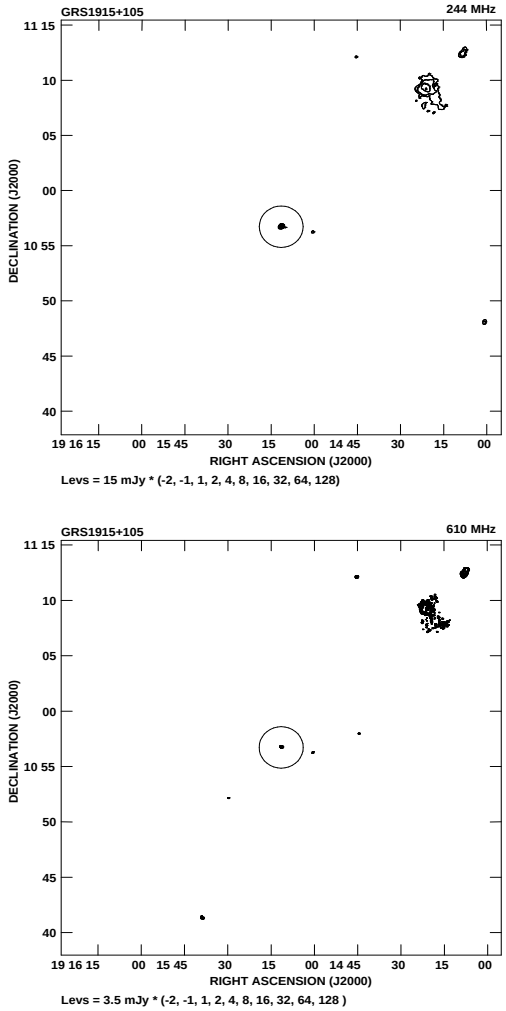

Figure 3.18: Field of GRS 1915+105 at 0.61 and 0.235 GHz. The circle drawn at the central region is only to help to locate the GRS 1915+105, which is at the center of this circle. The rest of the sources in the field are likely to be unrelated to GRS 1915+105.

population of low energy electrons accumulated due to repeated flaring activities forming optically thin plasma.

In the next section, we will discuss the possible geometry of the emission and compare the radio properties of GRS 1915+105 with other well known micro-quasars.

Radio emission geometry at low frequency: for GRS 1915+105 supports the formation of radio lobes. In this case the jet is not compact but conical in nature (Hjellming and Johnston, 1988). Hence, the low frequency emission is not self absorbed (Ishwara-Chandra et al. 2005a). In this model, the infra-red emission occurs shortly after the ejection of the plasma from the accretion disk and radio emission follows with a time delay (Mirabel et al. 1998).

As the plasma moves out wards, it also undergoes expansion and becomes optically thin. The peak of the emission moves progressively to lower frequencies, as explained in chapter 1. The plasma will continue to expand if the ambient medium is not dense enough to slow down or stop the ex-

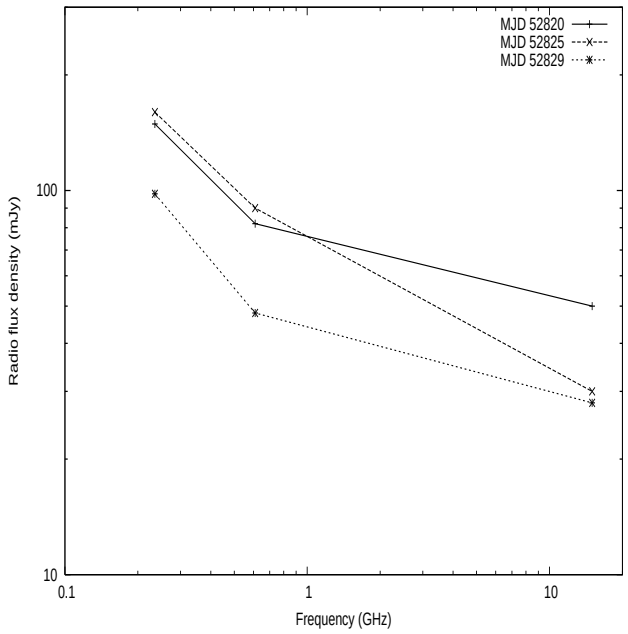

Figure 3.19: Spectral index plot between 0.610 and 0.244 GHz from MJD 52825 – MJD 52829

pansion. Under such conditions, lobes will be formed at the end of the jet, similar to case of AGNs (Figure 3.21). Thus the radio spectrum from centimeter to meter wavelength will show emission from two different components, the emission at centimeter wavelength dominated by radio emission from compact jet while the emission from lobe dominates at meter-wavelengths, as seen in the table 3.13. Under such conditions, no absorption effects will be seen at low frequencies and the spectra will continue to be optically thin.

Comparison with the low frequency nature of other micro-quasars: as seen in the earlier part of this chapter, the micro-quasars, Cyg X-1, Cyg X-3, LSI+61303 and Sco X-1 show clear spectral turn-over at low radio frequencies. The spectral turnover is understood as synchrotron self-absorption which suggests that the emitting region is compact. This is possible if the jet is continuously fed by new streams of plasma or if the expansion of the jet is limited by the dense surrounding. Similarly, the micro-quasar V4641 Sgr also exhibits spectral turnover at low radio frequencies during radio flaring episode (Ishwara-Chandra and Pramesh Rao 2005b). However, in the case of GRS 1915+105, the spectral turnover was not observed suggesting that the emitting region at this frequency is not compact.

It is important to understand whether the extended low frequency radio emission in GRS 1915+105 is present at times when there are no flares at higher frequencies. It is clearly seen from the GMRT data over several epochs that, the source is simultaneously detected at 0.235 and 0.61 GHz, during flaring activity at 15 GHz. During radio quite state the source is not detected at both the frequencies. This suggest that the low frequency component is formed only during radio flares. In radio active state, the high frequency radio emission is coupled to the activities of the accretion disk, and the plasmon will expand out wards and the peak of the radio emission shifts to lower radio frequencies. The plasma eventually decouples from the disk and disperse into ISM.

Summary: we have presented for the first time, detailed low frequency radio observations of the

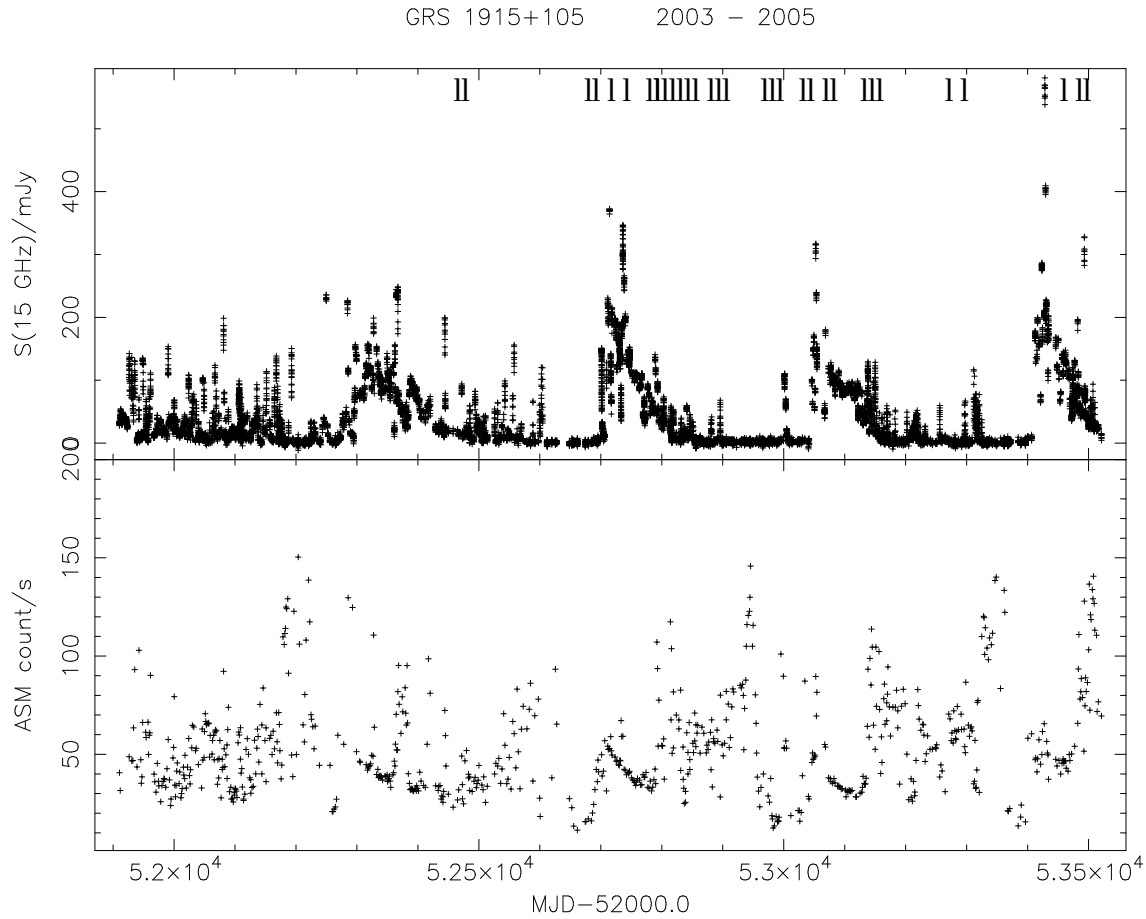

Figure 3.20: GRS 1915+105: Radio (15 GHz) (top) and RXTE/ASM (bottom) light-curves; during the interval MJD 52796 = 2003 Jun 06 to MJD 53392 = 2005 Jan 22. The dates of GMRT observations with positive detections are marked with vertical lines.

galactic micro-quasar GRS 1915+105 with GMRT. The observations have been carried out at several epochs at 1.28, 0.610 and 0.244 GHz, during various X-ray states. There exists a good correlation in the radio/X-ray states. The radio emissions are quenched in high/soft X-ray state and detected in the low/hard X-ray state. Our results suggest that, during flaring episodes there is no spectral turn over even at low radio frequencies of 0.244 GHz (Ishwara-Chandra et. al 2005a). While the radio emission at high radio frequencies could predominantly come from compact jets, the lower frequency emission is likely to come from regions far from the accretion disk. It is proposed that, radio lobes are formed at the end of the radio jet. The relativistic plasma which was ejected from the accretion disk will move out wards during radio flares, it will loose energy both by radiation and by expansion and will form these lobe, similar to the case of AGNs. The radio lobes acts as a reservoir of low energy electrons and is likely to be the origin for optically thin low frequency radio emission in the case of GRS 1915+105.

Thus it can be seen from the above discussions that, the micro-quasars are interesting candidates to study at various wavelengths. Each source has unique nature of its own and they show different

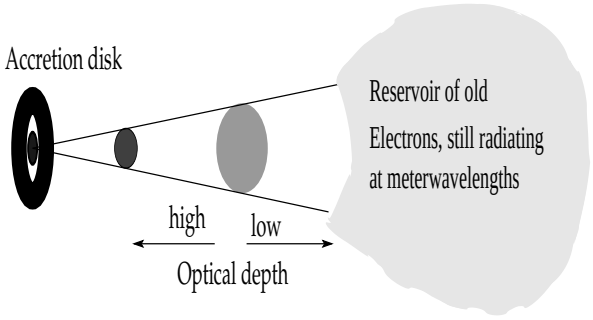

Figure 3.21: Toy model to suggest the possible location for the low frequency radio emission.

trends of variability and spectral behavior at various time scales. In the next section, we will discuss about the effect of RISS on the flux density fluctuation of micro-quasars.

3.3.5 Scintillation effects at low radio frequencies

A significant variability was seen in the radio flux density of micro-quasars during our continuous monitoring program. In most of the cases the variability is intrinsic to source; however, in a few cases the flux density fluctuation at meter-wavelength may be partly due to RISS. We have already discussed about RISS in the second chapter. In this section, we will discuss about the expected scintillation time scale for each micro-quasar and its relevance with the GMRT data. We have carefully investigated the low frequency GMRT data for micro-quasars to look for the signatures of radio flux density fluctuations due to RISS. We have also estimated the scattering angle and the scintillation time scale for all the micro-quasars using, NE2001 code (http://rsd-www.nrl.navy.mil/7213/lazio/ne.model/) developed to study the interstellar scattering and scintillation of radio wavefronts. Table 3.15 lists the angular broadening and scintillation time-scale calculated for all the micro-quasars at 0.235, 0.61 and 1.28 GHz. It is evident from Table 3 that angular broadening is dominant at lower frequencies.

At 0.61 GHz the scintillation time-scale estimated for Cyg X-1 is the least ($\sim$ two days) and our observations shows the flux density fluctuations on similar timescales. Hence we confirm that the flux density fluctuations in the case of Cyg X-1 data is affected by isotropic refractive interstellar scintillation. A detailed work is presented in Pandey et al. (2006c). A similar agreement with the scintillation effect can be seen in the SS433 data. In the case of Cyg X-3 the scintillation time scale is maximum (Table 3.15) due to anisotropic interstellar refractive scintillation. Therefore, the flux

Table 3.15: Scintillation time scale expected at GMRT frequencies

Source	Scintillation-angle			Scintillation-time			Variability (radio) type
	$\theta_{0.235GHz}$ (mas)	$\theta_{0.61GHz}$ (mas)	$\theta_{1.28GHz}$ (mas)	$T_{0.235GHz}$ (days)	$T_{0.61GHz}$ (days)	$T_{1.28GHz}$ (days)	
	HMXB						
LSI+61303	5.46	0.67	0.13	125.83	15.44	2.99	V_I/V_S
V4641 Sgr	135.49	16.62	3.25	15612.15	1915.08	374.49	V_I
LS 5039	15.11	1.85	0.36	452.68	55.42	10.78	V_I/V_S
SS433	5.70	0.70	0.14	315.26	38.72	7.74	V_I/V_S
Cyg X-1	2.47	0.30	0.06	56.92	6.91	1.38	V_I/V_S
Cyg X-3	6640	814.06	159.41	765109.33	93801.94	18368.39	V_I
	LMXB						
XTE J1118+480	9.46	1.16	0.23	218.01	26.73	6.94	V_I/V_S
Cir X-1	144.78	17.76	3.48	9175.43	1125.54	220.55	V_I
XTE J1550−564	132.88	16.30	3.19	8115.04	995.45	194.81	V_I
Sco X-1	12.18	1.49	0.29	392.97	48.07	9.36	V_I/V_S
GROJ1655	46.16	5.66	1.11	1702.05	208.69	40.93	V_I
GX339-04	78.40	9.62	1.88	3613.53	443.39	86.65	V_I
1E1740.7−2942	450.43	55.24	10.82	44116.56	5410.38	1059.75	V_I
XTE J1748−288	541.39	66.39	13.00	56144.62	6884.95	1348.16	V_I
GRS 1758−258	330.93	40.58	7.95	32412.34	3974.54	778.65	V_I
GRS 1915+105	169.94	20.84	4.08	24477.16	3001.67	587.66	V_I

ref:http://rsd−www.nrl.navy.mil/7213/lazio/ne.model/

density variations seen in the case of Cyg X-3 is most likely intrinsic to the source. The anisotropy in the scintillation effects in Cyg X-3 is due to position of the source in the direction of Cyg OB2 association (Pandey et al. 2006c, Pandey et. al. 2006d, Pandey et. al. 2006e, Wilkinson et al. 1994, Mioduszewski et al. 2001). In the case of LSI+61303, LS 5039, Sco X-1, and XTE J1118+480 scintillation time-scale is small but its effect on the flux density variations have not been checked at low frequencies due to inadequate data. However, the flux density variations at the time scale of the order of one week at 1 GHz for these sources can be due to RISS. In the case of Sco X-1 though the scintillation time-scale is small at 1.28 GHz ($\sim$ 2 weeks), the data was checked for RISS and no evidence for fluctuation at these timescales was found, hence the flux density variations is intrinsic to the source. In the case of all the other micro-quasars the scintillation time-scale is found to be larger than the observed flux density variation timescales, hence these variability in the flux density seen at low frequencies is most likely due to intrinsic emission mechanism. In Table 3.15 the variability due to scintillation is marked as V_S and intrinsic variability of the source is marked as V_I.

Source	S_ν (mJy)	beam (arc-sec)^2	ν (GHz)	T_B (K)	B (mgauss)	$L_{radio-jet}$ (ergs/sec)
	HMXB					
LSI+61303	87.32/ 25.63	39.12/ 236.47	0.61/ 0.235	$\geq 1.86\times10^8$/ $\geq 1.00\times10^7$	$\geq$1.18/ $\geq$0.18	2.41×10^{29}/ 7.07×10^{28}
V4641 Sgr	49.41	139.86	1.28	$\geq 1.86\times10^6$	$\geq$0.26	71.5×10^{29}
LS 5039	28.55/ 65.04	58.24/ 159.02	0.61/ 0.235	$\geq 2.74\times10^7$/ $\geq 5.65\times10^7$	$\geq$0.55/ $\geq$0.22	1.66×10^{29}/ 1.45×10^{29}
SS433	1473.64/ 2972.50	23.94/ 181.31	0.61/ 0.235	$\geq 8.38\times10^9$/ $\geq 1.98\times10^9$	$\geq$3.15/ $\geq$0.52	234.24×10^{29}/ 182.02×10^{29}
Cyg X-1	9.07/ 11.97	40.68/ 218.84	0.61/ 0.235	$\geq 1.78\times10^7$/ $\geq 5.49\times10^6$	$\geq$0.59/ $\geq$0.12	2.51×10^{28}/ 1.27×10^{28}
Cyg X-3	41.45/ 14.65	41.93/ 216.19	0.61/ 0.235	$\geq 7.68\times10^7$/ $\geq 6.88\times10^6$	$\geq$0.57/ $\geq$0.08	2.86×10^{30}/ 3.89×10^{29}
	LMXB					
XTE J1118+480	-	-		-	-	
Cir X-1	-	-		-	-	2.99×10^{29}
XTE J1550−564	-	-		-	-	
Sco X-1	41.25	50.82	0.61	$\geq 5.20\times10^7$	$\geq$0.69	2.23×10^{29}
GRO J1655−40	-	-		-	-	
GX339-04	15	16.54	1.28	$\geq 4.06\times10^7$	$\geq$1.33	1.52×10^{29}
1E1740.7−2942	-	-		-	-	
XTE J1748−288	-	-		-	-	
GRS 1758−258	-	-		-	-	
GRS 1915+105	49.98/ 118.99	50.46/ 145.56	0.61/ 0.235	$\geq 6.39\times10^7$/ $\geq 1.23\times10^8$ 0.19	$\geq$0.48/ $\geq$0.19	5.39×10^{30}/ 4.94×10^{30}

Table 3.16: Physical parameters of micro-quasars at GMRT frequencies

3.3.6 Comparative radio parameters at GMRT frequencies

Table 3.16 and 3.17 lists the observed and estimated parameters of all the sources at centimeter and meter-wavelengths. The information in table 3.17 has been complied from literature. The compilation is not exhaustive or complete, but rather representative. The mean radio flux density quoted in the tables are during quiescence or flaring phase of the respective source. The angular size in the case of table 3.16 is the size of the synthesized beam because all the sources remained unresolved and in the case of table 3.17 it was taken from various references mentioned in the footnote. Following important parameters were calculated using these informations:

$$Brightness\ \ Temperature, \qquad T_B = \frac{S\lambda^2}{2K\theta^2} \tag{3.1}$$

$$Radio\ \ Luminosity, \qquad L_{radio-jet} = 4\pi d^2 S\nu \tag{3.2}$$

$$Equipartition\ \ magnetic field, \qquad B = 2.3\left(\frac{aAL_{radio-jet}}{V}\right)^{2/7} \tag{3.3}$$

where, θ, is the source size, d, is the distance of the source, and S, is the flux density. a, in equation 3.2 is the ratio of total energetic particle energy to the total electron energy within the emitting source. A constant value of 50, is assumed for this parameter near the Earth (Moffet et al.1965), A, is the constant shape factor = 1.057×10^{12} cgs units (Moffet et al.1965), and V, is the volume of the emitting region. It should be noted the brightness temperature and equipartition magnetic field mentioned in table 3.16 are lower limits since the intrinsic source size is smaller than the synthesized beam which is used for the calculations. It can be seen from the tables that HMXBs have comparatively high magnetic field.

The source size is inversely proportional to the frequency due to scatter broadening (Tables 3.16 & 3.17). As seen in the tables, the radio flux density is less at lower radio frequencies due absorption effects within the jet medium (Section 3.3.3) However, in a few cases the flux density is rising towards low frequency suggesting no absorption effects at low frequencies (eg: SS433, LS 5039). The brightness temperature calculations ($\leq 10^8$ K) suggests that the radio emission is nonthermal in origin. The equipartition magnetic field in the case of V4641 Sgr is comparable to LMXBs and in the case of Sco X-1 is comparable to HMXBs. These calculations suggest that magnetic field of the order of 10 gauss and above is necessary for the source to be persistent at radio frequencies.

The REXBs with accretion disc type (B) or (C) and with magnetic field of the order of gauss and below are transient in nature at radio frequencies, refer tables 3.1, 3.16, and 3.17. Thus above information suggest that HMXBs with accretion disc type (A) or (C) are efficient systems and have highly developed magnetic field which can accelerate electrons to higher energies within the jet medium as discussed in chapter 1. These population of electrons will continue to emit at low radio frequencies due to increased magnetic field even after loosing energies due to expansion. In the case of LMXBs the radio emission is seen only during flares where high energy electrons are ejected.

3.4 Summary

This chapter presents the results of first ever low frequency radio observations of the galactic microquasars with GMRT. The GMRT observations were carried out at 0.235, 0.610 and 1.28 GHz while the archival GBI data at 2.3 and 8.2 GHz were considered. We have also used the Ryle telescope data at 15 GHz to derive some important informations at centimeter wavelengths. A detailed study of the

Table 3.17: Comparative radio parameters at high frequencies

Source	S_ν (mJy)	size (arc sec)^2	$\nu_.$ (GHz)	T_B (K)	$L_{radio-jet}$ (ergs/sec)	B (mgauss)
	HMXB					
LSI+61303	21.6	0.61	5	1.85×10^{9}	4.88×10^{29}	51.22
V4641 Sgr	400	0.250	4.9	8.35×10^{10}	2.22×10^{32}	159.13
LS 5039	16	0.012	5	6.96×10^{10}	7.61×10^{29}	1226.40
SS433	90	0.010	5	4.69×10^{11}	1.17×10^{31}	2032.45
Cyg X-1	15	0.0005	15	1.74×10^{11}	1.59×10^{30}	26203.70
Cyg X-3	45	0.145	15	1.89×10^{9}	7.63×10^{31}	187.07
Cyg X-3	4000	0.016	5	1.30×10^{13}	2.26×10^{33}	4833.78
	LMXB					
XTE J1118+480	5.3	0.015	8	7.39×10^{9}	1.73×10^{29}	953.18
Cir X-1	280	0.2	5	7.31×10^{10}	4.78×10^{31}	207.40
XTE J1550−564	10	2	8.4	1.05×10^{8}	2.66×10^{30}	13.03
Sco X-1	8	0.0001	5	4.17×10^{12}	3.55×10^{29}	61552.47
GRO J1655−40	2000	1	1.4	1.16×10^{12}	3.24×10^{31}	74.31
GX339-04	0.9	0.0081	8.6	2.33×10^{9}	1.40×10^{29}	803.84
GRS 1915+105	655	1.2	8.6	1.14×10^{10}	9.95×10^{32}	52.6

ref:(1)- J. M Paredes et al. 2005, arXiv.astro-ph/0409226, Chinese journal of A&A

radio spectrum of micro-quasars was carried out in this chapter. The RXTE/ASM X-ray data was used for this work to derive the X-ray state of the source. The results of study is listed below,

- The X-ray light-curve reveals that micro-quasars have 3 classes of accretion disc types; (A)- with no flaring events, (B)- with rare flaring events, and (C)- with frequent flaring events. Most of the HMXBs have accretion disc type (A) and (C) and they are persistent at radio frequencies except V4641 Sgr with accretion disc type (B) which is transient in nature. LMXBs have accretion disc type (B) and (C) and are transient in nature at radio frequencies except Sco X-1 with accretion disc type (A) which is persistent in nature.

- A few of the micro-quasars like GRO J1655−40, XTE J1118+480, and XTE J1748−288 were never detected by GMRT.

- Persistent micro-quasars like 1E1740.7−2942 and GRS 1758−258, which are weak radio emitter at high radio frequencies showed no radio detection at meter-wavelengths suggesting that the radio spectra is flat or inverted.

- GX339-04 and V4641 Sgr were detected on two occasion during radio flares. These flares followed X-ray activity.

- The persistent micro-quasars, Cyg X-1, Cyg X-3, LSI+61303, and Sco X-1 emit at meter-wavelengths and show SSA at these frequencies. Sco X-1 is self absorbed below 0.61 GHz.

- The near simultaneous multi-wavelength monitoring (radio/X-ray/Gamma-ray) data on Cyg X-1 shows a shift in the peak of the spectrum from shorter to longer wavelengths. The delay in the peak is of the order of $\sim$2 days.

- LS 5039 and SS433 show higher flux at 0.235 GHz as compared to 0.61 GHz, with a spectral index of $\sim$ -0.85. This suggest that there is no turn over in these sources upto 0.235 GHz. Further low frequency observations at 150 MHz or lower may help to locate the turn over frequency.

- GRS 1915+105 was extensively monitored at low frequencies during various X-ray states. There exits a good correlation in the X-ray and radio light curve as seen from the 15 GHz data. Radio emission from the source is suppressed in high/soft X-ray and radio activity is seen in the low/hard X-ray state. The simultaneous data at 0.235, 0.61 GHz and near simultaneous observations at 15 GHz suggests that the radio spectrum shows emission from dual components. The centimeter wavelength emission is from the compact jet and the meter wavelength emission is from an extended region at the end of the jet. This extended region acts like a reservoir of low frequency emitting electrons. It is important to note here that, the low frequency component is detected only during radio flares, suggesting that it is coupled with the jet activity. Also a delay in the peak of the radio spectrum from centimeter to meter wavelength is seen. The low frequency emitting component shows a slow rise and decay time.

- Two transient micro-quasars, viz., XTE J1550$-$564 and Cir X-1 were not observed by GMRT due to declination constraints.

- Significant variability is seen in the low frequency data in these sources. Hence, we checked for the effects of RISS. It was found that Cyg X-1 and SS433 is most likely affected by scintillation. LSI+61303, LS 5039, Sco X-1, and XTE J1118+480 may be affected by scintillation; however, detailed series of observations needs to be performed at low frequencies to check this effect. Most of the other micro-quasars appear not to be affected by refractive interstellar scintillation.

- Some of the sources showed spectral index evolution during the flaring activities strongly suggesting the ejection of expanding blobs of plasma. In these cases, the radio jet is optically thick at low radio frequencies during the initial phases of the radio outbursts and subsequently becomes optically thin as the flare evolves.

- Important radio parameters like size, brightness temperature, equipartition magnetic field and radio luminosity were estimated. The brightness temperature suggest that the radio emission is synchrotron in origin. However, at meter wavelengths only an upper limit to brightness temperature and equipartition magnetic field was obtained, since the source remained unresolved and the size of the synthesized beam was used. From the VLBI observations at centimeter wavelengths, it is clear that the equipartition magnetic field is high for HMXBs as compared to LMXBs. Also the size of the source increases at low frequencies due to angular broadening.

Further systematic observations of these sources at low radio frequencies in various radio states is of great importance to further explore the spectral behavior at these frequencies. Simultaneous radio data at various frequencies is necessary to obtain reliable life times, size and various jet parameters of the varying components.

Chapter 4

Radio survey of new gamma-ray sources discovered by INTEGRAL satellite

The INTEGRAL gamma-ray observatory has discovered a variety of hard X-ray/gamma-ray sources in the Galactic plane. Using GMRT, repeated observations were made on these sources to search for the radio counterparts of forty of them at low frequencies. This survey was conducted in order, to study radio emissions from these sources, to provide precise position and to identify new micro-quasar candidates. The source positions were taken from the various ATEL and IAUC announcements reporting their discovery. From the observations we find that 24 of the X-ray sources have radio candidates within the INTEGRAL error circle. Based on the radio morphology, variability and information available from different wavelengths (NVSS, DSS, 2MASS and NED), we categorize them as seventeen Galactic sources (4 unresolved, 7 extended, 6 extended sources in diffuse region) and seven extra-galactic sources (2 unresolved, 5 extended). Detailed account for each of these sources is presented in this chapter.

In this chapter we also present the first ever low frequency radio images of these hard X-ray sources and the best fit positions for the positive detections. We also discuss the radio spectrum of a few sources. The relevance of SSA is discussed in the case of IGR J18406−0539 and power law decay in the case of IGR J06074+2205. The extrapolation of simple SSA model obtained from high frequencies fails to reproduce and under predicts the observed flux density of IGR J17091−3624 at GMRT frequencies. The X-ray variability for some of the sources within the time scales of 100 s to 1 ks as seen in the RXTE/PCA light curves suggests their Galactic origin and possible binary nature. We discuss in detail about four unresolved sources, viz IGR J17091−3624, IGR J17303−0601, IGR J17464−3213, and IGR J18406−0539 which are possible micro-quasars. These sources have been associated with compact sources variable in radio and X-rays. The remaining sources have extended radio morphology and are either diffuse Galactic regions or extra-galactic in origin. A brief description of a few typical sources belonging to each sub-category is provided in this chapter.

4.1 Introduction

Micro-quasars are the recent addition to the list of high energy gamma−ray sources detected by EGRET. Gamma−ray emitting counterpart are recently detected within the field of micro-quasars e.g. LS 5039 and LSI+61303 (Paredes et al. 2005). Relativistic shocks encountered by jets in the ISM gives rise to gamma−ray emissions. Due to lack of highly sensitive gamma−ray instruments

with low background noise, the gamma−ray survey on these sources was not carried out in past. Recently HESS instrument has detected a compact TeV gamma-rays emitting counterpart for the micro-quasar LS 5039. This result has opened a new window to explore the nature of micro-quasars at this wavelength.

Since its launch in Oct 2002 the International Gamma Ray Astrophysics Laboratory, (*INTEGRAL*), has discovered a number of new hard X-ray/ soft γ-ray sources[1] within the Galactic plain mainly towards the Galactic center region. These sources were discovered with the IBIS instrument, which has a large field of view of $29^{\circ} \times 29^{\circ}$ and a sensitivity up to 1 MeV (Ubertini et al. 2003, Lebrun et al. 2003). The IBIS instrument has a point source location accuracy (PSLA) of typically 1 – $3'$. A majority of these soft gamma-ray emitters sources are believed to be Galactic X-ray binaries with a compact object orbiting a companion star (Bird et al. 2004). Some of these sources are identified as AGNs, radio galaxies, pulsars, CVs and dwarf nova. A detailed study of X-ray sources in the multi-wavelength band is essential to understand the emission mechanism and the accretion process on to the compact companion NS or black holes BH. The radio imaging of these sources can establish whether some of these are REXBs and show any micro-quasar like features. Due to their similarity with quasars, the jet feature in micro-quasars provide important information about the underlying physical phenomenon and the possible disk-jet connection which may power the observed emission in different wave bands. Their X-ray, infrared and radio properties can lead to classification schemes.

Since observations of superluminal outflows during the transient burst of GRS 1915+105 (Mirabel & Rodríguez, 1994), a new subclass, characterized by the presence of jets in X-ray binaries, has been established. They are named as micro-quasars. A compact core and two sided radio jets have been commonly observed in these sources during VLBI observations(Mirabel et al. 1999). In most of these sources the compact object is believed to be a BHC; however, for Sco X-1, CI Cam and Cir X-1, the compact companion is determined to be a neutron star. Variability pattern in the radio light curve were seen for GRS 1915+105 (Mirabel et al. 1994, 1997, 1998). The X-ray emission from this source has also revealed a rich class of flux variability and temporal pattern.

We have been carrying out a programme of monitoring of the new *INTEGRAL* sources since Aug 2003 with the GMRT with a view:

1. to map the field of new X-ray sources at low frequencies in order to find the radio counterparts and provide the exact position coordinates with the arcsec resolution of GMRT at meter wavelengths.

2. to determine a possible association of the source by combining the radio, infrared and X-ray data and to establish the nature (low mass X-ray binary (LMXB) or high mass X-ray binary (HMXB)) of the source based on the magnitude of any infrared counterpart. Both these systems have a NS or BH as one of the component. In the case of HMXB the other component is a massive star, usually a Be star or a blue super-giant of $\sim 8 -- 20$ M$\odot$. For LMXBs the second component (donor) is a main sequence star. In some cases the donor can either be a degenerate or an evolved (sub-giant or red giant).

3. to distinguish between Galactic (compact) and extra-galactic (extended) sources based on their statistically known radio morphology.

The radio data at different frequencies can help in unveiling the nature of these new sources and physics underlying the emission/absorption processes (Revnivtsev et al. 2003a).

[1]See http://isdc.unige.ch/∼rodrigue/html/igrsources.html for an updated information on the list of all *INTEGRAL* sources

In this chapter we report the results obtained from radio observations performed on seventeen new sources with GMRT at 0.61 GHz and 1.28 GHz. The selection criteria applied to detect possible radio-X-ray association discussed below are derived from our rigorous study of the known XRBs and BH jet sources. This was initiated in 2001 using GMRT (Pandey et al. 2004) to establish the long term spectral behavior of these sources at radio frequencies correlated to their X-ray properties.

The selection criteria for a true radio-X-ray association of the X-ray sources is as follows:

1. The number of extra-galactic sources with flux densities above 2.5 mJy in the sky at 0.61 GHz in $10' \times 10'$ area is typically ~ 5 whereas the number of sources expected above the flux density of 1.1 mJy in $10' \times 10'$ area at 1.28 GHz is typically ~ 2 (Condon et al. 1999). The number of sources decreases with: (i) the increase in flux density and (ii) decrease in the field area. The above source counts (number of sources) are used as typical limit for the extra-galactic sources in the given area. The number of sources above this limit in the given area are considered as Galactic sources. The occurrence of number of Galactic radio sources in the field of *INTEGRAL* source within the X-ray position error circle is statistically higher in number compared to extra-galactic radio sources. Also this source count varies from the Galactic center to further away along the Galactic plane with lower probability in the latter region.

2. The X-ray binaries have compact radio morphology with the radio emission being non-thermal in origin. The variability in the radio flux density is a prominent feature in these sources. The radio spectra of micro-quasars show flattening or power law decay at high radio frequencies with radio emission coming from the jet, e.g. GRS 1915+105, SS433, Cyg X-1, and spectral turnover at low radio frequencies with radio emission coming from the radio lobe (Ishwara-Chandra et al. 2004). The radio emission is quenched when the source is in a high soft X-ray state. Also the radio emission from a few of these sources is synchrotron self absorbed below 1.28 GHz, e.g. X1812−121, XTE J1720−318, 1E1740.7−294 (Pandey et al. 2004). The X-ray characteristics include prominent fluorescent emission from the iron line at 6.4 keV and a hard X-ray tail showing rapid variability of the order of $\sim 10 - - 100$ s. The infrared and optical counterparts are associated with the X-ray binary source. The infrared emission originates from circumstellar disks undergoing major expansion coincident with phases of X-ray activity and the evaporation of the disk material due to heating gives rise to optical emission. Thus a compact radio source within the 3σ X-ray position uncertainty limit satisfying the above criteria is very likely to be associated with the Galactic X-ray source.

3. The radio sources with extended radio morphology and with their radio emission being non-thermal in origin have a spectral index, $\alpha \sim -0.7$ ($S_\nu = \nu^\alpha$), are classified as extra-galactic radio sources. Their radio emission is mostly non-variable. The X-ray light curve shows variability on larger time-scales; however, variability of the order of ~ 100 s is reported for a few extra-galactic sources. Thus a radio source within the 3σ X-ray position uncertainty limit satisfying the above criteria is most likely not associated with the Galactic X-ray source.

The observations of these forty sources presented here were made between Aug 2003 – Aug 2004 observation cycle with GMRT. The target sources are those discovered during the *INTEGRAL* observation scans on the Galactic plane, and during guest observations and Crab calibrations; they are listed in Table 4.1 and 4.2.

Source	Type	Integral Pos. Unc. 1.6σ	Variable 100s–1ks $\frac{\text{IBIS}}{\text{ISGRI}}$	X-ray Flux 15–40 keV (mCrab)	X-ray/optical/UV/IR/Radio sources in X-ray error circ.
IGRJ00370+6122	HMXB[1,2]	$2'$	Yes		BD+6073
IGRJ01363+6610	HMXB[2]	$2'$	Yes	17	HD9603
IGRJ06074+2205		$2'$	Yes	15	high soft
IGRJ15479−4529		$2'$	Yes	2	
IGRJ16167−4957		$6''$		2	
IGRJ16195−4945	HMXB(?)[3,4]	$16''$			HD146628
IGRJ16207−5129		$2'$			HD146803
IGRJ16316−4028		$3'$	Yes	25	
IGRJ16318−4848	sgB(e) HMXB	$4''$	Yes	50–100	
IGRJ16320−4751	HMXB(?)	$4''$	Yes	10–50	
IGRJ16358−4726	LMXB(?)[5,6] Pulsar[7]	$0.6''$	Yes	20–50 4.63	2MASS J163553−472539
IGRJ16393−4643	HMXB(?) Pulsar[7,8,9,10]	$2'$	Yes	3	
IGRJ16418−4532		$2'$		2	
IGRJ16479−4514		$3'$	Yes	12	
IGRJ16558−5203		$8''$			1RXS J165605−520345 USNO-B1.0 0379−00008129
IGRJ17091−3624	XB[11,12](BHC) ?	$0.8'$	Yes	40	
IGRJ17195−4100		$8''$	Yes		1RXS J171935−410054 USNO-B1.0 0489−00511283
IGRJ17200−3116		$9''$	Yes		1RXS J172006−311702
IGRJ17252−3616	HMXB[13] Pulsar	$2'$			IRAS 17220−3615 NVSS J172510−361614 HD319824
IGRJ17254−3257		$14''$			1RXS J172525−325717 USNO-B1.0 0570−00727635

Table 4.1: Details of INTEGRAL sources observed with GMRT

[2]High mass X-ray binary[1], Reig et al. 2005[2], http://isdc.unige.ch/ rodrigue/html/igrsources.html[3], Sidoli et al. 2005[4], Bird et al. 2004[5], Low mass X-ray binary[6], Revnivtsev et al. 2004[7], Lutovinov et al. 2005[8],Boudaghee et al. 2005[9], Soldi et al. 2005[10], Revnivtsev et al. 2003[11], X-ray binary[12], Zurita et al. 2005[13]

Source	Type	Integral Pos. Unc. 1.6σ	Variable 100s–1ks $\frac{\text{IBIS}}{\text{ISGRI}}$	X-ray Flux 15–40 keV (mCrab)	X-ray/optical/UV/IR/Radio sources in X-ray error circ.
IGRJ17285−2922	XB[1]	2′	Yes		IRAS17252−2922
					[T66b]320
IGR J17303−0601	LMXB	7′′	Yes		H1726−058
					USNO−A2.0 0825−10606993
					1RXS J173021.5−055933
IGR J17391−3021	Be/(NS)	1′′	Yes	150	
	HMXB[2]?	Chandra			
IGR J17456−2901		1′			1LC G359.923−00.013
IGR J17460−3047		2′			
IGR J17464−3213	BHC[1]	0.5′	Yes	60	H1743−322
	LMXB[3]				2MASS 17461525-3213542
					USNO-A2.0 0525-294112269
IGR J17475−2822	Sgr B2[4]	2–3′			
IGR J17488−3253		12′′	Yes		1RXS J174854.7−325444
IGR J17544−2619	HMXB(?)	4′′	Yes	60	
IGR J17597−2201	NS, LMXB	2′	Yes	5	
IGR J18027−1455	Extragalactic[5]	2′	Yes		
IGR J18027−2016	Pulsar[6]	1′		4.06	HD312525
					1LC G000.683−0.035
					IRAS 17594−2021
IGR J18325−0756		2–3′	Yes		
IGR J18406−0539		2–3′			IRAS 18379−0546
					AX J1840.4−0537
					NVSS J184037−054317
					GSC2.2
IGR J18450−0435		2–3′			IRAS 18422−0437
					PMN J1845−0433
IGR J18483−0311		2′	Yes	10	
IGR J18490−0000		2–3′			
IGR J18539+0727	XB[7]	3′	Yes	20	
	(BHC)				
IGR J19140+0951	HMXB[8]	1.3′	Yes	50–100	
	(NS)				
IGR J21247+5058	Radio Galaxy	2′	Yes		

Table 4.2: Details of INTEGRAL sources observed with GMRT

[3] http://isdc.unige.ch/ rodrigue/html/igrsources.html[1], Smith et al. 2003[2], Bird et al. 2004[3], Revnivtsev et al. 2004[4], Masetti et al. 2004[5], Lutovinov et al. 2005[6], Revnivtsev et al. 2003[7], Rodrigue et al. 2005[8]

4.2 Observations and analysis

The radio observations were carried out at 0.61 GHz and 1.28 GHz with a bandwidth of 16/32 MHz using the GMRT (Swarup 1991). The half power beam width for the GMRT antenna at 0.61 GHz is $\sim 43'$ and at 1.28 GHz is $\sim 26'$. The measured position offset of the possible GMRT radio counterparts with respect to the X-ray sources is below $\sim 5'$, hence primary beam corrections do not contribute a signifi cant change to the images. The gain decreases signifi cantly in the fi eld at low radio frequencies, i.e 0.61 GHz, hence gain depression corrections or system temperature corrections were applied to the flux densities of the radio counterparts. The flux density scale was set by observing the primary calibrators 3C286, 3C147 and 3C48. Phase calibrators were observed near the target source for $\sim$ 5 min scans interleaved with 25 min scans on the *INTEGRAL* sources. The sample time was 16 s. The data recorded from GMRT were converted into FITS fi les and analyzed using the Astronomical Image Processing System (AIPS), as per described in Chapter 2. A self calibration on the data was performed to correct for phase related errors and improve the image quality. 7–10% of the data was affected by interference and was carefully removed. Ionospheric scintillation effects were not seen in the 0.61 and 1.28 GHz data during our observations. Possible radio counterparts were detected for twenty four out of forty sources and for other sources no possible radio counterpart was detected within the 3σ error box of the X-ray source.

Tables 4.3, 4.4, 4.5, 4.6, 4.7 and 4.8 summarizes our results for the new discovered hard X-ray sources along with best-fi t radio positions for the counterpart and the position offsets of this counterpart with respect to the X-ray positions. Column 1, 2 and 3 gives the name, date and frequency of observation of the source. Column 4 gives the peak and total flux density for the point and extended source respectively. The rms noise given in column 5 corresponds to the average background noise in the image fi eld and is higher in the Galactic plane. Column 6 and 7 gives the radio poition and the offset in the position with respect to the X-ray source. Column 8 gives the information about the radio morphology of the source and column 9 gives the radio flux density at 1.4 GHz from the NVSS survey.

In the radio images presented in this chapter, the boxes show the known fi eld sources (X-ray, gamma-ray, optical, infrared, radio) from the fi les available from the NASA extragalactic Database (NED), NVSS (Condon et al. 1998), 2MASS and Digital Sky Survey (DSS). The number of infrared and optical sources expected within a $10'$ area in the Galactic region was derived from the image obtained from FITS fi les available from the 2MASS and DSS surveys at: http://skys.gsfc.nasa.gov/cgi-bin/skvadvanced.pl.

The expected number of infrared and optical sources are ~ 6 and ~ 1.2 respectively; however, in the radio images shown in this chapter, only the sources in close proximity to the radio source have been marked. We also discuss briefly the spectral properties in the radio band (non-simultaneous radio observations) of the radio counterparts for which other data are available. The bold circle marked with 'A' indicates a possible GMRT radio counterpart close to the X-ray source.

Imaging at radio wavelengths are specially important since interferometry has the intrinsic capability to provide a precise sub-arcsec position measurements, thus improving the error boxes obtained from X-ray data. In addition, interstellar extinction has very little effect at low radio wavelengths.

4.3 Results

Based on the radio observations performed on the INTEGRAL sources they can be further divided into sources with possible radio counterparts and sources with no radio counterparts. Based on the

radio morphology of each source, they are grouped into point and extended sources. In this section we will discuss the sources belonging to each group in detail.

4.3.1 Point radio sources within the field of *INTEGRAL* sources:

Galactic point sources:

IGR J17091−3624 : This micro-quasar was discovered at a flux density level of $\sim$ 20 mCrab between 40–100 keV (Kuulkers et al. 2003). BeppoSAX detected the source at a flux density level of 14–20 mCrab in the 2–10 keV band, suggesting a very steep photon spectrum consistent with a spectral index of 3.0$\pm$0.4 or kT = 4.3$\pm$1.4 keV from the thermal bremsstrahlung (Zand et al. 2003). During a 3 ks observation of the source with RXTE/PCA in the 2–20 keV band, the observed flux density was $\sim$ 4 mCrab. The X-ray light curve of the source shows a large variability on time scales from several tenths to several tens of seconds. The energy spectrum of the source was fitted by a power law index of 1.43$\pm$ 0.03. No visible absorption was detected at the lower energies (Lutovinov & Revnivtsev 2003b). The combined X-ray data from BeppoSAX and *INTEGRAL* also suggest a variable nature of the source with flare episodes in Apr 2003 and Sep 2003 (Kuulkers et al. 2003). The radio emission from the source region was detected during observations with the Very Large Array (VLA) at 4.9 GHz with a flux density of 1.8$\pm$0.3 mJy and they showed significant variability in flux density (Rupen et al. 2003a).

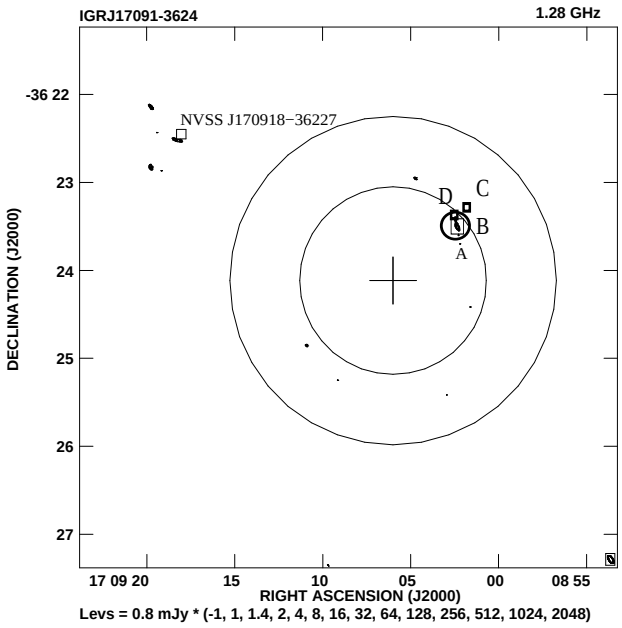

Figure 4.1: GMRT image of IGR J17091−3624 at 1.28 GHz with the *INTEGRAL* position marked with +. The small and large circles shows the *INTEGRAL* uncertainty error circles of 1.6σ and 3σ. The bold circle marked with 'A' show the radio source detected by GMRT. The boxes show the known field sources, B: NVSS 17092−3624, C: DSS J170901−3623 and D: 2MASS J170902−3623.

In our observation with GMRT, a radio source was detected within the 1.6σ position uncertainty

of the X-ray sources at a radio flux density of 1.10±0.16 mJy at 1.28 GHz, at a J2000 position of RA: 17h 09m 02.3s and DEC: −36d 23′ 33″. The rms noise was 0.19 mJy b^{-1}. The flux density at 0.61 GHz was measured to be 2.50±0.73 mJy.

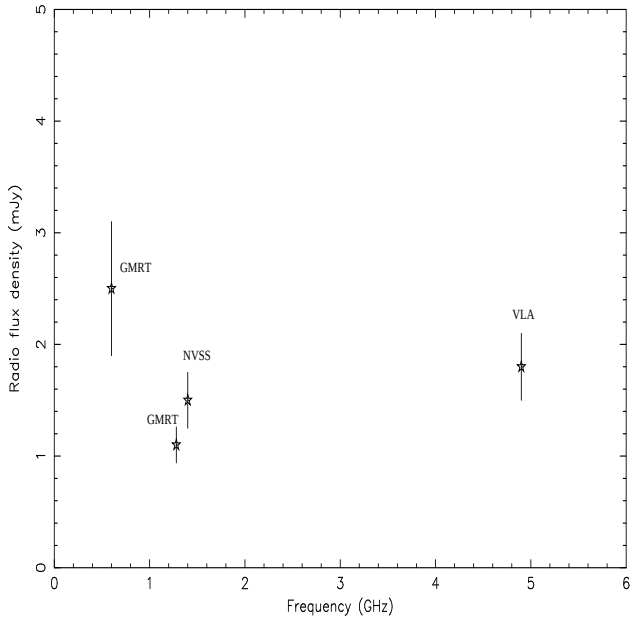

Figure 4.2: Radio spectrum for IGR J17091−3624

The GMRT image of the field is shown in Fig. 4.1. The source morphology is consistent with a point source. The compact nature of the radio source is also inferred from the Gaussian fit to the source flux density using the AIPS routine 'JMFIT'. In our analysis of the NVSS FITS files, we have detected a weak radio source with a flux density of $\sim 1.50\pm0.25$ mJy at the same position. The radio source marked 'A' in the figure lies within the *INTEGRAL* position error circle of the source and is the most likely radio counterpart of the X-ray source. The GMRT (A) and NVSS (B) radio counterparts are coincident in position. The infrared source, (D), and the optical source, (C), coincide in position with the radio source. Thus we confirm that the sources (B), (C) and (D) are associated with the X-ray binary source. Thus the infrared emission may come from a circumstellar disk undergoing major expansion coincident with phases of X-ray activity and the optical emissions are due to heating and evaporation of the disk material. In order to enhance the significance of the possible association of the GMRT source with the X-ray object, we have plotted the radio flux density measurements of the source region at GMRT frequencies of 0.61 and 1.28 GHz in Fig. 4.2. The observed flux density values for the NVSS source at 1.4 GHz and the VLA flux density value at 4.9 GHz are also plotted in the figure for reference. However, the observations are non-simultaneous. The spectral fit to the GMRT data corresponds to the falling power law of the form ($S \propto \nu^{\alpha}$) with $\alpha = -0.62$. This is consistent with the radio emission from the other X-ray binary sources. If the high frequency observations are associated with the same emission region, the radio spectral fit will require a clear inflection to positive slope with $\alpha = +2.73$. This suggests a composite of two separate radio emitting regions for

the source.

IGR J17303−0601 : This source was detected in the Norma arm region (Walter et al. 2004) and in coincidence with the *ROSAT* source 1RXS J173021.5−055933 (Voges et al. 1999, Stephen et al. 2005). Two optical objects with $R \sim 15.5$ and $R \sim 18$ are found within the *ROSAT* error box of $7''$ in the Digitized Sky Survey (DSS) field (Monet et al. 2003, Stephen et al. 2005). Two near-infrared sources in the (2-MASS survey) are also coincident with the optical sources. The optical spectra of both these sources acquired with the Bologna Astronomical Observatory show features identical to other X-ray emitting objects (Masetti et al. 2004). The brighter source within the *ROSAT* error box was considered to be the optical counterpart to IGR J17303−0601. All the optical emission lines of this object are at red shift zero, indicating its Galactic origin. The presence of the He II line strongly indicates that this object is undergoing mass accretion onto a compact star (e.g. van Paradijs & McClintock 1995), thereby suggesting the X-ray source to be a low mass X-ray binary. The optical photometry of the source; however, suggests the hard X-ray source to be an intermediate polar with a spin period of 128 s (Gansicke et al. 2005).

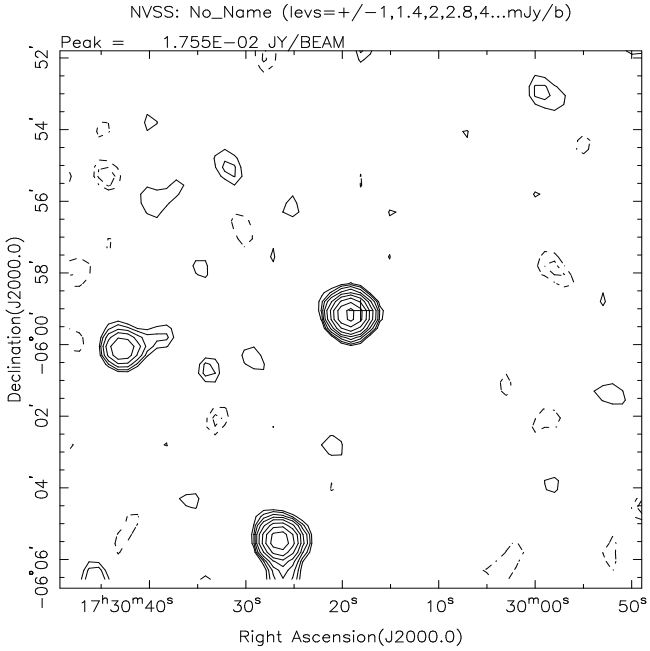

Figure 4.3: NVSS image of IGR J17303−0601 at 1.4 GHz with the *INTEGRAL* position marked with +. Source 'A' is coincident in position with IGR J17303−0601. Sources 'B' and 'C' are field sources. The circle shows the *INTEGRAL* uncertainty error circle of 3σ ($14''$).

The NVSS data at 1.4 GHz with the VLA (Condon et al. 1998) was analyzed to look for radio counterpart. The radio image of the field is shown in Fig. 4.3. A compact point source 'A' of ∼18 mJy at 1.4 GHz is detected coincident with the *INTEGRAL* and *ROSAT* source position. The precise position with the radio observations is RA: 17h 30m 21.50s and DEC: -05^0 $59'$ $33.5''$ (J2000). Two other compact field sources 'B' with radio flux density ∼5 mJy and RA: 17h 30m 45.48 and DEC: -06^0 $01'$ $57.17''$ and 'C' with radio flux density ∼16 mJy and RA: 17h 30m 28.41 and DEC: -06^0 $05'$ $56.27''$, were clearly detected within the field and lie outside the *INTEGRAL* error circle. In order

Source	Date	ν (GHz)	S_ν (mJy)	σ $\frac{mJy}{b}$	Radio Pos. RA & DEC	Pos. off. w.r.t Integral Pos.	Radio Struc.	S_ν (Total) NVSS 1.4 GHz (mJy)
IGR J17091−3624	16/09/03	0.61	2.50±0.73	0.60	17h 09m 02s±0.191	0.99′	P	1.5
					−36d 23′ 33′′±2.84		G	
	02/02/04	1.28	1.10±0.16	0.19				
IGR J17303−0601	25/06/04	0.61	17.28±2.38	2.21	17h 30m 18.11s±0.18	1.94′	P	18
					-05d 59′ 03.01′′±0.16		G	
IGR J17464−3213	25/07/04	0.61	2.75±0.52	0.50	17h 46m 16.14s±0.28	1.03′	P	≤2.4
					-32d 13′ 26.67′′±0.21		G	
IGR J18406−0539	23/07/04	0.61	28.03±0.76	0.76	18h 40m 37.61s±0.12	4.31′	P	165
					-05d 43′ 17.99′′±0.18		G	

Table 4.3: Possible Galactic compact radio counterparts of target INTEGRAL sources observed with GMRT

[4]P: Point, G: Galactic

to search for the radio source at lower frequencies GMRT observations on this source was performed at 0.61 GHz. No radio source was found coincident in position with the NVSS source 'A' during our observations at 0.61 GHz. The 3σ upper limit in the GMRT image was $\sim$6 mJy and the rms noise was $\sim$1.84 mJy beam^{-1}. The sources 'B' and 'C' with radio flux density $\sim$18 mJy and $\sim$15.5 mJy were clearly detected coincident in position with the NVSS sources.

At radio wavelengths the detection at 1.4 GHz and non-detection at 0.61 GHz with positive detection of other field sources suggest that IGR J17303−0601 is a radio emitting X-ray binary (REXB). And the source is highly variable or absorbed at low frequencies. The absorption may be due to synchrotron self absorption process dominant at low frequencies as seen for most of the X-ray binaries (Pandey et al. 2004, Pandey et al. 2006). In both the cases, a non-thermal origin of the radio emission is favored. Thus from the above observational facts, we suggest that IGR J17303−0601 may be a possible new micro-quasar candidate. Like a few other sources in the Norma Arm region even this source was highly absorbed at low frequencies (Pandey et al. 2005b). even this source was highly absorbed at low frequencies (Pandey et al. 2005b).

The source also staisfies our classification scheme discussed in chapter 3 based on the X-ray light-curve and nature of the companion star. The RXTE/ASM X-ray light-curve for the source is quasi-persistent in nature and the companion star in this case is a LMXB, this points towards the transient nature of the radio counterpart, as seen above.

IGR J17464−3213 : This transient BH candidate was detected by the *INTEGRAL* satellite on 21st March, 2003 (Revnivtsev et al. 2003). The position of the source is consistent with the position of the HEAO source H1743−322 (Markwardt & Swank 2003, Gursky et al. 1978). The spectral fit to the JEM-X/IBIS data shows the presence of a soft component fitted by a multi color disk black body and a hard power-law tail with photon index of 2.2 which extends to 80 keV. The observations made during the outburst shows that the light curve is typical of a X-ray nova (Steeghs et al. 2003). It is therefore believed that IGR J17464−3213 is a classical X-ray nova – a LMXB harboring a BH – which experienced a recurrent outburst in 2003 (Lutovinov et al. 2005).

The RXTE pointed observations on 28th March, 2003 gave mean fluxes 50, 200 and 220 mCrab in 2 – 10, 15 – 40 and 40 – 100 keV range respectively. A strong quasi periodic oscillation (QPO) with the period $\sim$ 20 s was also seen in the X-ray light curve. The X-ray spectrum is consistent with an absorbed power law with photon index 1.49$\pm$0.01 and an absorption column of 2.4×10^{22} cm^{-2}. Compton reflection signatures are seen in the continuum spectrum (Grebenev et al. 2003, Capitanio et al. 2005).

The RXTE monitoring of the source between May – July, 2004 observed IGR J17464−3213 in several BH states and revealed various types of variability, including QPOs of 7.8 Hz (Homan et al. 2005).

During the follow up observations with the VLA on 30th, March and 1st April, 2003 a compact, variable source was detected at 4.8 GHz at, RA: 17h 46m 15.61 $\pm$ 0.01s, DEC: -32^0 $13'$ $59.9 \pm 1.0''$ (J2000) and approximately $0.64'$ from the original *INTEGRAL* position. It is consistent with the position of H1743−322 (Swank et al. 2004). The source flux was 4 mJy on 30th March, and had brightened by about 50% on 1 April. A strong radio flare was detected on 8th April, 2003 (Rupen et al. 2003a). The ATCA radio observations of H1743−322 performed from Nov, 2003 – June, 2004 led to the discovery of large-scale radio jets on each side of the BHC H1743−322 (Corbel et al. 2005).

The optical observations in the *I*-filter at the radio position show a marginal detection of an optical counterpart at a level of $I_{mag} \sim 20$ (Khamitov et al. 2003, Remillard et al. 2003, Steeghs et al. 2003, Rupen et al. 2003b).

On 3rd Jul, 2004 a second outburst was detected in the X-ray light curve of IGR J17464−3213

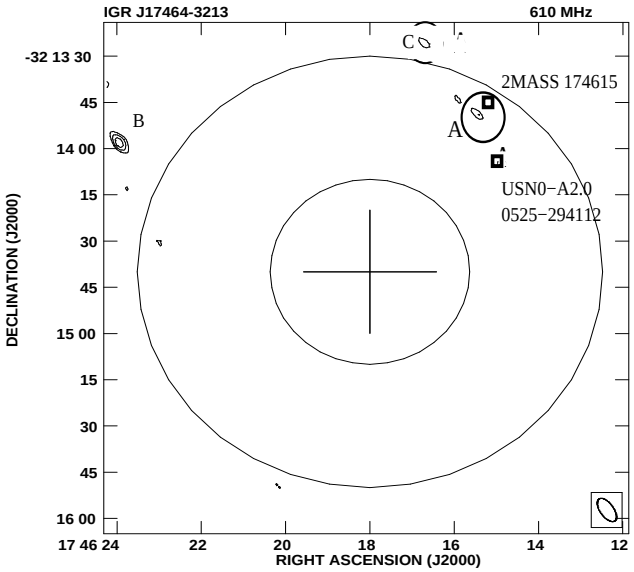

Figure 4.4: GMRT image of IGR J17464−3213 at 0.61 GHz with the *INTEGRAL* position marked with +. The small and large circles shows the *INTEGRAL* uncertainty error circles of 1.6σ and 3σ. The contour levels are 2 mJy × 1, 1.4, 2. The field sources 2MASS 17461525-3213542 and USNO-A2.0 0525-294112269 are marked in the figure

and it went into hard X-ray state (Swank et al. 2004). During the end of the X-ray state, the radio source was not detected at the position mentioned by Rupen et al. (2003a) until 4th Aug 2004 during VLA observations at 4.86 GHz; however, it was positively detected by VLA on 5th Aug 2004, with a flux density of 1.96±0.15 mJy (Rupen et al. 2004). During GMRT observations on 25th July, 2004, a radio source was detected coincident with the VLA position reported by Rupen et al. 2003a, at a radio flux density of 2.75±0.52 mJy (source 'A' in Fig. 4.4). It is also interesting to note that two compact sources, (B) of flux level 6 mJy at position coordinates, RA: 17h 46m 24.17s and DEC: $-32^0\ 13'\ 59.92''$ and (C) of flux level 2 mJy at position coordinates, RA: 17h 46m 16.55s and DEC: $-32^0\ 13'\ 29.89''$ are also detected within the field of IGR J17464−3213; however, they clearly lie outside the *INTEGRAL* 3σ position error circle. The analysis of the NVSS data at 1.4 GHz shows no point sources coincident with the radio sources (A) and (B), detected by the GMRT; however, the source (C) was positively detected in the NVSS field at a flux level of ∼1.05 mJy. There were no other radio observations reported at this epoch. Hence two variable radio sources (A, B) are detected within the field of *INTEGRAL* source; however, the source (A) is most likely to be associated with the hard X-ray source and it clearly shows transient behavior at radio wavelengths like other LMXBs. Thus from the above observational facts, we suggest that IGR J17464−3213 may be a possible new micro-quasar candidate.

In order to determine IR and optical counterparts, we have analyzed the 2MASS and USNO data near the radio source (A) position for the field of IGR J17464−3213. An IR point source, 2MASS 17461525-3213542 with coordinates RA: 17h 46m 15.25s and DEC: $-32^0\ 13'\ 54.2''$ and magnitudes, $J = 16.2, H = 13.8, K = 13.16$ and an optical source, USNO−A2.0 0525−294112269 with position coordinates RA: 17h 46m 14.77s and DEC: $-32^0\ 14'\ 06.02''$ and magnitudes, $B = 19.6, R = 17.4$ lies

within the error circle of the hard X-ray source but separated from the radio source more than the position error box (Voges et al. 2004). Thus, if H1743 322 is most likely associated with IGR J17464 3213, then no optical and infrared counterpart has been found.

IGR J18406−0539 : The source was discovered during the observations of the Sagittarius arm region by IBIS telescope during the spring of 2003 (Belanger et al. 2004). We have carried out cross identification of this source with the data available from various catalogues, to identify the nature of the source. A hard X-ray source, AX J1840.4−0537 discovered during ASCA observations with RA: 18h 40m 24s and DEC: -05^0 37′ 00″ lies within the position error circle of the source (Bamba et al. 2003). The field is further complicated by the presence of an optical source, GSC2.2 with magnitudes $B = 16$ and $R = 19$ and position RA: 18h 40m 38.094s and DEC: -05^0 43′ 19.30″ lying within error circle (Monet et al. 1998).

An IR point source, IRAS J18379−0546 (Cutri et al. 2003), with coordinates RA: 18h 40m 38.04s, DEC: -05^0 43′ 20″ and magnitudes $J = 12.89$, $H = 11.91$, $K = 11.61$, also lies within the 2σ position error ellipse of the hard X-ray source. Masetti et. al 2006, based on their optical observations suggest that the source is a high mass X-ray binary.

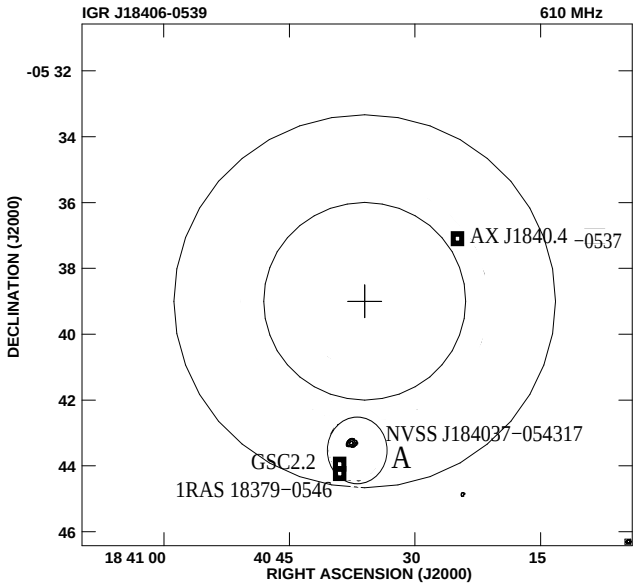

Figure 4.5: GMRT image of IGR J18406−0539 at 0.61 GHz with the *INTEGRAL* position marked with +. The small and large circles shows the *INTEGRAL* uncertainty error circles of 1.6σ and 3σ. The contour levels are 5.5 mJy × 1, 2, 4, 8. The boxes show the ASCA, optical and IR sources within the *INTEGRAL* error circle. The field sources AX J1840.4−0537, 1RAS 18379−0546, NVSS J184037−054317 and GSC2.2 are marked in the figure

During GMRT observations a point source was detected with radio flux density of ∼ 28 mJy and at RA: 18h 40m 37.61s and DEC: -05^0 43′ 17.99″, which is 4.31′ away from the hard X-ray source. The NVSS image of the field also shows a point source of 165 mJy coincident with the GMRT position. Fig. 4.5 shows the radio image of the field of IGR J18406−0539 at 0.61 GHz with the other known field sources.

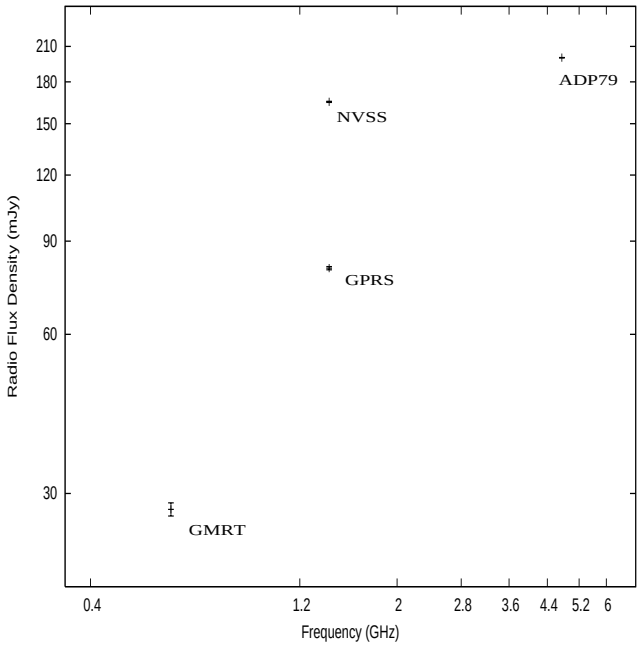

Figure 4.6: Radio spectrum for IGR J18406−0539

Using the various radio survey, we have computed the radio spectrum for the source (non-simultaneous measurement) in Fig. 4.6. It can be seen from the figure that the spectrum is highly inverted at meter wavelengths. It is interesting to note that the NVSS survey at 1.4 GHz and the Galactic Plane Radio-source Survey at 1.4 GHz (Zoonematkermani et al. 1990) for the compact Galactic source at different epochs gave the radio flux density of 165 mJy and 80 mJy respectively. A variability in the radio flux density by a factor of two is clearly measured. The Galactic plane survey at 4.87 GHz by (Altenhoff et al. 1979) gave the radio flux density for the source as 200 mJy. This information implies that the source is variable in nature and a possible micro-quasar candidate. As can be seen in fig.3, the radio source detected with GMRT (and coincident with the VLA/NVSS source), has no IR/optical counterpart. It is important to do further observations in the optical and infrared band to find the counterpart and establish the nature of the companion star.

IGR J18406−0539 staisfies our classification scheme discussed in chapter 3 based on the X-ray light-curve and nature of the companion star. Though the RXTE/ASM X-ray light-curve for the source is not available, the companion star in this case is a HMXB, this points towards the persistent nature of the radio counterpart, as seen above.

Compact extra-galactic sources:

IGR J06074+2205 : The transient X-ray source IGR J06074+2205 was detected with a flux density of ~ 7 mCrab between 3–10 keV by *INTEGRAL* (Chenevez et al. 2004). The hardness ratio derived from the RXTE/ASM light curve suggests that the source was in a high state during our observations. The EGRET source 3EG J0617+2238 lies close to the X-ray source; however, it is likely to be associated with the SNR IC443 (Torres et al. 2003). GMRT observations for the source were made on four occasions during Feb – May 2004 and a radio source was discovered within the *INTEGRAL* position uncertainty limit of 1.6σ (~ 2').

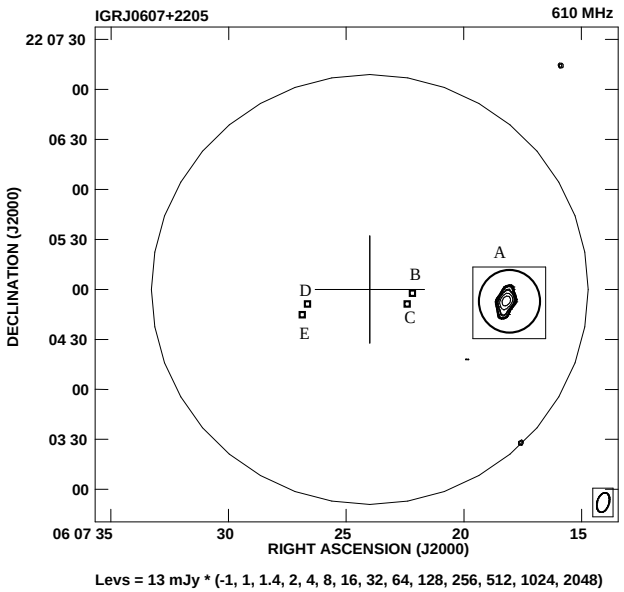

Figure 4.7: GMRT image of IGR J06074+2205 at 0.61 GHz with the X-ray source position in the center marked with + . The large circle represents the *INTEGRAL* uncertainty error circle of 1.6σ. The bold circle marked with 'A' shows the radio source detected by GMRT. The box indicates the known NED field source, A: NVSS J060718+220452, B: DSS J060722+220500, C: 2MASS J060722+220453, D: DSS J060727+220453 and E: 2MASS J060727+220445

Fig. 4.7. shows the GMRT radio image of the IGR J06074+2205 field at 0.61 GHz with a source with a flux density level of $\sim$ 80 mJy close to the X-ray source position (offset of 1.29 $'$ with respect to the *INTEGRAL* position). The compact nature of the radio source is inferred from the Gaussian fit to the source. The GMRT position coordinates are (J2000) RA: 06h 07m 18.45s and DEC: +22d 04$'$ 52.49$''$. The source was also detected at 1.28 GHz by GMRT on 1st Feb 2004 at a flux density of $\sim$ 36 mJy. An observation of this region with the Ryle Telescope at 15 GHz on 29th Jan 2004, 3 days before our observations, showed an unresolved flux density of 4.0$\pm$0.2 mJy, at the NVSS J2000 position (Pooley 2004). The positive detection of the source at different epochs with GMRT at 0.61 GHz clearly suggests a persistent nature for the source in the radio region. The source has shown small variability in the radio flux density.

In Fig. 4.8, we plot the radio spectrum of the source using all available data. It is seen from the figure that the data can be represented by a power-law of the form ($S_\nu \sim \nu^\alpha$). The spectral index at higher frequencies is derived as -0.70 ± 0.08. A power-law nature of the radio spectrum is typical for a non-thermal emission arising from an optically thin medium similar to that produced in the jets interacting with the ambient medium, as seen in extragalactic sources. The hypothesis of a continuous jet can also lead to X-ray emission in the hard X-ray band due to inverse Comptonization of thermal disk photons by a corona (e.g. Markoff & Nowak 2004). Fig. 4.7 also shows infrared (2MASS J060727+220453, C and 2MASS J060727+220445, E) and optical (DSS J060727+220453, D and DSS J060722+220500, B) sources present in the 1.6σ error circle lying close to the X-ray source and thus showing no possible association between the radio and the infrared/optical sources.

Source	Date	ν (GHz)	S_ν (mJy)	σ $\frac{mJy}{b}$	Radio Pos. RA & DEC	Pos. off. w.r.t Integral Pos.	Radio Struc.	S_ν (Total) NVSS 1.4 GHz (mJy)
IGR J06074+2205	01/02/04	1.28	36.00±1.12	0.64	06h 07m 18.45s±0.005	1.29′	P	36
					22d 04′ 52.49′′±0.03		E	
	09/04/04	0.61	78.65±1.29	1.33				
	12/04/04	0.61	83.49±1.30	0.65				
	02/05/04	0.61	79.86±1.42	1.57				
IGR J18027−1455	02/05/04	0.61	10.72±2.25	2.32	18h 02m 42.75s±0.134	4.18′	P	12.3
					−14d 50′ 49.21′′±3.93		E	

Table 4.4: Extragalactic compact radio sources detected in the fi eld of target INTEGRAL sources observed with GMRT

[5]P: Point, E: Extragalactic

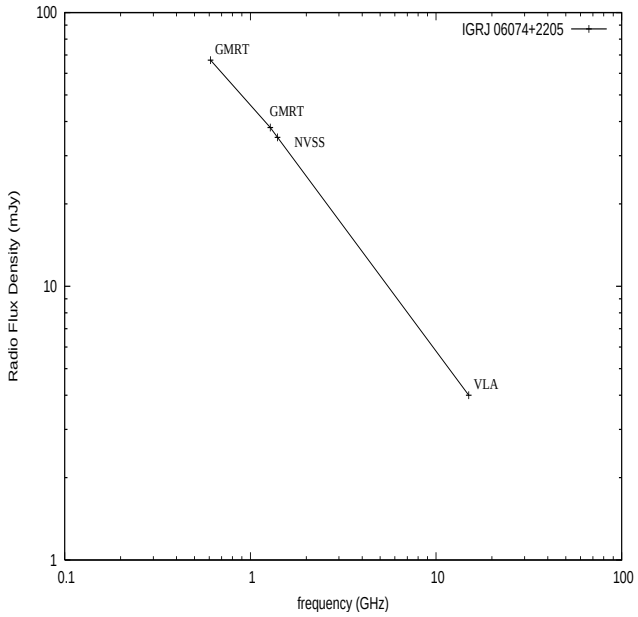

Figure 4.8: Radio spectrum for IGR J06074+2205

IGR J18027−1455 : This source is an AGN candidate located in the Norma arm region (Walter et al. 2004, Masetti et al. 2004). A faint ROSAT X-ray source 1RXS J180245.5−145432 (Voges et al. 2000) lies well within the IBIS/ISGRI error circle. Two weak radio sources were discovered in the NVSS field at 1.4 GHz (Combi et al. 2004). The first source, NVSS J180239−145453, located at J2000.0 ICRS position of RA: 18h 02m 39.94s($\pm$0.25s), DEC: $-$14d 54′ 53.6″($\pm$3.3″) and 0.51 arcmin away from the X-ray source has a flux density of 6.9 mJy. The 2MASS image of the field gives an infrared source, 2MASS J180239−145453, coincident in position with the radio source NVSS J180239−145453. The second source, NVSS J180247−145451, at J2000.0 ICRS position of RA: 18h 02m 47.37s($\pm$0.13s), DEC: $-$14d 54′ 51.6″($\pm$2.2″) is located 0.28 arcmin away from the X-ray position and has a flux density of 10.5 mJy. The field is further complicated by the presence of an extended IR source, 2MASXi J1802473−145454, with coordinates RA: 18h 02m 47.3s, DEC: $-$14d 54′ 55″ and magnitudes $J = 13.18$, $H = 12.02$, $K = 10.94$, within the 2σ position error ellipse of the second radio source. The average optical magnitudes of this IR source are $B = 19.3$, $R = 14.9$ and $I = 13.8$ in the USNO-B1.0 catalog (Combi et al. 2005). The source has an optical counterpart DSS J180241−145453. The sources NVSS J180247−145451, 2MASXi J1802473−145454, DSS J180241−145453 and 1RXS J180245.5−145432 are therefore likely to be associated with the counterparts of IGR J18027−1455 (Combi et al. 2005).

The GMRT observations were made at 0.61 GHz and a image of the field is shown in Fig. 4.9. It is seen from the figure that GMRT data did not yield any significant flux from the directions of NVSS J180239−145453 (E), NVSS J180247−145451 (C), 2MASS source (F) or the ROSAT (B) source position. The only point radio source seen in the GMRT data, (A), was at a flux density of 10.72$\pm$2.25 mJy and is coincident with the NVSS source J180242−145049. The GMRT position for the radio source is RA: 18h 02m 42.75s and DEC: $-$14d 50′ 49.21″ with position offset 4.18′ with respect to the *INTEGRAL* position. The rms noise was 2.3 mJy b^{-1} and the NVSS flux density for the source is 12.3 mJy. With the detection of a higher flux density at 0.61 GHz compared with NVSS data, we can infer that NVSS J180242−145049 is a flat spectrum source in the 0.61 GHz to 1.4 GHz

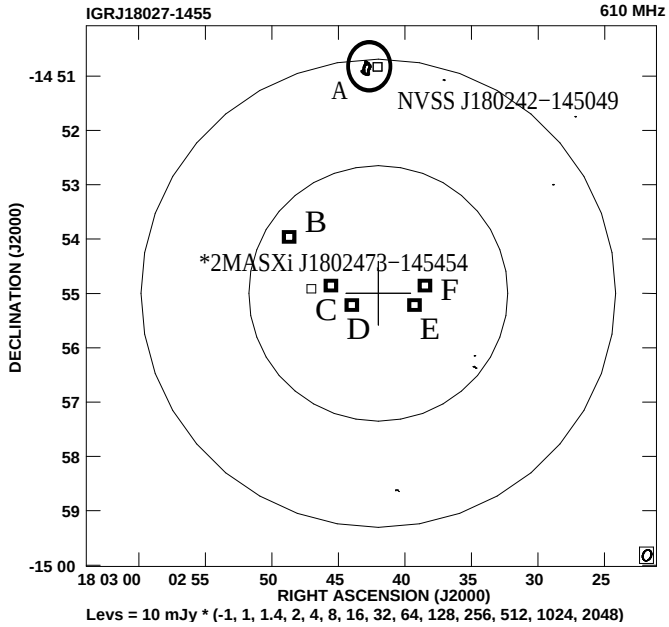

Figure 4.9: GMRT image of IGR J18027−1455 at 0.61 GHz with the *INTEGRAL* position marked with +. The small and large circles shows the *INTEGRAL* uncertainty error circles of 1.6σ and 3σ. The bold circle marked with 'A' shows a radio source detected by GMRT. The boxes show known field sources, B: 1RXS J180245.5−145432, C: NVSS J180247−145451, D: DSS J180241−145453, E: NVSS J180239−145453.6 and F: 2MASS J180239−145453.

range, assuming that the source is persistent in nature.

Non- detection of the 2 radio sources closest to the *INTEGRAL* X-ray source position during our observation, suggests that the radio sources show spectral turnover at low frequencies or are variable in nature. However, in both the cases, a non-thermal origin of the radio emission is clearly favoured. Thus considering the NVSS flux density at 1.4 GHz for the source NVSS J180247−145451 and the upper limit of <7 mJy from GMRT observations at 0.6 GHz, the spectral index derived is $\alpha = 0.48$. The RXTE/ASM light curve for the hardness ratio of the X-ray source suggests that it was in a high soft state during our observations. Thus, NVSS J180247−145451 (C) is a possible radio counterpart of the X-ray source. The non-detection of NVSS J180239−145453 (E) and NVSS J180247−145451 (C) with GMRT in May 2004 and a clear detection in the NVSS survey is consistent with the binary nature of the X-ray source.

However, observation of IGR J18027−1455 region with the GMRT (2nd Mar 2005) showed an evolution of the previous trends followed by the source in the radio regime. We have detected radio emission at 0.61 GHz in the direction of the *INTEGRAL* source coincident in position with the NVSS (E) and (C) sources; see Fig. 4.9. The radio morphology reveals the extended nature of the sources. The (E) and (C) sources have GMRT flux densities of 9.00 ± 0.33 and 5.00 ± 0.35 mJy, respectively. A clear low frequency radio variability is established for the source by our observations. The ASM light curve for the source shows a flaring episode during MJD 53350 – 53360 i.e 1st – 11th Dec 2004. This enhances the significance of the radio–X-ray association.

The above results accomplishes the major goal of this work. The other information available later

in this chapter forms an important by product of this work. In the next section, we will discuss about the next class of hard X-ray sources with extended possible radio counterparts.

4.3.2 Extended radio sources within the field of *INTEGRAL* sources:

Extended Galactic sources:

Among the rest eighteen sources, thirteen hard X-ray sources do show extended radio morphology within the position error circle. The available X-ray spectra on a few of these sources suggest their binary nature and galactic origin (refer table 1). No known extragalactic radio sources from the NED catalogue lie in the position error circle of these *INTEGRAL* sources and in coincidence with GMRT position. The observed radio emission with morphology non similar to the radio galaxies and with no known extragalactic identification therefore suggests that these extended sources may most probably be associated with the radio emitting regions within the galaxy.

From the GMRT data, based on their radio morphology, the thirteen *INTEGRAL* hard X-ray sources can be grouped in two classes; (a) extended Galactic source and (b) extended source typical of the diffuse emission regions. Seven sources belong to group (a) and six sources belong to group (b). We describe below a few typical examples from each group.

IGR J15479−4529 : This source was discovered by *INTEGRAL* in Feb, 2003 observations of Black Hole Candidates (BHC) 4U 1630−47 at a flux density level of $\sim$ 3 mCrab between 20–40 keV (Tomsick et al. 2004). An X-ray source 1RXS J154814.5−452845, which lies at the distance of $3'$ from IGR J15479−4529 has been detected during XMM-Newton observation of the source field in the energy range below 10 keV (Haberl et al. 2002).

During the GMRT observation, a radio source with a total flux density of 22.2 mJy was detected within the position error box of 3σ of the hard X-ray source and is shown in Fig. 4.10. The GMRT position of the source is (J2000), RA: 15h 47m 44.26s and DEC: -45d $32'$ $35.22''$. The rms noise in the GMRT data was 0.5 mJy b^{-1} in the source direction. The position offset with respect to the *INTEGRAL* position is $3.98'$. The radio morphology of the source suggests that the source is extended in nature. No NVSS image is available for comparison to our measurement. In the absence of RXTE/ASM light curve, it is difficult to comment whether the X-ray source was in the high soft or low hard state during our measurements. It is seen from the figure that the position coordinates of the radio source do not coincide with those of IRXS J154814.5− 452845 (D) but they coincide with those of the infrared (2MASS J1547−4532, C) and optical (DSS J1547−4532, B) sources in position, thus suggesting a possible association of the radio and optical/infrared sources. From the above information we conclude that the radio source is not associated with the X-ray source. Since the X-ray counterpart is expected to fall in 90% of the *INTEGRAL* position error circle, i.e, within a distance of 1.6σ, this X-ray source may be a possible candidate for further observations to look for counterparts.

IGR J16479−4514 : is a weak hard X-ray transient source with an observed flux density of $\sim$ 8 mCrab between 25–50 keV (Molkov et al. 2003). The EGRET source 3EG J1655−4554 (Romero et al. 1999) is located close to the X-ray source. The RXTE/ASM hardness ratio suggests that the source was in a high soft state during our observations. The ASM light curve for the source shows that the X-ray flux density between 1st Jan and 28th Feb 2003 was relatively constant, though irregular large random spikes were seen.

During our observations with GMRT in Feb 2004, a bright radio source was detected within the

Source	Date	ν (GHz)	S_ν (mJy)	σ $\frac{mJy}{b}$	Radio Pos. RA & DEC	Pos. off. w.r.t Integral Pos.	Radio Struc.	S_ν (Total) NVSS 1.4 GHz (mJy)
IGR J15479−4529	02/02/04	1.28	22.2	0.5	15h 47m 44.26s±0.105 −45d 32′ 35.22′′±1.76	3.98′	E G	N/A
IGR J16207−5129	30/07/04	0.61	60.50	0.78	16h 20m 48.54s±0.77 -51d 29′ 50.01′′±0.98	1.33′	E G	N/A
IGR J16479−4514	02/02/04	1.28	2445.45	1.24	16h 47m 47.75s±0.153 −45d 17′ 07′′±1.97	3.30′	E G	N/A
IGR J16558−5203	30/07/04	0.61	27.24	0.78	16h 55m 46s±0.04 -52d 03′ 58′′±1.04	0.69′	E G	N/A
IGR J17285−2922	25/07/04	0.61	74.88	0.59	17h 28m 28.75s±0.07 -29d 21′ 04.51′′±1.24	0.96′	E G	$\leq$2.7
IGR J17460−3047	30/07/04	0.61	2.50	0.46	17h 45m 59.69s±0.03 -30d 46′ 58.00′′±2.33	0.076′	E G	$\leq$2.3
IGR J18450−0435	23/07/04	0.61	207.94	0.76	18h 45m 12.05s±1.06 -04d 40′ 05.99′′±1.69	5.90′	E G	74

Table 4.5: Extended radio sources detected in the fi eld of target INTEGRAL sources observed with GMRT

[6]G: Galactic, E: Extended

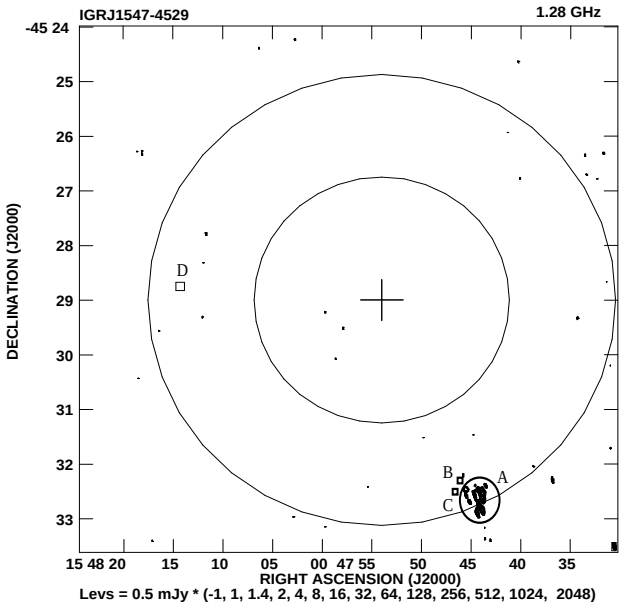

Figure 4.10: GMRT image of IGR J15479−4529 at 1.28 GHz with the *INTEGRAL* position marked with + in the center. The small and large circles in the figure represent the *INTEGRAL* position uncertainty error circles of 1.6σ and 3σ. The bold circle marked with 'A' shows the radio source detected by GMRT. The boxes show the known NED field sources, B: DSS J1547−4532, C: 2MASS J1547−4532 and D: IRXS J154814.5−452845.

INTEGRAL position uncertainty limit of 1.6σ. The flux density recorded at 1.28 GHz is $\sim$ 2.50 Jy with the rms noise of $\sim$ 1.24 mJy. Fig. 4.12. shows the 10′ image of the field of IGR J16479−4514.

The position offset is 3.30′ with respect to the X-ray source position. The radio position of the source is (J2000) RA: 16h 47m 47.75s and DEC: −45d 17′ 07′′. There is no NVSS image of the field. Radio morphology of the source suggests it is an HII region. While the photoelectric effect heats the gas in the compact HII region leading to ionized hydrogen, the dominant cooling process is mainly through recombination giving rise to free-free radio emission. Thus radio emission from this source should be thermal in nature. The infrared source 2MASS J164745−451653 (B) coincides in position with the radio source. Due to the extended nature of the radio source we conclude from our observations that the radio and infrared sources are not associated with the Galactic X-ray source.

In the Fig. 4.12 we have plotted representative radio images for the group. The image shown in figure 4.11 is similar to reminscent of the molecular clouds while figure 4.12 is the one having an extended jet emission. The remaining five hard X-ray sources, namely, IGR J16207−5129, IGR J16558−5203, IGR J17285−2922, IGR J17460−3047 and IGR J18450−0435 also belongs to group (a) and their information is listed in Table 4.5. Except IGR J17285-2922, all sources are located in the Norma Arm region and have high probability of being galactic in nature. The X-ray spectrum of IGR J17285−2922 shows XB characteristics (Barlow et al. 2004); however, the nature of remaining sources is not yet identified. Positive detection of extended radio emission at low frequencies, associated with the galactic X-ray sources seen in the GMRT data suggests the presence of a new class of galactic extended radio sources.

Extended Galactic sources in diffuse region:

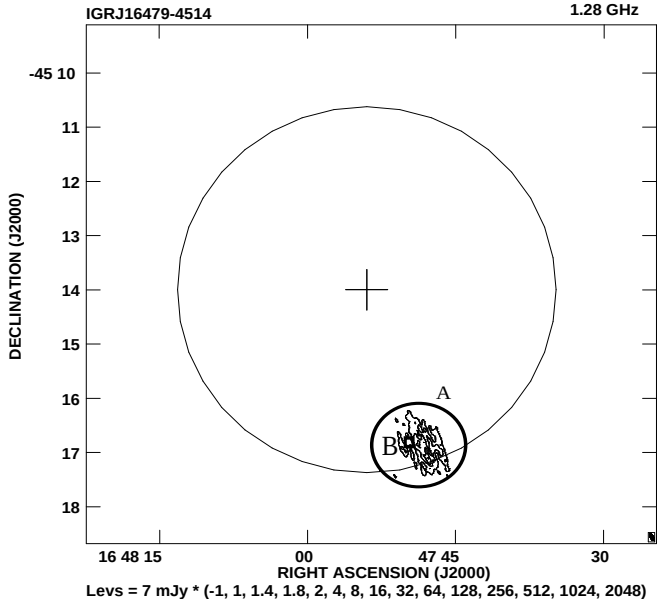

Figure 4.11: GMRT image of IGR J16479−4514 at 1.28 GHz with the *INTEGRAL* position marked with + . The circle shows the *INTEGRAL* uncertainty error circles of 1.6σ. The bold circle marked with 'A' shows the radio source detected by GMRT and the box shows the known field source, B: 2MASS J164745−451653.

Six sources, viz IGR J16167−4957, IGR J16195−4945, IGR J16393−4643, IGR J17252−3616, IGR J17254−3257, and IGR J17475−2822 belongs to group (b). Except IGR J17475−2822, all the sources in this group were detected in the Norma Arm region (refer table 4.1, 4.2 and 4.6).

As seen from Fig. 4.13, due to the large extent of the radio emission, it is difficult to associate a single region with the X-ray source, even though the radio emission lies within the position error circle of the X-ray source. The sources IGR J16393−4643, IGR J17456−2901, IGR J17460−3047 and IGR J17475−2822 have crowded fields with large number of field sources >20, as expected from the diffuse regions. Therefore, we conclude that, none of these radio sources may be associated with the *INTEGRAL* sources.

Extended extragalactic sources:

The Galactic binary X-ray sources are mostly unresolved at arcsec scale (Pandey et al. 2005a). The extended sources can thus be catagorized as extragalactic in nature. From our GMRT observations, we find that for the remaining five sources, the radio emission observed in their direction are extended in nature and having a double source morphology, which is typical of the extragalactic sources. Hence, I classify these as extragalactic radio sources. In Fig. 4.14, I have plotted the GMRT image of IGR J17195-4100 taken at 0.61 MHz. The data clearly suggests the sources to be a a radio galaxy. The cross identification with the NED catalogue (Voges et al. 1999, Condon et al. 1982, Pappa et al. 2001) also confirms their extragalactic nature of both these regions. In regards to the true association of the radio source with the hard X-ray source, it is quite likely that the X-ray sources are indeed extragalactic. No X-ray spectral data is yet available to infer the galactic origin of the source.

Source	Date	ν (GHz)	S_ν (mJy)	σ $\frac{mJy}{b}$	Radio Pos. RA & DEC	Pos. off. w.r.t Integral Pos.	Radio Struc.	S_ν (Total) NVSS 1.4 GHz (mJy)
IGR J16167−4957	23/07/04	0.61	725	2.90	16h 16m 44.29s±0.91 -49d 57′ 10.02′′±0.71	0.12′	E DG	N/A
IGR J16195−4945	30/07/04	0.61	256.4	0.84	16h 19m 35.07s±0.21 -49d 44′ 59.01′′±0.28	0.84′	E DG	N/A
IGR J16393−4643	23/07/04	0.61	79.25	1.63	16h 39m 03.9s±0.51 -46d 42′ 15.55′′±0.59	2.58′	E DG	N/A
IGR J17252−3616	25/07/04	0.61	36.74	1.88	17h 25m 11.09s±1.71 -36d 16′ 48.01′′±0.20	0.82′	E DG	700
IGR J17254−3257	25/07/04	0.61	359.65	0.43	17h 25m 24s±1.22 -32d 55′ 10′′±1.33	3.12′	E DG	$\leq$2.5
IGR J17475−2822	23/07/04	0.61	12.50	1.27	17h 47m 25.68s±0.62 -28d 22′ 21.96′′±1.21	1.02′	E DG	1920

Table 4.6: Extended radio sources in diffuse regions detected in the fi eld of target INTEGRAL sources observed with GMRT
[7]DG: Diffuse Galactic sourc, E: Extended

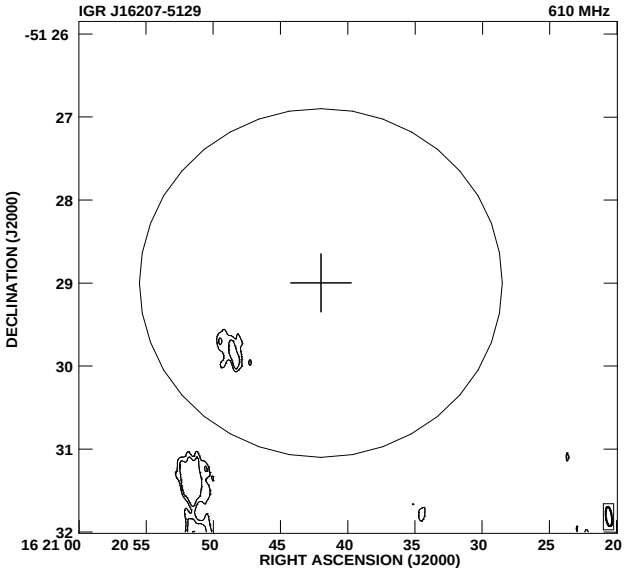

Figure 4.12: GMRT image of IGR J16207−5129 at 0.61 GHz with the *INTEGRAL* position marked with + . The circle shows the *INTEGRAL* uncertainty error circle of 1.6σ. The countour levels are 3.0 mJy × 1.0, 1.2, 2.0, 2.8, 4.0, 8.0, 16.0, 32.0.

However, if the X-ray sources are galactic in origin, then the observed radio association will be a case of fortutious line of sight coincindence. We have listed the known field sources within the *INTEGRAL* error circle in Table 4.1 and 4.2. The optical counter part for IGR J17195−4100 in the table is listed from USNO catalogue.

We discuss further the two most interesting examples of this class of sources.

IGR J18539+0727 : This source was discovered with the IBIS/ISGRI detector in Apr 2003 (Lutovinov et al. 2003a). With the measured photon fluxes of 20 mCrab between 15–40 keV and ∼ 20 mCrab between 40–100 keV, IGR J18539+0727 has the most unusual flat spectrum among the known X-ray sources in hard X-ray band.

In a later observation of the source with RXTE/PCA, an average flux density level of ∼ 6 mCrab was found with large variability on time scales from milli-seconds to seconds, but without any prominent features associated with quasi-periodic oscillations (QPO). The energy spectrum of the source fits a power law with spectral index ∼ −1.5, and has appreciable low energy attenuation due to neutral hydrogen of $n_H \sim (1.5 \pm 0.4) \times 10^{22}$ and a fluorescent iron emission line at 6.4 keV. The observed spectral and temporal characteristics of the X-ray source fits well with the standard model of AGNs (Ceballos et al. 2004).

During GMRT observations of the field, a fully resolved double point source with a flux density of ∼ 5.25±0.25 mJy and ∼ 5.85±0.50 mJy was detected from the J2000 position of, RA: 18h 53m 52.54s±0.03 and DEC: +07d 30′ 39.07″±0.43 and RA: 18h 53m 52.19s±0.023 and DEC: +07d 30′ 37.31″±0.32, respectively, which lies within the 1.6σ position error circle of 3′ of the X-ray source. The radio morphology resembles IGR J18027−1455 or an AGN.

Source	Date	ν (GHz)	S_ν (mJy)	σ $\frac{mJy}{b}$	Radio Pos. RA & DEC	Pos. off. w.r.t Integral Pos.	Radio Struc.	S_ν (Total) NVSS 1.4 GHz (mJy)
IGR J17195−4100	23/07/04	0.61	33.44	0.56	17h 19m 34s±0.22	0.98′	E	N/A
					-41d 00′ 00′′±1.24		DS-E	
IGR J17200−3116	23/07/04	0.61	33.03	0.51	17h 19m 55s±0.74	0.55′	E	20
					-31d 16′ 01′′±0.70		DS-E	
IGR J17456−2901	23/07/04	0.61	23.11	1.53	17h 45m 38.07s±0.04	0.56′	E	17200
					-29d 00′ 40.00′′±1.87		DS-E	
IGR J18539+0727	02/02/04	1.28	5.25±0.25	0.16	18h 53m 52.54s±0.028	3.64′	E	6
					+07d 30′ 39.07′′±0.43		DS-E	
			5.85±0.50		18h 53m 52.19s±0.023			
					+07d 30′ 37.31′′±0.32			
IGR J21247+5058	07/04/04	0.61	184.81±1.59	1.25	21h 24m 39.63s±0.004	0.57′	DS-E	237
					50d 58′ 25.55′′±0.04		E	
	09/04/04	0.61	178.41±1.38	1.61				
	12/04/04	0.61	173.81±1.59	1.71				
	02/05/04	0.61	177.71±1.17	1.52				

Table 4.7: Extragalactic radio sources detected in the fi eld of INTEGRAL sources observed with GMRT

[8]DS-E: Double source Extragalactic, E: Extended

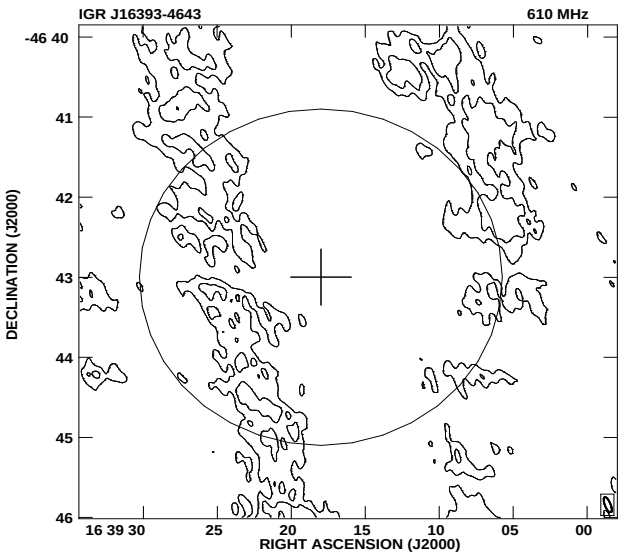

Figure 4.13: GMRT image of IGR J16393−4643 at 0.61 GHz with the *INTEGRAL* position marked with + . The circle shows the *INTEGRAL* uncertainty error circle of 1.6σ. The countour levels are 2.0 mJy × 1, 2, 4, 18, 16, 32, 64.

The computed position offset from the field center is 3.82′ and 3.64′ respectively as shown in Fig. 4.16. The GMRT source is coincident with the NVSS unresolved radio source in the field, for which the flux density is estimated as ∼ 6 mJy at 1.4 GHz. The radio flux density measurements, although done at different epochs are consistent with a flat spectrum source between 1.28 and 1.4 GHz and its persistent nature. Fig. 4.15 also shows the 2MASS J18535+0731 (infrared, E) and DSS J18535+07315 (optical, C) are coincident in position with the radio source, thus suggesting a possible association with the radio source. A power law X-ray spectrum with strong photoabsorption at low energies and fluorescent iron emission line at 6.4 keV clearly points to a binary nature for IGR J18539+0727, in which the emission may arise due to the reflection of the hard X-radiation of inner accretion-flow regions from an optically thick, cold accretion disk. Furthermore, the power density spectrum of the source shows a cutoff below a frequency of ∼ 0.01 Hz, which places it in the category of a compact companion to a BHC (Van der Klis et al. 1999). The presence of infrared and optical counterparts also supports the disk-jet morphology. Thus the hard X-ray source is associated with the radio counterpart detected by GMRT and we conclude from our result that IGR J18539+0727 is an AGN.

IGR J21247+5058 : This source was discovered in the Norma arm region (Walter et al. 2004). The X-ray source has been identified with the core of a bright radio galaxy, 4C 50.55, also known as GPSR 93.319+0.394, KR2, NRAO 659 or BG 2122+50 (Ribo et al. 2004, Combi et al. 2005) and is also coincident with the IR source 2MASS J21243932+5058259. The optical spectrum of the source is very peculiar, having a broad hump around 6700 ÅHα line typical of elliptical or spiral bulge (Barth et al. 2001). While the observed Na, Ca and Mg features are consistent with redshift $z = 0$, the identification of the Hα feature leads to a redshift $z = 0.020 \pm 0.001$. In addition, the photometric magnitudes indicate an increased reddening from *R* to the near infrared band. Masetti et

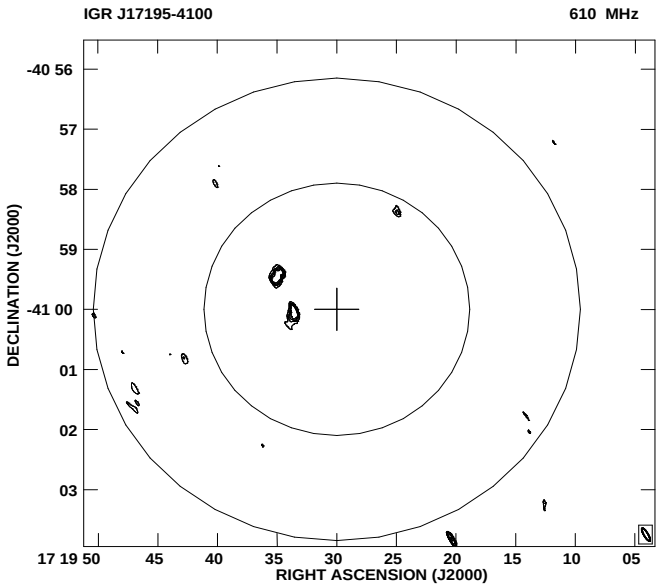

Figure 4.14: GMRT image of IGR J17195−4100 at 0.61 GHz with the *INTEGRAL* position marked with + . The small and large circles shows the *INTEGRAL* uncertainty error circles of 1.6σ and 3σ. The countour levels are 2.3 mJy × 1.0, 1.2, 1.3, 1.4, 2.0, 2.8, 4.0, 8.0, 16.0, 32.0

al. 2004 therefore propose that the observed spectral features in the optical band are caused by the chance alignment of a F-type star with the radio galaxy. The radio observations of the region with GMRT were carried out on 4 occasions between Apr – May 2004. The observation details are listed in Table. 4.3 – 4.8. A radio flux density of $\sim$ 180 mJy at 0.61 GHz from the core was observed on each occasion (Table. 4.7).

In Fig. 4.17 we have plotted the high resolution GMRT image of the source along with the other radio sources detected in this region in previous surveys. It is seen from the figure that morphology of the GMRT radio image resembles that of a radio galaxy with the bright core marked 'A' and extended radio lobes. However, the field is very complex and contains multiple objects within the 3σ position error circle of the *INTEGRAL* source, and some of them are not seen in the GMRT data. Apart from the GMRT source marked 'A', radio sources 28P206 (D) and 87GB212310.9 (I) lie within the 1.6σ position error circle of the X-ray source. However, the alignment of these sources towards the radio lobes clearly suggests that sources (D) and (I) represent regions of radio lobes that were brighter during the respective observations.

The observed GMRT flux density for the radio core varied between 173 mJy and 185 mJy at 0.61 GHz during our four observations the total flux densities for the radio lobes was measured to be $\sim$ 1.8 Jy and $\sim$ 0.85 Jy. Using NVSS flux density values for the core and the extended radio lobes, the spectrum for the extended region was fit with a power law spectrum ($S_\nu \propto \nu^\alpha$) with a spectral index of $\alpha \sim -0.6$ which is consistent with the synchrotron emission from a optically thin medium. The spectral index of the radio core is $\alpha \sim 0.5$, which clearly points towards an inverted spectrum due to strong absorption in the optically thick medium at low frequencies. Our observation at low frequency (0.61 GHz) with GMRT is indicative of the true spectral nature of the core of IGR J21247+5058. The discovery of the X-ray source in the hard X-ray band, the Hα hump in the optical spectrum and

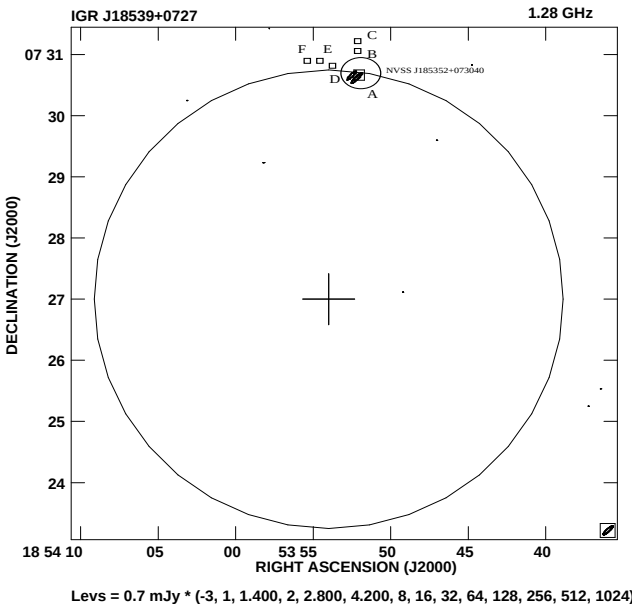

Figure 4.15: Figure shows the GMRT image of IGR J18539+0727 at 1.28 GHz with the *INTEGRAL* position marked with +. The circle shows the *INTEGRAL* uncertainty error circle of 1.6σ. The bold circle marked with 'A' shows the radio source detected by GMRT. The boxes show the known field sources, B: 2MASS J18535+0731, C: DSS J18535+07315, D: 2MASS J185352+07305, E: 2MASS J185353+07305 and F: DSS J185353+07305.

its spectral nature in the radio and X-ray bands suggest that IGR J21247−5058 is a partially obscured extragalactic X-ray source similar to NGC1068 and NGC4579.

In the previous sections we have discussed about the hard X-ray sources with radio sources detcetd within the X-ray position error circle. In the next section we will discuss about the last class of hard X-ray sources with no radio counterparts detected within their field.

4.3.3 Sources with no radio counterpart

Sixteen hard X-ray/gamma-ray sources have no radio counterpart within the X-ray position error circle. They are listed in Table 4.8. Most among these sources are X-ray binaries refer Table 4.1 and 4.2. Hence either these sources are not REXBs or these are synchrotron self absorbed at low frequencies at which our observations were made or these are highly variable in radio band. Follow up observations in the radio window is necessary to confirm the variable nature of these sources. We discuss below a few examples among these sources.

IGR J16316−4028 : This source was discovered at a flux density level of $\sim$ 25 mCrab between 20 and 40 keV during the *INTEGRAL* survey (Rodriguez & Goldwurm 2003). The X-ray source is transient in nature, and variability of the X-ray flux density on timescales of $\sim$ 2000 s has been observed from the source along with the flaring events during its discovery (Rodriguez et al. 2003). An EGRET gamma ray source 3EG 1631−4033 lies in the field direction at a distance of 10′ with respect to the source, IGR J16316−4028 (Rodriguez et al. 2003) suggesting a possible association of the two

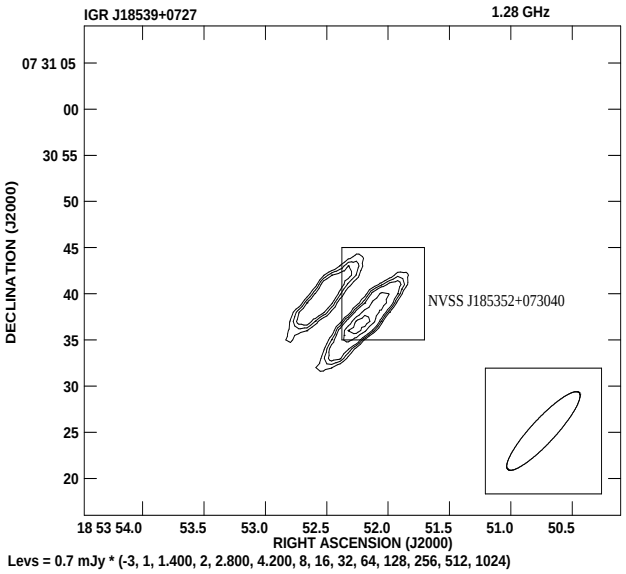

Figure 4.16: Figure shows the blown up image of GMRT radio counterpart

due to large position uncertainty of the gamma ray source. During our observations with GMRT at 0.61 GHz and 1.28 GHz, no radio source was detected within the X-ray position error box of 3σ and upper limits of ~ 0.8 mJy b^{-1} and ~ 6 mJy b^{-1} respectively were measured.

IGR J16318−4848 : This transient source was discovered by *INTEGRAL* in the Norma arm. The observed flux density in the $15 -- 40$ keV band was $50 -- 100$ mCrab. The X-ray flux data show signifi cant temporal variations on the time scale of 1000 s. A bright 9th mag infrared source in the *J*, *H*, *K* bands, coincident with the X-ray source position is clearly seen in the 2MASS and Mid course Space Experiment (MSX) data. The source is highly absorbed at 8 micron flux density and Galactic in nature (Courvoisier et al. 2003). The best fi t position (J2000) determined from the infrared and the XMM measurement corresponds to RA: 16h 31m 48.3s, DEC: -48d $49' 01''$ (Schartel et al. 2003, de Plaa et al. 2003, Revnivtsev et al. 2003). The infrared and optical observations of the counterpart have revealed the high mass X-ray binary nature of the source, there being a compact, companion around a super-giant primary B[e] star (Filliatre et al. 2004). Strong photo absorption and the fluorescent emission line of neutral iron (6.4 keV) are seen in the XMM data thereby suggesting accretion due to a stellar wind (Matt et al. 2003). A search for the radio emission from the source at 4.8 and 8.6 GHz was made by Walter et al. 2003 with ATCA, but no signifi cant radio flux density was detected from the source with a 1σ upper limit of 0.1 mJy. We made repeated observations at 0.61 GHz using GMRT at various epochs during 2003 and 2004 observing cycles. No positive detection was made in any of these observations. An upper limit of ~ 7 mJy for the radio emission within the 3σ position uncertainty circle is derived. The typical rms noise in the fi eld is measured to be ~ 2.2 mJy. A non detection at radio frequencies may be due to the highly absorbed nature of the source due to its location in the Galactic plane. The present observation may also correspond to high soft state of the source during which the radio emission is believed to be quenched. There is also a possibility of non existence of the radio jet in the source, as in the case of pulsars.

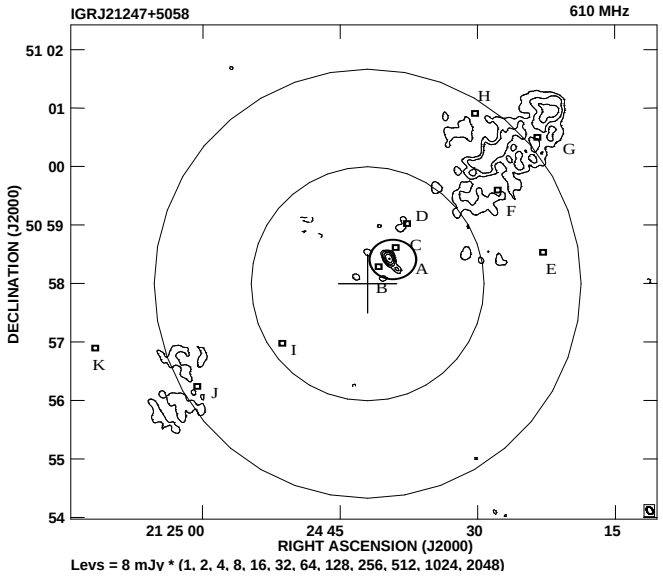

Figure 4.17: A high resolution GMRT image of IGR J21247+5058 at 0.61 GHz. The core is marked with 'A'. The X-ray position is marked with +. The boxes show the known field sources, B: 2MASS J2124+5058, C: NVSS 21247+5058, D: 28P206, E: MG4 J2124+5058, F: *87GB 2122+5046, G: 7C 2122+5047, H: NRAO 0659, I: *87GB 2123+5044, J: *87GB 2123+5043, K: MG4 J212511+5056.

IGR J16320−4751 : The variable hard X-ray source, IGR J16320−4751, was discovered during Feb 2003 (Tomsick et al. 2003). The hard X-ray source position is consistent with that of the source AX J1631.9−4752. The ASCA/GIS observations also suggest a variable nature of the source (Sugizaki et al. 2001a) and its energy spectrum fits an absorbed power law and so it is believed to be a high-mass X-ray binary system. The variations of the spectral index in different observations by XMM-Newton, ASCA and BeppoSAX suggest that the source undergoes a spectral transition similar to those in the other XRBs. The EGRET source 3EG J1639−4702 (Romero et al. 1999) could be associated with the X-ray source considering the large position uncertainties. The infrared images from the 2MASS database and the optical observations indicate a bright and massive companion for the X-ray source (Rodriguez et al. 2003). GMRT observation of the field did not show any significant radio source within the 3σ position uncertainty limit during different observations at various frequencies. A 3σ upper limit for the radio flux density was ~ 3 mJy at 1.28 GHz with a rms noise of ~ 0.83 mJy b^{-1}, while the 3σ upper limit at 0.61 GHz correspond to 4 mJy with rms noise typically ~ 1.04 mJy b^{-1}. No NVSS data is available for comparison of the field and also there is no RXTE/ASM data to determine the X-ray state of the source during our observation. The non detection of the source at low frequency clearly points out either an absorption of the jet in the ambient medium or a lack of a radio jet.

IGR J16418−4532 : This hard X-ray source was discovered in the IBIS/ISGRI data at the flux density level of ~ 3 mCrab in the $20 -- 40$ keV bands (Tomsick et al. 2004). The X-ray source is located in the Norma arm region. The GMRT observations at 0.61 GHz were made in Feb 2004, to search for the radio counterpart of the X-ray source. No significant radio flux density was detected

within the *INTEGRAL* position uncertainty limit of $2'$. The 3σ upper limit is 1 mJy at 1.28 GHz with a rms noise of ~ 0.33 mJy b^{-1}. No RXTE/ASM X-ray light curve or the NVSS image is available. Thus suggesting a non existence of the radio emission from the X-ray source during our observations.

IGR J17391−3021 : Hard X-ray emission in the $18 -- 50$ keV bands from the transient HMXB source, IGR J17391−3021, was discovered in Aug 2003 at a flux density level of ~ 70 mCrab (Sunyaev et al. 2003a). The position coordinates of the source overlap with the X-ray source XTE J1739−302 with J2000 position of, RA: 17h 39m 11.1s and DEC: -30d $20'$ $37''$. Using CHANDRA observations, the position has been refined to $1''$. Within the improved position, an optical counterpart of the source is identified with the object 0525 28760590 in the USNO A2 catalog. It is also a 2MASS source and is a highly reddened O star (Smith et al. 2003). A radio source was detected in a VLA observations at 4.9 GHz at a flux density of 0.9 ± 0.2 mJy, and a J2000 position of, RA: 17h 39m 01.52s and DEC: -30d $19'$ $34.9''$ within $3'$ error circle *INTEGRAL* position but well outside the CHANDRA error circle (Rupen et al. 2003b). The EGRET source 3EG J1736−2908 is located near the X-ray source. The source was observed with GMRT at 1.28 GHz and no radio emission was detected from the field within 3σ position uncertainty of $2'$, as determined from CHANDRA data. The 3σ upper limit for the radio flux density from GMRT data is ≤ 1 mJy and the rms noise was 0.2 mJy b^{-1}. No significant radio flux from the X-ray source position was detected in the analysis of the NVSS data and the 3σ upper limit for the radio flux density is derived as 2.5 mJy. Nevertheless, during our observations, we did detect a radio source coincident in position with the NVSS source with radio flux density of 8.9 mJy and rms noise of 0.19 mJy b $^{-1}$ at J2000 position of, RA: 17h 39m 06s and DEC: -30d $18'$ $12''$ which lies $2.4'$ away from the X-ray source position. Thus we confirm from the above data that the radio source detected by VLA in the field of the X-ray source is not associated with the Galactic X-ray source.

IGR J17544−2619 : This transient source was discovered with *INTEGRAL* at a flux density of ~ 160 mCrab in the $18 -- 25$ keV bands (Sunyaev et al. 2003b). The X-ray variability with time scales of $1.5 -- 2$ hrs seen in the data is ascribed to the binary nature of the X-ray source and is associated with the accretion-emission processes (Rodriguez et al. 2003). A ROSAT source IRXS J175428.3−262035 with the count rate of 0.08 ± 0.02 counts s^{-1} ($0.1 -- 2.4$ keV) lies within the field of IGR J17544−2619. Optical and infrared parameters observed in the 2MASS survey give the magnitude $J = 8.79 \pm 0.02$, $H = 8.31 \pm 0.03$, $K = 8.02 \pm 0.03$, thus suggesting the companion star to be an early O-type star.
The GMRT image of the field of source IGR J17544−2619 at 0.61 GHz showed no significant radio flux density within the 3σ position uncertainty of the X-ray source. A 3σ upper limit for the radio emission from the GMRT data is <7 mJy with the rms noise of ~ 2.2 mJy b^{-1}. No radio emission from the source region is seen even in the NVSS image. A 3σ upper limit from the NVSS data is estimated to be ~ 3 mJy. The RXTE/ASM hardness ratio data for the source suggests that it was in the high soft state during our observations. A non detection of radio emission within the $4''$ (1.6σ) (Gonzalez-Riestra et al. 2004) position limit from XMM-Newton observations, during a high soft X-ray state of the source suggests that there is no associated radio source for the X-ray source; however, the radio emission, if present, may be synchrotron self-absorbed at low frequency or highly variable, similar to some of the HMXBs below 1 GHz.

IGR J17597−2201 : The X-ray source is a weak transient source with a flux density level of 5 mCrab in $15 -- 40$ keV energy band (Lutovinov et al. 2003). The RXTE observation shows variability of the source. The PCA spectra is, however, consistent with a power law with an additional

Source	Date	ν (GHz)	S_ν (mJy)	σ $\frac{mJy}{b}$	Radio Pos. RA & DEC	Pos. off. w.r.t Integral Pos.	Radio Struc.	S_ν (Total) NVSS 1.4 GHz (mJy)
IGR J00370+6122	25/06/04	0.61	≤7.00	2.18				≤1.6
IGR J01363+6610	25/06/04	0.61	≤7.00	2.31				≤2.5
IGR J16316−4028	02/02/04	1.28	≤0.8	0.19				N/A
	09/04/04	0.61	≤6.00	1.35				
	12/04/04	0.61	≤4.80	1.18				
IGR J16318−4848	04/08/03	0.61	≤6.50	2.13				N/A
	15/09/03	0.61	≤6.60	2.20				
	09/04/04	0.61	≤7.00	2.41				
IGR J16320−4751	29/07/03	1.28	≤3.00	0.83				N/A
	04/08/03	0.61	≤4.00	1.23				
	15/09/03	0.61	≤4.00	1.04				
IGR J16358−4726	31/07/04	0.61	≤7.50	2.5				N/A
IGR J16418−4532	02/02/04	1.28	≤1.00	0.33				N/A
IGR J17391−3021	02/02/04	1.28	≤1.04	0.19				≤2.5
IGR J17488−3253	30/07/04	0.61	≤2.10	0.67				≤1.6
IGR J17544−2619	12/04/04	0.61	≤7.35	2.46				≤3
IGR J17597−2201	16/09/03	0.61	≤7.90	2.42				≤3.5
IGR J18027−2016	25/06/04	0.61	≤7.00	2.32				≤1.3
IGR J18325−0756	16/09/03	0.61	≤3.00	0.75				≤3.5
IGR J18483−0311	16/09/03	0.61	≤4.24	1.27				≤1.6
	02/02/04	1.28	≤1.00	0.15				
IGR J18490−0000	23/07/04	0.61	≤3.5	1.25				≤1.4
IGR J19140+0951	21/06/03	0.61	≤5.50	1.28				≤1.6
	29/07/03	1.28	≤0.80	0.15				
	04/08/03	0.61	≤5.50	1.23				
	09/09/03	0.61	≤5.00	1.14				
	15/09/03	0.61	≤5.70	1.90				
	02/02/04	1.28	≤0.50	0.15				
	07/04/04	0.61	≤5.00	1.43				
	12/04/04	0.61	≤5.00	1.28				
	02/05/04	0.61	≤5.00	1.64				
	03/05/04	0.61	≤5.00	1.20				

Table 4.8: No radio counterparts detected for the target INTEGRAL sources observed with GMRT

soft X-ray excess. The measured spectral indices in the hard X-ray band range between 1.8 and 2.9. An Fe K emission line at 6.5 keV has been detected (Markwardt et al. 2003) in the X-rays. These observations suggest that IGR J17597−2201 is a binary system containing a neutron star as the compact companion. The GMRT observations on 16th Sep 2003 at 0.61 GHz were taken immediately after the discovery of the source with *INTEGRAL*. The radio image of the field showed no significant radio source within the 3σ position uncertainty circle of the X-ray source position. A 3σ upper limit for the radio flux density is derived as <7 mJy with the rms noise of $\sim$ 2.14 mJy b $^{-1}$. The analysis of the NVSS data also did not yield any radio flux density at 1.4 GHz and a 3σ upper limit is obtained as 3.5 mJy. An upper limit for the radio emission from the source clearly implies that if the prompt radio emission was indeed present, then either it was highly absorbed at low frequency or was variable.

IGR J18325−0756 : This is a transient, flat spectrum X-ray source discovered with IBIS at a flux density level of $\sim$ 10 mCrab in the 15 −− 40 keV band and $\sim$ 5 mCrab in the 40 −− 100 keV band. The source is variable in X-ray regime (Lutovinov et al. 2003). We observed the source with GMRT at 0.61 GHz during AO3 to look for any residual low frequency flux density from the active phase. No significant radio source was detected within the 3σ *INTEGRAL* position error circle. The GMRT 3σ upper limit for the radio flux density is $\leq$ 3 mJy. Thus our conclusion for non detection of radio emission is similar to IGR J17597−2201.

IGR J18483−0311 : This new transient source was discovered in Apr 2003 with a X-ray flux density of $\sim$ 10 mCrab in the 15 −− 40 keV band and a flaring behavior in the X-ray light curve was seen from the source (Chernyakova et al. 2003). The radio image of the field of IGR J18483−0311 with GMRT at 1.28 GHz showed no significant radio source within the 3σ upper limit of 4 mJy either at 0.61 GHz or 1.28 GHz. No significant source was detected even in the NVSS data. The 3σ upper limit at 1.2 GHz was 1 mJy. A non detection of the radio emission supports our previous conclusion.

IGR J19140+0951 : The X-ray source was discovered with IBIS/ISGRI at a flux density of $\sim$ 50 −− 100 mCrab between 15 and 40 keV (Hannikainen et al. 2003). The RXTE light curve of the source shows variations on short time scale. No QPO was seen in the power density spectrum of the source in the PCA/RXTE data, the X-ray spectrum is; however, well fitted by power-law + thermal component (Cabanac et al. 2004a). A broad ionized iron line is also seen in the spectral data. The source shows strong spectral variability more typical of X-ray binaries. A comparison of the ISGRI/JEMX and RXTE/PCA spectra reveals a state transition in the source from 'steep power-law' to 'low hard' (Schultz et al. 2004). Such a transition in spectral state is a characteristic of a BH LMXB (McClintock et al. 2003) thus suggesting the possibility of IGR J19140+0951 being a BH LMXB, though the absence of QPO does not fit this hypothesis. However; Rodriguez (private communication) suggests the HMXB nature of the source, with a neutron star as the central engine based on available RXTE and *INTEGRAL* data. We performed a series of ten radio observations with GMRT for the source at 0.61 and 1.28 GHz during the 2003 and 2004 observing seasons. No positive radio detection within the 1.6σ position error circle of 1.3′ around the new refined position coordinate (Cabanac et al. 2004b) of the source was found during our observations. The upper limit for the GMRT radio flux density towards the source direction is derived as $\leq$ 5.5 mJy. No radio source corresponding to the X-ray source position was seen even in the NVSS data at 1.4 GHz. The absence of radio emission from the source as seen in other micro-quasars, viz XTE J1748−288, GRS 1758−258 below 1.4 GHz is also seen in IGR J19140+0951. Thus we confirm from our observations that the X-ray source has no radio counterpart, or if present, it is highly absorbed below 1.4 GHz.

The remaining sources in this group i.e. IGR J00370+6122, IGR J01363+6610, IGR J16358−4726, IGR J17488−3253, IGR J18027−2016 and IGR J18490−0000 hold similar explanation for non-detection at radio wavelengths.

4.4 Discussion

Radio survey of newly discovered hard X-ray/Gamma-ray sources is of substantial interest as some of the micro-quasars have shown hard X-ray/Gamma-ray counterparts. A radio survey was performed with the GMRT to study the radio behavior of the new sources discovered by the Gamma-ray satellite, INTEGRAL. The aim of this work was to look for new micro-quasar candidates and to provide presice measurement of position at arc second accuracy via radio observations. The information available from various surveys at different wavelengths was also used to explore the multi-wavelength nature of these source. The cross-correlation of the data available at radio, IR, optical, UV and X-rays along with the GMRT data was done to achieve this result.

Among the forty Gamma-ray sources for which GMRT data is presented in this chapter, radio counterparts are detected for twenty four objects that lie within the 3σ position error circle of the *INTEGRAL* source positions. Among these, four radio sources viz, IGR J17303−0601, IGR J17091−3624, IGR J7464−3213 and IGR J18450−0432 are classified as possible micro-quasars. The detailed explanation and multi-wavelength behavior of these sources are discussed in Pandey et. al 2006a and Pandey et. al 2006b. IGR J17303−0601, IGR J17091−3624, and IGR J7464−3213 are LMXBs and IGR J18450−0432 is a HMXB. IGR J17091−3624 and IGR J7464−3213 are persistent in nature and IGR J17303−0601 and IGR J18450−0432 are transient in nature at radio frequencies. All of these sources have shown variability trends at radio frequencies. In the case of IGR J17464−3213 large-scale radio jets were discovered during ATCA observations. High resolution observations have to be performed for the remaining 3 sources to map their jet structures. Also repeated simultaneous observations have to be performed for all these sources to look for their variability pattern.

The information about the other hard X-ray sources forms an important byproduct of this work. Based on the radio morphology of these source important informations can be derived. The morphology for IGR J16479−4514 resembles a HII region while that of IGR J18539+0727 and IGR J21247+5058 indicates a radio galaxy. In the case of IGR J15479−4529, GMRT data do not fit a point source model, thereby suggesting an extended morphology more likely to be a reminiscent of molecular cloud. The sources IGR J06074+2205 and IGR J18027−1455 are unresolved source with extragalactic properties and are probably AGNs. The sources IGR J16318−4848, IGR J16320−4751, IGR J17544−2619, IGR J17597−2201 and IGR J19140+0951 are suggested as X-ray binaries from the *INTEGRAL* studies; however, their radio counterparts are not yet detected, suggesting that either they are synchrotron self absorbed at low frequencies or have no current radio emission. The sources IGR J16316−4028, IGR J16418−4532, IGR J17391−3021, IGR J18325−0756 and IGR J18483−0311 do not have low frequency radio counterparts and were not identified based on our survey. This points to either a variable nature of the radio emission or a persistent emission at much lower flux density than the GMRT threshold.

As seen in the tables, the position off-set of the possible radio counterparts with respect to the X-ray source position are of the order of a few arc-minutes and well within the 3σ error circle of the X-ray position. Hence such possible identifications are a reason to conduct even deeper optical and infrared follow-up observations. Infact, based on our published results there were observations carried out at other wavelengths by various international groups. The data is being analyzed for publications

by these groups.

A large number of accreting binary systems show a transient behavior in the X-ray band. The radio emission from X-ray binaries can be classified into two broad classes (1) X-ray sources with persistent radio emission are generally binary systems containing a BH or a NS with low magnetic field; (2) the sources with a highly variable and bright radio emission, are associated with jet-like outflows from their compact objects. On the basis of X-ray spectral characteristics, their transient nature and their discovery in the high energy band, a majority of the *INTEGRAL* sources are believed to be Galactic HMXB. It is, therefore likely that during the transient outbursts, most of these sources will produce relativistic outflows, thereby giving rise to strong radio emission. Therefore, non-detection of radio flux density from a number of *INTEGRAL* sources may be due to the different X-ray state of the source at the time of our observations. Thus, near simultaneous observations in different wave bands are necessary to reveal the true nature of most of the *INTEGRAL* high energy sources.

Chapter 5

Conclusion and future work

In this chapter we will briefly summarize the over all results and discuss the future work that can be carried out in this field.

5.1 Results

This thesis consists of statistical study of radio observations of sixteen micro-quasars- XRBs with stellar mass BH and radio jet, performed at low radio frequencies. This was the first ever effort to explore the nature of these source at meter-wavelengths. We present the characteristics of these sources in chapter 1 along with their nature known at various wavelengths. These sources are Galactic counterparts of distant quasars- harboring BH of the order of 10^8 solar mass. The low frequency radio study has helped to study the geometry and emission mechanism of these sources.

The thesis also lists the results of a radio survey carried out on forty newly discovered hard X-ray/ gamma-ray sources detected via INTEGRAL satellite. This study was performed to explore the nature of newly discovered X-ray sources at radio wavelengths and to look for new micro-quasar candidates. The results on prominent sources and possible micro-quasar candidates are investigated in detail.

All the micro-quasars show compact radio morphology at low radio frequencies, except SS433, which shows marginal extended structure at 0.235 GHz. The radio emission is non-thermal in origin at low frequencies and undergo various emission and absorption processes. The prime goal was to derive the low frequency radio spectra of these sources. We have made repeated observations with GMRT on these sources to study their variability pattern. The work also includes the estimation of the size of the emitting region and their magnetic field strength using equi-partition assumption.

For a few sources, we have obtained a near-simultaneous spectra with GMRT and Ryle telescope, which led to various interesting information that would not have been available via single frequency observations. We have also used the information available from the ASM X-ray data to interpret the X-ray state of the source. It is important to note that for micro-quasars the X-ray and radio variability are anti-correlated, except Cyg X-3, which shows both correlation and anti-correlation depending on the strength of the flare. It can also be seen that radio emission is mostly detected when the source is in low/hard or intermediate X-ray state, while the source is not detected in radio in its high/soft X-ray state. These arguments led us to organize the observations only on the sources which were in low/hard and intermediate state.

We summarize below the results obtained from this thesis in brief.

5.1.1 Observation of microquasars at 1.28, 0.61 and 0.235 GHz

Statistical study of micro-quasars: We have presented for the first time, detailed low frequency radio observations of the galactic micro-quasars with GMRT. The data from various radio frequencies was also complied in order to understand the behavior of these sources from centi-meter to meter-wavelength and to derive the correlation in the emitting regions. The GMRT observations were carried out at 0.235, 0.61 and 1.28 GHz while the archival GBI data at 2.3 and 8.2 GHz were considered to study the nature of these sources at centi-meter wavelengths. The data at 15 GHz from Ryle telescope was used to derive some important informations at high radio frequencies. And the RXTE/ASM X-ray data was used to study the radio/X-ray correlation in various X-ray states. The main results on micro-quasars are listed below

- There exits an anti-correlation in the X-ray and radio light curve of micro-quasars. The source is detected at the radio wavelengths following activity in X-rays. The radio emission is suppressed in high/soft X-ray state and the source is radio loud in low/hard X-ray state. This indicates the disk-jet coupling in micro-quasar. The formation/filling up of the matter in the accretion disk is characterized by high/soft X-ray state. And, the collapsing of matter into the accretion disk and its ejection is characterized by low/hard X-ray state.

- The X-ray light-curve reveals that micro-quasars have 3 classes of accretion disc types; (A)-persistent, (B)- quasi-persistent, and (C)- transient. Except V4641 Sgr, most of the HMXBs have persistent or transient accretion disc and they are persistent at radio frequencies. In the case of V4641 Sgr, it does not exhibit frequent flaring in both X-rays and at radio wavelengths. Except Sco X-1, which is persistent radio emitter, most of the LMXBs show transient behavior in X-rays and radio wavelengths. Among these, only GRS1915+105 shows frequent variability at different amplitudes and timescales while rest of them show only occasional flaring activity.

- A few of the micro-quasars like GRO J1655-40, XTE J1118+480, and XTE J1748-288 were never detected by GMRT due to their X-ray inactive state since more than last six years.

- GX339-04 and V4641 Sgr were detected on two occasion during radio flares. These flares followed X-ray activity.

- Persistent micro-quasars like 1E1740.7−2942 and GRS 1758−258, which are weak radio emitter at high radio frequencies showed no radio detection at meter-wavelengths suggesting that the radio spectra is flat or inverted.

- Cyg X-1, Cyg X-3, Sco X-1, and LSI+61303 are persistent at radio wavelenths and show SSA at low frequencies.

- SS433 and LS 5039 show increase in the flux density at low radio frequencies, with a power-law spectra. This suggest that there is no turn over in these sources down to 0.235 GHz. Further low frequency observations at 150 MHz or lower (with SFA, LOFAR) may help to locate the turn over frequency.

- GRS 1915+105, show excellent radio/X-ray correlation with radio emission suppressed during high/soft state and enhanced radio emission during low/hard state. The radio emission are first detected at centi-meter wavelengths followed by a delay in detection at meter wavelength. The radio spectra is substantially steeper towards lower frequencies, suggesting that the radio emission originates from two different components, viz, jet emission dominating at higher

radio frequencies and radio lobes at the end of the jet contributing significantly at low radio frequencies. These lobes acts like a reservoir of electrons emitting at low radio frequencies. A variability in the spectral index of the source from flat or inverted to steep was noticed on a few of the flaring episodes.

- The low frequency data is also checked for the effects of RISS, which is know to dominate at meter wavelengths and cause flux density fluctuations. It is seen in the case of Cyg X-1 and SS433 that, part of the flux density variations at meter wavelengths is indeed due to RISS. Our calculations show that, LSI+61303, LS 5039, Sco X-1, and XTE J1118+480 may be affected by scintillation; however, detailed series of observations needs to be performed at low frequencies to check this effect. Most of the other micro-quasars appear not to be affected by refractive interstellar scintillation.

- Based on the multi-frequency data, important radio parameters like size, brightness temperature, equipartition magnetic field and radio luminosity were calculated. The brightness temperature suggest that the radio emission is synchrotron in origin. However, at meter wavelengths only an upper limit to brightness temperature and equipartition magnetic field was obtained, since the source remained unresolved and the size of the synthesized beam was used. From the VLBI observations at centimeter wavelengths, it is clear that the equipartition magnetic field is high for HMXBs as compared to LMXBs. Also the size of the source increases at low frequencies due to angular broadening.

We will discuss below the results obtained on prominent micro-quasars.

Cyg X-1: the first ever low frequency study was performed on Cyg X-1 using GMRT at 0.235, 0.61and 1.28 GHz. The observations were performed simultaneously at 0.235 and 0.61 GHz and the near simultaneous data from Ryle Telescope at 15 GHz was used. The near simultaneous multi-wavelength monitoring (radio/X-ray/Gamma-ray) data on the source shows a shift in the peak of the spectrum from shorter to longer wavelengths. The delay in the peak is of the order of $\sim$2 days. It was seen for the first time that Cyg X-1 could be affected by RISS at low radio frequencies. The mean radio flux is $\sim$7.5 mJy at low radio frequencies ($\leq$ 2 GHz). A spectral turn over at lower frequencies is seen in the case of Cyg X-1 due to SSA. The radio spectrum is flat from 2 to 220 GHz, which is explained by super position of individual synchrotron emitting plasma, each of them is optically thick at range of frequencies. The positive detection of Cyg X-1 at 0.235, 0.61 to 1.2 GHz on several occasions, along with the spectral turnover at low frequencies, conclusively supports the synchrotron origin of the radio photons contrary to its ambiguous thermal or non-thermal nature as concluded from earlier measurements (Fender et al. 2000).

Cyg X-3: The results of first ever simultaneous (0.610 and 0.235 GHz) low radio frequency study of Cyg X-3 is presented in this section. Cyg X-3 is a persistent source at low frequencies and shows spectral turn over due to SSA. Continuous blobs of plasmoids are known to be emitted within the jet medium at centi-meter wavelengths. However, the lifetime of the individual blob in the case of Cyg X-3 is smaller than in the case of Cyg X-1, hence no flatness in the spectrum is seen. The scintillation time scale derived in the case of Cyg X-3 is unexpectedly high due to presence of local inhomogenity in the electron density . Hence we conclude from the present data that the source variability is due to intrinsic effects.

Sco X-1: the extensive observation of Sco X-1 at low radio frequencies was carried out to study the variability of the source. The source shows SSA below 0.61 GHz. It also shows significant short and

long term variability in the radio flux density. From the radio light curve, we derive 3 different stages of evolution of the radio emission from the source, viz., slow rising stage, plateau stage, and slow decaying stage. From the GMRT observations, it is also suggested that the background NE and SW sources are not associated with Sco X-1.

GRS 1915+105: The first ever detailed low frequency radio observations and results of the galactic micro-quasar GRS 1915+105 with the GMRT, is presented in this section. The observations have been carried out at several epochs at 1.28, 0.610 and 0.244 GHz, during various X-ray states. There exists a good correlation in the radio/X-ray states. The radio emissions are quenched in high/soft X-ray state and detected in the low/hard X-ray and intermediate state. Our results suggest that, during flaring episodes there is no spectral turn over even at low radio frequencies of 0.244 GHz. While the radio emission at high radio frequencies could predominantly come from compact jets, the lower frequency emission is likely to come from regions far from the accretion disk. It is proposed that, radio lobes are formed at the end of the radio jet. The relativistic plasma which was ejected from the accretion disk will move outwards during radio flares, it will loose energy both by radiation and by expansion and will form these lobe, similar to the case of AGNs. The radio lobes acts as a reservoir of low energy electrons and is likely to be the origin for optically thin low frequency radio emission in the case of GRS 1915+105.

5.1.2 Results of radio observations of newly discovered Gamma-ray sources by the INTEGRAL satellite at 1.28 and 0.61 GHz

We have performed a radio survey on forty new discovered hard X-ray/Gamma-ray sources via INTEGRAL satellite. Based on the radio morphology of these source important informations can be derived. We group the sources with compact and extended radio morphology and discuss their nature based on the information available at other wavelengths.

Possible micro-quasar candidates Four possible new micro-quasar candidates viz, IGR J17303−0601, IGR J17091−3624, IGR J7464−3213 and IGR J18450−0432 were detected by the radio survey performed on forty new discovered hard X-ray/Gamma-ray sources discovered by the INTEGRAL satellite.

- They show multi-colour disk black body spectra with hard power law tail and variability patterns in the X-ray domain similar to X-ray binaries.
- The RXTE/ASM X-ray light curve of the LMXB, IGR J17303−0601, is quasi-persistent in nature and show transient behavior at radio frequencies as discussed in chapter 3. The RXTE/ASM data on the remaining three sources are not available.
- The HMXB IGR J18450−0432 is persistent at radio frequnecies; however, it shows variable radio flux.
- The variability in the radio data was seen during X-ray acitivities.
- IGR J17303−0601, IGR J17091−3624, IGR J7464−3213, and IGR J18450−0432 show compact radio morphology. In the case of IGR J7464−3213, a large scale radio jet was detected during ATCA observations (Corbel et. al. 2005).

- A precise measurement of position at arc second accuracy is provided for the possible radio counterparts of INTEGRAL sources from GMRT radio observations.
- We have also cross-correlated the information available from various surveys at radio, IR, optical, UV and X-rays to enhance the signifi cance of this result.

Gamma-ray sources with no association with the radio source: The results on the remaining thirty-six Gamma-ray sources with no association with the radio source detected within the X-ray position error circle is discussed in this section.

- Among the remaining thirty-six Gamma-ray sources, radio emissions from the direction of twenty sources are detected at low radio frequencies. These sources are further grouped into, Galactic extended sources, sources in diffuse Galactic region and extra galactic sources.
- Seven sources, viz., IGR J15479−4529, IGR J16207−5129, IGR J16479−4514, IGR J16558−5203, IGR J17285−2922, IGR J17460−3047, and IGR J18450−0435 show extended radio morphology similar to extended Galactic sources.
- The radio morphology of IGR J15479−4529 resembles to a reminiscent of molecular cloud.
- The radio morphology of IGR J16479−4514 resembles a HII region.
- Six gamma-ray sources, viz., IGR J16167−4957, IGR J16195−4945, IGR J16393−4643, IGR J17252−3616, IGR J17254−3257, and IGR J17475−2822, show radio morphology similar to sources in diffuse Galactic region.
- Seven sources, viz., IGR J06074+2205, IGR J17195−4100, IGR J17200−3116, IGR J17456−2901, IGR J18027−1455, IGR J18539+0727, and IGR J21247+5058 show characteristics double source morphology similar to extra galactic radio sources.
- We have performed repeated observations on the compact source IGR J06074+2205 to look for variability pattern. The source shows characteristics of an active galactic nuclei and is not associated to the hard X-ray/Gamma-ray source.
- The source IGR J18027−1455 is also an extra galactic compact source. The extra galactic nature is inferred based on its optical characteristics. We have confi rmed its variable nature at low frequencies based on our observations at low frequencies.
- The morphology of IGR J18539+0727 and IGR J21247+5058 resembles to extended radio galaxies.
- Sixteen sources have no radio counterparts within their X-ray position error circle. The sources IGR J16318−4848, IGR J16320−4751, IGR J17544−2619, IGR J17597−2201 and IGR J19140+0951 are suggested to be X-ray binaries from the *INTEGRAL* studies; however, their radio counterparts are not yet detected, suggesting that either they are synchrotron self absorbed at low frequencies or have no current radio emission. The sources IGR J16316−4028, IGR J16418−4532, IGR J17391−3021, IGR J18325−0756 and IGR J18483−0311 do not have low frequency radio counterparts and were not identifi ed based on our survey. This points to either a variable nature of the radio emission or a persistent emission at much lower flux density than the GMRT threshold.

The XRBs are known to show interesting variability pattern extending from centimeter to gamma-rays. In this work we have further explored the nature of these source at meter wavelengths. It is confirmed from this work that the variations at lower frequencies is coupled with the disk-jet activity. This thesis we have attempted to unify the nature of accreting objects through the behavior of the X-ray light curve, the radio lightcurve and morphology and the mass of the companion star. The low frequency synchrotron radiations in these sources are quenched in high/soft X-ray state and are detected in the low/hard X-ray and intermediate states. Short and long term variability is noted in the radio behavior of the source e.g. Sco X-1 and Cyg X-1. And a delay in the peak of the radio emission is noted at low frequencies as expected from synchrotron bubble model. In the case of HMXBs the radio emissions are persistent even at low frequencies suggesting a strong magnetic field in these systems. LMXBs are transient in nature at meter-wavelengths. The flaring episodes in the case of LMXBs may give rise to formation of radio lobes at the end of the jet, for e.g. GRS 1915+105. Thus, it can be seen from the above discussion that BHXBs are interesting candidates for monitoring studies. It is also important to discover new micro-quasar candidates and check their nature as suggested in this thesis. We will list below the further work that can be carried out in this domain.

5.2 Future Prospects at low radio frequencies

We would like to perform observations on flaring micro-quasars in future with the GMRT in the simultaneous dual frequency mode to trace the evolution of radio spectra. The deep imaging of six persistent micro-quasars at lower radio frequencies will help to detect, if any, radio emitting features associated or powered by the microquasar. The low frequency observations are also required for SS433 and LS5039 in-order to locate the turn over frequency. Simultaneous data at various frequencies will help in studying the broad band radio behavior of micro-quasars. Multi wavelength observations during radio flares will also help to study the over all behavior of the source and the various emission mechanism.

5.2.1 Follow up radio observations of newly discovered binaries by X-ray/Gamma-ray satellites

Repeated radio observations of possible micro-quasar sources discovered by INTEGRAL satellite need to be carried out tolook for the radio variability pattern in these sources. Further observations of new discovered sources from recently launched X-ray/Gamma-ray satellites are also useful. This will be an important effort towards looking for new micro-quasar candidates and towards exploring the radio nature of these new discovered sources.

5.3 Micro-quasars with future multi-wavelength facilities

As we have described in chapter 1, micro-quasars are good candidates for multi-wavelength studies. Over the past decade, important simultaneous multi-wavelength observations have provided remarkable insights into accretion and outflow around accreting relativistic objects. The detailed comparative studies for this class of objects are just beginning to be made and holds an important subject of many future research.

SKA: is a giant square kilometer radio array expected to be operational by 2020. It will play a crucial role in the study of micro-quasars. With the increase by two orders of magnitude in the sensitivity and angular resolution of the order of VLBI scale, it will be possible to resolve relativistic events from a large number of X-ray binaries. It will be also possible to detect the unresolved radio emissions from the radio cores at very low radio luminosities. The broad band frequency of SKA will allow to determine the behavior of radio spectrum, which changes with the X-ray state. The simultaneous multi frequency facility of SKA will help to determine the synchrotron time delay in micro-quasars, which will give a direct insight of the scale of radio jet.

GLAST: GLAST is an imaging gamma-ray telescope designed for the study of gamma-ray bursts. It has a superior area of > 8000 cm^2, and an angular resolution of $< 3.5^0$ at 100 MeV and $< 0.15^0$ at $>$10 GeV. The field of view is > 2 sr. It will provide a factor of 30 or more advance in sensitivity, as well as provide capability for the study of transient phenomena via the GLAST Burst Monitor.

Its design permits to investigate the great range of astrophysical phenomena best studied in high-energy gamma rays. GLAST is likely to be lanuched in August 2007. GLAST will enable identification of the EGRET sources for which no counterparts are known at other wavelengths by providing much smaller error boxes. More than 60% of the EGRET sources are unidentified. Considering their distribution on the sky, less than one third of these are extra galactic (probably blazar AGNs), with the rest most likely within the Milky Way. Apparently steady sources are likely to be radio-quiet pulsars and GLAST will be able to directly search for periods in sources at least down to EGRET's flux limit. Some of the unidentified sources discovered by Gamma-ray satellite, EGRET are associated with recently discovered Galactic micro-quasars. This association represent interactions of binaries with the ambient interstellar medium.

HESS: Recent High Energy Stereoscopic System (HESS) observations show that micro-quasars in high-mass systems are sources of very high energy gamma-rays. A model for micro-quasar gamma-ray emission is developed. And the results are applied to gamma-ray observations of micro-quasar LS 5039. It is shown that (1) the TeV emission measured with HESS cannot result only from Compton-scattered stellar radiation (CSSR), but could be synchrotron self-Compton (SSC) emission or a combination of CSSR and SSC. Similar observations can be performed on other micro-quasars and their Gamma-ray nature can be explored.

Further systematic observations of these sources at low radio frequencies and at multi-wavelengths are of great importance to resolve the mystery of micro-quasars. It is important to acquire longer duration data to test the theoretical suggestions. Simultaneous radio data at various frequencies is necessary to obtain reliable life times, size and various jet parameters of the varying components.

Bibliography

[] Apparao, K. M. V., 2000, A&A, 356, 972

[] Altenhoff, W. J., Downes, D., Pauls, T., et al., 1979, A&As, 35, 23

[] Bamba A., Ueno M., Koyama K. and Yamauchi S., 2003, ApJ, 589, 253-260

[] Barlow E., Bird, A., Clark J., et al., 2004, A&A 437, L27-L30

[] Barth A., Luis H., Filippenko A., et al., 2001, ApJ., 546, 205-209

[] Basko M., Sunyaev R., Titarchuk L., 1974, Astron. Astroph. 31, 249

[] Becker, R. H.; White, R. L.; McLean, B. J., et al., 1990, ApJ, 358, 485

[] Belanger G., Goldwurm A., Goldoni P., et al., 2004, ApJ, L163, 601

[] Belloni T., Mendez M., King A., et al., 1997, ApJ, 488, L109

[] Belloni, T., Klein-Wolt, M., Mendez, M. et al. 2000, A&A, 355, 271

[] Bodaghee A., R. Walter, J.A. Zurita Heras, A.J. Bird, et al., 2005, A&A, accepted, astro-ph 0510112

[] Bolton. C, 1972, Nature, 240, 124

[] Bird A., Barlow E., Bassani L., et al., 2004, ApJ, 607, L33

[] Blandford, R. D., 1989, Theory of accretion Disks ed. P. Meyer, W. Duschl, J. Frank, E. Meyer-Hofmeister (Dordrecht: Kluwer), 35

[] Braes, L. & Miley, G., 1971, Nature, 232, 246

[] Bradt & McClintock, et al., 1983, ARA&A, 21, 13

[] Bradshaw, C. F.; Geldzahler, B. J.; Fomalont, E. B., 1997, ApJ, 481, 489

[] Brocksopp, C. et al, 1999, MNRAS, 309, 1063

[] C. O' Dea, et al., 1998, ApJ, 488, L109

[] Cabanac C., Rodriguez J., Hannikainen D., et al., 2004a, ATEL 272

[] Cabanac C., Rodriguez J., Petrucci P., et al., 2004b, RMxAC, 20, 209

[] Capitanio F., Ubertini P., Bazzano A., et al., 2005, ApJ, 622, 503

[] Castro-Tirado, A. J., Brandt, S., Lund, N., 1992, IAUC, 5590

[] Ceballos M. and Barcons X., 2004, Multiwavelength AGN surveys conference proceedings, Cozumel, 17

[] Chakrabarti, S., Nandi, Anuj, Manickam, S. G., et. al., 2002, ApJ, 579L, 21

[] Chakrabarti, S., Anandarao, B. G.; Pal, S., et al., 2005, MNRAS, 362, 957

[] Chenevez J., Budtz-Jorgensen C., Lund N., et al., 2004, ATEL 223

[] Chernyakova M., Lutovinov A., et al., 2003, ATEL 157

[] Coles, W. A., Frehlich R., Rickett B., et al. 1987, ApJ, 315, 666

[] Combi, J., Ribó, M. & Mirabel, I.F., 2004, ATEL 246

[] Combi, J., Ribó, M.,& Mirabel, I.F., 2005, Proceedings f 'Multiwavelength Approach to Unidentifi ed Gamma-Ray Sources', eds. K. S. Cheng and G. E. Romero, Ap&SS, 297, 385

[] Condon, J. J., Cotton, W. D., Greisen, E., et al., 1998, AJ, 115, 1693

[] Condon J., 1999, Proc. Natl. Acad. Sci., Vol. 96, pp. 4756-4758

[] Condon, J. J., Condon M., Hazard C., 1982, AJ, 87, 739

[] Corbel S., Kaaret P., Fender R., et al., 2005, ApJ, 632, 504-513

[] Corbel, S.; Fender, R. P.; Tzioumis, A. K, et al., 2002, Sci, 298, 196

[] Corbel, S., Fender, R. P., Tzioumis, A. K., et al. 2000, A&A, 359, 251

[] Cordes, J. & Lazio, J., 1993, ASPC, 47, 143

[] Cordes, J. M., Chatterjee, S., Lazio, T., 2003, ASPC, 302, 225

[] Cordes, J. M., Lazio T., 2003, The Cordes-Lazio NE2001 Galactic Free Electron Density Model, http://rsd-www.nrl.navy.mil/7213/lazio/ne_model/

[] Cordes, J. M., Lazio T., 2004, ASPC, 317, 211

[] Cordier B., Goldwurm A., Laurent P., et al., 1991, Adv.Sp.Res. 11, 169

[] Cornwell & Perley, 1999, Synthesis Imaging in Radio Astronomy II, Eds: Taylor, G. B.; Carilli, C. L.; Perley, R. A., 1999, ASPC, 180

[] Courvoisier T., Walter R., Rodriguez J., et al., 2003, IAUC 8063

[] Cui, W., 1999, 'High Energy Processes in Accreting Black Holes' ed. J. Poutanen & R. Svensson, (San Francisco: Astron Soc Pacifi c), p.97

[] Cutri R.M., Skrutskie M.F., Van Dyk S., et al., 2003, 2MASS All-Sky Catalog of Point Sources

[] Dhawan, V., Mirabel, I. F., Rodriǵuez, L. F., 2000, ApJ, 543, 373

[] de Plaa J., Hartog den P., Kaastra J., et al., 2003, ATEL 119

[] Eikenberry, S. S., Matthews, K., Morgan, E. H., Remillard, R. A., Nelson, R. W.,1998, ApJ, 494, L61 (E98)

[] Dickey. J, 1983, ApJ, 273L, 71

[] Fabrika, S., Revnivtsev, M., et al., 2006, A&A, 447, 545

[] Fender, R. P.; Bell Burnell, S. J.; Garrington, S. T.; Spencer, R. E.; Pooley, G. G, 1995, MNRAS, 274, 633

[] Fender, R. P., Pooley, G. G., et al., 1997, MNRAS, 292, 925

[] Fender, R. P., Pooley, G. G., 1998, MNRAS, 300, 573 (F98)

[] Fender, R. P., Garrington, S. T., McKay, D. J., Muxlow, T. W. B., Pooley, G. G., et. al., 1999, MNRAS, 304, 865

[] Fender R. P., Pooley G. G., Durouchoux P., et al., 2000, MNRAS, 312, Issue 4, pp. 853-858

[] Fender, R. & Hendry, A., 2000, MNRAS, 317, 1

[] Fender, R. P.; Kuulkers, E., 2001, MNRAS, 324, 923

[] Fenimore E., Cannon M., 1978, Appl. opt. 17, 337

[] Filliatre & Chaty, 2004, ApJ, 616, 496

[] Fomalont, E. B.; Bradshaw, C. F.; Geldzahler, B. J., 1998, ASPC, 144, 339

[] Fomalont, E. B.; Geldzahler, B. J.; Bradshaw, C. F., 2001, ApJ, 558, 283

[] Frail, D. A.& Hjellming, R. M., 1991, AJ, 101, 2126

[] Chaty, S.; Rodrguez, L. F.; Mirabel, I. F., et al., 2001, A&A, 366, 1035

[] Fuchs, Y.; Rodriguez, J.; Mirabel, I. F.; Chaty, S., et al., 2003, A&A, 409L, 35

[] Fuchs, Y.; Rodriguez, J.; Shaw, S. E., 2004, inun.conf., 321

[] G. Matt & Guainazzi, et al., 2003, MNRAS, 341, L 13

[] Gansicke, B. T., Marsh, T. R., Edge, A., Rodriguez-Gil, et al., 2005, ATEL, 463

[] Gallo, E., et al. 2005, Nature 436, 819

[] Gallo, E.; Fender, R. P.; Pooley, G. G., 2004, NuPhS, 132, 363

[] Gallo, E., Fender, R., & Pooley G., 2003, MNRAS, 344, 60

[] Gonzalez-Riestra E., Oosterbroek T., Kuulkers E., et al., 2004, A&A, 420, 589

[] Gies D., Bolton C., 1982, ApJ, 260, 240

[] Gies D., Bolton C., 1986, ApJ, 304, 371

[] Gies, D. R.; Huang, W.; McSwain, M. V., 2002, ApJ, 578L, 67

[] Gierlinski, M., Zdziarski, A., et al. 1977, MNRAS, 288, 958

[] Gierliski, M., Zdziarski, A., Poutanen, J., et . al., 1999, MNRAS, 309, 496

[] Gleissner, T. et al, 2004, A&A, 425, 1061

[] Greiner, J., Castro-Tirado, Alberto J., Paredes, Josep M., 2001, miqu.book

[] Greiner, J., Cuby, J. G., McCaughrean, M. J., 2001, Nature, 414, 522

[] Grebenev, S., Lutovinov, A., Sunyaev, R., et al., 2003, ATEL, 189

[] Gursky, H., Bradt, H., Doxsey, R., et al., 1978, ApJ, 223, 973

[] Haardt & Maraschi, et al., 1991, ApJ, 380L, 51

[] Hannikainen, Diana; Wu, Kinwah; Campbell-Wilson, Duncan; Hunstead, Richard; Lovell, Jim; McIntyre, Vince; Reynolds, John; Soria, Roberto; Tzioumis, Tasso, 2001, egru.conf, 291

[] Hannikainen D., Rodriguez J., Pottschmidt K., et al., 2003, IAUC 8088

[] Hanson, M. M., Still, M. D., Fender, R. P., 1999, AAS, 195, 3906

[] Haberl F., Motch C., Zickgraf F., 2002, A&A., 387, 201H

[] Hjellming, R. M., Johnston, K. J., 1988, ApJ, 328, 600

[] Hjellming, R., Gibson, D., Owen, F., et al. 1975, Nature, 256, 111

[] Hjellming, R., Han, X., 1995, ‘X-ray Binaries’, ed W.H.G.Lewin, J. Van Paradijs & E.P.J. van den Heuvel (Cambridge: Cambridge University Press)

[] Hjellming, M. & Rupen, M., 1995, Nature, 375, 464

[] Hjellming, R. M.; Rupen, M. P.; Mioduszewski, A. J.; Smith, D. A.; Harmon, B. A.; Waltman, E. B.; Ghigo, F. D.; Pooley, G. G., 1998, AAS, 19310308

[] Homan J., Miller J., Wijnands Rudy, et al., 2005, ApJ, 623, 383

[] Harmon, B. A., Deal, K. J., Paciesas, W. S., Zhang, S. N., Robinson, C. R., Gerad, E., Rodriguez, L. F., Mirabel, I. F., 1997, ApJ, 477, L85

[] Hutchings, B. & Crampton, D., 1981, ApJ, 251, 604

[] Ishwara-Chandra, C. H.; Yadav, J. S.; Pramesh Rao, A, 2002, A&A, 388L, 33I

[] Ishwara-Chandra, A. P.Rao, Pandey M., et al., 2005a, ChJAA, 5, 87-92

[] Ishwara-Chandra & A. P.Rao, 2005b, ChJAA, 5, 269

[] Jackson C. A., 1999, PASA, 16, 2, 124

[] Kaiser, C. R., Gunn, K. F., Brocksopp, C., Sokoloski, J. L., astro-ph/0405206

[] Khamitov, I., Parmaksizoglu, M., Revnivtsev, M., et al., 2003, ATEL, 140

[] Konigl, A., Ruden, S. P., 1992 Protostars and Planets III, ed. E.H. Levy & J. I. Lunine (Univ. of Arizona Press)

[] Konigl, A., 1989 ApJ 342, 208

[] Kuulkers, Erik; Fender, R. P.; Spencer, Ralph E.; Davis, Richard J.; Morison, Ian, 1999, MNRAS, 306, 919

[] Kuulkers E., Lutovinov A., Parmar A., et al., 2003, ATEL 149

[] Leahy, D. A., 2001, A&A, 380, 516

[] Lebrun F., Leray J., Lavocat P., et al., 2003, A&A, v.411, pL141-148

[] Levine, A. M., Cui, W., Remillard, R., et al. 1996, AAS, 189, 3511

[] Liu, Q. Z.; Hang, H. R.; Wu, G. J.; Chang, J.; Zhu, Z. X., 2000, A&A, 359, 646

[] Longair, M., 1994, High energy astrophysics. Vol.2: Stars, the galaxy and the interstellar medium

[] Lutovinov A., Revnivtsev M., Molkov S., et al., 2005, A&A, 430, 997

[] Lutovinov A., Rodriguez J., et al., 2003a, ATEL 151

[] Lutovinov A., Shaw S., et al., 2003c, ATEL 154

[] Lutovinov A., Walter R., et al., 2003b, ATEL 155

[] Malizia A., Bassani L., et al., 2004, ATEL 227

[] Malzac, J., 2006, A&A, 448, 1125

[] Manchanda, R. K., 2002, J. Astrophys. Astr., 23, 197

[] Maraschi, L.; Treves, A.; Tanzi, E. G., 1981, ApJ, 248, 1010

[] Margon, B.; Anderson, S. F.; Aller, L. H.; Downes, R. A.; Keyes, C. D., 1984, ApJ, 281, 313

[] Markoff S. & Nowak M. 2004, ApJ, 609, 972

[] Markwardt, Swank J., et al., 2003, ATEL 156

[] Markwardt, C. & Swank, J., 2003, ATEL, 136, 1

[] Peracaula, M.; Paredes, J. M.; Mart, J., 1998, NewAR, 42, 645

[] Mart, Josep; Paredes, Josep M.; Peracaula, Marta, 2000, ApJ, 545, 939

[] Marti J., Paredes J. M., Peracaula M., 2001, A&A, 375, 476

[] Mart, J.; Mirabel, I. F.; Rodrguez, L. F.; Smith, I. A., 2002, A&A, 386, 571

[] Mason, K. O., Sanford, P. W., 1979, MNRAS, 189P, 9

[] Massey P., Johnson K., Degioia-Eastwood, et al., 1995, ApJ, 454, 151

[] Massi, M., 2004, A&A, 422, 267

[] Massi, M.; Rib, M.; Paredes, J. M.; Garrington, S. T.; Peracaula, M.; Mart, J., 2004b, A&A, 414L, 1

[] Massi, M.; Rib, M.; Paredes, J. M.; Peracaula, M.; Estalella, R., 2001, A&A, 376, 217

[] Masetti N., Palazzi E., Bassani L., et al., 2004, A&A, 426, L41

[] Masetti, N.; Pretorius, M. L.; Palazzi, E.; Bassani, L., et. al., 2006, A&A, 449, 1139

[] McClintock J., Remillard R. 2003, 'Compact Stellar X-ray sources, eds, Cam. Univ. Press'

[] McCollough, M.L., Robinson, C. R., Zang, S. N. et al, 1999, ApJ, 517, 951

[] Mendelson, Haim; Mazeh, Tsevi, 1989, MNRAS, 239, 733

[] Monet D., Bird A., Canzian B., et al., 1998, USNO-A2.0 Catalogue of Astrometric Standards

[] Monet, D., Levine, S., Canzian, B., et al., 2003, AJ, 125, 984

[] Miller-Jones, J. C. A., Blundell, K. M., Rupen, M. P., et. al., 2004, ApJ, 600, 368

[] Mioduszewski, Amy J., Rupen, Michael P., Hjellming, Robert M., et al. 2001, ApJ, 553, 766

[] Mioduszewski, A. J.; Dhawan, V.; Rupen, M. P., 2005, ASPC, 340, 281

[] Mirabel, I. F., Rodriǵuez, L. F., 1994, Nature, 371, 46

[] Mirabel F., Gerard E., Rodríguez L. 1994, IAU Circ., 5958

[] Mirabel F., Harmon B., Deal K., et al., 1997, ApJ, 477, L85

[] Mirabel F., Marti J., Chaty S., et al., 1998, New Aston. Rev., 42, 9-10, 621-624

[] Mirabel, I. F., Dhawan, V., Chaty, S., Rodriǵuez, L. F., Marti, J., Robinson, C. R., Swank, J., Geballe, T., 1998, A&A, 330, L9 (M98)

[] Mirabel F. and Rodríguez L. 1999, ARA&A, 37, 409

[] Mirabel, I. F., Rodríguez, L. F., Cordier, B., et al, 1992, Nature, 358, 215

[] Mirabel, I. F.; Rodriguez, L. F.; Cordier, B.; Paul, J.; Lebrun, F., 1993, A&AS, 97, 193

[] Mirabel, F.;Dhawan, V.; Pooley, G. G.; Ogley, R. N., 2000, IAUC.7395, 2

[] Moffet A., et. al., 1962, A.P.J. Suppl., 7, 93

[] Molkov S., Mowlavi N., Goldwurm A., et al., 2003, ATEL 176

[] Muno, M. P., Remillard, R. A., Morgan, E. H., Waltman, E. B., Dhawan, V., Hjellming, R. M., Pooley, G. G., 2001, ApJ, 556, 515

[] Nityananda R., Rao, A., et. al. 2004, 'Serc School on Radio Interferometry'

[] Pandey M., Durouchoux Ph., Manchanda R., et al., 2004, 5th INTEGRAL workshop proceedings held in Munich, ESA, SP-552, 695

[] Pandey, M.; Manchanda, R. K.; Rao, A. P.; Durouchoux, P.; Ishwara-Chandra, 2006, A&A, 446, 471

[] Pandey, M.; Rao, A. P.; Pooley, G. G.; Durouchoux, P.; Manchanda, R. K.; Ishwara-Chandra, C. H., 2006, A&A, 447, 525

[] Pandey M., Rao, A. P.; Manchanda R. K. et al., 2006c, A&A, in press

[] Pandey M., Rao A. P., Manchanda R. K. et al., 2006d, Advance Space Reseaech, Cospar meeting, Jan 2005, in press

[] Pandey M., Rao A. P., Durouchoux Ph., et al., 'Low frequency radio monitoring of microquasars', 2006e, submitted

[] Pandey M., Rao A. P., Durouchoux Ph., et al., 'Low frequency radio monitoring of GRS1915+105', 2006f, submitted

[] Pandey M., Manchanda R., Durouchoux Ph., et al., 'Radio survey of INTEGRAL sources', 2006g, JApA, submitted

[] Pappa A., Stewart G, Georgantopoulous I., et al., 2001, MNRAS, 327, 499

[] Paragi, Z.; Vermeulen, R. C.; Fejes, I.; Schilizzi, R. T.; Spencer, R. E.; Stirling, A. M., 1999, A&A, 348, 910

[] Paredes, J., Bosch-Ramon, V., Torres, D. F., 2005, ChJAA, 5S, 284

[] Paredes, J. M.; Rib, M.; Ros, E.; Mart, J.; Massi, M., 2002, A&A, 393L, 99

[] Paredes, J. M.; Marti, J.; Ribo, M.; Massi, M., 2000,evnconf, 163

[] Paredes, J. M., Peracaula, M.; Marti, J., 1997, A&A, 328, 283

[] Paredes, J. M.; Marti, J.; Estalella, R.; Sarrate, J., 1991, A&A, 248, 124

[] Paredes, J. M.; Figueras, F., 1986, A&A, 154L, 30

[] Paradijs V., & McClintock J. 1995, in X-ray Binaries, ed. W. H. G. Lewin, J. van

[] Paradijs, & E. P. J. van den Heuvel, Cambridge Univ. Press, 58

[] Predehl P., Wilms J., Nowak M. A., et al., 2002, Proceedings of 3rd Micro-quasar workshop, 41

[] Persi, P., Ferrari-Toniolo, M., Grasdalen, G. L., et al, 1980, A&A, 92, 238

[] Pooley, G., Brocksopp, C., Fender, R. P., et al., 1999, MNRAS, 309, 1063

[] Pooley, G. G., Fender, R. P., 1997, MNRAS, 292, 925

[] Pooley G. 2004, ATEL 226

[] Poutanen, Juri; Svensson, Roland, 1996, ApJ, 470, 249

[] Poutanen & Coppi, 1998, tx19, confE, 355

[] Ray, P. S.; Foster, R. S.; Waltman, E. B.; Tavani, M.; Ghigo, F. D., 1997, ApJ, 491, 381

[] Reig P., Negueruela I., Papamastorakis G., et al., 2005, A&A, 440, 637

[] Remillard, R., 2003, ATEL, 138

[] Revnivtsev, M., Chernyakova, M., Capitanio, F., et al., 2003, ATEL, 132, 1

[] Revnivtsev M., Astron. Astroph. 2003a, A&A, 411, 329

[] Revnivtsev M., Lutovinov A. 2003b, Astron. Letters, Vol. 29, No. 11, pp.719-723

[] Revnivtsev, M. G.; Sunyaev, R. A.; Varshalovich, D. A.; et al., 2004, Cat, 90300430

[] Revnivtsev, M., Churazov, E., Sazonov, S., et al., 2005, A&A 425, L49-L52

[] Ribo M., Combi J., Mirabel I.F., 2004, ATEL 235

[] Rickett, B.J.,1990, ARA&A 28, 561

[] Rybicki, G., Lightman, A., 1979. ‘Radiative processes in Astrophysics’ (New York: Wiley)

[] Rickett, B. J., Coles, W. A., Bourgois, G., 1984, A&A, 134, 390

[] Rodriguez J., Foschini L., Goldwurm A., et al., 2004, ATEL 253

[] Rodriguez J., Goldwurm A. 2003, ATEL 201

[] Rodriguez J., Tomsick J. 2003, Foschini L., et al., IAUC 8096

[] Rodriguez J., 2003, ATEL 194

[] Rodriguez J.,Cabanac, C., Hannikainen, et al., 2005, A&A, 432, 235

[] Rodriguez, L. F.; Mirable, F., Cordier, B.; Paul, J.; Lebrun, F., 1993, A&AS, 97, 193

[] Rodríguez, L., Mirabel, F., Martí, J., 1992, ApJ, 544, 443

[] Romero A., Gaztanaga E., Barriga., et al., 1999, A&A, 348

[] Rupen M., Mioduszewski A., Dhawan V. 2003a, ATEL 152

[] Rupen M., Mioduszewski A., Dhawan V. 2003b, ATEL 184

[] Rupen M., Midoduszewski, A. and Dhawan, V., 2003a, ATEL 137

[] Rupen M., Midoduszewski, A. and Dhawan, V., 2003b, ATEL 139

[] Rupen M., Midoduszewski, A. and Dhawan, V., 2004, ATEL 314

[] Schalinski, C. J., Johnston, K. J., Witzel, A., et al. 1998, A&A, 329, 504

[] Schalinski, C.; Witzel, A.; Johnson, K.; Pavelin, P.; Davis, R. J.; Spencer, R. E.; Umana, G., 1993, sara.conf, 22

[] Schartel N., Ehle M., Breitfellner M., et al., 2003, IAUC 8072

[] Schultz J., Hannikainen D., Vilu O., et al., 2004, A&A, 423L,

[] Shakura & Sunyave, 1973, A&A, 24, 337

[] Shapiro, S. L.; Lightman, A. P.; Eardley, D. M., 1976, ApJ, 204, 187

[] Shklovsky, I., 1965, Nature, 206, 176

[] Smith D., Heindl W., Swank J., et al., 2003, ATEL 182

[] Soldi S., Brandt S., Garau A., et al., 2005, ATEL 456

[] Spencer R. and Jowett, Frederick H., 1995, conf, 12, 'MERLIN Observations of the Radio Jets of SS433'

[] Spencer, R. E., 1984, MNRAS, 209, 869

[] Sidoli L., Vercellone S., Mereghetti S., Tavani M., et al., 2005, A&A, 429, L47-L50

[] Stephen J., Bassini L., Molina M., et al., 2005, A&A, 432, L49

[] Steeghs, D., Miller, J., Kaplan, D., et al., 2003, ATEL, 146, 1

[] Stewart, R. T.; Caswell, J. L.; Haynes, R. F.; Nelson, G. J., 1993, MNRAS, 261, 593

[] Stinebring, D.R., Smirnova, T.V., Hankins, T. et al. 2000, ApJ, 539

[] Stirling A., Spencer R., de la Force C., 2001, MNRAS, 327, 1273

[] Sugizaki M., Matsuzaki K., Kaneda H., et al. 2001(a), AIPC, 599, 959

[] Sugizaki M., Matsuzaki K., Kaneda H., et al. 2001(b), Ap.J. Suppl. 134, 77

[] Sunyaev R., Lotovinov A., et al. 2003a, ATEL 181

[] Sunyaev R., Grebenev S., Lutovinov A., et al., 2003b, ATEL 190

[] Sunyaev, R. A.; Titarchuk, L. G., 1980, A&A, 86, 121

[] Swarup G. 1991, Radio Interferometry techn.:Proceedings of 131st IAU Coll.,Astr. Scty. Pac., p.376-380

[] Swank, J. H., Markwardt, C. B., 2004, ATEL, 358, 1

[] Taylor, G. B.; Vermeulen, R. C.; Readhead, A. C. S.; Pearson, T. J.; Henstock, D. R.; Wilkinson, P. N., 1996, ApJS, 107, 37

[] Tingay, S. J.; Jauncey, D. L.; Preston, R. A.; Reynolds, J. E.; Meier, D. L.; et al., 1995, Nature, 374, 141

[] Tomsick J., Lingenfelter R., et al., 2003, IAUC 8076

[] Tomsick J., Lingenfelter R., Corbel S., et al., 2004, ATEL 224

[] Torres D., Romero G., Dame T., et al., 2003, Phys. Rep., 382, 303

[] Ubertini P., Bazzano A., Cocchi M., et al., 1999, Astroph.Lett.Comm. 38, 301

[] Ubertini P., Lebrun F., Di Cocco G., et al., 2003, A&A, 411, 131

[] Van der Klis M., Wijnands R. 1999, Astrophys.J. 514, 939

[] van der Klis, M., Janson, F. A., 1985, Nature, 313, 768

[] van der Laan, H., 1966, Nature, 211, 1131

[] Velusamy, T., Rao, A. P. & Sukumar,S.:OSRT observations of Sco X-1 region at 327 MHz, MNRAS.-Vol. 213 (1985) 735

[] Voges W., Aschenbach B., Boller T., et al., 1999, A&A, 349, 389

[] Voges W., Aschenbach B., Boller, Th., et al., 2000, VizieR online Data Catalog, IX/29 (http://cdsweb.u-strasbg.fr/viz-bin/Cat?IX/29)

[] van Kerkwjick, M. H., Gebelle, T. R., King, D. L. et al., 1996, A&A, 314,521

[] Waltman, E. B., Fiedler, R. L., Johnston, K. L. et al., 1994, AJ, 108, 179

[] Waltman, E. B., Ghigo, F. D., Johnston, K. J., 1995, AJ, 110, 290

[] Walter R., Bodaghee A., et al., 2004, ATEL 229

[] Watanabe, H., Kitamoto, S, Miyamoto, S. et al : 1994, ApJ, 433, 350

[] Wilkinson, P. N., Narayan, R., Spencer, R. E., 1994, MNRAS, 269, 67

[] Zamanov, R. K.; Mart, J., 2000, ASPC, 214, 731

[] Zdziarski, Andrzej A.; Grove, J. Eric; Poutanen, Juri; Rao, A. R.; Vadawale, S. V., 2001, ApJ, 554L, 45

[] Zoonematkermani S., Helfand D., Becker R., White R., Perley R., et al., 1990, ApJS, 74, 181

[] Zurita Heras, J., Cesare, G., Walter, R., et al., 2005, astro-ph/0511115

[] in’t Zand J. J. M., Heise J., et al., 2003, ATEL 229 ()

Appendix A

Inter Stellar Scintillation at meter wavelengths

Several classes of flux density variations are seen at radio wavelengths. The large-amplitude, broad-band, pulse-to-pulse variations seen for most point sources are thought to be intrinsic to the source emission mechanism. When averaged over many pulses to smooth out these variations, the intensity fluctuations occurring over time-scales ranging from minutes to hours, are explained in terms of propagation of radio waves through the irregular interstellar plasma (Scheuer 1968, Rickett 1969). Random variations of electron densities in the interstellar medium (ISM) gives rise to phase perturbations, leading to scattering of radio waves. As they propagate, the scattered waves interfere with each other, causing large variations of amplitude with frequency and position. The relative motion between the point source, observer and the density irregularities translates the spatial amplitude variations into temporal variations at a given point, leading to a typical time-scale of intensity fading, called the scintillation time-scale. Other observable consequence of this phenomenon are angular broadening of compact radio sources at low frequencies. We proceed further with a brief description of Inter Stellar scattering. Let us consider the inhomogeneities distorting the wave consist of variations in the electron density n_e with a single typical size, a. The phases of the radio waves are perturbed by these distortion due to the change in the refractive index, $\delta\mu$. After propagation through an inhomogeneity of length a, a wave of frequency ν experiences a phase shift of

$$\delta\phi = \delta k a \tag{A.1}$$

where $k = (2\pi/c)\mu\nu$. The corresponding phase shift is

$$\delta\phi = \delta k a = \frac{2e^2}{m_e c}\frac{a\delta n_e}{\nu} \tag{A.2}$$

After traversing a distance d between the compact source and the Earth, the radio wave has encountered a total of about d/a such irregularities in n_e, resulting into a rms phase variation

$$\Delta\phi = \sqrt{d/a}\delta\phi = \frac{2e^2}{m_e c}\frac{\sqrt{ad}\delta n_e}{\nu} \tag{A.3}$$

This phase difference $\Delta\phi$ causes a bending of wavefronts by an angle θ_0 at a screen of scale a located midway between the Earth and the compact source, where

$$\theta_0 = \frac{\Delta\phi/k}{a} = \frac{\Delta\phi c}{2\pi a\nu} = \sqrt{\frac{d}{a}}\frac{e^2}{\pi m_e}\frac{\delta n_e}{\nu^2} \tag{A.4}$$

As a result the observer sees a scatter broadened image as a diffuse disk centered around the compact source with an angular radius

$$\theta_d = \theta_0/2 = \sqrt{\frac{d}{a}}\frac{e^2}{2\pi m_e}\frac{\delta n_e}{\nu^2} \tag{A.5}$$

An angular Intensity distribution

$$I(\theta)d(\theta) \propto exp(-\theta^2/{\theta_d}^2)2\pi\theta d\theta \tag{A.6}$$

is seen.
Rays received by the observer at an angle θ arrive slightly later than those traveled undefected. The geometric delay

$$\Delta t(\theta) = \frac{\theta^2 d}{c} \tag{A.7}$$

can be used to derive the observed intensity as a function of time:

$$I(t) \propto exp(-c\Delta t/({\theta_d}^2 d)) = e^{-\Delta t/\tau_s} \tag{A.8}$$

where

$$\tau_s = \frac{\theta^2 d}{c} = \frac{e^4}{4\pi^2 {m_e}^2}\frac{\delta n_e^2}{a} d^2\nu^{-4} \tag{A.9}$$

Thus,

$$\tau_s \propto d^2\nu^{-4} \tag{A.10}$$

Thus the radio wave emitted by the compact object is measured by the observer as a one-sided exponential function with a scattering time scale τ_s. With the increase in the size of the scattering disk the time delay increases. And scattering strongly depends upon the frequency of observation and the distance of the source. The signal received over the time τ_s shows a variety of phases given by $\delta\phi = 2\pi\nu\tau_s$. The interference pattern is produced with reduced and enhanced intensity patches and moves over the observer due to relative motions of the compact source, the scattering medium and the observer. Thus a change in intensity with a time scale of Δt that depend upon the relative velocity is seen.

Interference can occur only if the phases of the waves do not differ by more than about 1 radian. Phases depend upon frequency, a limitation in bandwidth of interfering waves, i.e waves of frequencies outside a decorrelation bandwidth, also referred to as the scintillation bandwidth $\Delta\nu$ will not contribute. The condition for interference in therefore

$$2\pi\Delta\nu\tau_s \sim 1 \tag{A.11}$$

which implies the scaling $\Delta\nu \propto 1/\tau_s \propto \nu^4$. Thus a pattern of intensity variation with respect to frequency and time is produces by scintillation effect .

Depending upon the size of the electron inhomogeneities in the ISM and the distance of the compact source different kinds of scintillation can be observed. They are weak and strong scintillation, strong scintillation can be further classifi ed into (a) diffractive and (b) refractive scintillation.

Weak and strong scintillation Consider the radio waves are passing through a thin-scattering screen mid-way between us and the compact source. The screen disturbs the phases of the waves so that they are scattered into an angular spectrum of ($e^{-1/2}$) width θ_d. At some distance d the phase modulation caused by the screen produces an amplitude modulation and, hence a interference pattern is seen in the observer plane. The weak and strong scintillation depends upon the size of the total phase perturbations at this distance. This regime can be determined by considering the size of the circular region on the scattering screen centered around the source at which the phase differences are less than or equal to 1 radian. The size of this region is known as field coherence scale $s_0 = 1/(k\theta_d)$. This field coherence scale can be compared with the Fresnel scale, I_F known from diffractive optics when we observe an interference pattern. The radius of a first Fresnel zone

$$I_F = \sqrt{\frac{d}{k}} = 1.2 \times 10^9 m (\frac{d}{kpc})^{1/2} (\frac{\nu}{GHz})^{-1/2} \tag{A.12}$$

For the case $s_0 >> I_F$, the phase fluctuation within I_F are very small. At the observer's plane at distance d for which this condition holds, intensity variations can be caused only be small phase perturbations within the Fresnel zone that lead to weak scintillation. The Fresnel scale is the domination length for weak scintillation.

At larger distance the far field is considered where we enter into the regime of Fraunhofer diffraction in which large phase perturbations of many radians across the screen are effective. This occurs when $s_0 << I_F$. On this scale the effective screen also contains many points with stationary phases. This leads to multi-path propagation which leads to observed pulse scatter broadening. In terms of geometric optics, a distance is reached where rays of different parts of the screen can cross, leading to large intensity variations and, hence strong scintillation.

As discussed before, strong scintillation consists of two branches: (a) diffractive: (b) refractive scintillation. While diffractive: scintillation is described by the simple picture mentioned above - caused by interference between components of the angular spectrum - the refractive branch corresponds to the larger sizes of the scattering disk. This defines the refractive scale

$$I_R = d\theta_d = \frac{d}{ks_0} = \frac{I_F^2}{s_0} \tag{A.13}$$

$$I_F^2 = \frac{d}{k} = I_R s_0 \tag{A.14}$$

this implies that,

$$I_F^2 = \frac{d}{k} = Imagesize \times s_0 \tag{A.15}$$

Or

$$I_F^2 = \frac{d}{k} = Imagesize \times s_0 = d\theta_d \times s_0 \tag{A.16}$$

Thus the diffractive scale

$$s_0 = \frac{1}{k\theta_d} = \frac{\lambda}{2\pi\theta_d} \tag{A.17}$$

The above equation shows that the diffractive scale is dependent upon the observation frequency and scattering angle. Refractive scintillation causes small-amplitude intensity variations from the large scale focusing and defocussing of the radiation.

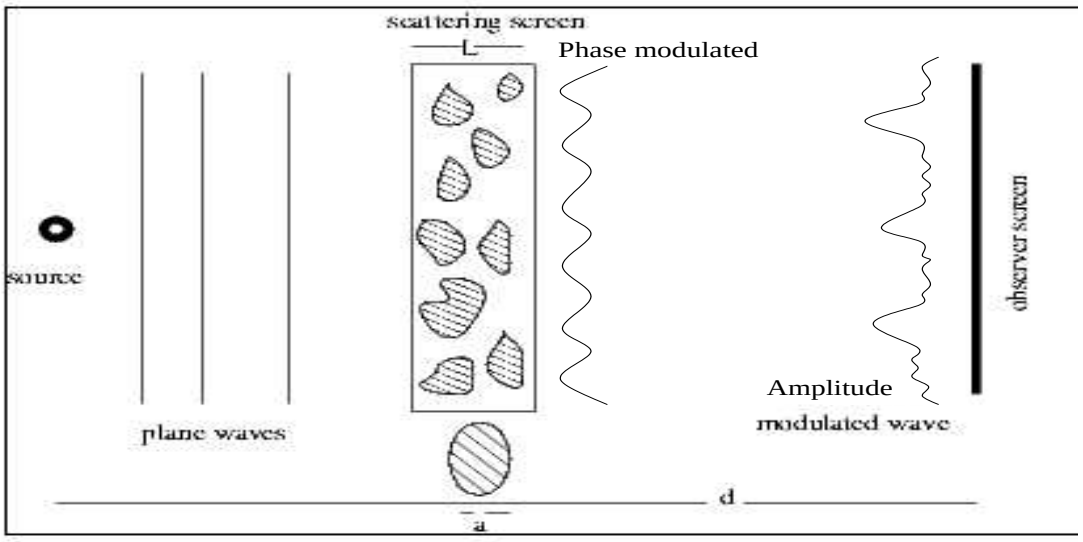

Figure A.1: DISS Phenomenon

Diffractive Inter Stellar scintillation (DISS)

DISS occurs in the strong scintillation regime, when $s_0 >> I_F$ or when phase perturbations are large at the distance of the observer and scintillation bandwidth > 1. It gives rise to strong intensity variation in both time and frequency. For DISS, the dominating length scale is the fi eld coherence scale, s_0, so that DISS time scale is

$$\Delta t_{DISS} = \frac{S_0}{V_{ISS}} \tag{A.18}$$

Where V_{ISS} is the transverse speed of the compact object. Thus it is a narrow band phenomenon occurring at shorter time scale of the order of a few seconds (Rickett 1977).

Refractive Inter Stellar scintillation (RISS)

The discovery of long term ($\sim$days to month) flux variations (Cole et al. 1970, Huguenin et al. 1973) and subsequent correlation of these time-scales with dispersion measure (DM; Sieber 1982) led to the recognition of a second class of propagation effects (Rickett et al. 1984), which has become known as refractive interstellar scintillation (RISS). In RISS, the modulations are fairly broadband in nature. RISS is the preferred explanation of slow flux variability at meter wavelengths (Rickett et al. 1986). Besides flux modulations, RISS is also thought to produce slow modulations of decorrelation bandwidth and scintillation time-scales. RISS occurs when, $s_0 << I_F$. It involves much larger refractive time scale

$$\Delta t_{RISS} = \frac{I_R}{V_{ISS}} = \frac{I_F^2}{s_0 V_{ISS}} = \frac{{I_F}^2}{{s_0}^2}\frac{s_0}{V_{ISS}} = \frac{{I_F}^2}{{s_0}^2}\Delta t_{DISS} \tag{A.19}$$

Or,

$$\Delta t_{RISS} = \frac{I_R}{V_{ISS}} = \frac{d\theta_d}{V_{ISS}} = \frac{Imagesize}{V_{ISS}} \tag{A.20}$$

Thus RISS time scale involves DISS time scale. And it is a broad band phenomenon occurring at larger time scale.

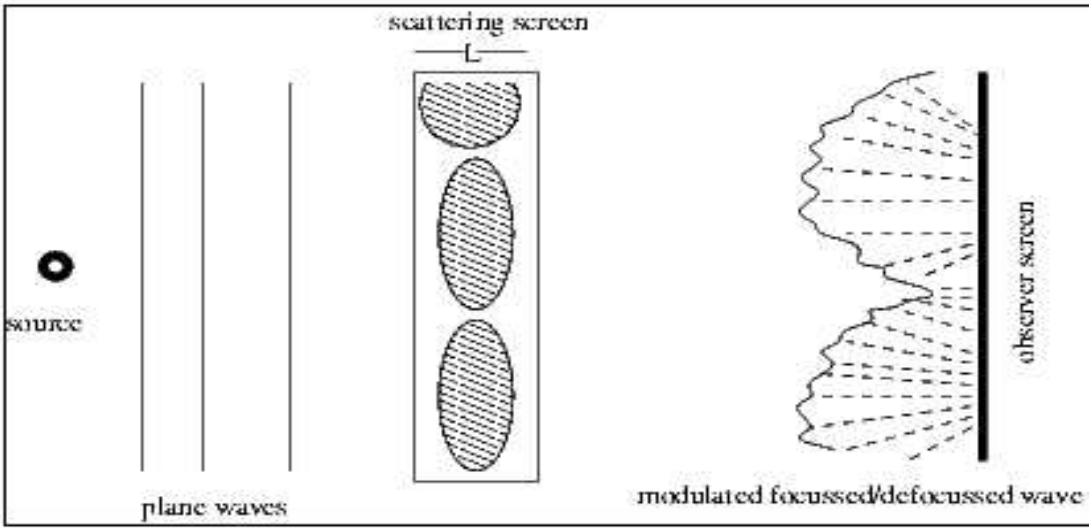

Figure A.2: RISS Phenomenon

The above mentioned phenomenon have been successfully used to answer the intensity fluctuations in compact sources. Due to our long term monitoring programme of micro-quasar, it was easy to check and confirm if the data of these variable sources were also affected by RISS.

With the earlier mentioned theory of micro-quasar (chapter 1) and the observational strategy applied (chapter 2), the important results obtained from this work is discussed in next two following chapters.